Pontifícia Universidade Católica do Rio Grande do Sul
Faculdade de Biociências
Programa de Pós-Graduação em Biologia Celular e Molecular

Ardala Breda

Caracterização Biofísico-Química da Enzima Orotato Fosforibosiltransferase (OPRT, EC 2.4.2.10) de *Mycobacterium tuberculosis* H37Rv: Modelo para o Desenvolvimento de Novas Drogas Anti-Tuberculose

Porto Alegre
Março, 2011

Pontifícia Universidade Católica do Rio Grande do Sul
Faculdade de Biociências
Programa de Pós-Graduação em Biologia Celular e Molecular

Caracterização Biofísico-Química da Enzima Orotato Fosforibosiltransferase (OPRT, EC 2.4.2.10) de *Mycobacterium tuberculosis* H37Rv: Modelo para o Desenvolvimento de Novas Drogas Anti- Tuberculose

Tese apresentada ao Programa de Pós-Graduação em Biologia Celular e Molecular como requisito para a obtenção do grau de Doutora.

Ardala Breda

Orientador:
Prof. Dr. Diógenes Santiago Santos

Co-Orientador:
Prof. Dr. Luiz Augusto Basso

Porto Alegre
Março, 2011

Ardala Breda

Caracterização Biofísico-Química da Enzima Orotato Fosforibosiltransferase (OPRT, EC 2.4.2.10) de *Mycobacterium tuberculosis* H37Rv: Modelo para o Desenvolvimento de Novas Drogas Anti- Tuberculose

Tese apresentada ao Programa de Pós-Graduação em Biologia Celular e Molecular como requisito para a obtenção do grau de Doutora.

Aprovada em _____ de _____ de _____.

BANCA EXAMINADORA:

Dr. Francisco Gorgonio da Nobrega – UNESP

Dr. Diogo Onofre Gomes de Souza – UFRGS

Dr^{a}. Nadja Schoder – PUCRS (relatora)

Dedico esta tese ao meu avô,
José Octávio Breda.

So dance if you wanna dance
- Noel Gallagher

O que você não entende pode significar qualquer coisa
- Chuck Palahniuk

Agradecimentos

Agradeço ao Professore Diógenes Santiago Santos pela confiança, pela oportunidade, pela paciência e pelos conselhos e ensinamentos ao longo destes anos. Agradeço ao Professor Luiz Augusto Basso pela oportunidade, pelos ensinamentos, paciência e discussões de resultados, essenciais para o desenvolvimento deste trabalho.

Muito obrigada aos amigos e colegas do CPBMF/4G, pelos momentos sérios e momentos de descontração, em especial à Dra. Jocelei Chies, Claudinha Paiva Nuves, Gaby Renard e Tina Dias.

Todos os “obrigadas” do mundo aos meus amigos Zé, Thiago, Júnior e Léo Rosado, por sempre me fazerem rir, por me aguentarem chorando na sala de espectro e por me ensinarem a me levar menos a sério; e às minhas amigas Jojo e Dai, pelas jantinhas das meninas, pelas conversas sérias, pelas conversas nada sérias, pelo companheirismo do começo ao fim.

Resumo

A tuberculose é uma doença infecciosa crônica, causada principalmente pelo *Mycobacterium tuberculosis*, e requer novas iniciativas urgentes para o seu tratamento e cura em decorrência do surgimento de cepas resistentes a drogas, sua abrangência global, e o significativo aumento de pessoas infectadas entre pacientes imunodeprimidos; além do grande número de pessoas infectadas com a forma latente da tuberculose, que atuam como reservatório da doença. As enzimas que constituem as vias de metabolismo de nucleotídeos são alvos promissores para o desenvolvimento de novas drogas para o tratamento da tuberculose, tanto na sua forma ativa quanto latente. A enzima orotato fosforibosiltransferase (OPRT), pertencente à via de síntese *de novo* de nucleotídeos de pirimidina, catalisa a transferência reversível do grupamento fosforibosil da molécula de 5'-fosfo-α-D-ribose 1'-difosfato (PRPP) para o ácido orótico (OA), formando orotidina 5'-monofosfato (OMP), molécula precursora dos demais nucleotídeo de pirimidina. Este trabalho descreve a clonagem, amplificação e caracterização do produto do gene *pyrE* de *M. tuberculosis* H37Rv como uma enzima OPRT funcional; a determinação de suas constantes cinéticas aparentes e verdadeiras para as reações direta e inversa; ensaio de inibição pelos produtos; e a determinação do mecanismo cinético da reação como sendo Mono-Iso Ordenado Bi Bi, mecanismo que até então não havia sido descrito para uma enzima pertencente à família das fosforibosiltransferases do tipo I. As constantes termodinâmicas e o perfil de discriminação termodinâmica permitiram a identificação dos modos de interação dos substratos naturais da enzima com seu sítio de ligação. A caracterização da reação catalisada pela enzima OPRT micobacteriana é uma etapa essencial para o desenvolvimento de novas drogas de ação específica que permitam o melhor controle da tuberculose. Os dados resultantes da caracterização da enzima foram utilizados como ponto de partida para o planejamento, seleção e teste de inibidores seletivos contra a OPRT de *M. tuberculosis*. Um composto inicial, com valores de K_i na faixa de concentração de nanomolar, foi identificado como potencial composto líder, sendo submetido a diferentes protocolos de derivatizaçao química, permitindo a obtenção de uma molécula derivada com valores de constantes inibitórias e perfil de discriminação termodinâmica aprimorados. Estes dois compostos foram caracterizados como inibidores competitivos e incompetitivos em relação aos substratos naturais da OPRT, OA e PRPP, respectivamente; onde o conhecimento do singular mecanismo cinético de reação da enzima de *M. tuberculosis* foi utilizado para o planejamento de moléculas capazes de formar um complexo ternário não catalítico ($E \cdot PRPP \cdot I$), inibindo a síntese de nucleotídeos de pirimidina e sequestrando moléculas de PRPP do meio celular, afetando ainda, outros processos metabólicos essenciais. Os resultados deste trabalho colaboram ainda para uma melhor compreensão do metabolismo de nucleotídeos de micobactérias e fornecem informações relevantes para o avanço do desenvolvimento de inibidores de ação seletiva sobre alvos moleculares específicos para o tratamento e profilaxia da tuberculose.

Abstratc

Tuberculosis is a chronic infectious disease mainly caused by *Mycobacterium tuberculosis* that requires urgent new efforts towards its treatment and cure face the emergence of drug-resistant strains, its world spreading, the increasing number of infected patients among immune compromised populations, and the large number of latent infected individuals that are reservoir to the disease. Nucleotides metabolism pathways provide promising molecular targets for the development of novel drugs against active tuberculosis and might also target its latent forms. The orotate phosphoribosyltransferase (OPRT) enzyme of the *de novo* pyrimidine synthesis pathway catalyzes the reversible phosphoribosyl transfer from 5'-phospho-α-D-ribose 1'-diphosphate (PRPP) to orotic acid (OA), forming orotidine 5'-monophosphate (OMP), precursor of remaining pyrimidine nucleotides. This work describes cloning, amplification and characterization of *M. tuberculosis* H37Rv *pyrE* gene as encoding a functional OPRT, its apparent and true kinetic constants for forward and reverse reactions, product inhibition profile, and kinetic mechanism assignment as Mono-Iso Ordered Bi Bi, not previously described for an enzyme member of type I phosphoribosyltransferase family. Thermodynamic constants and discrimination profile allowed natural enzyme's substrates binding patterns identification. Characterization of the reaction catalyzed by mycobacterial OPRT is essential to structure-based drug development, aiming to advance towards tuberculosis control. Resulting data from enzyme's characterization were the starting point for OPRT specific inhibitors planning, selection and testing. A starting compound was identified as promising lead molecule, with K_i values in nanomolar range, and was further submitted to several chemical replacement experiments, leading to a derived molecule with lower inhibitory constants and improved thermodynamic discrimination profile. Both compounds identified were characterized as competitive and uncompetitive inhibitors towards OPRT substrates OA and PRPP, respectively. Advantage of *M. tuberculosis* unique kinetic mechanism among homologues OPRTs was taken in order to plan a specific molecule that might trap the enzyme in a non-catalytic ternary complex $E \cdot PRPP \cdot I$, both inhibiting pyrimidine synthesis and sequestering PRPP from cellular pool, thereby affecting other metabolic pathways. *M. tuberculosis* OPRT characterization and results on primary inhibitors identification are crucial step towards a potential novel drug development for tuberculosis treatment and prophylaxis. Results from this work are believed to enhance the understanding of mycobacterial nucleotide metabolism and provide pertinent data to advance towards specific molecular targets inhibitors development, aiming tuberculosis control.

Lista de Abreviaturas e Siglas

5FU: 5-fluoruracil

A: adenina

AMPc: adenosina 5'-monofosfato cíclico

ATP: adenosina 5'-trifosfato

C: citosina

CTP: citidina 5'-trifosfato

DMSO: dimetilsulfóxido

DNA: ácido desoxirribonucléico, do inglês *deoxiribonucleic acid*

FAD: flavina-adenina dinucleotídeo

FMN: flavina mononucleotídeo

G: guanina

GMP: guanosina 5'-monofosfato

GMPc: guanosina 5'-monosfosfato cíclico

GTP: guanosina 5'-trifosfato

HIV: síndrome da imunodeficiência adquirida humana, do inglês *human imunodeficiency virus*

HPLC: cromatografia líquida de alto desempenho, do inglês *high performance liquid cromatography*

IMP: inosina 5'-monofosfato

LB: Luria-Bertani

LNLS: Laboratório Nacional de Luz Sincrotron

MDR-TB: tuberculose resistente a múltiplas drogas, do inglês *multi drug-resistant tuberculosis*

MIC: concentração mínima inibitória, do inglês *minimal inhibitory concentration*

MTB: *Mycobacterium tuberculosis*

NAD^+: nicotinamida adenina dinucleotídeo, forma oxidada

$NADP^+$: nicotinamida adenina dinucleotídeo fosfato, forma oxidada

OMP: orotidina 5'-monofosfato

OMS: Organização Mundial da Saúde

OPRT: orotato fosforibosiltransferase, do inglês *orotate phosphoribosyltransferase*

PCR: reação em cadeia da polimerase, do inglês *polymerase chain reaction*

PDB: *Protein Data Bank*

PNP: fosforilase de nucleosídeos de purina, do inglês *purine nucleoside phosphorylase*

PRPP: 5'-fosfo-α-D-ribose 1'-difosfato

PRTase: fosforibosiltransferase

PyNP: fosforilase de nucleosídeos de pirimidina, do inglês *pyrimidine nucleoside phosphorylase*

R-1-P: ribose 1-fosfato

RNA: ácido ribonucléico, do inglês *ribonucleic acid*

T: timina

TB: tuberculose

TBSGC: *Tuberculosis Structural Genome Consortium*

TP: timidina fosforilase, do inglês *thymidine phosphorylase*

U: uracil

UMP: uridina 5'-monofosfato

UP1: uridina fosforilase 1, do inglês *uridine phosphorylase 1*

UP2: uridina fosforilase 2, do inglês *uridina phosphorylase 2*

UPRT: uracil fosforibosiltransferase, do inglês *uracil phosphoribosyltransferase*

UTP: uridina 5'-trifosfato

UV: ultra-violeta

XDR-TB: tuberculose extensivamente resistente a drogas, do inglês *extensively drug-resistant tuberculosis*

X-Gal: 5-bromo-4-cloro-3-indolil-β-D-galactopiranosídeo

Lista de Símbolos

mM: mili molar

µL: micro litro

vol/vol: proporção volume/volume

°C: temperatura em graus Celsius

M: molar

w/vol: proporção massa/volume

pb: pares de base

µM: micro molar

kb: quilo base

µg mL^{-1}: microgramas por mili litro

mL: mili litro

rpm: rotações por minuto

Sumário

Anexos

Capítulo 1

1. Introdução

I. A Tuberculose e o Metabolismo de Nucleotídeos

A tuberculose (TB), doença infecto-contagiosa causada principalmente pelo bacilo *Mycobacterium tuberculosis* (MTB), é responsável pela morte de mais de dois milhões de pessoas por ano, segundo a Organização Mundial da Saúde (OMS) (1). Dados epidemiológicos apontam um total de 8.9-9.9 milhões de casos estimados, 1.1-1.7 milhões de mortes entre pacientes não portadores do vírus do HIV, e 0.45-0.62 milhões de mortes entre pacientes soropositivos (os dados destes pacientes inicialmente eram classificados como mortes decorrentes da infecção por HIV). O número de casos notificados no ano de 2008 chegou a 67% do total de casos incidentes, aproximando-se da meta estabelecida pela OMS (2). A incidência global da TB é menor nas Américas, onde ocorrem 46 casos de TB a cada 100.000 habitantes, e maior na África, com 290 casos a cada 100.000 habitantes, onde está relacionada com a alta prevalência da infecção por HIV (3).

O Brasil ocupa o 15º lugar entre os 22 países responsáveis por 80% do total de casos de TB no mundo. Estima-se uma prevalência de 50 milhões de infectados com cerca de 111.000 casos novos e 6.000 óbitos ocorrendo anualmente (1). Segundo dados do Sistema de Informação de Agravos de Notificação (Sinan/MS), são notificados anualmente 85 mil casos novos (correspondendo a um coeficiente de incidência de 47/100.000 habitantes) no Brasil (4), sendo 0.9% destes novos casos de TB correspondentes a cepas resistentes a múltiplas drogas (MDR-TB) (2). No ano de 2008 foram notificados quase 30 000 casos de MDR-TB, estando a maior parte (85%) em países europeus. No entanto, a OMS estima que estes números correspondam a apenas 11% do total de casos de tuberculose causada por cepas resistentes a drogas (1).

As cepas MDR-TB se caracterizam por apresentarem resistência a um dos dois principais medicamentos de primeira linha contra a TB, rifampicina e isoniazida,

requerendo a administração de medicamentos de segunda linha, que são menos efetivos, mais tóxicos e mais custosos quando comparadas às drogas de primeira linha (5, 6). Em 2006 a OMS reportou a identificação de cepas extensivamente resistentes (XDR-TB), as quais, além de resistência a rifampicina e isoniazida, são também resistentes a três ou mais medicamentos de segunda linha (7, 8). Mais recentemente, em 2010, foram reportadas cepas de MTB resistentes a todas as drogas de primeira linha e a todas as drogas de segunda linha testadas, sendo classificadas como cepas totalmente resistentes a drogas (TDR-TB) (9). Estas cepas apresentam ainda morfologia distinta da MDR-TB e XDR-TB, com espessamento significativo da camada de ácidos micólicos no seu envelope celular (10).

A baixa adesão ao tratamento, o surgimento decorrente das cepas resistentes às drogas de primeira e segunda linha, além da incidência mundial da TB ressaltam a necessidade de busca de novas drogas para o seu combate e controle (11, 12). Dentre as possíveis rotas metabólicas passíveis de serem utilizadas como alvo para o desenvolvimento de novos inibidores anti-TB, encontra-se o metabolismo de nucleotídeos, uma via essencial para a viabilidade e replicação da micobactéria (13).

O metabolismo de nucleotídeos é conservado entre eucariotos e procariotos, incluindo MTB. Embora as vias de síntese de nucleotídeos a partir de precursores simples (via *de novo*) e a via de reciclagem de bases (via de salvamento) não sejam amplamente detalhadas nas micobactérias, é sabido que o MTB expressa enzimas presentes em ambas as vias (14). A oscilação do metabolismo de MTB entre as vias de síntese *de novo* e de salvamento ainda é uma questão pouco compreendida (11), (15, 16). O MTB é capaz de adaptar o seu metabolismo durante os diferentes estágios de infecção da TB, em resposta aos microambientes formados nas regiões necróticas típicas da doença e que se localizam em cavidades do pulmão do hospedeiro, onde a disponibilidade de oxigênio e nutrientes provavelmente é limitada

(15), e esta restrição de nutrientes a que o MTB está submetido nos granulomas (16, 17) é considerada um elemento essencial para a sua sobrevivência no estado latente (18). Estudos já demonstraram que mesmo em fase de latência, a enzima ribonucleotídeo redutase (responsável pela conversão de ribonucleotídeos em deoxi-nucleotídeos para a incorporação ao DNA) de MTB se mantém ativa (19).

Após a inalação de aerossóis contendo MTB, a resposta inata mediada por macrófagos é iniciada nos pulmões; células dendríticas que entram em contato direto com o MTB ou com macrófagos infectados iniciam a resposta adaptativa, mediada por células T, que ativam mais macrófagos e induzem a formação de granulomas nos pulmões e a contenção do patógeno (20). A formação de granulomas pode resultar na eliminação do MTB, mas também apenas na prevenção da sua replicação, levando-o a entrar no estado de latência (20, 21).

Em 5-7% dos casos a contenção da TB pela formação de granulomas não é eficaz, com a replicação intracelular do MTB causando morte celular dos macrófagos, induzindo necrose e apoptose celular no interior dos granulomas e permitindo a disseminação do MTB para outros tecidos ou através da via aérea; havendo então o contágio de outras pessoas (20, 22).

Embora os mecanismos que levam à falha do granuloma em conter a infecção causada pelo MTB não sejam ainda completamente compreendidos, assim como o estado metabólico do MTB no período de latência e as causas da sua reativação; sabe-se, no caso da reativação, que tanto fatores relacionados ao próprio MTB como ao hospedeiro (supressão imunológica, congênita ou causada por outras infecções, como HIV ou por medicamentos) estão relacionados com a indução da apoptose e necrose celular no interior do granuloma, ocasionando a disseminação do MTB (11).

Evidências experimentais indicam a ocorrência de uma alteração do uso de carboidratos pela micobactéria como principal fonte de carbono nas primeiras semanas após o contágio, para ácidos graxos e colesterol nas etapas subsequentes da infecção (15); no entanto, poucas proteínas de transporte responsáveis pela absorção de nutrientes essenciais foram identificadas na membrana interna e externa do MTB (16). Desta forma, ainda não é claro se o MTB depende da absorção de moléculas complexas provenientes do hospedeiro para a manutenção do seu metabolismo, ou se realiza a síntese de moléculas essenciais a partir de precursores simples e capazes de se difundir passivamente pelas suas membranas.

A via de síntese *de novo* de nucleotídeos de pirimidina já foi comprovada como sendo essencial para a virulência de *Toxoplasma gondii* (23) e *Plasmodium vivax* (24), onde a sua interrupção origina cepas dependentes nutricionais de uracil e completamente avirulentas (23).

A busca por melhores drogas anti-TB requer a identificação e caracterização de alvos moleculares essenciais à sobrevivência do MTB, os quais devem ser validados quanto a seu potencial farmacológico (25). A profilaxia da TB, através da imunização com a vacina BCG apresenta eficiência amplamente variável, sendo baixa ou mesmo nula em certas populações humanas (26). Nesse sentido, genes e rotas metabólicas essenciais ao crescimento e persistência do MTB (como é o provável caso da via de salvamento e de síntese *de novo* de nucleotídeos) constituem uma boa opção para o desenvolvimento de novas drogas de ação específica, pois a inibição de suas funções deve resultar na morte ou atenuação do bacilo, auxiliando no tratamento, controle e profilaxia da tuberculose.

II. Metabolismo de Nucleotídeos

Nucleotídeos são ésteres fosfato de pentoses que apresentam uma base nitrogenada ligada covalentemente ao carbono C1' da porção açúcar (**Figura 1**). A grande maioria das células apresenta as rotas metabólicas de síntese e degradação de nucleotídeos (27), o que salienta a sua importância em diversos processos bioquímicos, por exemplo:

- trifosfatos de nucleosídeos servem como precursores ativados na síntese de DNA e RNA, constituindo as unidades monoméricas das cadeias de ácidos nucléicos;
- a hidrólise dos grupamentos fosfato ligados ao grupamento hidroxila 5' dos ribonucleotídeos ATP, UTP, GTP e CTP (denominados α, β e γ a partir da ribose) provê energia química para diversas reações celulares (30KJ/mol na hidrólise das ligações fosfoanidro entre os fosfatos α/β e β/γ e 14KJ/mol na hidrólise da ligação éster entre o fosfato α e a ribose);
- nucleotídeos de adenina são componentes dos cofatores enzimáticos NAD^+, $NADP^+$, FMN, FAD e coenzima A, e embora a porção adenosina não participe diretamente da função primária destas coenzimas, a sua remoção reduz drasticamente a sua atividade;
- atuam como segundo mensageiros no processo de transdução de sinal, principalmente na forma de AMP cíclico (AMPc) e GMP cíclico (GMPc) (28).

As bases nitrogenadas de ocorrência mais comum são divididas em bases púricas, cuja estrutura é formada por dois anéis – adenina (A) e guanina (G) - e bases pirimídicas, com apenas um anel em sua estrutura – timina (T), citosina (C) e uracil (U). A ligação glicosídica entre a base nitrogenada e o anel da ribose se dá através do carbono C1' da ribose e o nitrogênio N1 para as bases púricas e N9 para as pirimidinas (29) (**Figura 2**).

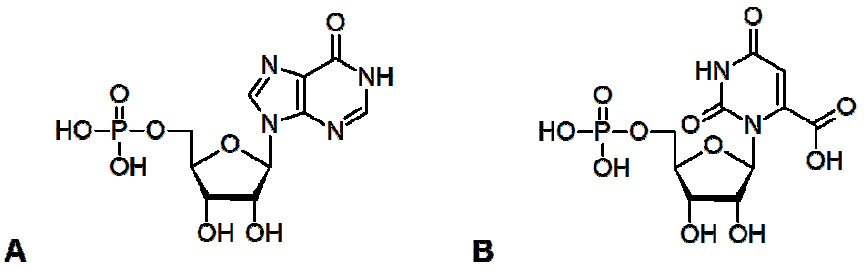

Figura 1. Estrutura de um ribonucleotídeo de purina (A) e pirimidina (B). O açúcar encontrado nas moléculas de DNA (2'-deoxi-D-ribose) apresenta apenas um átomo de hidrogênio ligado ao carbono C2' do anel, substituindo o grupamento hidroxila observado no RNA. Os nucleotídeos mostrados são IMP (A) e OMP (B).

As rotas metabólicas de síntese e de degradação de nucleotídeos estão fortemente relacionadas com as rotas correlatas do metabolismo de aminoácidos, apresentando diversos intermediários metabólicos em comum, com aminoácidos sendo incorporados na estrutura de purinas e de pirimidinas e com parte da base nitrogenada das purinas podendo ser incorporada na estrutura do aminoácido histidina (30).

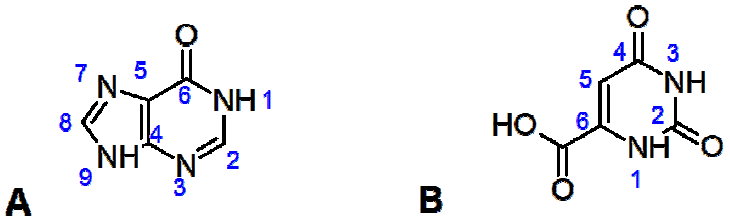

Figura 2. Numeração dos átomos da base nitrogenada nos nucleotídeos de purinas (**A**) e pirimidinas (**B**).

O metabolismo de nucleotídeos requer um controle fino, pois estes devem estar presentes em quantidades específicas e no momento correto para a síntese de ácidos nucléicos, permitindo a replicação celular e a síntese de proteínas, além de serem moléculas carregadas negativamente, cujos níveis devem ser controlados para manter o balanço eletroquímico das células (28). Em humanos, a obtenção de nucleotídeos diretamente da dieta é mínima, pois as enzimas deoxiribonuclease e

ribonuclease, secretadas pelo pâncreas, juntamente com a atividade da fosfatase alcalina das células epiteliais intestinais, são responsáveis pela degradação dos nucleotídeos em nucleosídeos. Células do próprio epitélio intestinal metabolizam estes nucleosídeos para suas necessidades energéticas, de forma que apenas cerca de 5% dos nucleotídeos ingeridos chegam à circulação como bases livres ou nucleosídeos (31).

Duas rotas metabólicas são responsáveis pela síntese de nucleotídeos, a via *de novo* e a via de salvamento, tanto para purinas como pirimidinas. A síntese *de novo* se dá a partir de precursores simples, como aminoácidos, ribose-5-fosfato, CO_2 e NH_3, enquanto a via de salvamento está relacionada à reciclagem de bases livres e nucleosídeos formados no catabolismo de nucleotídeos (27).

As vias de síntese *de novo* e de salvamento de purinas e de pirimidinas são distintas nos seus mecanismos e em sua regulação, apresentando, no entanto, alguns precursores comuns, como o aminoácido glutamina como fonte de grupamentos amino, e PRPP (5'-fosfo-α-D-ribose 1'-difosfato) como fonte da porção pentose (32).

Síntese de novo e Via de Salvamento de Purinas

Síntese de novo

Os nucleotídeos de purinas são sintetizados a partir de PRPP, que atua como fonte da porção ribose. O PRPP é obtido a partir de ribose 5'-fosfato, obtida da via das pentose fosfato (32), e de ATP, em reação catalisada pela enzima PRPP sintase (**Figura 3**).

A etapa de comprometimento desta via é catalisada pela glutamina fosforibosilamidotransferase, que adiciona o átomo de nitrogênio 9 (N9) da base nitrogenada ao PRPP. Os demais átomos da base são adicionados nas reações

subsequentes, com consumo de seis moléculas de ATP até a formação de IMP (monofosfato de inosina). Os átomos de carbono 4 (C4) e 5 (C5) e nitrogênio 7 (N7) são obtidos de um resíduo do aminoácido glicina, carbono 8 (C8) é obtido de N^{10}-formil tetrahidrofolato, nitrogênio 3 (N3) de um resíduo de aminoácido glutamina, carbono 6 (C6) é obtido do CO_2, nitrogênio 1 (N1) provém de um resíduo de aminoácido aspartato e carbono 2 (C2) é obtido a partir de formil tetrahidrofolato.

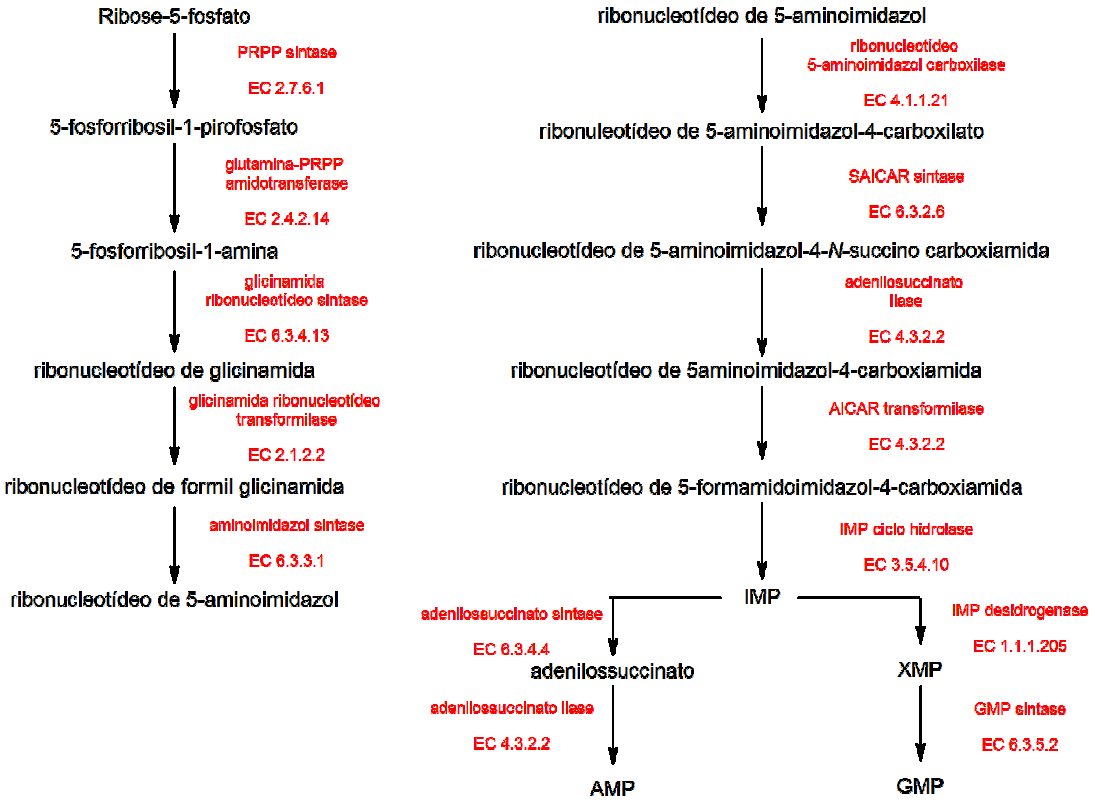

Figura 3. Síntese *de novo* de purinas. A via inicia com a formação de PRPP a partir de ribose-5-fosfato e ATP pela ação da enzima PRPP sintase.

Os nucleotídeos AMP e GMP são sintetizados a partir de IMP, podendo ser posteriormente fosfatados às formas di e trifosfato por cinases específicas (31). As reações catalisadas pelas enzimas PRPP sintase, glutamina fosforibosilamidotransferase, adenilossuccinato sintase e IMP desidrogenase são as etapas reguladas da via, sendo que as duas primeiras enzimas controlam a síntese de IMP e as duas últimas controlam a síntese de AMP e GMP, respectivamente.

Via de Salvamento

A maioria das células é capaz de utilizar a via de salvamento para a reciclagem de bases livres e nucleosídeos tecidos (31). As principais enzimas responsáveis pela interconversão de bases livres, nucleosídeos e nucleotídeos são a fosforilase de nucleosídeos púricos (PNP – do inglês *purine nucleoside phosphorylase*), fosforibosiltransferases e deaminases. A via de salvamento de purinas é mostrada na **Figura 4**.

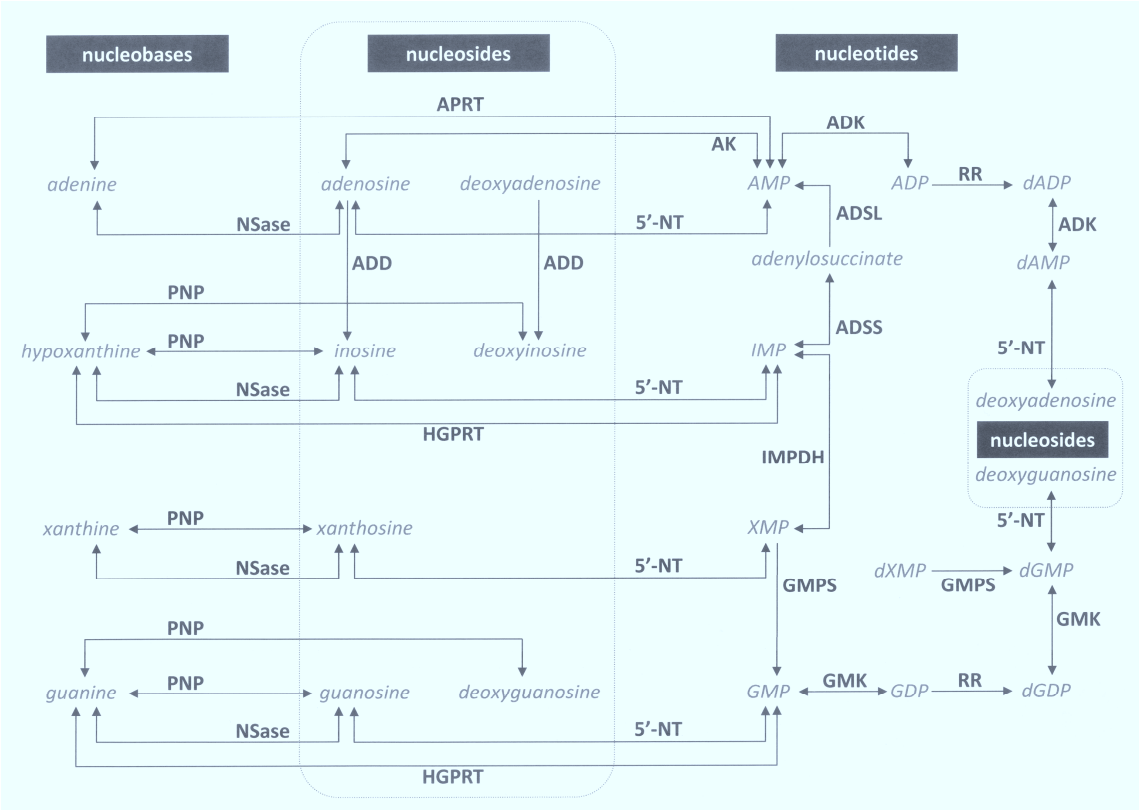

Figura 4. Via de salvamento de bases púricas. Adaptado de (33).

A enzima PNP catalisa a fosforólise da ligação glicosídica entre o átomo C1' da ribose e N9 da base nitrogenada. Assim, nucleosídeos são convertidos em bases livres, liberando ribose-1-fosfato (R-1-P), que pode ser isomerizada em ribose-5-fosfato. As bases livres geradas podem ser convertidas de volta a nucleotídeos pela ação de fosforibosiltransferases específicas da via de salvamento, ou degradadas.

Adenosina e AMP podem ser deaminados por suas deaminases específicas a inosina e IMP para entrar na via de salvamento, ou ainda a conversão de nucleosídeo a nucleotídeo pode ocorrer diretamente pela ação da adenosina cinase (31).

As reações catalisadas pelas enzimas da via de salvamento de purinas são reversíveis e atuam também no catabolismo destes nucleotídeos, sendo o sentido das reações (salvamento ou catabolismo) determinado pelas condições da célula. No catabolismo, a base livre hipoxantina gerada pela clivagem do IMP é convertida em xantina pela xantina oxidase, e guanina é deaminada a xantina pela ação da guanase. Xantina é convertida em ácido úrico pela xantina oxidase, que é excretado na urina. Pouca energia é obtida da degradação de purinas, o que torna a via de salvamento energeticamente mais favorável para a célula.

Síntese de novo e Via de Salvamento de Pirimidinas

Síntese de novo

Em contraste com a síntese *de novo* de purinas, nas pirimidinas a base nitrogenada é sintetizada e depois ligada à ribose. A via começa com a formação de carbamoil fosfato a partir de glutamina, CO_2 e duas moléculas de ATP, em uma reação catalisada pela carbamoil fosfato sintetase II. Esta reação é a etapa regulada da via e é análoga à primeira reação do ciclo da uréia, catalisada pela carbamoil fosfato sintetase I; no entanto, a reação catalisada pela carbamoil fosfato sintetase II ocorre no citosol e utiliza glutamina como fonte de nitrogênio, ao contrário da reação observada no ciclo da uréia, que ocorre no interior da mitocôndria e utiliza amônia como fonte de nitrogênio (31). A via completa de síntese *de novo* de pirimidinas, com seus intermediários e enzimas, é mostrada na **Figura 5**.

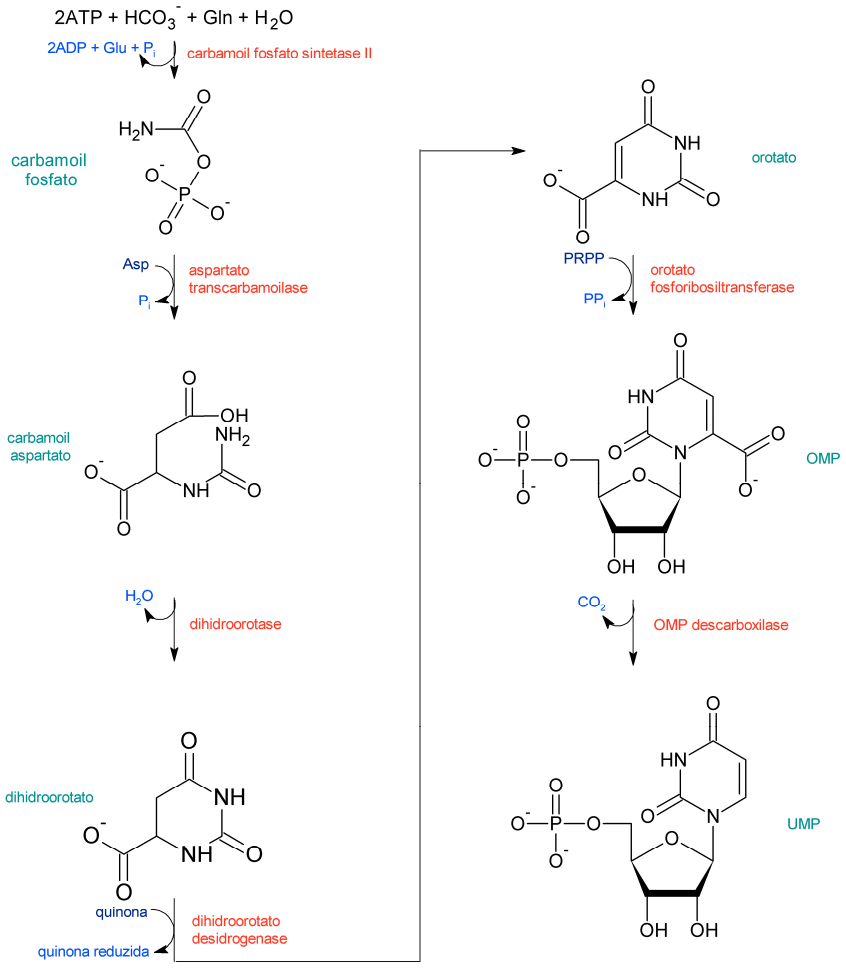

Figura 5. Síntese *de novo* de pirimidinas. A via inicia com a formação de carbamoil fosfato a partir de glutamina, CO_2 a duas moléculas de ATP, pela ação da enzima carbamoil fosfato sintetase II.

Os seis átomos que compõem a base nitrogenada das pirimidinas são oriundos da glutamina (nitrogênio 3 – N3), CO_2 (C2) e do aminoácido aspartato (nitrogênio 1 – N1 e carbono 4, 5 e 6 – C4, C5, C6). A adição dos átomos N1, C4, C5 e C6, à base nitrogenada ocorre pela ação da enzima aspartato transcarbamoilase, segunda reação da via, que é também a sua etapa de comprometimento. Uma vez formada a base nitrogenada, a enzima orotato fosforibosiltransferase catalisa a transferência da ribose-5-fosfato do PRPP para o orotato, formando OMP, que é descarboxilado a UMP (34, 35).

Cada uma das etapas da síntese *de novo* de pirimidinas é catalisada por uma enzima individual, codificada por genes distintos nos procariotos e fungos. Nos organismos eucariotos, exceto fungos, as três primeiras enzimas da via estão localizadas na mesma cadeia polipeptídica, assim como a orotato fosforibosiltransferase e a OMP desidrogenase, que formam o polipeptídeo UMP sintase (36, 37). O nucleotídeo UMP formado pode então ser fosforilado a UTP e originar CTP pela adição de um grupamento amina a partir de um aminoácido glutamina.

Via de Salvamento

A via de salvamento de pirimidinas compreende a conversão direta de bases livre de uracil no seu nucleotídeo correspondente (UMP), pela ação da enzima uracil fosforibosiltransferase, e ainda reações em duas etapas: a primeira é a conversão de bases livres em seus respectivos nucleosídeos por pirimidina nucleosídeo fosforilases, que podem ser específicas para uridina (UP1 e UP2 – do inglês *uridine phosphorylase*) ou para timidina (TP – do inglês *thymidine phosphorylase*), como nos mamíferos, ou por pirimidina nucleosídeo fosforilases com afinidade tanto para uridina quanto timidina, como no caso de bactérias, sendo denominada PyNP (do inglês *pyrimidine nucleoside phosphorylase*). Na segunda etapa desta conversão, nucleosídeo cinases específicas promovem a conversão dos nucleosídeos em nucleotídeos (**Figura 6**) (34).

Assim como na via de salvamento de purinas, as reações catalisadas pelas PyNPs são reversíveis, fazendo parte também do catabolismo destes nucleotídeos. Os nucleosídeos são clivados formando R-1-P e as bases livres citosina, uracil e timina. Citosina é deaminada em uracil e convertida em CO_2, NH_4^+ e β-alanina. Timina é convertida em CO_2 e NH_4^+. Estes produtos são excretados, exceto pela β-

alanina que é convertida em metilmalonil semialdeído pela aminotransferase, que por sua vez é ativado a malonil CoA (27).

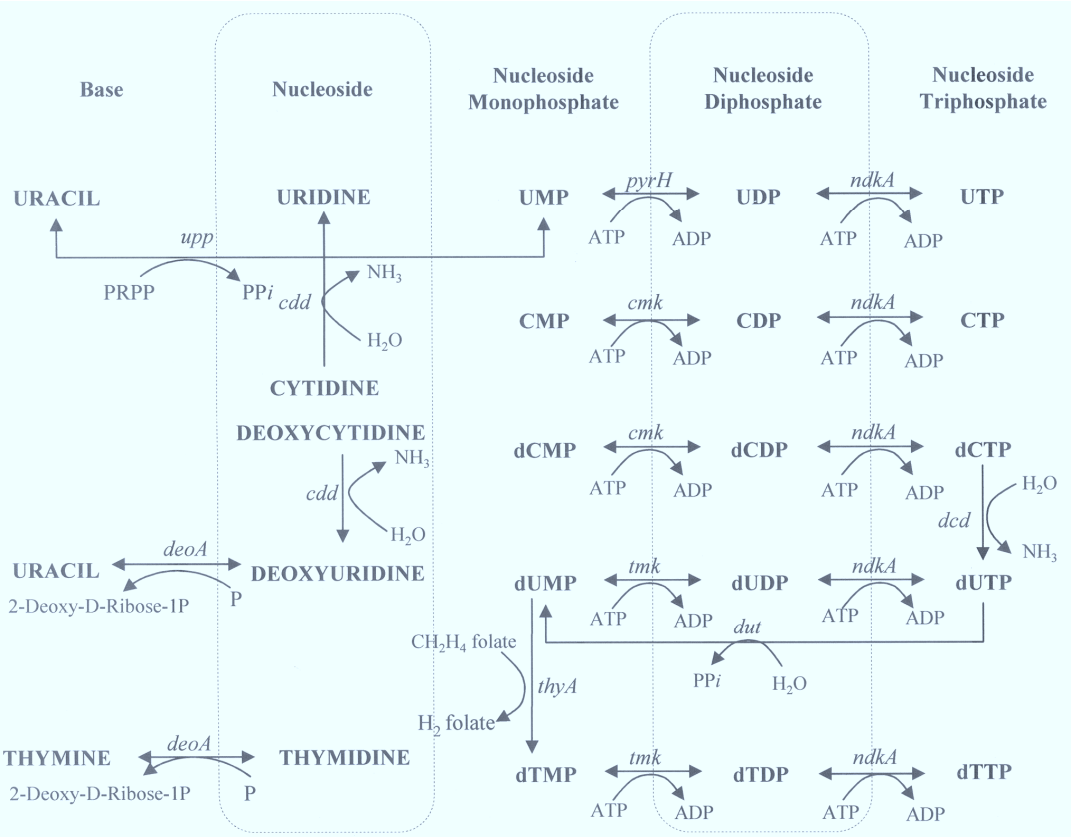

Figura 6. Via de salvamento de bases púricas. Adaptado de (38).

III. A Enzima OPRT de *Mycobacterium tuberculosis*

A quinta enzima da via de síntese *de novo* de pirimidinas (**Figura 5**), a enzima orotato fosforibosiltransferase (OPRT, do inglês *orotate phosphoribosyltransferase*) catalisa a reação reversível de síntese de orotidina 5'-fosfato ou orotidilato (OMP) a partir de orotato (OA) e 5'-fosfo-α-D-ribose 1'-difosfato (PRPP), com a formação de uma ligação covalente entre o átomo N1 do orotato e o átomo C1' do PRPP, em presença de Mg^{2+} (39) (**Figura 7**). A reação de formação de OMP, na via de síntese *de novo* de pirimidinas, é seguida pela reação de descarboxilação do OMP em UMP, precursor de todas as demais bases pirimídicas (36).

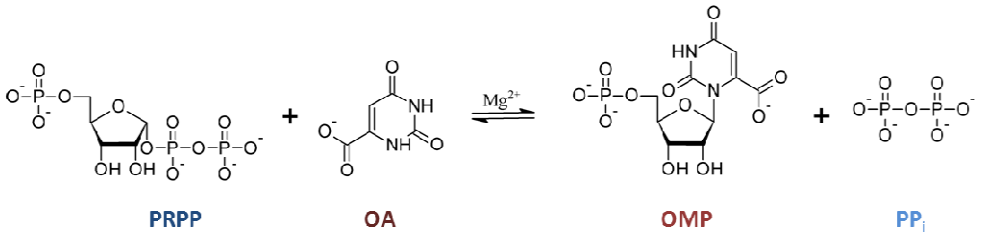

Figura 7. Reação catalisada pela enzima OPRT.

A enzima de MTB é codificada pelo gene *pyrE* (Rv0382c), e ao contrário do que é observado em eucariotos, não forma um complexo bifuncional com a enzima OMP descarboxilase. De baixa homologia com a enzima humana (~12 % de identidade entre as sequências primárias, quando comparada à forma bifuncional da enzima humana, e 23% de identidade quando apenas a porção com atividade OPRT da enzima humana é considerada), a OPRT de MTB é considerada potencial alvo para o desenvolvimento de novas drogas contra a TB.

A não conservação da estrutura primária entre as proteínas homólogas OPRT de diferentes organismos é descrita como uma característica das enzimas que constituem a família PRTase (do inglês *phosphoribosiltransferase*) (40), as quais apresentam conservação apenas das estruturas terciária e quaternária (41, 42), e não de suas sequências de aminoácidos, exceto pelo motivo de ligação ao PRPP,

composto por 13 aminoácidos, e pelo loop catalítico que encobre o sítio ativo da enzima (40). As enzimas que fazem parte da família da PRTs que são encontradas nas rotas metabólicas de síntese e salvamento de nucleotídeo são classificadas como PRTases do tipo I, compreendendo as enzimas responsáveis pela transferência de PRPP a nucleófilos que contenham nitrogênio, como amônia, adenina, guanina, hipoxantina, xantina, orotato e uracil. As demais PRTases não apresentam o motivo de ligação do PRPP em suas sequências primárias e nem a conservação estrutural observada entre as enzimas PRTases do tipo I, e estão envolvidas nas vias de síntese e salvamento dos aminoácidos triptofano e histidina e da nicotinamida, sendo classificadas de modo geral como PRTases do tipo II (40).

A enzima OPRT tem sido alvo de estudos para o desenvolvimento de drogas contra a malária (24, 43-45) e toxoplasmose (46); além de ser alvo para o desenvolvimento de drogas contra o câncer pelo seu papel na ativação de 5FU (47, 48). Seu papel na síntese *de novo* de nucleotídeos de pirimidina e a sua baixa homologia com a enzima humana tornam a OPRT de MTB um interessante alvo para o desenvolvimento de novas drogas para o tratamento da tuberculose. A interrupção desta rota metabólica pode ser letal para a micobactéria, viabilizando o desenvolvimento de inibidores específicos, ou ainda gerar uma cepa atenuada dependente da via de salvamento de pirimidinas, tornando-a um alvo para o desenvolvimento de potenciais amostras vacinais, de acordo com a metodologia proposta por Fox & Bzik para *Toxoplasma gondii* (23, 49). Além de seu papel no controle e profilaxia da TB, a caracterização da OPRT possibilitará a maior a compreensão do metabolismo de nucleotídeos em MTB, demonstrando a sua maior ou menor dependência da via de síntese *de novo* de nucleotídeos ou de salvamento de bases livres.

2. Objetivos

I. Hipótese de Trabalho

A via de síntese *de novo* de nucleotídeos de pirimidina constitui uma rota metabólica essencial para a viabilidade de diversos organismos parasitas obrigatórios. As enzimas que constituem esta rota, já identificadas na micobactéria *Mycobacterium tuberculosis*, agente causador da tuberculose, dentre elas a enzima Orotato Fosforibosiltransferase (EC 2.4.2.10), são potenciais alvos moleculares para o desenvolvimento de inibidores de ação específica para o tratamento da tuberculose na sua forma ativa, podendo ainda ser eficazes para o tratamento da forma latente desta doença.

II. Objetivos Gerais

Caracterização da enzima OPRT (EC 2.4.2.10), codificada pelo gene *pyrE*, de MTB H37Rv como alvo para o desenvolvimento de novas drogas de ação específica contra o microorganismo *Mycobacterium tuberculosis* para o tratamento da TB.

III. Objetivos Específicos

1. Caracterização da enzima OPRT de *Mycobacterium tuberculosis*, codificada pelo gene *pyrE*, através de amplificação, clonagem, expressão e purificação da enzima recombinante.
2. Determinação das constantes cinéticas aparentes e verdadeiras da reação reversível catalisada pela enzima, bem como estabelecer seu mecanismo cinético de reação e as constantes termodinâmicas associadas a este mecanismo.

3. Identificação, desenvolvimento e caracterização de inibidores específicos da enzima OPRT através de metodologia de derivatização química, cinética enzimática e microcalorimetria.
4. Determinação da estrutura terciária e quaternária da enzima OPRT através de cristalografia por difração de raios X, utilizando a técnica de *hanging drop* para a obtenção de cristais.
5. Determinação da essencialidade da enzima OPRT e desenvolvimento de uma provável amostra vacinal de MTB para o tratamento da TB através de nocaute gênico da sequência de DNA correspondente ao seu gene codificante, *pyrE*.

Os resultados obtidos em cada etapa de trabalho estão organizados da seguinte forma: Amplificação do gene *pyrE* Rv0382c a partir de DNA genômico total de MTB H37Rv; clonagem em vetor de expressão procariótico; sequenciamento e expressão da enzima recombinante em diferentes cepas de *Escherichia coli* a fim de obtê-las na sua forma solúvel; purificação da proteína recombinante por cromatografia líquida de alta performance (HPLC); quantificação total de proteína; análise da pureza e identidade da proteína recombinante homogênea por espectrometria de massa e sequenciamento de aminoácidos (**Objetivo Específico 1**); testes de atividade enzimática; determinação das constantes cinéticas e mecanismo cinético de reação da enzima; caracterização do mecanismo de ligação das enzimas aos seus substratos utilizando técnicas de espectrofotometria e microcalorimetria (**Objetivo Específico 2**) – compilados em forma de artigo científico apresentado no **Capítulo 2**.

Seleção de compostos análogos de substrato da reação catalisada pela enzima OPRT como prováveis agentes de ação inibitória; caracterização do mecanismo de inibição e determinação das constantes inibitórias através de técnicas

de espectrofotometria e microcalorimetria; substituição de grupamento químicos presentes nas moléculas selecionadas visando a melhoria de suas propriedades inibitórias e aumento da sua afinidade pela enzima (**Objetivo Específico 3**) – resultados compilados em forma de artigo científico apresentado no **Capítulo 3**.

Triagem de condições de cristalização da enzima OPRT pela metodologia de *hanging-drop*, utilizando a enzima recombinante homogênea na sua forma apo (não complexada aos substratos ou produtos da reação catalisada, ou a inibidores), e em presença de ligantes, através do uso de diferentes tampões de incubação e condições de temperatura; obtenção de cristais da enzima adequados para a difração de raios X, determinação da estrutura tridimensional da enzima OPRT de *Mycobacterium tuberculosis* (**Objetivo Específico 4**) – resultados apresentados no **Capítulo 4**.

Amplificação das regiões flanqueadoras *upstream* e *downstream* ao gene *pyrE*; construção de um plasmídeo suicida utilizando vetores da série pNIL/pGOAL; eletroporação do plasmídeo suicida em células da linhagem MTB H37Rv; isolamento, seleção e contra seleção de linhagens mutantes de MTB por troca alélica; caracterização microbiológica e bioquímica das linhagens mutantes obtidas (**Objetivo Específico 5**) – resultados parciais apresentados no **Capítulo 5**.

No corpo da tese, foi ainda incluído um artigo científico de revisão sobre a metodologia de seleção virtual de inibidores, ferramenta que possibilita a triagem computacional de compostos com potencial ação inibitória sobre um alvo molecular específico, uma vez que os dados acerca da sua estrutura tridimensional sejam conhecidos (**Capítulo 6**). Os resultados apresentados neste capítulo serão futuramente combinados aos dados apresentados no Capítulo 4, possibilitando a seleção e identificação de novos compostos líderes de ação inibitória sobre a enzima OPRT de *Mycobacterium tuberculosis*.

Capítulo 2

MOLECULAR, KINETIC AND THERMODYNAMIC CHARACTERIZATION OF *Mycobacterium tuberculosis* OROTATE PHOSPHORYBOSILTRANSFERASE

Artigo submetido ao *The Journal of Biological Chemistry*.

MOLECULAR, KINETIC AND THERMODYNAMIC CHARACTERIZATION OF *Mycobacterium tuberculosis* OROTATE PHOSPHORYBOSILTRANSFERASE

Ardala Breda[1,2,3], Leonardo Astolfi Rosado[1,2,4], Daniel Macedo Lorenzini[1,2], Luiz Augusto Basso[1,2,3] and Diógenes Santiago Santos[1,2,3]

Instituto Nacional de Ciência e Tecnologia em Tuberculose[1], Centro de Pesquisas em Biologia Molecular e Funcional [2], Programa de Pós-Graduação em Biologia Celular e Molecular[3], and Programa de Pós-Graduação em Medicina e Ciências da Saúde[4], Pontifícia Universidade Católica do Rio Grande do Sul, Porto Alegre, Rio Grande do Sul, Brazil

Running head: *Mt*OPRT molecular, kinetic and thermodynamic characterization

Address correspondence to: Luiz Augusto Basso or Diógenes Santiago Santos, Avenida Ipiranga 6900 Prédio 92A – TECNOPUC. 90619-900 Porto Alegre, RS, Brazil. Phone/Fax: +55 51 3320 3629. E-mail: luiz.basso@pucrs.br, diogenes@pucrs.br

Tuberculosis (TB) is a chronic infectious disease caused mainly by *Mycobacterium tuberculosis*. The worldwide emergence of drug-resistant strains, the increasing number of infected patients among immune compromised populations, and the large number of latent infected individuals that are reservoir to the disease have underscored the urgent need of new strategies to treat TB. The nucleotide metabolism pathways provide promising molecular targets for the development of novel drugs against active TB and may, hopefully, also be effective against latent forms of the pathogen. The orotate phosphoribosyltransferase (OPRT) enzyme of *de novo* pyrimidine synthesis pathway catalyzes the reversible phosphoribosyl transfer from 5'-phospho-α-D-ribose 1'-diphosphate (PRPP) to orotic acid (OA), forming pyrophosphate and orotidine 5'-monophosphate (OMP). Here we describe cloning and characterization of *pyrE* gene of *M. tuberculosis* H37Rv strain as encoding a homodimeric functional OPRT. The *M. tuberculosis* OPRT true kinetic constants for forward reaction and product inhibition results suggest a Mono-Iso Ordered Bi Bi kinetic mechanism, which has not been previously described for this enzyme family. Absence of detection of half reaction and isothermal titration calorimetry (ITC) data support the proposed mechanism. ITC data also provided thermodynamic signatures of non-covalent interactions between substrate/product and *M. tuberculosis* OPRT. These data provide a solid foundation on which to base target-based rational design of anti-TB agents and should inform us how to better design inhibitors of *M. tuberculosis* OPRT.

Tuberculosis (TB) is a chronic infection disease caused mainly by *Mycobacterium tuberculosis* (MTB) (1), killing over 2 million people annually (2). The latest survey by the World Health Organization (WHO) on TB global burden for 2008 showed 8.9-9.9 million estimated cases, 9.6-13.3 million prevalent cases, 1.1-1.7 million deaths among HIV negative patients, and 0.45-0.62 million deaths among HIV positive cases (originally classified as HIV deaths). The number of notified cases in 2008 rose up to 67% incident cases, approaching the 71% milestone established by Stop TB initiative. As a positive result, 86% patients from 2007 cohort had access to treatment, exceeding the 85% task. Almost 30 000 cases of multi-drug resistant TB were notified only in 2008, where 27 countries, 15 at the European region, account for 85% of these cases. The WHO estimates that such number correspond for solely 11% of total drug resistant cases (3). Patients' non-compliance to the current treatments, along with HIV infection emergence, leads to the occurrence of multi drug-resistant and extensively drug-resistant TB strains, and to an increasing number of new cases (2). Recently, TB infections with totally resistant strains, denoted as TDR-TB have been described, which are resistant to all first and second line classes of anti-TB drugs tested (4, 5). Novel TB treatments should ideally be able to also eliminate latent forms of TB that are a significant infection reservoir (6). Approximately 32% of the world population is positive on tuberculin purified protein derivative (PPD) skin test (2), of which 10% will lead to reactivation of infection during lifetime, raising to 50% in HIV positive subjects (7, 8).

Although being an ancient human disease (7), little is known about the nutritional adaptability of MTB in the course of TB infection (9, 10). Experimental evidence points to a shift from carbohydrate carbon source at the first weeks of TB contagion to fatty acid and cholesterol

carbon sources later during infection (9). However, the identity of inner and outer membrane transporter for essential nutrients in MTB is largely unknown, despite availability of genetic data (10). Whether MTB relies on complex nutrient molecules uptake from host or on essential molecules synthesis from simple and passive diffusible precursors is still not clear. Granuloma formation is thought to benefit not only the host by containing and restricting mycobacteria, but also the MTB providing and optimal environment for its persistence (10, 11). It might be viewed as establishment of an equilibrium in which progress of infection is arrested but intracellular bacteria are still viable, although at minimal replication rate (12-14). Nutrient starvation is considered an essential element for this long-term survival of mycobacteria during latent infection (15), in response to microenvironments such as necrotic or caseous regions that are remote from the cavity surface of host lungs, where the availability of oxygen and nutrients is likely to be restricted (16). The metabolism required for sustaining mycobacterial survival during TB latency is still poorly understood. Transcriptional profiling has shown that a ribonucleotide reductase encoded by *nrdZ* is up-regulated in latent bacillus, which indicates that a pool of deoxyribonucleotides is required either for maintenance of chromosomal integrity or DNA repair and replication that are expected to occur during TB reactivation (17).

The nucleotide metabolism is an essential pathway for microorganism viability; and the *de novo* pyrimidine biosynthesis has been shown to be required for virulence of obligatory parasites as *Toxoplama gondii* (18) and *Plasmodium vivax* (19). Disruption of this pathway leads to uracil auxotrophs that are completely avirulent (18) and free nucleotide uptake from host may not be possible due to pathology's characteristics (19) such as the tubercle structure in TB (20). Orotate phosphoribosyltransferase (OPRT, EC 2.4.2.10) catalyses the fifth reaction in the *de novo* synthesis of pyrimidine nucleotides, in which orotate (OA) and 5'-phospho-α-D-ribose 1'-diphosphate (PRPP) are converted to orotidine 5'-monophosphate (OMP), and pyrophosphate (PP_i), in the presence of Mg^{2+} (Fig. 1). OPRT catalyses the last step in such pathway for which there is no chemical intermediate that can be derived from pyrimidine salvage pathway (21). Accordingly, this reaction may be considered a commitment step of the *de novo* pathway, which has been shown to be essential for survival of MTB and *Mycobacterium bovis* BCG (22). Although being well conserved among all prokaryotes and eukaryotes organisms, the mammalian homologue is expressed as a bifunctional complex with OMP decarboxylase, which catalyses decarboxylation of OMP to form uridine 5'-monophosphate (UMP) (23). The bifunctional enzyme is encoded by a single gene, *pyr5* (GenBank accession code: NP_000364.1).

Here we describe cloning of *pyrE* (Rv0382c) from *M. tuberculosis*, and expression and purification of recombinant protein. Functional studies demonstrate that this gene encodes a homodimeric functional OPRT (*Mt*OPRT). Determination of true steady-state kinetic parameters for the forward reaction, product inhibition patterns, half-reaction measurements and isothermal titration calorimetry (ITC) measurements of substrate/product binding to *Mt*OPRT suggest that it follows a Mono-Iso Ordered Bi Bi kinetic mechanism, which has not been previously described for this enzyme family. ITC data also provided thermodynamic signatures of non-covalent interactions between substrate/product and *Mt*OPRT, which are consistent with catalytic loop motions upon substrate binding and product release. The results presented here should contribute to function-based design of *Mt*OPRT enzyme inhibitors. It is hoped that the results described here may contribute to better understanding of the biology of MTB, and may also be useful to chemical biologists interested in designing loss-of-function (inhibitors) or gain-of-function (activators) chemical compounds to reveal the biological role of *Mt*OPRT in the context of whole MTB cells.

Experimental Procedures

Gene amplification – The *pyrE* gene (Rv0382c) was PCR amplified from total genomic DNA of MTB H37Rv strain using specific primers designed to contain *Nde*I (primer sense 5'gaa**catatg**gccggacctgaccgcgcagagttggc3') and *Hind*III (primer antisense 5'gc**aagctt**ctaatccagccccagatcggccaggcc3') restriction sites (highlighted in bold). PCR cycling parameters were 35 cycles of denaturation at 98°C (30 sec), annealing at 55°C (45 sec) and extension at 72°C (2 min). The PCR product was visualized on 1% agarose gel and purified from the gel using QIAGEN QIAquick

gel extraction kit. The purified fragment was initially cloned into pCR-Blunt vector (Invitrogen) and subcloned into pET-23a(+) expression vector (Novagen), previously digested with *Nde*I and *Hind*III restriction enzymes. The integrity of constructs was confirmed in all cases by appropriate selections and digests with appropriated restriction enzymes (New England Biolabs). Inserted sequences were confirmed by DNA sequencing in all cases.

Recombinant protein expression, purification and molar absorption coefficient determination – Competent *Escherichia coli* BL21(DE3) cells were electroporated with pET-23a(+)::*pyrE* recombinant vector. Cells were grown overnight at 37°C and 180 rpm in 100 mL Luria-Bertani (LB) medium containing ampicillin 50 μg mL^{-1}. A volume of 13 mL of this culture was used to inoculate 500 mL LB medium supplemented with ampicillin (50 μg mL^{-1}), grown at 37°C and 180 rpm to an optical density (OD_{600nm}) of 0.4, and induced with 1 mM isopropyl α-D-thiogalactopyranoside (IPTG). Cells were harvested by centrifugation (8000 *g*) 12 h after induction, at 4°C and immediately submitted to purification protocol steps. All protein purification steps were performed at 4°C or on ice. Chromatographic steps were performed by High-Performance Liquid Chromatography (HPLC) on Äkta Purifier System (GE HealthCare). Cell pellet (12 g) was suspended in 60 mL of buffer A (Tris HCl 50 mM pH 8.0) and stirred by 30 min. Lysozyme (Sigma Aldrich) was added to a final concentration of 0.2 mg mL^{-1} and incubated for 30 min at constant stirring. The mixture was sonicated (15 pulses of 10 sec, spaced by 1 min), the lysate was centrifuged for 30 min at 48000 *g*. Streptomycin sulfate (Sigma Aldrich) was added to the supernatant to a final concentration of 1%, centrifuged for 30 min at 48000 *g*. The supernatant was dialyzed against buffer A (2 times against 2 L for 3 h each, and a third time against 2 L overnight), and clarified by centrifugation at 48000 *g* for 30 min. The supernatant was loaded on an anionic exchange chromatographic column (HiPrep Q-XL 16/10, GE HealthCare) equilibrated with buffer A, washed with 8 column volumes (CV) of buffer A, followed by 20 CV of 0-70% linear gradient of buffer B (Tris HCl 50 mM NaCl 500 mM, pH 8.0) at 1 mL min^{-1} flow rate. Fractions containing the recombinant enzyme, as inferred by 12% SDS-PAGE polyacrilamide electrophoresis stained with Coomassie Blue, were pooled, concentrated to a final volume of 9 mL using a 50 mL stirred ultrafiltration cell (Millipore) with 10 kDa cutoff filter. The concentrated recombinant protein was loaded into a size exclusion chromatographic column (HiPrep 26/60 Sephacryl S200 HR, GE HealthCare) equilibrated with buffer A. Proteins were eluted in isocratic conditions with 1 CV of buffer A at 0.2 mL min^{-1} flow rate. Fractions containing *Mt*OPRT were treated with Tris HCl 50 mM $(NH_4)_2SO_4$ 2 M pH 8.0 to a final concentration of Tris HCl 50 mM $(NH_4)_2SO_4$ 1 M pH 8.0 (buffer C), at constant stirring for 30 min, and centrifuged for 30 min at 48000 *g*. The supernatant was then loaded on a hydrophobic interaction chromatographic column (HiLoad 16/10 Phenyl Sepharose HP, GE HeathCare) equilibrated with buffer C. The hydrophobic interaction column was washed with 10 CV of buffer C and the homogeneous recombinant *Mt*OPRT was eluted using a 20 CV linear gradient of 0-65% of buffer A, at a 1 mL min^{-1} flow rate. Eluted fractions containing homogeneous *Mt*OPRT were dialyzed against 2 L buffer A for 2 h, concentrated to 1 mg mL^{-1} and stored at -80°C in 5% glycerol. Under these conditions *Mt*OPRT is stable up to 12 months. Protein concentration was determined either by the method of Bradford (24) or by direct absorbance measurement. A value of 11570 $M^{-1}cm^{-1}$ was determined by the method of Edelhoch (25, 26) for the molar absorption coefficient at 280 nm (ε_{280nm}) of *Mt*OPRT in buffer A.

Identification of MtOPRT by mass spectrometry – 1.Gel electrophoresis and staining: Samples containing *Mt*OPRT were mixed with sample loading buffer (Laemmli loading dye (27)) at a 1:1 final volume before loading onto 12% SDS-PAGE polyacrilamide gel and submitted to vertical electrophoresis at 120 V for 1 h. For protein staining, gels were fixed with Coomassie Blue for 20 min and destained with 10% acetic acid/25% methanol until the background was clear. Gel cutting was performed manually with a sterile scalpel. *2. In-gel digestion:* In-gel digestion was performed according to Shevchenko (28). Briefly, excised gel band corresponding to *Mt*OPRT was cut into small pieces and destained in 25 mM NH_4HCO_3 and 50% acetonitrile, dehydrated with acetonitrile, and dried. Gel pieces were then rehydrated with 12.5 ng μL^{-1} trypsin solution (in 25 mM NH_4HCO_3) and incubated overnight at 37°C. Peptides were extracted twice with a solution containing 5% formic acid and 50% acetonitrile

followed by a final extraction with acetonitrile. Samples were dried with a speed-vacuum centrifugation before analysis. *3. Mass spectrometry (MS)*: Tryptic digest of *Mt*OPRT was separated on a homemade column (solid phase Kinetex C18 of 2.6 µm particles, 0.1 × 1000 mm) using a nanoUPLC (nanoLC Ultra 1D plus, Eksigent, USA) and eluted directly to a nanospray ion source connected to a hybrid mass spectrometer (LTQ-XL and LTQ Orbitrap Discovery, Thermo, USA). The flow rate was set to 1 µL min^{-1} and the mass spectrometer was set to acquire one MS survey scan for the *m*/*z* range of 400–2000 (30000 resolution) and MS/MS spectra for the ten most intense ions from the survey scan during the gradient. An isolation mass window of 15 ppm was used for the precursor ion selection, and the normalized collision energy value of 35% was used for fragmentation. Dynamic exclusion lasting for 30 sec was used to acquire MS/MS spectra from low intensity ions. In MS survey, the preview mode for FTMS master scan was turned on, and only doubly and triply charged ions were selected for MS/MS. LC-MS/MS data was processed with Proteome Discoverer 1.0 (Thermo, USA) for comparison of MS/MS spectra with theoretical spectra generated from in-silico tryptic digestion of MTB H37Rv proteome (downloaded from ftp://ftp.ncbi.nih.gov/genomes/). The search parameters were as follows: trypsin digestion, two missed cleavage allowance, carbamidomethylation on cysteine, variable oxidation on methionine, precursor tolerance of 10 ppm, and fragment tolerance of 0.8 Da. To exclude false identifications, only matches with XCore > 2.0 for doubly charged peptides and XCore > 2.5 for triply charged peptides were accepted.

Determination of MtOPRT molecular mass – The homogeneous *Mt*OPRT was processed for removal of salts using homemade Poros 50 R2 (Applied Biosystems, USA) reverse phase tips, reconstituted in ACN 50%/FA 0.1% and loaded on offline emitter (PicoTip Econotip, New Objective, Woburn, MA, USA). The emitter was submitted to electrospray ionization on a nanospray ion source (settings: Source Voltage 1.8 kV, Capillary Temperature 200°C, Capillary Voltage 9V, Tube Lens Voltage 125V) and averaged spectra were collected during 1 min on a Thermo Orbitrap Discovery XL. The average spectrum was processed with the software MagTran (29) for charge state deconvolution.

Analytical HPLC Gel Filtration – Determination of *Mt*OPRT molecular mass in solution was performed using a Superdex 200 HR 10/30 size exclusion column (GE HealthCare) at 0.4 mL min^{-1} flow rate and isocratic elution with 1 CV of Tris HCl 50 mM NaCl 200 mM pH 7.5. Proteins were detected at 215, 254 and 280 nm. The LMW and HMW Gel Filtration Calibration Kits (GE Healthcare) were used to prepare a calibration curve. The elution volumes (V_e) of standard proteins (ferritin, catalase, aldolase, coalbumin, ovalbumin, ribonuclease A) were used to calculate their corresponding partition coefficient, K_{AV} - **Eq. (1).** Blue dextran 2000 (GE Healthcare) was used to determine the void volume (V_0). V_t is the total bead volume of the column. The K_{AV} value for each protein was plotted against the log of their corresponding molecular mass, yielding a linear function with the values for *y*-intercept and slope given in **Eq. (2)**. A final volume of 100 µL of recombinant enzyme sample was applied to the column at three distinct concentrations (7 µM, 11 µM and 53 µM) to determine the V_e value for *Mt*OPRT. Substitution of the latter in **Eq. (2)** allowed determination of the molecular mass of recombinant enzyme in its apo form in solution.

$$K_{AV} = (V_e - V_0)/(V_t - V_0) \quad \textbf{Eq. (1)}$$

$$K_{AV} = 0{,}9669 - 0{,}3087 \log kDa \quad \textbf{Eq. (2)}$$

Enzymatic activity assay – All chemicals in enzyme activity measurements were purchased from Sigma Aldrich. *Mt*OPRT activity was measured both for the forward (phosphoribosyltransferase) and reverse (pyrophosphorolysis) reactions, by a continuous assay measuring, respectively, a decrease or increase in OA concentration. The assay was performed in quartz cuvettes with UV-visible Shimadzu spectrophotometer UV2550 equipped with a temperature-controlled cuvette holder. For the forward reaction ($OA + PRPP \rightarrow OMP + PP_i$), the reaction mixture (500 µL) contained Tris HCl 50 mM $MgCl_2$ 20 mM pH8.0 and varied concentrations of OA and PRPP. Reaction was started by addition of enzyme, and followed a linear progress of absorbance change at 295 nm for 60 sec at 25°C. The extinction coefficient of this conversion was 3950 $M^{-1}cm^{-1}$ (30). For the reverse reaction, ($OMP + PP_i \rightarrow OA + PRPP$) the reaction mixture (500 µL) contained Tris HCl 50 mM $MgCl_2$ 20 mM pH8.0 and varied concentrations of OMP and PP_i. Reaction was started by addition of enzyme, and followed a linear progress of absorbance change at 303 nm for 60 sec at 25°C. The extinction

coefficient of this conversion was 2200 $M^{-1}cm^{-1}$ (31).

Steady state kinetics – Kinetic assays for forward and reverse reactions were performed using homogeneous *Mt*OPRT (25-50 nM per reaction), at the same assay conditions as described above. For optimal $MgCl_2$ concentration determination, saturating concentrations of OA (100 μM) and PRPP (500 μM) were employed and *Mt*OPRT concentration was 98 nM. $MgCl_2$ concentration was varied from 0 to 30 mM, in Tris HCl 50 mM pH 8.0 at 25°C. The decrease in OA concentration was monitored at 295 nm. Based on these results, subsequent experiments employed $MgCl_2$ at fixed 20 mM concentration (Tris HCl 50 mM $MgCl_2$ 20 mM pH 8.0 - buffer D). K_M and V_{max} values for OA, PRPP, OMP and PP_i were determined by initial velocity measurement in duplicate or triplicate with at least five substrate concentrations. In the forward reaction, a 500 μL final volume reaction contained buffer D and 2-100 μM OA and 25-500 μM PRPP. In the reverse reaction, K_M^{app} and V_{max}^{app} were determined in a 500 μL final volume reaction containing buffer D and varied OMP concentrations (2-12 μM) in the presence of PP_i 100 μM and varied PP_i concentrations (6-105 μM) in the presence of 400 μM OMP. The k_{cat} values were calculated from **Eq. (3)** (32).

$$V_{max} = k_{cat}[E]_t \qquad \textbf{Eq. (3)}$$

Data from initial velocity double reciprocal plots for the forward reaction were best fitted to equation **Eq. (4)** for double-displacement or Ping-Pong bisubstrate kinetic mechanism using SigmaPlot 10 Software; in which v, V, A, and B correspond to, respectively, steady-state reaction rate, maximum reaction rate (V_{max}), substrate A and substrate B concentrations. K_a and K_b are the K_M values for substrate A and substrate B.

$$v = VAB/(K_aB + K_bA + AB) \qquad \textbf{Eq. (4)}$$

PP_i detection assay – Release of PP_i by *Mt*OPRT in the forward reaction was monitored indirectly with EnzCheck® Pyrophosphate Assay E-6645 detection kit (Molecular Probes, Invitrogen). This kit employs two enzymes in a coupled assay to measure changes in PP_i concentration. First, PP_i released by *Mt*OPRT reaction is converted to P_i by inorganic pyrophosphatase. Second, the P_i released into solution is a co-substrate for phosphorolysis of 2-amino-6-mercapto-7-methylpurine ribonucleoside (MESG) into ribose 1-phosphate and 2-amino-6-mercapto-7-methylpurine catalyzed by purine nucleoside phosphorylase (PNP). Enzymatic conversion of MESG into 2-amino-6-mercapto-7-methylpurine was measured at 360 nm ($\Delta\varepsilon_{360nm}$ 11000 $M^{-1}cm^{-1}$) which is the result of a spectrophotometric shift in maximum absorbance from 330 nm for the substrate to 360 nm for the product. The PP_i detection assay was performed at 22°C, in a final 500 μL reaction volume containing buffer D, MESG 1 mM, PNP 100 U mL^{-1}, inorganic pyrophosphatase 3 U mL^{-1}, PRPP 5-40 μM and *Mt*OPRT 50 nM, in either the presence or absence of OA 100 μM. PRPP was varied in a range were PNP catalyzed P_i consumption was linear under the assay conditions. All reagents were incubated for 10 min at 22°C and the reaction was started by addition of *Mt*OPRT.

Product inhibition assay – Product inhibition assays were carried out in 500 μL reaction volume at 25°C, monitoring the decrease in OA concentration upon conversion to OMP at 295 nm for 60 sec. These assays employed either a constant saturating concentration (5 times its $K_M$value) or sub-saturating concentration (half its K_M value) of one substrate, and varying concentrations of the co-substrate (OA: 6-75 μM, PRPP: 25-400 μM), in the absence and presence of varying concentrations of each product (OMP: 3-60 μM, PP_i: 25-125 μM). Product inhibition assays were performed in buffer D, and the enzyme-catalyzed chemical reactions started upon addition of 25-50 nM *Mt*OPRT to assay mixtures. Double reciprocal data were fitted to **Eq. (5)** for noncompetitive inhibition mechanism, in which v, V, A, K, K_i and α correspond to, respectively, steady-state reaction rate, maximum reaction rate (V_{max}), varying concentration of substrate A, Michaelis-Menten constant, inhibition dissociation constant, and the factor α reflects the effect of inhibitor on the affinity of the enzyme for its substrate (or the effect of the substrate on the affinity of the enzyme for the inhibitor).

$$v = VA/A(1 + I/\alpha K_i) + K(1 + I/K_i) \qquad \textbf{Eq. (5)}$$

ITC binding assays – Ligand binding to *Mt*OPRT were evaluated by isothermal titration calorimetry (ITC) using an iTC_{200} Microcalorimeter (Microcal, Inc., Northampton, MA). Reference cell (200 μL) was loaded with Millie-Q water during all assays. The injection syringe (39.7 μL) was filled with substrate(s) or product(s) at different concentrations (PRPP 4 mM, OA 9 mM, OMP 750 μM and PP_i 10 mM), and the ligand binding isotherms were measured

by direct titration (ligand into macromolecule). First injection (0.5 μL) of ligand was followed by seventeen injections of 2.26 μL each spaced by 180 sec, into 100 μM apo *Mt*OPRT (sample cell). The titration first injection was not used in data analysis. *Mt*OPRT and all ligand solutions contained $MgCl_2$ 20mM in buffer Gly-Gly 100 mM pH 8.0 (buffer E), the latter substituted for buffer D due to the high enthalpy of ionization of Tris (33). Control titrations (ligand into buffer) were performed to subtract the heats of dilution and mixing for each experiment prior to data analysis. To assess $MtOPRT{:}PPi{:}OA$ dead-end complex formation, *Mt*OPRT (90 μM) was incubated with PP_i (900 μM) in the sample cell prior to OA titration (800 μM syringe concentration). $MtOPRT{:}PPi{:}OA$ ternary complex formation was also assessed by pre-incubating *Mt*OPRT (90 μM) with OA (800 μM), followed by titration with PP_i (900 μM syringe concentration). ITC data were fitted to **Eq. (6)**, in which ΔH is the enthalpy of binding, ΔG is the Gibbs free energy change, ΔS is the entropy change, T is the absolute temperature in Kelvin, R is the gas constant (1.987 cal K^{-1} mol^{-1}), and K_a is the association constant. The dissociation constant, K_d, was calculated as the inverse of K_a. All data were evaluated using the Origin 7 SR4 software (Microcal, Inc.). Entropy values are depicted as $-T\Delta S$.

$$\Delta G = \Delta H - T\Delta S = RT \ln K_a \quad \textbf{Eq. (6)}$$

RESULTS

MtOPRT amplification, cloning, expression and purification – The *pyrE* gene was PCR amplified in the presence of 10% DMSO, cloned into pCR-Blunt cloning vector, and sub-cloned into pET-23a(+) expression vector. The nucleotide sequence of the insert was confirmed by automated sequencing, revealing a discrepancy between the *pyrE* gene sequence available at TubercuList (http://genolist.pasteur.fr/TubercuList/) database and our clone at position 99. The third base of the 33rd codon changed from thymine (TAT) given by the genome sequencing to cytosine (TAC) as described here. Nevertheless, both codons are for tyrosine, and it might have been introduced by PCR amplification or be a misannotation of the Rv0382c locus in MTB H37Rv (34). The pET-23a(+)::*pyrE* recombinant vector was electroporated into *E. coli* BL21(DE3) host cells and the best experimental conditions for *Mt*OPRT recombinant protein expression in soluble form were 12 h of growth after induction with 1 mM IPTG at 37°C. SDS-PAGE analysis showed expression of *Mt*OPRT recombinant enzyme with apparent subunit molecular mass of ~ 20 kDa in agreement with predicted molecular mass (18.8 kDa). *Mt*OPRT was purified to homogeneity by a three-step protocol. *Mt*OPRT adsorbed on HiPrep Q-XL 16/10 anion exchange resin and was desorbed by approximately 300 mM salt concentration. Eluted samples were concentrated and loaded on HiPrep 26/60 Sephacryl S-200 HR to remove salt from recombinant protein samples, which, however, was accompanied by significant activity loss (Table 1). Pooled fractions containing *Mt*OPRT were loaded on HiLoad 16/10 Phenyl Sepharose HP hydrophobic interaction column, from which homogeneous recombinant protein eluted at 26-42% gradient of buffer A (660 mM salt concentration), yielding 6.65 mg. Activity loss observed after size exclusion chromatography step was reversed after hydrophobic interaction chromatography. Dialysis against buffer A prior to enzyme storage did not affect its specific activity.

Identification of MtOPRT by mass spectrometry and molecular mass determination – Purified *Mt*OPRT digested with trypsin was submitted to LC-MS/MS analysis, and 343 spectra were identified to 8 peptides from the *Mt*OPRT amino acid sequence (Table I – *Supplemental Data*), representing 73% of the whole *Mt*OPRT sequence. Mass spectrometry spectra showed peaks corresponding to charged states (from 15^+ to 25^+) of *Mt*OPRT recombinant protein, and deconvolution of these spectra gave a single peak corresponding to an average molecular mass value of 18761 Da for *Mt*OPRT (Fig. I – *Supplemental Data*).

Analytical HPLC Gel Filtration – Recombinant active *Mt*OPRT was loaded on a Superdex 200 HR 10/30 size exclusion column using three distinct concentrations (7 μM, 11 μM and 53 μM), showing molecular masses of 38.67 kDa, 37.499 kDa and 36.01 kDa, according to data fitting to **Eq. (2)**. Molecular masses values divided by *Mt*OPRT subunit molecular mass (18.761 kDa) indicate that *Mt*OPRT has a homodimeric quaternary structure in solution, in the protein concentration range here presented.

Kinetic properties of recombinant MtOPRT – Prior to embarking on determination of steady-state kinetic parameter for the forward reaction, the optimal concentration range of $MgCl_2$ to be

employed in initial rate measurements was determined to be 15-30 mM (*data not shown*). Accordingly, $MgCl_2$ concentration was fixed at 20 mM to all further experiments. The true macroscopic kinetic constants for the forward reaction of *Mt*OPRT are summarized in Table 2. On the other hand, in Table 2 are presented the apparent kinetic constant for the reverse reaction. The true kinetic parameters for forward reaction were determined from primary double-reciprocal plots of the steady-state initial velocity kinetics data fitted to **Eq. (4)** for a double-displacement (or Ping-Pong) bisubstrate kinetic mechanism, which is suggested by the parallel lines pattern observed for both substrates (Fig. 2). The $k_{cat\text{forward}}/k_{cat\text{reverse}}$ for *Mt*OPRT enzyme is 2.16, an indicative that forward reaction is faster than the reverse one.

Half-reaction detection by PP_i consumption measurement – In case *Mt*OPRT followed a Ping-Pong mechanism in which PRPP would transfer 5-phosphate ribose to *Mt*OPRT enzyme active site, detection of PP_i release in solution was assessed by a coupled assay. As a positive control, OA at saturating concentration (100 μM) was added to the reaction mixture, a condition in which PP_i released is certain to occur. As PRPP was varied (5-40 μM) in the presence of OA, an increase in 2-amino-6-mercapto-7-methylpurine formation was observed indicating that there was an increase in PP_i formation by *Mt*OPRT (Fig. 3). No significant activity could be detected when the experiment was performed at the same conditions in the absence of OA. These data show that there is no half-reaction in the absence of OA, thereby proving that *Mt*OPRT cannot transfer 5'-phosphate ribose from PRPP to the enzyme active site in the absence of the second reaction substrate. Minimal activity detected is due to PRPP contamination with PP_i, largely accounted for by pre-incubation prior to adding *Mt*OPRT to start the reaction.

Enzymatic reaction mechanism determination by product inhibition assays – Product inhibition assays were carried out for the forward reaction, using both OMP and PP_i products as inhibitors. When varying PRPP (25-400 μM) and the product OMP (12-25 μM) at saturating concentration of OA (50 μM) or varying OMP (3-12 μM) at non-saturating concentration of OA (6 μM), mixed-type inhibitions were observed. Similar results were observed when OA (6-75 μM) and the product PP_i (25-120 μM) were varied in the presence of both saturating (400 μM) and non-saturating (50 μM) concentrations of PRPP. For varying concentrations of OA substrate (6-75 μM) and product OMP (24-60 μM) in the presence of saturating concentration of PRPP (400 μM), a noncompetitive inhibition profile was obtained. On the other hand, for varying concentrations of OA substrate (6-75 μM) and product OMP (6-25 μM) in the presence of non-saturating concentration of PRPP (50 μM), a mixed-type inhibition was observed instead. Variation of substrate PRPP (25-400 μM) and product PP_i (25-125 μM) in the presence of saturating OA concentration (50 μM) also showed a noncompetitive inhibition pattern that changed to a mixed-type one when OA was fixed at a non saturating concentration (6 μM) and fixed-varied PP_i concentration range was 25-75 μM (Table 3). The observed product inhibition pattern is in agreement with a Mono-Iso Ordered Bi Bi kinetic mechanism (Fig. 4). Values of α indicating whether a product inhibitor has higher affinity for free enzyme ($\alpha > 1$), or increased affinity for enzyme-substrate(s) complex(es) as compared to free enzyme ($0 < \alpha < 1$), or equal affinity for all enzyme forms ($\alpha = 1$) (35) are also given in Table 3.

ITC ligand binding assays – Binding assays carried out at 25°C showed that PRPP and OMP can bind to free *Mt*OPRT enzyme (Figs. 5A and 5B). ITC data on PRPP and OMP binding were fitted to, respectively, sequential binding sites and one set of sites models (where the number of ligand sites was set to two for the sequential model). ITC data fitting yielded the thermodynamic constants ΔH and K_a, whereas ΔS and ΔGvalues were calculated using **Eq. (6)**, and K_d was calculated as the inverse of K_a (Table 4). The value near unity for the number of sites (N) given by ITC data fitting to one set of sites model for OMP suggests that there is one ligand molecule bound to each subunit of homodimeric *Mt*OPRT enzyme (Table 4). On the other hand, no binding to free *Mt*OPRT enzyme could be detected for OA and PP_i even when ligand concentrations were 600-fold and 900-fold larger their K_M values (Figs. 5C and 5D). These results are in agreement with Mono-Iso Ordered Bi Bi kinetic mechanism in which PRPP binding to free enzyme is followed by OA binding to form a ternary complex, and PP_i product release is followed by OMP dissociation from $MtOPRT{:}OMP$ binary complex to yield free enzyme (Fig. 4). The thermodynamic signatures of non-covalent interactions to each binding process indicate a net favorable

(negative ΔH) enthalpy and unfavorable entropy (positive $-T\Delta S$ or negative ΔS) for both PRPP and OMP binding to *Mt*OPRT (Fig. 6). ITC data on OA binding to $MtOPRT{:}PPi$ binary complex (Fig. 7A) and PP_i binding to $MtOPRT{:}OA$ binary complex (Fig. 7B) clearly demonstrate that there is dead-end complex formation. These ITC data were fitted to a sequential binding model with the number of ligand sites set to 4 (Table 4). Thermodynamic discrimination profiles for $MtOPRT{:}PPi{:}OA$ dead-end complex formation displayed two patterns: two binding events were driven by favorable enthalpy and unfavorable entropy, and two other binding events displayed unfavorable enthalpy and favorable entropy (Table 4).

DISCUSSION

Amplification, cloning, expression and purification – DNA sequencing of *pyrE*-encoded *Mt*OPRT introduced in pET-23a(+) expression vector revealed a silent mutation, which fortunately did not hamper further efforts. Interestingly, the size exclusion chromatography of the three-step purification protocol of recombinant *Mt*OPRT produced by *E. coli* host cells resulted in a decrease in the enzyme specific activity (Table 1). It has been reported that 40-50 mM of Na_2SO_4, $(NH_4)_2SO_4$ and K_2HPO_4 inhibit *E. coli* OPRT enzyme activity, whereas NaCl at concentration up to 200 mM showed no inhibitory effect on the enzyme's activity (36). It is thus puzzling that NaCl salt removal of *Mt*OPRT by size exclusion chromatography lowered the enzyme activity. Notwithstanding, this reduction in *Mt*OPRT activity was reverted after elution at approximately 660 mM $(NH_4)_2SO_4$ from the hydrophobic interaction column. Although the purification protocol described here involves three chromatographic steps, this protocol yielded ~ 64% of homogeneous *Mt*OPRT protein, which is approximately 3 times larger than a single-step OMP column affinity (37) and Ni^{2+} affinity purification protocols published for OPRT homologues (19, 38). Homogeneous recombinant *Mt*OPRT was dialyzed against buffer A to remove $(NH_4)_2SO_4$, and stored up to 12 months at -80°C in the presence of 5% glycerol with no loss of enzyme activity. As described for the yeast and *Plasmodium falciparum* homologues (30, 39), significant activity loss was observed when the enzyme was stored at 4°C, with a half-life of 24 hours. The specific activity of OPRTs from *Saccharomyces cerevisiae*, *Rhizobium leguminosarum*, *Salmonella typhimurium* and *E. coli* were reported to be, respectively, 40 U mg^{-1} (40), 53 U mg^{-1} (38), 70-85 U mg^{-1} (41, 42), and 400 U mg^{-1} (43). The specific activity value of 105 U mg^{-1} for *Mt*OPRT is thus amongst the largest values reported.

Mass spectrometry identification and molecular mass determination – Mass spectrometry data indicated a value of 18761 Da for subunit molecular mass of *Mt*OPRT, which is in agreement with the theoretical value for the 179 amino acids of its primary sequence. The UniProt database (44, 45) reported 460 reviewed amino acid sequences of OPRT enzymes, largely divided into monofunctional and bifunctional homologues that are greatly distinct by their primary sequence length. Monofunctional OPRTs range from 166 to 238 amino acids, comprising Archaea (34 organisms), Bacteria (403 organisms) and Eukaryota (Fungae, 13 organisms). Bifunctional eukaryotic homologues (10 organisms) have longer sequences from 461 to 494 amino acids whose single polypeptide chains contain both OPRT and OMP decarboxylase activities. The filamentous nitrogen-fixing cyanobacterium *Anabaena* sp. strain PCC 7120 is the only bacteria so far identified as expressing a bifunctional OPRT (46), even though its enzyme activity has being inferred solely by sequence homology. Among monofunctional enzymes, Archaea have some of the shortest sequences (from 166 to 203 amino acids), and the *Mycobacterium* genus correspond to the shortest OPRT sequences described so far among Eubacteria (179 amino acids long). Neighbor-joining multi sequence alignment (Fig. 8) showed that longer primary sequences of OPRTs present an insertion of 19-20 amino acids between amino acids 114 and 115 in *Mt*OPRT, as well as N and C-terminal extensions. Bacterial OPRTs have been divided in two major groups based on their sequence identities, one sharing up to 70% sequence identity and a second one comprising OPRTs with lower sequence identity (47). However, 'Type I PRTases' (phosphoribosyltransferases), which are involved in nucleotide synthesis or salvage pathways, are known to present remarkable tertiary and quaternary structure conservation (48, 49) regardless the conservation of their primary structure. Exception to the observed high variation in amino acid sequence is a conserved PRPP binding motif of 13 amino

acids, shared with the PRPP synthases (50), being the main unifying characteristic of the primary structure for this group of enzymes (16). The PRPP binding motif is conserved in *Mt*OPRT primary sequence, comprising amino acids 116 to 128 (VLVVEDTSTTGNS – Fig. 8, underlined), as well as an 11-amino acid long conserved flexible loop (amino acids 94 to 104 – RKSAKAHGMQR, Fig. 8, shaded in gray) involved in PRPP substrate binding and partial exclusion of solvent from the enzyme active site (36, 49, 51-53). Another shared feature of Type I PRTases is the catalytic role of conserved lysine residues (Fig. 8, bold) (31, 54), involved in the binding of highly charged Mg^{2+}:PRPP complex and anionic form of OA at pH 8.0. Site-directed mutagenesis and crystallographic structures of *S. typhimurium* demonstrated that Lys26 (equivalent to *Mt*OPRT Ser31) interact with ribose-5-phosphate moiety of PRPP and OMP (54) as well as with the carboxylic group of OA (55); whereas Lys100 and Lys103 (corresponding to Lys109 and Lys111 in *Mt*OPRT) interact with PP_i moiety of PRPP (54). The Lys73 residue has also been implicated in catalysis, adopting distinct conformations for forward or reverse chemical reactions in *S. typhimurium* OPRT active site (31, 54, 55). Although these residues are generally conserved in OPRTs, Ser31 and Gly79 in MTB substitute for, respectively, Lys26 and Lys73 in *S. typhimurium*. Blastp (56) analyses indicate that *Mt*OPRT has larger similarity to *Corynebacterium* genus homologues (75% identity), where *C. ammoniagenes* OPRT also lacks Lys26 and Lys73 (57) as *Mt*OPRT. *C. ammoniagenes* is proposed to follow a different catalytic pathway, since Lys73 is believed to be responsible for catalysis initiation in *S. typhimurium* (31), along with other distinct properties observed for *C. ammoniagenes* as higher optimal pH for the forward reaction (10.5 to 11.5) (57).

Analytical HPLC Gel Filtration – As Type I PRTases are homodimeric (50), size exclusion results presented here showing that *Mt*OPRT is a homodimer of approximately 38 kDa in solution suggest that it belongs to Type I PRTases. OPRTs from other organisms have also been shown to be homodimers (38, 40, 42, 43, 58) including *P. falciparum* (19). However, the latter was shown to be expressed as a 140 kDa enzyme complex containing two OPRT subunits and two OMP decarboxylase subunits (59). Although encoded by separate genes, and capable of catalyzing individual reactions, tetramer assembly seems to enhance *P. falciparum* OPRT and OMP decarboxylase activities and stability (60). Crystallographic structures determination indicated that loop closure upon substrate binding occurs between adjacent subunits, locating OPRTs two active sites at such interfaces, indicating that the catalytic lysine residue in the loop (*Mt*OPRT Lys111) actually plays this role in the active site of the adjacent subunit (36, 49, 51-53, 55, 61-63). OPRT active sites are thus formed by amino acids of both subunits, and the homodimeric quaternary structure corresponds to the biologically active form. The key role of Lys111 might explain its complete conservation in OPRTs, whereas positions 31 and 79 appear to have been under lesser selective pressure in *Mycobacterium* and *Corynebacterium* genus.

Kinetic mechanism determination – Divalent metal ion activation of substrate PRPP has already been demonstrated as essential for phosphoribosyltransferase-catalyzed reactions (40), in which the binary 1:1 Mg^{2+}:PRPP complex was proved to be the true substrate for OPRT reaction (41). Although *S. typhimurium* OPRT has been shown to have residual activity of 1 U mg^{-1} in the absence of Mg^{2+} (41), no activity could be detected when Mg^{2+} was omitted from the reaction mixture for the *Mt*OPRT (*data not shown*). This data indicate that Mg^{2+}:PRPP is the true substrate for *Mt*OPRT, in agreement with Type I PRTases (50). The set of *Mt*OPRT kinetic constants listed on Table 2 showed an approximately 10-fold larger value for the overall dissociation constant (K_M) of PRPP as compared to OA for the forward reaction, and an approximately 6-fold larger K_M value for PP_i in comparison to OMP for the reverse reaction. Higher OA affinities over PRPP have also been described for *P. falciparum* (1.5-fold) (19) and *C. ammoniagenes* (2-fold) (57). In addition, OMP is the preferred substrate for the reverse reaction for *S. typhimurium* (42, 48) and *S. cerevisiae* homologues (64). *Mt*OPRT presents larger K_M values as compared to the human homologue (Table 2). However, human OPRT is a bifunctional enzyme encoded by a single gene (*pyr5*) whose N-terminal portion has OPRT activity while the C-terminal portion presents OMP decarboxylase activity (23). Accordingly, the K_M values for OA and OMP substrates of human OPRT (Table 2) actually correspond to, respectively, OPRT and OMP decarboxylase

portions, and not directly to the reversal of phosphoribosyltransferase reaction. In addition to the ligands given in Table 2, *P. falciparum* (19), *S. typhimurium* (41) and human (48) homologues have been shown to also employ, respectively, 5-fluororotate, uracil and 5-fluoruracil as alternative substrates. However, *Mt*OPRT showed no activity towards uracil or 5-fluoruracil (*data not shown*). The $k_{cat\,\text{forward}}/k_{cat\,\text{reverse}}$ ratio indicates that the forward reaction is faster than the reverse reaction for *Mt*OPRT. The k_{cat} value for *Mt*OPRT demonstrates low catalytic efficiency in comparison to *P. falciparum* (19), *S. cerevisiae* (64) and *Homo sapiens* (23) homologues (Table 2). A possible explanation is that active site lysine residues that play catalytic roles (Lys26 and Lys73 in *S. typhimurium*) are replaced with Ser31 and Gly79 in *Mt*OPRT, thereby reducing the catalytic constant of the latter. Notwithstanding, site-directed mutagenesis efforts should be pursued to lend or not support to this proposal. Double reciprocal pattern of parallel lines for forward reaction (Fig. 2) is an indicative that the reaction catalyzed by *Mt*OPRT obeys a double-displacement or Ping-Pong kinetic mechanism, in which the binding of first substrate is followed by the release of first product prior to second substrate binding to the active site. Nonetheless, sequential mechanisms have been suggested as one of the characteristics of Type I PRTases (19, 48, 50), where the sole exception was *S. cerevisiae* OPRT, for it a Ping-Pong was initially attributed (40), but later it was demonstrated to also follow a sequential mechanism (65), most likely a Theorell-Chance variant (64). To try to address this issue, the experiments described below were pursued.

Half-reaction detection by PPi consumption measurement – In bi-substrate reaction where a portion of a molecule is transferred to a second one, the donor molecule usually binds first and transfers to enzyme active site a molecular group (35). In case the PRPP substrate binds first and transfers its 5-phosphate ribose moiety to *Mt*OPRT enzyme active site prior to OA binding to form OMP by two separated half-reactions ($E + PRPP \rightarrow E{:}\,PRib + PP_i$, and $E{:}\,PRib + OA \rightarrow E + OMP$), the release of PP_i into solution should be detectable in the absence of OA. Fig. 3 shows that release of PP_i by the reaction catalyzed by *Mt*OPRT can only be detected in the presence of OA, thereby ruling out a Ping-Pong mechanism in which PRPP would transfer 5-phosphate ribose moiety to the enzyme. In addition, there are some conditions where lines that seem parallel and indicate Ping-Pong mechanisms (32, 66), but in reality are sequential mechanisms that can the distinguished by a complete set of product inhibition experiments (67, 68).

Enzymatic reaction mechanism determination by product inhibition assays – Product inhibition results (Table 3) are consistent with a Mono-Iso Ordered Bi Bi kinetic mechanism (68, 69) (Fig. 4A). Although product inhibition results allow identification of substrate-product pairs (PRPP and PP_i, OA and OMP); they do not unambiguously indicate the order of substrate addition and product release, as the inhibition patterns are symmetrical (32, 67). The Mono-Iso Ordered Bi Bi kinetic mechanism implies that *Mt*OPRT undergoes an isomerization of the transitory ternary complex formed upon binding of substrates prior to release of products, and the "product" form of free enzyme has to isomerize back to the "substrate" form (70). Enzymes that isomerize slowly enough to influence the rate of catalytic turnovers are said to have "Iso mechanisms" (68). Based on steady-state kinetics data and product inhibition studies a fractional reduction of the maximal velocity (f_{iso}= the average impact of the isomerization on the maximal velocities of the reaction in the forward and reverse directions together) can be estimated by the following equation: $f_{iso} = (K_{is}/K_{ii})/[(V_{reverse}/V_{forward}) + 1]$ (68). The value of f_{iso} will range from zero, when an Iso mechanism is insignificant, to one, when the isomerization is rate limiting (68). Fitting the steady-state kinetics data (Table 2) and product inhibition data (Table 3) to this equation yielded ambiguous results. For instance, a value of 1.2 was estimated for f_{iso} at fixed-saturating PRPP substrate concentration and varied OA in the presence of PP_i product. On the other hand, a value of 0.06 was estimated at fixed-unsaturated OA concentration and varied PRPP concentration in the presence of PP_i product. Solvent-exposed loop closure during catalysis has been proposed to shield the active site of *S. typhimurium* OPRT (48), as well as for other PRTases (16, 50), and was corroborated by crystallographic structure determination of *S. typhimurium* in the presence of ligands (55, 62). Loop closure of *S. typhimurium* OPRT has also been proposed to be essential for transition-state stabilization during phosphoribosyl group transfer and to shield the transition state from

bulk solvent, accompanied by a partially rate-limiting loop opening after substrate to product conversion (49).

ITC ligand binding assays – ITC measurements were carried out to both determine the order, if any, of addition of substrate and the order of product release to yield free enzyme. ITC data on PRPP and OMP binding to *Mt*OPRT show that both ligands can bind to free enzyme to form binary complexes (Fig. 5A and 5B). However, no OA and PP_i binding to free *Mt*OPRT enzyme could be detected by ITC direct titration experiments, even when titrated ligand concentrations were raised to, respectively, 9 mM and 10 mM (Fig. 5C and 5D). Enthalpy variation (0.2 kcal/mol and 0.35 kcal/mol) and hyperbolic-like profile observed on both cases (if graphic axis was adjusted to fit scale on Fig. 5C and 5D) might indicate that larger concentrations, solubility permitting, of OA and PP_i may bind to free *Mt*OPRT. However, it is unlikely to be relevant in the intracellular context. A calculated value of 0.6 for α from product inhibition data suggests that when the substrate PP_i is varied along with OA in the presence of a fixed-saturating concentration of PRPP (Table 3), PP_i has higher affinity for enzyme forms other than free *Mt*OPRT, suggesting that PP_i and OA can both occupy the enzyme's active site simultaneously in a dead-end complex. ITC ligand binding assay confirmed that OA can bind to *Mt*OPRT in the presence of saturating PP_i concentration (900 μM; Fig. 7A), and that PP_i can bind to *Mt*OPRT in the presence of saturating OA concentration (800 μM; Fig. 7B). Although the ITC results clearly showed $MtOPRT{:}PPi{:}OA$ ternary complex formation according to a sequential binding sites model, how can one reconcile $MtOPRT{:}PPi{:}OA$ abortive complex formation with lack of enzyme-ligand binary complex formation? The abortive complex ($MtOPRT{:}PPi{:}OA$) formation has been supported by isotopic exchange and equilibrium binding assays of *S. typhimurium* OPRT that showed stronger PP_i binding to OPRT enzyme in the presence of OA as compared to weak binding of PP_i to free enzyme (48, 49). Presence of both PP_i and OA, in the absence of PRPP and OMP, might result in a synergic positive cooperative binding (71). Although a site other than the active site that can bind either OA or PP_i could be invoked, the ITC data were best fitted to a sequential binding model with the number of ligand sites set to 4. There is thus no evidence for a second binding site for these ligands in *Mt*OPRT. However, it could be speculated that for the reverse reaction binding of OA moiety of OMP could result in conformational changes that increase PP_i binding. A $MtOPRT{:}PRPP{:}OMP$ dead-end complex is not expected to form because of overlapping in the enzyme active site (67). Data presented in Table 4 show that the four binding events of two PP_i and two OA molecules all have similar ΔG values, an indicative of enthalpy-entropy compensation (71, 72). ITC data on PRPP binding to free *Mt*OPRT were best fitted to sequential binding sites model, yielding the values given in Table 4 and depicted in Fig. 6. It is noteworthy that binding of the first PRPP molecule appears to trigger large conformational changes likely in *Mt*OPRT protein upon binary complex formation as suggested by the entropically unfavorable (negative ΔS) contribution to non-covalent interactions to the binding process (73). Binding of the second PRPP molecule is accompanied by smaller unfavorable entropic contribution. At any rate, there appears to be enthalpy-entropy compensation as ΔG values are similar (Table 4). ITC data on OMP binding to free *Mt*OPRT were best fitted to one set of sites binding model, indicating that one molecule of OMP binds to each enzyme active site (1:1 stoichiometry) with equal affinity (Table 4, Fig. 6). These results corroborate the Mono-Iso Ordered Bi Bi kinetic mechanism, where PRPP binds to *Mt*OPRT first followed by OA binding, there occurs an enzyme conformational change, and PP_i is the first product to dissociate followed by OMP release to yield the "product" form of free enzyme that has to isomerize back to the "substrate" form (Fig. 4B). Thermodynamic signatures of non-covalent interactions of PRPP and OMP binding to *Mt*OPRT (Fig. 6) show a net favorable (negative ΔH) redistribution of the network of interatomic interactions (e.g., hydrogen bonds and/or van der Waals interactions) between the reacting species. Dominant negative enthalpies arise largely as a result of changes in interatomic interactions. The larger ΔH value for OMP as compared to PRPP is probably due to more H bonds and hydrophobic contacts of the former with the enzyme's active site, as indicated by crystallographic data available (53). The negative values for Gibbs energy changes demonstrate that these binding events are favorable. The entropically unfavorable

(negative ΔS) contributions to the binding processes are likely due to conformational changes in either the ligand or protein upon binary complex formation (73). The larger entropic contribution to the first event of PRPP binding is more likely due to protein conformational changes prior to a second PRPP molecule binding, and not to positive cooperativity as ΔH and K_a thermodynamic constants are approximately the same for both binding events. ΔG values for binding of PRPP first and second molecules to the enzyme are also equivalent, indicating an enthalpy-entropy compensation, discarding an allosteric effect of PRPP binding to *Mt*OPRT (71, 72). Movements of the flexible loop appear to be integral to catalysis of Type I PRTases, both covering the active site and recruiting essential residues to the catalytic locus (48). Accordingly, PRPP and OMP binding to *Mt*OPRT are enthalpy-driven processes, and are accompanied by an unfavorable entropy contribution that likely reflects enzyme's loop closure.

Currently anti-TB available drugs are considered not completely efficacious (74) due to natural and emerging disease characteristics that might impose some obstacles to its treatment (75). TB control and eradication thus require the identification of novel molecular targets for the rational design of inhibitors and development of novel treatments regimens to improve patient compliance (2, 76). In addition, trials and follow-up studies including high infection risk populations (as infants, pregnant women, and HIV positive individuals) (77) should be pursued to evaluate the effects of proposed novel drugs on TB pandemic (75, 78). The lack of bactericidal and sterilizing activities of DOTS (2) against drug-resistant mycobacteria (75, 78) also drive the current efforts to find new therapeutics. The target-based rational design of new agents with anti-TB activity includes functional and structural efforts. Accordingly, mechanistic analysis should be included in enzyme-targeted drug programs aiming at the rational design of potent enzyme inhibitors (79). Accordingly, understanding the mode of action of *Mt*OPRT will inform us on how to better design inhibitors targeting this enzyme with potential therapeutic application in TB chemotherapy. For instance, knowledge of chemical and non-chemical steps have been employed to enhance effectiveness of inhibitors of inosine monophosphate dehydrogenase enzyme activity (80). Moreover, understanding the mode of action of *Mt*OPRT may also be useful to chemical biologists interested in designing function-based chemical compounds to elucidate the biological role of this enzyme in the context of whole MTB cells. Efforts towards understanding *Mt*OPRT function in cell-like dense conditions are also currently underway since it has been shown that molecular crowding can affect protein structure, stability, function and activity (81). Moreover, attempts to ascertain the role of *Mt*OPRT in MTB survival *in vivo* during both active and latent TB are currently ongoing. Whether it proves to be essential to MTB survival, persistence, or both, *Mt*OPRT molecular, kinetic and molecular characterization data presented here provide a solid foundation on which to base inhibitor development.

REFERENCES

1. Ducati, R. G. , et al. (2006) *Mem. Inst. Oswaldo Cruz.* **101**, 697-714.
2. World Health Organization Report 2009. (August, 2009) ww.who.int/tb/publications/global_report/2009.
3. World Health Organization (2010) *Global tuberculosis control: a short update to the 2009 report.* WHO Pres, Switzerland.
4. Velayati, A. A. , Farnia, P. , Masjedi, M. R. , Ibrahim, T. A. , Tabarsi, P. , Haroun, R. Z. , Kuan, H. O. , Ghanavi, J. , Farnia, P. , and Varahram, M. (2009) *Eur. Respir. J.* **34**, 1202-1203.
5. Velayati, A. A. , Masjedi, M. R. , Farnia, P. , Tabarsi, P. , Ghanavi, J. , ZiaZarifi, A. H. , and Hoffner, S. E. (2009) *Chest.***136**, 420-425.
6. Gomez, J. E. , and McKinney, J. D. (2004) *Tuberculosis.* **84**, 29-44.
7. Rustad, T. R. , Sherrid, A. M. , Minch, K. J. , and Sherman, D. R. (2009) *Cell. Microbiol.* **11,** 1151-1159.
8. Saunders, B. M. , and Britton, W. J. (2007) *Immunol. Cell Biol.* **85**, 103-111.

9. Eisenreich, W. , Dandekar, T. , Heesemann, J. , and Goebel, W. (2010) *Nat. Rev. Microbiol.* **8**, 401-412.
10. Niederweis, M. (2008) *Microbiology.* **154**, 679-692.
11. Davis, J. M. , and Ramakrishnan, L. (2009) *Cell.* **136**, 38-49.
12. Bold, T. D. , and Ernst, J. D. (2009) *Cell.* **136**, 17-19.
13. Meena, L. S. , and Rajni. (2010) *FEBS J.* **277**, 2416-2427.
14. Tischler, A. D. , and McKinney, J. D. (2010) *Curr. Opin. Microbiol.* **13**, 93-99.
15. Raupach, B. , and Kaufmann, S.H.E. (2010) *Curr. Opin. Immunol.* **13**, 417-428.
16. Ducati, R. G. , Breda, A. , Basso, L. A. , and Santos, D. S. (2010) *Curr. Med. Chem.* in press.
17. Boshoff, H. I. M. , and Barry, C. E. 3rd. (2005) *Nat. Rev. Microbiol.* **3**, 70-80.
18. Fox, B. A. , and Bzik, D. J. (2002) *Nature.* **415**, 926-930.
19. Krungkrai, S. R. , Aoki, S. , Palacpac, N. M. Q. , Sato, D. , Mitamura, T. , Krungkrai, J. , and Horii, T. (2004) *Mol. Biochem. Parasitol.* **134**, 245-255.
20. Russel, D. G. (2007) *Nat. Rev. Microbiol.* **5**, 39-47.
21. O'Donovan, G. A. , and Neuhard, J. (1970) *Bacteriol. Rev.* **34**, 278-343.
22. Sassetti, C. M. , Dana, H. B. , and Rubin, E. J. (2003) *Mol. Microbiol.* **48**, 77-84.
23. Yablonski, M. J, Pasek, D. A. , Han, B. D. , Jones, M. E. , and Traut, T. W. (1996) *J. Biol. Chem.* **271**, 10704-10708.
24. Bradford, M. M. (1976) *Anal. Biochem.* **72**, 248-254.
25. Edelhoch, H. (1976) *Biochemistry.* **6**, 1948-1954.
26. Pace, C. N. , Vajdos, F. , Fee, L. , Grimsley, G. , and Gray, T. (1995) *Protein Sci.* **4**, 2411-2423.
27. Laemmli, U. K. (1970) *Nature.* **227**, 680-685.
28. Shevchenko, A. , Wilm, M. , Vorm, O. , and Mann, M. (1996) *Anal. Chem.* **68**, 850-858.
29. Zhang, Z. , and Marshall, A. G. (1998) *J. Am. Soc. Mass Spectrom.* **9**, 225-233.
30. Krungkrai, S. R. , DelFraino, B. J. , Smiley, J. A. , Prapunwattana, P. , Mitamura, T. , Horii, T. , and Krungkrai, J. (2005) *Biochemistry.* **44**, 1643-1652.
31. Ozturk, D. H. , Dorfman, R. H. , Scapin, G. , Sacchettini, J. C. , and Grubmeyer, C. (1995) *Biochemistry.* **34**, 10755-10763.
32. Segel, I.H. (1993) *Enzyme kinetics - Behavior analysis of rapid equilibrium and steady-state enzyme systems.* 1st Ed. , Wyley-Interscience Publication, John Wiley & Sons, Inc.
33. Fukada, H. , and Takahashi, K. (1998) *Proteins.* **33**, 159-166.
34. Cole, S. T. , et al. (1998) *Nature.* **393**, 537-544.
35. Copeland, R. A. (2005) *Evaluation of Enzyme Inhibitors in Drug Discovery.* 1st Ed., John Wiley & Sons.
36. Henriksen, A. , Aghajari, N. , Jensen, K. F. , and Gajhede, M. (1996) *Biochemistry.* **35**, 3803-3809.
37. Dodin, G. (1981) *FEBS Lett.* **134**, 20-24.
38. Bayles, D. O. , Fennington Jr, G. J. , and Hughes, T. A. (1997) *Gene.* **195**, 329-336.
39. Umezu, K. , et al. (1971) *J. Biochem.* **70**, 249-262.
40. Victor, J. , Leo-Mensah, A. , and Sloan, D. L. (1979) *Biochemistry.* **18**, 3597-3604.
41. Bhatia, M. B. , and Grubmeyer, C. (1993) *Arch. Biochem. Biophys.* **302**, 321-325.
42. Bhatia, M. B. , Vinitsky, A. , and Grubmeyer, C. (1990) *Biochemistry.* **29**, 10480-10487.
43. Poulsen, P. , Jensen, K. F. , Valentin-Hansen, P. , Carlsson, P. , and Lundberg, L. G. (1983) *Eur. J. Biochem.* **135**, 223-229.
44. The UniProt Consortium. (2010) *Nucleic Acids Res.* **38**, D142-D148.
45. Jain, E. , et al. (2009) *BMC Bioinformatics.* **10**, 136.
46. Kaneko, T. , et al. (2001) *DNA Res.* **8**, 205-213.
47. Kim, M. K. , Song, H. E. , Kim, Y. S. , Rho, S. H. , Im, Y. J. , Lee, J. H. , Kang, G. B. , and Eom, S. H. (2003) *Mol. Cells.* **15**, 361-363.
48. Wang, G. P. , Lundegaard, C. , Jensen, K. F. , and Grubmeyer, C. (1999) *Biochemistry.* **38**, 275-283.
49. Wang, G. P. , Cahill, S. M. , Liu, X. , Girvin, M. E. , and Grubmeyer, C. (1999) *Biochemistry.* **38**, 284-295.
50. Sinha, S. C. , and Smith, J. L. (2001) *Curr. Opin. Struct. Biol.* **11**, 733-739.

51. Schumacher, M. A. , Carter, D. , Roos, D. S. , Ullman, B. , and Brennan, R. G. (1996) *Nat. Struct. Biol.* **3**, 881-887.
52. Smith, J. L. (1999) *Nat. Struct. Biol.* **6**, 502-504.
53. González-Segura, L. , Witte, J. F. , McClard, R. W. , and Hurley, T. D. (2007) *Biochemistry.* **46**, 14075-14086.
54. Grubmeyer, C. , Segura, E. , and Dorfman, R. (1993) *J. Biol. Chem.* **268**, 20299-20304.
55. Scapin, G. , Ozturk, D. H. , Grubmeyer, C. , and Sacchettini, J. C. (1995) *Biochemsitry.* **34**, 10744-10754.
56. Altschul, S. F. , Wootton, J. C. , Gertz, E. M. , Agarwala, R. , Morgulis, A. , Schäffer, A. A. , and Yu, Y. K. (2005) *FEBS J.* **272**, 5101-5109.
57. Wang, X. , Ma, C. , Wang, X. , and Xu, P. (2007) *J. Bacteriol.* **189**, 9030-9036.
58. Hamana, H. , and Shinozawa, T. (1999) *J. Biochem.* **125**, 109-114.
59. Kungkrai, S. R. , Prapunwattana, P. , Horii, T. , and Krungkrai, J. (2004) *Biochem. Biophys. Res. Commun.* **318**, 1012-1018.
60. Kanchanaphum, P. , and Kungkrai, J. (2009) *Biochem. Biphys. Res. Commun.* **309**, 337-341.
61. Ozturk, D. H. , Dorfman, R. H. , Scapin, G. , Sacchettini, J. C. , and Grubmeyer C. (1995) *Biochemistry.* **34**, 10764-10770.
62. Scapin, G. , Grubmeyer, C. , and Sacchetinni, J. C. (1994) *Biochemistry.* **33**, 1287-1294.
63. Liu, C. P. , et al. (2010) *Acta Crystallogr.* **F66**, 498-502.
64. McClard, R. W. , Holets, E. A. , MacKinnon, A. L. , and Witte J. F. (2006) *Biochemistry.* **45**, 5330-5342.
65. Witte, J. F. , Tsou, R. , and McClard, R. W. (1999) *Arch. Biochem. Biophys.* **361**, 106-112.
66. Bar-Tana, J. , and Cleland, W. W. (1974) *J. Biol. Chem.* **249**, 1271-1276.
67. Cooper, B. F. , and Rudolph, F. B. (1995) *Meth. Enzymol.* **249**, 188-210.
68. Rebholz, K. L. , and Northrop, D. B. (1995) *Meth. Enzymol.* **249**, 211-240.
69. Northrop, D. B. , and Rebholz, K. L. (1997) *Arch. Biochem. Biophys.* **342**, 317-321.
70. Leskovac, V. (2003) *Comprehensive enzyme kinetics.* Kluwer Academic, Plenum Publishers, NY.
71. Eftink, M. R. , Anusiem, A. C. , and Biltonen, R. L. (1983) *Biochemistry.* **22**, 3884-3896.
72. Brown, A. (2009) *Int. J. Mol. Sci.* **10**, 3457-3477.
73. O'Brien, R. , and Haq, I. (2004) Applications of Biocalorimetry: Binding, Stability and Enzyme Kinetics. [ed.] John E Ladbury e Michael L Doyle. *Biocalorimetry 2 Applications of calorimetry in the biological sciences.* 1st Ed. , John Wiley & Sons.
74. Zaleskis, R. (2006) *Eur. Respirat. Dis.* 47-49.
75. Ma, Z. , Lienhardt, C. , MdIlleton, H. , Nunn, A. J. , and Wang, X. (2010) *Lancet.* **375**, 2100-2109.
76. Spigelman, M. , Woosley, R. , and Gheuens, J. (2010) *Int. J. Tuberc. Lung Dis.* **14**, 663-664.
77. Donald, P. R. (2007) *SAMJ.* **97**, 992-994.
78. Russell, D. G. , Barry 3rd, C. E. , and Flynn, J. L. (2010) *Science.* **328**, 852-856.
79. Hasan, S. , Daugelat, S. , Srinivasa Rao, P. S. , and Schreiber M. (2006) *PLoS Comput. Biol.* **2**, e61.
80. Umejiego, N. N. , Li, C. , Riera, T. , Hedstrom, L. , and Striepen, B. (2004) *J. Biol. Chem.* **279**, 40320-40327.
81. Dhar, A. , Samiotakis, A. , Ebbinghaus, S. , Nienhaus, L. , Homouz, D. , Gruebele, M. , and Cheung, M. S. (2010) *Proc. Natl. Acad. Sci. USA*. **107**, 17586-17591.
82. Thompson, J. D. , Higgins, D. G. , and Gibson, T. J. (1994) *Nucleic Acis Res.* **22**, 4673-4680.

FOOTNOTES

* This work was supported by funds of Decit/SCTIE/MS-MCT-CNPq-FNDCT-CAPES to National Institute of Science and Technology on Tuberculosis (INCT-TB) to D.S.S. and L.A.B. L.A.B. and D.S.S. also acknowledge financial support awarded by FAPERGS-CNPq-PRONEX-2009. D.S.S. (CNPq, 304051/1975-06) and L.A.B. (CNPq, 520182/99-5) are Research Career Awardees of the National Research Council of Brazil (CNPq). A.B., L.A.R. and D.M.L. acknowledge scholarships awarded by, respectively, BNDES, CAPES and PNPD-CAPES.

The abbreviations used are: TB, tuberculosis; MTB, *Mycobacterium tuberculosis*; WHO, World Health Organization; TDR-TB, totally-drug resistant TB; OPRT, orotate phosphoribosyltransferase; OA, orotate; PRPP, 5'-phospho-α-D-ribose 1'-diphosphate; OMP, orotidine 5'-monophosphate; PPD, purified protein derivative; IPTG, isopropyl α-D-thiogalactopyranoside; ITC, isothermal titration calorimetry; LB, Luria-Bertani; MESG, 2-amino-6-mercapto-7-methylpurine ribonucleoside; UMP, uridine 5'-monophosphate; *Mt*OPRT, *Mycobacterium tuberculosis*' OPRT; PRTases, phosphoribosyltransferases.

FIGURE LEGENDS

Fig. 1. OPRT catalyzed conversion of OA and PRPP into OMP and PP_i by the formation of a N-glycosidic bond in the presence of Mg^{2+}, the fifth step of pyrimidine *de novo* synthesis pathway.

Fig. 2. Double reciprocal plots of the forward reaction of *Mt*OPRT. Steady-state initial velocity experiments were carried out as described in Experimental Procedures. (A) Concentration of OA was varied (2-100 μM) in the presence of seven fixed different concentrations of PRPP. (B) Concentration of PRPP was varied (25-500 μM) in the presence of five fixed different concentrations of OA. Data were fitted to **Eq. (4)**.

Fig. 3. PP_i release indirectly measurement by monitoring 2-amino-6-mercapto-7-methylpurine formation in the absence (■) and presence (●) of OA (100 μM) in the reaction mixture.

Fig. 4. (A) Kinetic mechanism of *Mt*OPRT as proposed by product inhibition assays. E and E' correspond to enzyme isoforms. A and B, P and Q indicate substrates and products of the reaction. (B) Order of substrates binding and products release from *Mt*OPRT binding site, inferred from ITC ligand binding assays.

Fig. 5. Ligand binding assays. PRPP (A) and OMP (B) ITC data were fitted to sequential binding and one set of sites binding models. Both OA (C) and PP_i (D) binding to *Mt*OPRT apo form could not be detected under experimental settings.

Fig. 6. Dead-end complex formation of product PP_i and substrate OA with *Mt*OPRT. (A) Incubation of enzyme and PP_i, titration of OA; (B) incubation of enzyme and OA, titration of PP_i.

Fig. 7. Enthalpy (ΔH), entropy ($-T\Delta S$) and Gibbs free energy (ΔG) thermodynamic profile for PRPP and OMP binding to *Mt*OPRT. As ITC data on PRPP binding were fitted to a sequential binding sites model, values are also given for each binding site of homodimeric *Mt*OPRT (PRPP 1 and PRPP 2).

Fig. 8. Neighbor-joining multi sequence alignment of MTB (TubercuList: Rv0382c), *H. sapiens* (GenBank: NP_000364.1), *S. cerevisiae* (UniProt: P13298), *S. thyphimurium* (GenBank: NP_462633), *C. ammoniagenes* (GenBank: EU123869) and *P. falciparum* (GenBank: XP_001351684) OPRT enzymes, performed with ClustalW (82). *P. falciparum* first 63 amino acids were omitted from sequence alignment. Conserved catalytic lysine residues, and amino acids comprising the catalytic loop and the PRPP binding site are highlighted in bold, shaded in gray and underlined respectively.

Table 1. Purification of *Mt*OPRT from *E. coli* BL21(DE3). Typical purification protocol starting from 12 g wet cell paste from 3 L culture.

Step	*Total protein (mg)*	*Specific activity* (U mg^{-1})*	*Total enzyme activity (U)*	*Yield %*	*Purification fold*
crude extract	131	8	1088.6	100	1
HP 16/10 Q XL	46.4	51	2354.4	216	6.4
Sephacryl S-200	10.6	40	423	39	5
Phenyl Sepharose HP	6.6	105	693	64	13

* One enzyme unit is the amount of *Mt*OPRT that converts 1 µmol of OA to OMP per minute at 25°C.

Table 2. *Mt*OPRT and some homologues OPRTs kinetic parameters.

Organism	*Kinetic constants*	*Ligand*			
		OA	*PRPP*	*OMP*	*PP_i*
Mycobacterium tuberculosis	K_M (µM)	10 ± 0.5	96 ± 4.1	2.6 ± 0.4*	16 ± 0.6*
	k_{cat} (s^{-1})	0.61 ± 0.01		0.280 ± 0.01*	0.280 ± 0.003*
	k_{cat}/K_M ($M^{-1}s^{-1}$)	60 (± 3)E3	6.0 (± 0.3)E3	100 (± 18.3)E3*	10 (± 0.7)E3*
Plasmodium falciparum (19)	K_M (µM)	18.2 ± 0.9	28.6 ± 1.3	25.1 ± 0.7	14.3 ± 0.1
	k_{cat} (s^{-1})	3.0 ± 0.1	3.2 ± 0.1	2.6 ± 0.1	1.3 ± 0.1
	k_{cat}/K_M ($M^{-1}s^{-1}$)	16.4E6	11.3E6	10.2E6	9.4E6
Saccharomyces cerevisiae (64)	K_M (µM)	18.7 ± 3.4	18.2 ± 4.5	3.4 ± 0.3	30.6 ± 2.5
	k_{cat} (s^{-1})	111 ± 5		35 ± 0.5	
	k_{cat}/K_M ($M^{-1}s^{-1}$)	5.9E6	6.1E6	10E6	1.1E6
Salmonella typhimurium (42)	K_M (µM)	27.5	44.1	3.1	31.1
	k_{cat} (s^{-1})	--	--	--	--
	k_{cat}/K_M ($M^{-1}s^{-1}$)	--	--	--	--
Salmonella typhimurium (48)	K_M (µM)	20 ± 2	18 ± 3	2.1 ± 0.2	47 ± 7
	k_{cat} (s^{-1})	--	--	--	--
	k_{cat}/K_M ($M^{-1}s^{-1}$)	--	--	--	--
Corynebacterium ammoniagenes (57)	K_M (µM)	33.09	63.53	44.84	36.1
	k_{cat} (s^{-1})	--	--	--	--
	k_{cat}/K_M ($M^{-1}s^{-1}$)	--	--	--	--
Homo sapiens (23)	K_M (µM)	2.1 ± 0.12	--	0.23 ± 0.87	--
	k_{cat} (s^{-1})	4.0	--	16	--
	k_{cat}/K_M ($M^{-1}s^{-1}$)	--	--	--	--

* Values corresponding to apparent kinetic constants.

Table 3. Product inhibition results for *Mt*OPRT forward reaction.

Inhibitor	*Varied substrate*	*Fixed substrate*	αK_i *(μM)*	K_i *(μM)*	α	*Inhibition type*
OMP	PRPP	OA saturated	107 ± 85	10 ± 2	11	Mixed-type
		OA unsaturated	44 ± 15	4.4 ± 0.8	10	Mixed-type
	OA	PRPP saturated	35 ± 4	35 ± 10	1	Noncompetitive
		PRPP unsaturated	10.7 ± 0.4	7.4 ± 0.7	1.4	Mixed-type
PP_i	PRPP	OA saturated	108 ± 9	108 ± 19	1	Noncompetitive
		OA unsaturated	310 ± 53	26 ± 3	12	Mixed-type
	OA	PRPP saturated	120 ± 14	209 ± 97	0.6	Mixed-type
		PRPP unsaturated	145 ± 17	29 ± 4	5	Mixed-type

Table 4. Thermodynamic, ligand binding affinity and dissociation constants; and number of ligands per subunit (N) for *Mt*OPRT.

	ΔH *(cal/mol)*	$-T\Delta S$ *(cal/mol/degree)*	ΔG *(cal/mol)*	K_a *(M^{-1})*	K_d *(μM)*	N
$PRPP_1$	-8.6 (± 0.3) × 10^3	2.7 (± 0.1) × 10^3	-6 (± 0.2) × 10^3	20 (± 2) × 10^3	52 (± 5)	--
$PRPP_2$	-6.3 ± (0.4) × 10^3	0.37 (± 0.02) × 10^3	-6 (± 0.3) × 10^3	21 (± 1) × 10^3	48 (± 2)	--
OMP	-25.7 (± 0.9) × 10^3	19 (± 0.6) × 10^3	-7 (± 0.2) × 10^3	124 (± 2) × 10^3	8 (± 1)	0.82 (± 0.02)
$PP_i{\cdot}OA_1$	-43 (± 2) × 10^3	37 (± 2) × 10^3	-6 (± 0.3) × 10^3	13 (± 2) × 10^3	75 (± 11)	--
$PP_i{\cdot}OA_2$	55 (± 4) × 10^3	-60 (± 4) × 10^3	-5 (± 0.3) × 10^3	4 (± 0.6) × 10^3	261 (± 41)	--
$PP_i{\cdot}OA_3$	13.1 (± 0.5) × 10^3	-20 (± 0.8) × 10^3	-7 (± 0.3) × 10^3	127 (± 20) × 10^3	8 (± 1)	--
$PP_i{\cdot}OA_4$	-43 (± 9) × 10^3	36 (± 7) × 10^3	-6 (± 1) × 10^3	58 (± 9) × 10^3	17 (± 2)	--

Figure 1

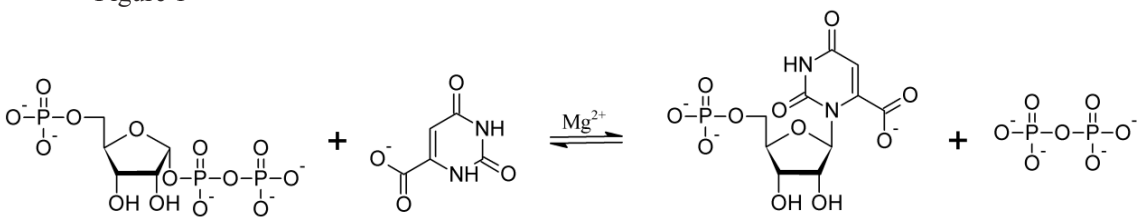

Figure 2

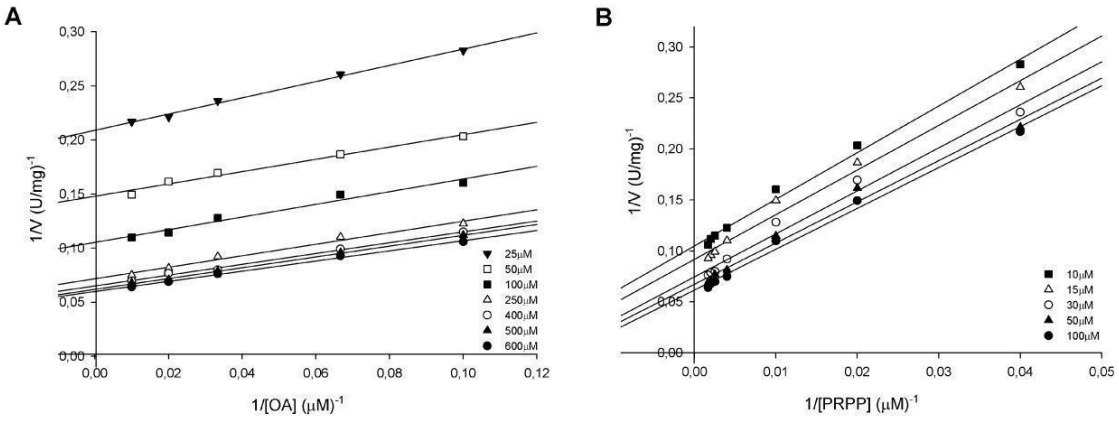
A
1/V (U/mg)-1
1/[OA] (μM)-1
25μM
50μM
100μM
250μM
400μM
500μM
600μM
B
1/V (U/mg)-1
1/[PRPP] (μM)-1
10μM
15μM
30μM
50μM
100μM

Figure 3

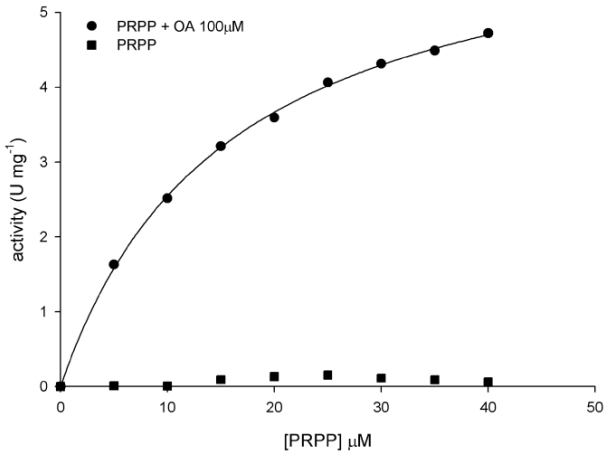
PRPP + OA 100μM
PRPP
activity (U mg-1)
[PRPP] μM
0
1
2
3
4
5
0
10
20
30
40
50

Figure 4

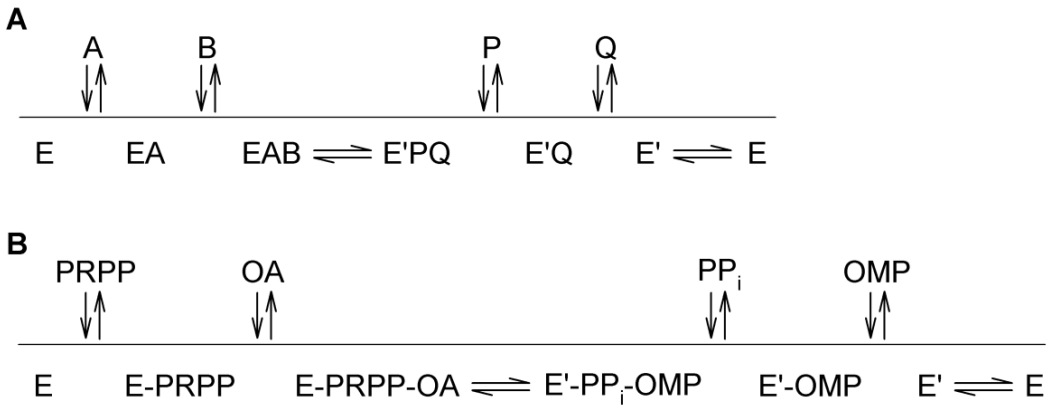
A
A
B
P
Q
E
EA
EAB ⇌ E'PQ
E'Q
E' ⇌ E
B
PRPP
OA
PPi
OMP
E
E-PRPP
E-PRPP-OA ⇌ E'-PPi-OMP
E'-OMP
E' ⇌ E

Figure 5

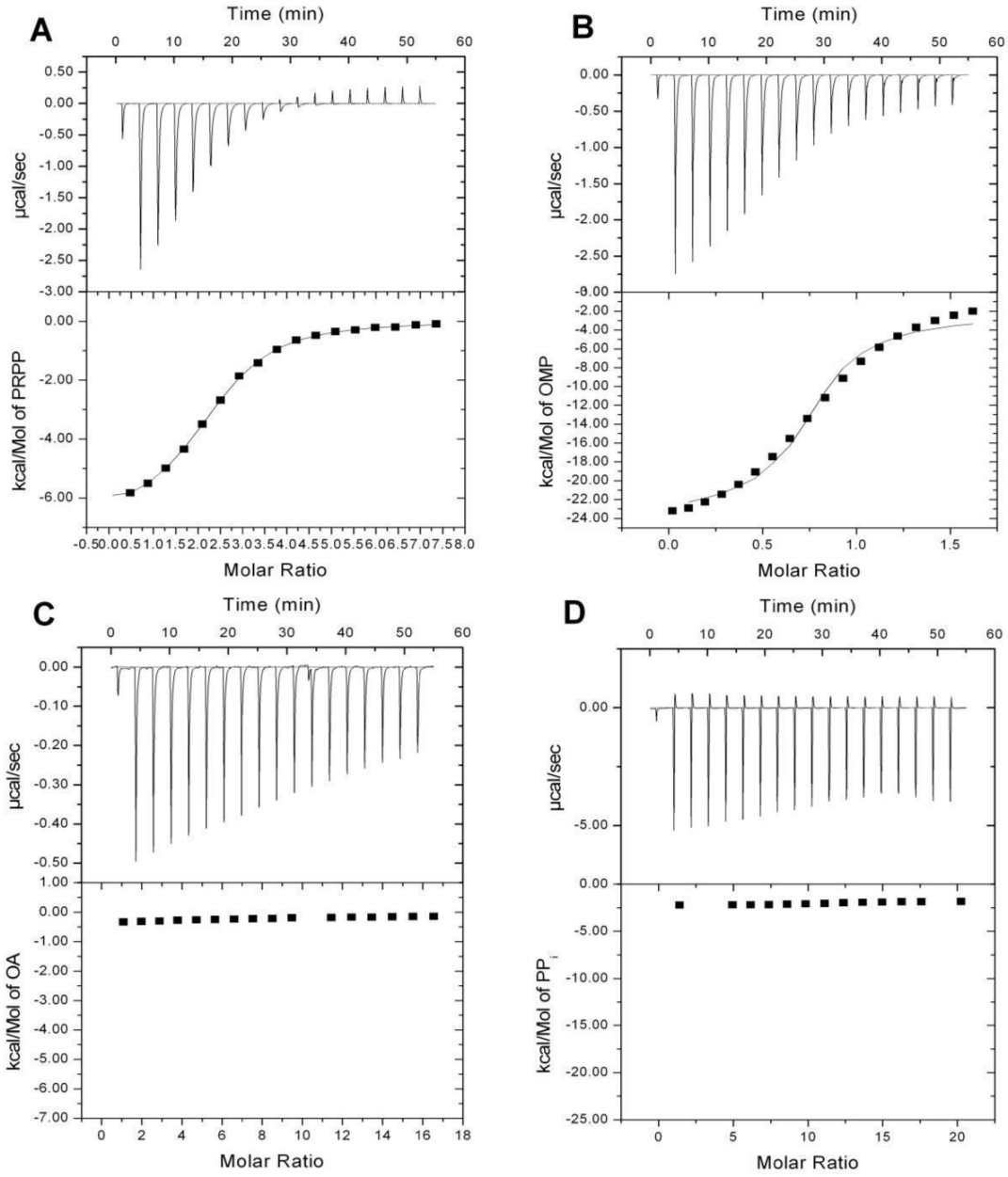
A
Time (min)
µcal/sec
kcal/Mol of PRPP
Molar Ratio
B
Time (min)
µcal/sec
kcal/Mol of OMP
Molar Ratio
C
Time (min)
µcal/sec
kcal/Mol of OA
Molar Ratio
D
Time (min)
µcal/sec
kcal/Mol of PPi
Molar Ratio

Figure 6

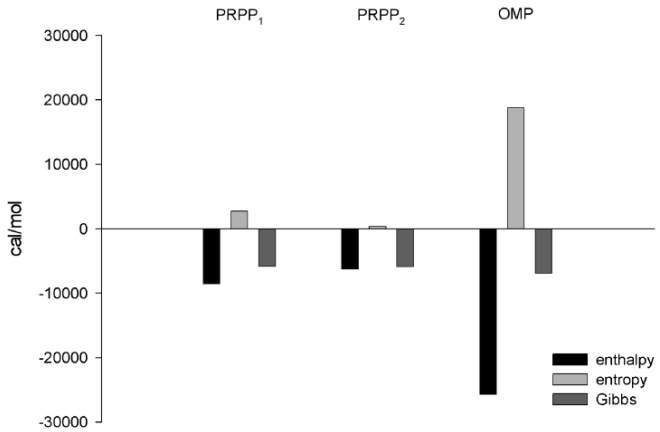
PRPP1
PRPP2
OMP
30000
20000
10000
0
-10000
-20000
-30000
cal/mol
enthalpy
entropy
Gibbs

Figure 7

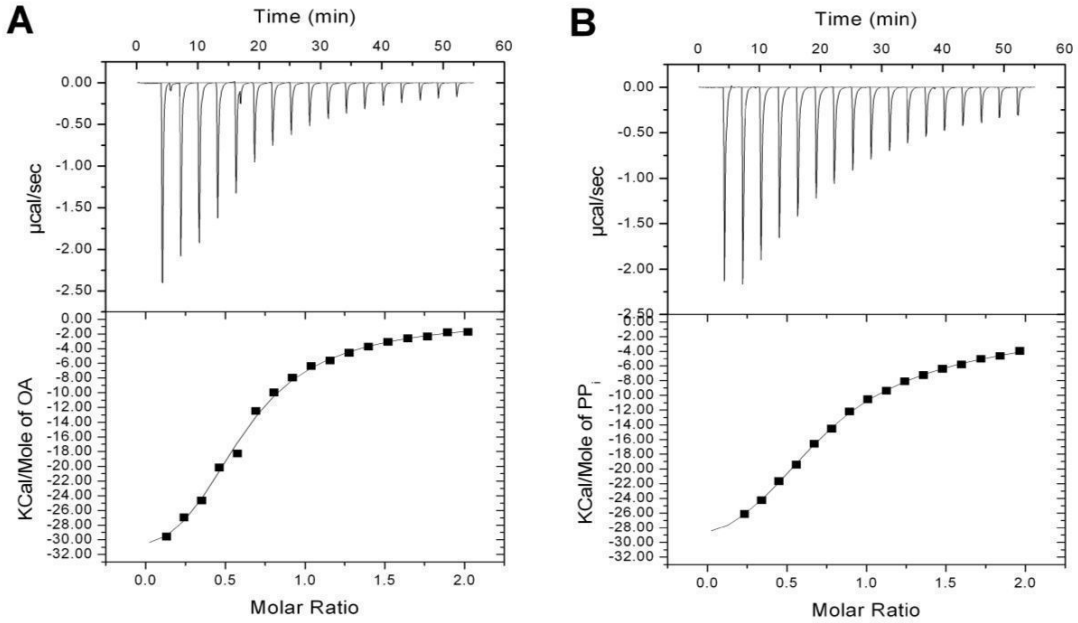
A
Time (min)
µcal/sec
KCal/Mole of OA
Molar Ratio
B
Time (min)
µcal/sec
KCal/Mole of PPi
Molar Ratio

Figure 8

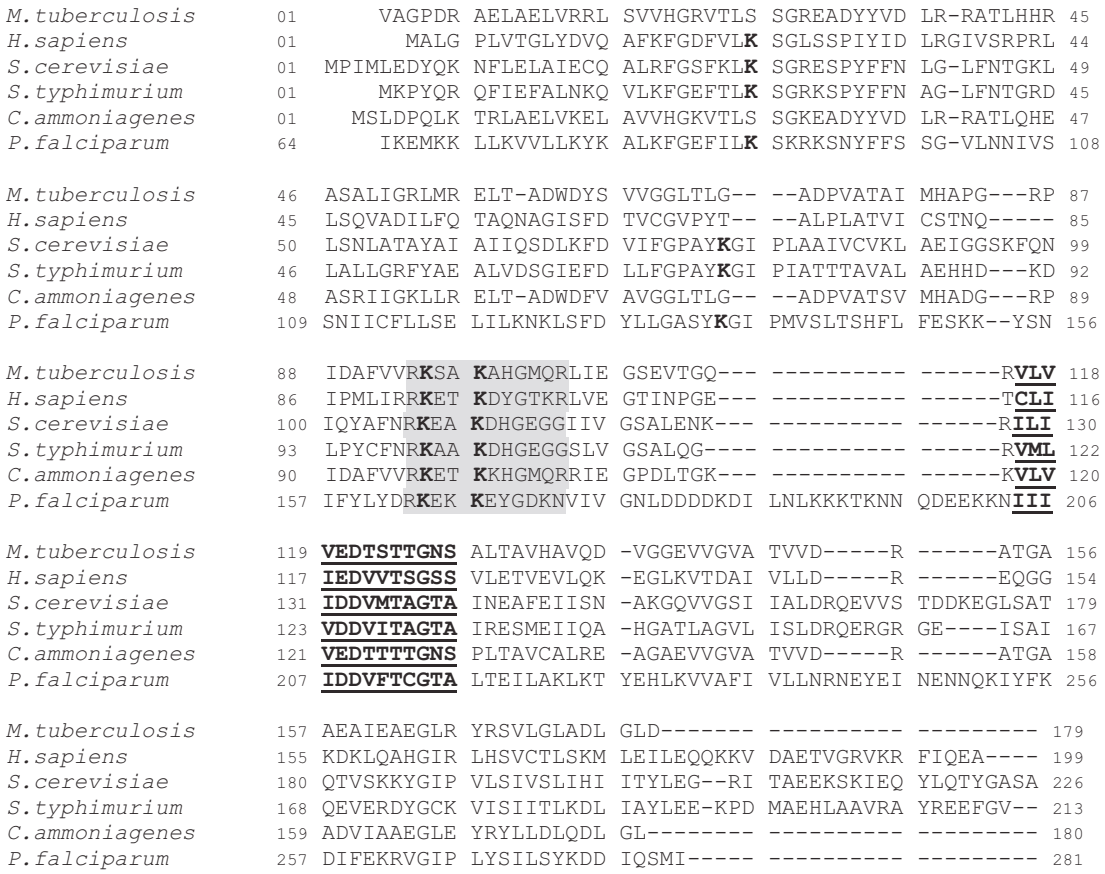
M.tuberculosis 01 VAGPDR AELAELVRRL SVVHGRVTLS SGREADYYVD LR-RATLHHR 45
H.sapiens 01 MALG PLVTGLYDVQ AFKFGDFVLK SGLSSPIYID LRGIVSRPRL 44
S.cerevisiae 01 MPIMLEDYQK NFLELAIECQ ALRFGSFKLK SGRESPYFFN LG-LFNTGKL 49
S.typhimurium 01 MKPYQR QFIEFALNKQ VLKFGEFTLK SGRKSPYFFN AG-LFNTGRD 45
C.ammoniagenes 01 MSLDPQLK TRLAELVKEL AVVHGKVTLS SGKEADYYVD LR-RATLQHE 47
P.falciparum 64 IKEMKK LLKVVLLKYK ALKFGEFILK SKRKSNYFFS SG-VLNNIVS 108
M.tuberculosis 46 ASALIGRLMR ELT-ADWDYS VVGGLTLG-- --ADPVATAI MHAPG---RP 87
H.sapiens 45 LSQVADILFQ TAQNAGISFD TVCGVPYT-- --ALPLATVI CSTNQ----- 85
S.cerevisiae 50 LSNLATAYAI AIIQSDLKFD VIFGPAYKGI PLAAIVCVKL AEIGGSKFQN 99
S.typhimurium 46 LALLGRFYAE ALVDSGIEFD LLFGPAYKGI PIATTTAVAL AEHHD---KD 92
C.ammoniagenes 48 ASRIIGKLLR ELT-ADWDFV AVGGLTLG-- --ADPVATSV MHADG---RP 89
P.falciparum 109 SNIICFLLSE LILKNKLSFD YLLGASYKGI PMVSLTSHFL FESKK--YSN 156
M.tuberculosis 88 IDAFVVRKSA KAHGMQRLIE GSEVTGQ--- ---------- ------RVLV 118
H.sapiens 86 IPMLIRRKET KDYGTKRLVE GTINPGE--- ---------- ------TCLI 116
S.cerevisiae 100 IQYAFNRKEA KDHGEGGIIV GSALENK--- ---------- ------RILI 130
S.typhimurium 93 LPYCFNRKAA KDHGEGGSLV GSALQG---- ---------- ------RVML 122
C.ammoniagenes 90 IDAFVVRKET KKHGMQRRIE GPDLTGK--- ---------- ------KVLV 120
P.falciparum 157 IFYLYDRKEK KEYGDKNVIV GNLDDDDKDI LNLKKKTKNN QDEEKKNIII 206
M.tuberculosis 119 VEDTSTTGNS ALTAVHAVQD -VGGEVVGVA TVVD-----R ------ATGA 156
H.sapiens 117 IEDVVTSGSS VLETVEVLQK -EGLKVTDAI VLLD-----R ------EQGG 154
S.cerevisiae 131 IDDVMTAGTA INEAFEIISN -AKGQVVGSI IALDRQEVVS TDDKEGLSAT 179
S.typhimurium 123 VDDVITAGTA IRESMEIIQA -HGATLAGVL ISLDRQERGR GE----ISAI 167
C.ammoniagenes 121 VEDTTTTGNS PLTAVCALRE -AGAEVVGVA TVVD-----R ------ATGA 158
P.falciparum 207 IDDVFTCGTA LTEILAKLKT YEHLKVVAFI VLLNRNEYEI NENNQKIYFK 256
M.tuberculosis 157 AEAIEAEGLR YRSVLGLADL GLD------- ---------- --------- 179
H.sapiens 155 KDKLQAHGIR LHSVCTLSKM LEILEQQKKV DAETVGRVKR FIQEA---- 199
S.cerevisiae 180 QTVSKKYGIP VLSIVSLIHI ITYLEG--RI TAEEKSKIEQ YLQTYGASA 226
S.typhimurium 168 QEVERDYGCK VISIITLKDL IAYLEE-KPD MAEHLAAVRA YREEFGV-- 213
C.ammoniagenes 159 ADVIAAEGLE YRYLLDLQDL GL-------- ---------- --------- 180
P.falciparum 257 DIFEKRVGIP LYSILSYKDD IQSMI----- ---------- --------- 281

SUPPLEMENTAL DATA

Fig. I. Averaged spectra collected from non digested *Mt*OPRT. Deconvoluted spectrum (insert) presents a single peak corresponding to the average molecular of *Mt*OPRT without the first amino acid methionine (18761 Da). Peaks in original spectrum are assigned to charged states (from 15^+ to 25^+) of *Mt*OPRT.

Table I. Peptides from *Mt*OPRT sequence identified by comparison of MS/MS spectra with theoretical spectra generated from *in silico* tryptic digestion of MTB H37Rv proteome.

Peptide	*Position*	*XCore*
AELAELVR	7-14	2.5
RLSVVHGR	15-22	2.47
EADYYVDLR	30-38	2.82
ELTADWDYSVVGGLTLGADPVATAIMHAPGRPIDAFVVR	56-94	4.5
LIEGSEVTGQR	105-115	3.1
VLVVEDTSTTGNSALTAVHAVQDVGGEVVGVATVVDR	116-152	7.41
ATGAAEAIEAEGLR	153-166	3.72
YRSVLGLADLGLD	167-179	3.42

Figure I

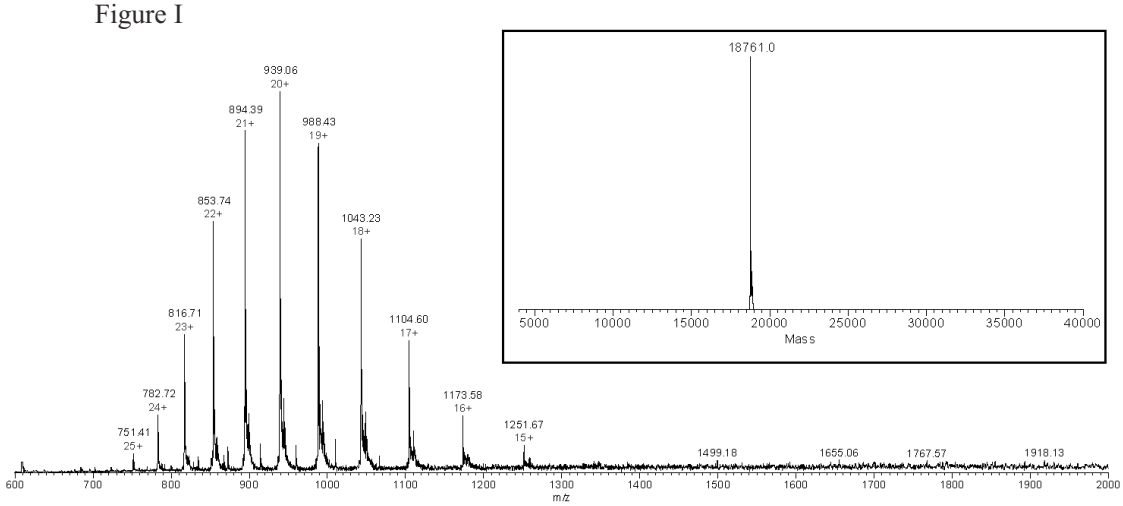
939.06
20+
894.39
21+
988.43
19+
853.74
22+
1043.23
18+
816.71
23+
1104.60
17+
782.72
24+
1173.58
16+
751.41
25+
1251.67
15+
1499.18
1655.06
1767.57
1918.13
600
700
800
900
1000
1100
1200
1300
1400
1500
1600
1700
1800
1900
2000
m/z
18761.0
5000
10000
15000
20000
25000
30000
35000
40000
Mass

Capítulo 3

PYRIDINONE-BASED INHIBITORS OF *Mycobacterium tuberculosis* OROTATE PHOSPHORIBOSYLTRANSFERASE

Artigo submetido ao *Bioorganic and Medicinal Chemistry Letters*

PYRIDINONE-BASED INHIBITORS OF *Mycobacterium tuberculosis* OROTATE PHOSPHORIBOSYLTRANSFERASE

Ardala Breda [a, b, c], Pablo Machado [a, b], Leonardo Astolfi Rosado [a, b, d], Luiz Augusto Basso [a, b, c], Andre Arigony Souto [a, b, c], and Diógenes Santiago Santos [a, b, c]

[a] Instituto Nacional de Ciência e Tecnologia em Tuberculose, [b] Centro de Pesquisas em Biologia Molecular e Funcional, [c] Programa de Pós-Graduação em Biologia Celular e Molecular, [d] Programa de Pós-Graduação em Medicina e Ciências da Saúde.
Pontifícia Universidade Católica do Rio Grande do Sul, Porto Alegre, Rio Grande do Sul, Brazil
Avenida Ipiranga 6900 Prédio 92A – TECNOPUC. 90619-900 Porto Alegre, RS, Brazil.
Phone/Fax: +55 51 3320 3629.

Corresponding authors: Diógenes Santiago Santos (diogenes@pucrs.br) and André Arigony Souto (arigony@pucrs.br)

Author's e-mails: ardala.breda@acad.pucrs.br, pablomachado.mail@gmail.com, leo.rosado@gmail.com, arigony@pucrs.br, luiz.basso@pucrs.br, diogenes@pucrs.br

Abstract

Tuberculosis (TB) is a chronic infection disease caused mainly by *Mycobacterium tuberculosis* and is considered a global emergence by the World Health Organization. The development of novel drugs is thus required to improve control, treatment and prophylaxis of TB. The nucleotide metabolism pathway enzymes provide promising molecular targets for the development of drugs, most probably targeting both active and latent tuberculosis forms. Molecular properties and kinetic mechanism of orotate phosphoribosyltransferase (OPRT), the fifth enzyme of *de novo* pyrimidine synthesis was explored for planning, selecting and synthesizing substrate analogs with potential inhibitory activity. Steady-state kinetic measurements of OPRT enzyme activity were employed to determine the mode of inhibition of chemical compounds. Compound **6** and derived molecule **13** showed inhibition at values in the nanomolar concentration range. Thermodynamic data show that binding of compounds **6** and **13** to OPRT have negative enthalpy (ΔH) and favorable Gibbs free energy (ΔG), an indicative of both molecules being complementary to the enzyme's binding pocket. Thermodynamic profile discrimination results suggest that improvement of compound **13** hydrophobic character by addition of a phenyl substituent resulted in inhibitor's entropic optimization with favorable negative entropic contribution ($-T\Delta S$) and negative enthalpy, resulting in negative favorable Gibbs energy that is characteristic of high affinity ligands.

Keywords: *Mycobacterium tuberculosis*, tuberculosis, pyrimidine synthesis, orotate phosphoribosyltransferase, selective inhibitors.

Abbreviations: TB – tuberculosis; MTB – *Mycobacterium tuberculosis*; OPRT – orotate phosphoribosyltransferase; OA – orotate; PRPP – α-D-5-phosphoribosyl-1-pyrophosphate; OMP – orotidine 5'-monophosphate; PP_i – pyrophosphate.

Tuberculosis (TB) is an ancient human chronic infection disease [1] caused mainly by *Mycobacterium tuberculosis* (MTB). [2] According to the World Health Organization this disease has been responsible for the death of over 2 million people annually, and in 2009 there were an estimated 26 deaths per 100 000 population. [3] TB treatment regimen includes six month therapy with rifampicin and isoniazid, supplemented with pyrazinamide and ethambutol in the first two months. [4, 3] The poor compliance to the current treatment, owing to its length and side-effects, [5] along with HIV infection emergence, leads to the occurrence of multi drug-resistant and extensively drug-resistant TB strains, for which the standard treatment shows no bactericidal and sterilizing activity. [4, 6] Recently, a totally resistant strain, denoted as TDR-TB, has been described as resistant to all first and second line classes of anti-TB drugs tested. [7, 8] Thus, novel TB treatments should be active against drug-resistant strains, and, ideally, be able to eliminate latent forms of TB. Latent TB represents a significant infection reservoir, [9] since almost 32% of world population is positive on tuberculin purified protein derivative skin test. [3]

The nucleotide metabolism is an essential pathway for microorganism viability, [10] including MTB and *Mycobacterium bovis* BCG. [11] In addition, *de novo* pyrimidine biosynthesis has already been shown to be required for virulence of other obligatory parasites, [12, 13] in which disruption of this pathway leads to avirulent pyrimidine auxotrophs. [12]

Orotate phosphoribosyltransferase (OPRT, EC 2.4.2.10) catalyzes the fifth reaction in the *de novo* synthesis of pyrimidine nucleotides, converting orotate (OA) and α-D-5-phosphoribosyl-1-pyrophosphate (PRPP) into orotidine 5'-monophosphate (OMP) and pyrophosphate (PP_i), in the presence of Mg^{2+} (Fig. 1).

(Fig. 1)

The metabolism required for sustaining mycobacterial survival during TB latency is still poorly understood, however, experimental evidence demonstrated the maintenance of nucleotide synthesis even in latent bacillus. [14] A specific inhibitor that targets a nucleotide synthesis enzyme has thus the potential of being effective against both active and latent TB.

Since disruption of *de novo* pyrimidine pathway gives rise to avirulent strains of obligatory parasites, [12, 13] MTB OPRT (*Mt*OPRT) might not only be target for TB treatment, but also prophylaxis, enhancing current TB BCG-based vaccines whose efficacy is highly inconsistent. [15] OPRT homologues are targets for the development of inhibitors to treat malaria [13, 16, 17, 18] and toxoplasmosis. [19] OPRT inhibitor development is also employed in cancer treatment for its role in 5-fluoruracil metabolism. [20, 21] *Salmonella typhimurium* OPRT inhibitors have also been already described. [22]

Molecular, kinetics and thermodynamic characterizations of *Mt*OPRT will be described elsewhere (Breda, et al. manuscript in preparation). Characterization of *Mt*OPRT prompted us to propose, synthesize and test several potential specific inhibitors. Accordingly, a series of derivatives (Schemes 1 and 2) of pyridine-2(1*H*)-one (Fig. 2) were synthesized, and their *in vitro* mode of inhibition of *Mt*OPRT enzyme activity were evaluated by steady-state kinetics. As data on *Mt*OPRT's substrate thermodynamic signatures and affinities (K_d) were previously collected, these values were compared with the ones for inhibitors of *Mt*OPRT enzyme activity. These results suggest that compound **6** is a promising lead molecule. In addition, compounds **2**, **5**, **7** and **8** showed slight inhibitory profile while their analogues **1**, **3** and **4** did not show any detectable inhibitory activity of *Mt*OPRT enzyme (Table 1).

(Fig. 2)

(Table 1)

It is noteworthy that inhibitory activity was increased by the presence of electron withdrawing groups attached at 3- and 5-position on the pyridine-2(1*H*)-one rings of tested compounds; where the compound 5-chloro-substituted **2** showed 18% of inhibitory activity while its analogue **1** showed no inhibitory activity. The same pattern could be observed for compounds **4** and **5**, where 3-nitro substituted compound **5** inhibited the enzymatic activity of *Mt*OPRT in 15% at 100 μM while compound **4** was ineffective in the same conditions. The presence of these groups can increase the acidity of the hydrogen bound to the nitrogen of heterocyclic pyridine-2(1*H*)-one rings improving the putative interactions via hydrogen bonds with *Mt*OPRT active site. There also seems to be a need for the presence of the nitrogen (NH) in the pyridinone system for inhibitory activity as compound **6** inhibitory activity (90%) is superior as compared to compound **7** (15%) both at 100 μM (Table 1). This result is in accordance with data from literature which showed that N1 of OA performs important interactions with *Toxoplasma gondii* OPRT active site. [19] Worth mentioning are the results exhibited by isoniazid (**8**), the most prescribed and commercially available anti-tuberculosis drug, [4, 3] which was able to inhibit the enzymatic activity of *Mt*OPRT in 10% at concentration of 100 μM. Therefore, at larger concentration values, OPRT activity can also be modulated by isoniazid; corroborating its role as a promiscuous drug towards MTB targets. [23] Isoniazid is a pro-drug that is activated by KatG, a catalase peroxidase that oxidizes the molecule to an acyl radical which binds covalently to NADH. This adduct is a potent inhibitor of NADH-dependent enoyl-acyl carrier protein reductase InhA [24], and, based on proteome analysis, shows high affinity for another 17 proteins in *M. tuberculosis*. [23]

Compounds **5** and **6** were thus selected for further optimization. Although compound **2** displayed a better inhibitory profile (18%) as compared to **5** (15%), we favored **5** over **2** since the former presents the nucleophilic 5-position unoccupied, an important feature for our initial strategy of introducing amino alcohol derivatives as side chains in pyridine-2(1*H*)-one rings **5** and **6**. Acyclic mimics of the ribooxacarbenium ion as transition state analogues of purine nucleoside phosphorylases led to synthesis of compounds with nanomolar

dissociation constants. [25] We relied on the possibility that such amino alcohol derivatives would mimic the α-D-ribose leading to compounds more structurally similar to OMP product of *Mt*OPRT enzyme.

Compounds **9-12** were synthesized by classical Mannich reaction [26] with 63-95% yields (Scheme 1). The reactions were performed starting from **5** in the presence of amine or amino alcohol and paraformaldehyde using methanol as solvent. The reaction mixture was heated in sealed tube at 100°C for 2-18 h. All such compounds showed spectrometric properties corresponding to the proposed structures; and were then tested as potential inhibitors of *Mt*OPRT enzyme activity. None of these compounds showed better inhibitory activity as compared to the parent compound (Table 1). Based on these disappointing results, our efforts were them directed at studying compound **6** and their derivatives.

(Scheme 1)

The hydrophobic character of **6** was improved by condensation reaction of benzaldehydes in the presence of ethanol as solvent (Scheme 2). The reactions were conducted on reflux for 16-24 h furnishing the compounds **13-14** in 15-22% yield. This low yield can be attributed to formation of lactones derivatives in these reactions. [28] The Mannich reaction was also employed to obtain the amino and amino alcohol derivatives of **6** (Scheme 2). Likewise the reactions for synthesis of **9-12** the compounds **15-16** were obtained by reaction of **6** and amino derivatives compounds in the presence of paraformaldehyde and methanol as solvent. The reaction mixtures were heated at 100°C for 2-3 h leading to synthesis of the respective compounds with 43-78% yield (Scheme 2). In all performed attempts the dialkylated compound **16** was obtained as major product although the molar ratio was 1:1 pyridine-2(1*H*)-one **6** and dimethylamine. All synthesized compounds **13-16** showed spectrometric properties corresponding to the proposed structures.

(Scheme 2)

As carried out for compounds **1-8**, measurements of *Mt*OPRT (26 nM) activity in presence of saturating concentrations of both substrates was considered 100% under assay conditions. Effects of compounds **13-16** at 100 μM final concentration on *Mt*OPRT activity were evaluated. Compound **13** showed better inhibitory activity (95%) as compared to **14** (60%), which suggests that the presence of a hydroxyl group attached at 2-position of the phenyl substituent reduce the inhibitory activity (Table 1). Therefore, modest changes in analogue structure seem to cause relatively large changes in the ability to inhibit *Mt*OPRT activity. Compounds **15** and **16** showed inhibitory activity of, respectively, 71% and 40%. Based on these data, the dialkylated compound **16** seems to possess steric restriction which could reduce its interaction with *Mt*OPRT. We have set a threshold of 60% inhibitory activity of a specific compound as a starting point to carry out detailed determination of the mode of inhibition. Accordingly, compounds **6**, **13-15** (Table 1) were selected for further studies. None of these compounds presented time-dependent inhibition, which was assessed by measuring *Mt*OPRT enzyme activity at varied times (up to 30 min) withdrawing aliquots of a reaction mixture containing enzyme and either compound **6**, **13**, **14** or **15** (*data not show*). [29]

Inhibition assays [30] for **6**, **13-15** showed that these compounds are competitive inhibitors with respect to OA substrate (Fig. I of Supplementary data). Accordingly, compounds **6**, **13-15** compete with OA for binding to free *Mt*OPRT enzyme ($E + OA \rightarrow E \cdot OA$), thereby indicating that they are structural mimics of OA substrate. [31] On the other hand, compounds **6**, **13-15** displayed uncompetitive inhibition with respect to PRPP substrate (Fig. I of Supplementary data). These data suggest that these compounds can only bind after PRPP binding to *Mt*OPRT. These results are in agreement with *Mt*OPRT Mono-Iso Ordered Bi Bi kinetic mechanism (Fig. 3). Hence, as compounds **6**, **13-15** are OA analogs and binding of PRPP must precede OA binding, compounds **6**, **13-15** compete with OA for molecular interactions with the $MtOPRT \cdot PRPP$ binary complex. On the other hand, as PRPP binding is followed by OA, compounds **6**, **13-15** behave as uncompetitive inhibitors with respect to PRPP, showing increased binding to increasing concentrations of $MtOPRT \cdot PRPP$ binary complex as PRPP concentration increases, and subsequent competitive inhibition towards OA binding to the binary complex.

(Fig. 3)

Binding of lead-like compounds **6** and **13** to *Mt*OPRT active site was further characterized by ITC assays. [32] The ITC data (Fig. II of Supplementary data) were fitted to one set of sites binding model, indicating that there is no difference of binding affinity between the two active sites of homodimeric *Mt*OPRT. Thermodynamic constants for **6** binding were: ΔH= -9.8 (± 0.1) x 10^3 cal/mol; $-T\Delta S$= 390 (± 6) cal/mol/deg; ΔG= -9.4 (± 0.1) x 10^3 cal/mol; K_a= 7 (± 1) x 10^6 M^{-1}; and K_d= 0.14 (± 0.03) μM. For **13**, thermodynamic constants are: ΔH= -6.59 (± 0.05) x 10^3 cal/mol; $-T\Delta S$= -3.04 (± 0.02) x 10^3 cal/mol/deg; ΔG= -9.63 (± 0.07) cal/mol; K_a= 12 (± 2) x 10^3 M^{-1}; and K_d= 0.09 (± 0.01) μM (Fig. 4). Both molecules displayed 1:1 binding stoichiometry (N = 0.962 ± 0.005 for **6** and 1.05 ± 0.03 for **13**), indicating that one molecule of inhibitor binds to each OPRT subunit.

(Fig. 4)

Thermodynamic data indicate a predominant negative enthalpy (ΔH) and favorable Gibbs free energy (ΔG) upon binding of compounds **6** and **13** to *Mt*OPRT. Taken together, these data are indicative that binding of compounds **6** and **13** to *Mt*OPRT are favorable spontaneous processes mainly ruled by formation of favorable hydrogen bonds and/or van der Waals interactions (negative ΔH). Binding of compound **13** appears to be accompanied by release of "bound" water molecules to bulk solvent (negative $-T\Delta S$). On the other hand, the negative entropic contribution (positive $-T\Delta S$ term) for compound **6** implies the occurrence of a conformational change upon binary complex formation. [33] It is likely that it corresponds to a protein isomerization step upon ligand binding, characteristic of enzymes that adopt Iso Mechanisms. [34] Moreover, it has been reported that movements of a catalytic flexible loop are integral to catalysis of

phosphoribosyltransferase enzymes, [35] allowing closing of active site, recruitment of catalytic essential residues, and displacement of water molecules to bulk solvent. [36] Binding of OMP to *Mt*OPRT displays similar thermodynamic discrimination profile (**Fig. 4**), which could be explained by conservation of OA and OMP pharmacophoric molecular scaffold as compound **6**. It is thus tempting to suggest that compounds **6** and **13** can make key enzyme-ligand contacts in *Mt*OPRT active site at positions N3, C4 and C6, in accordance with three-dimensional structures of OPRT homologues in complex with ligands, [37, 38, 39] and available data for *Toxoplasma gondii* enzyme. [19]

Interestingly, the favorable enthalpic and entropic contributions of molecule **13** binding to *Mt*OPRT are favorable thermodynamic profiles for high affinity ligands. [40] Gibbs free energy value for compound **13** is larger than the value for **6**, which results in lower dissociation constant for the former. Compound **13** binding process shows a slight loss in enthalpy and an improvement in entropy, which could be attributed to release of solvation water molecules of the aromatic ring of **13** not present in **6**. In addition, binding of compound **6** appears to be accompanied by small unfavorable conformational entropy change [41] (active site loop closure), which is not present in compound **13** binding process. It is thus tempting to suggest that the lower K_i values for **13** is due to entropy optimization by increasing its hydrophobicity, which is also reflected on the enhancement of its logP and logD values. These physical properties were, respectively, 0.714 and -3.92 for compound **6**, and 0.938 and -2.58 for compound **13** (pH 8.0).

Enthalpy and entropy simultaneous optimization are the major goal in drug discovery, which is not trivial due to enthalpy/entropy compensation. [40] Interestingly, the ITC data for compounds **6** and **13** binding to *Mt*OPRT suggest a compensatory system, since the values of ΔH and $-T\Delta S$ change drastically, while the free energy and affinity values are similar (**Fig. 4**).

In summary, the results presented here are expected to aid in the design of potent and selective *Mt*OPRT inhibitors. In addition, an entropically optimized *Mt*OPRT enzyme inhibitor compound was obtained from classical improvement of its hydrophobic character.

Acknowledgements
This work was supported by funds of National Institute of Science and Technology on Tuberculosis (INCT-TB), MCT-CNPq, Ministry of Health - Department of Science and Technology (DECIT) - Secretary of Health Policy (Brazil) to D.S.S. and L.A.B. L.A.B. and D.S.S. also acknowledge financial support awarded by FAPERGS-CNPq-PRONEX-2009. L.A.B. (CNPq, 520182/99-5) and D.S.S. (CNPq, 304051/1975-06) are Research Career Awardees of the National Research Council of Brazil (CNPq). A.B. acknowledges a scholarship awarded by BNDES. P.M. and L.A.R. acknowledge scholarships awarded by CNPq.

References

1. Rustad, T.; Sherrid, A.; Minch, K.; Sherman, D. Cell. Biol. 2009, 11, 1151-1159.
2. Ducati, R.; Ruffino-Netto, A.; Basso, L. A.; Santos, D. S. Mem. Instit. Oswaldo Cruz. 2006, 7, 697-714.
3. World Health Organization. Global Tuberculosis Control - Epidemiology, Strategy, Financing. 2009. Available from: www.who.int/tb/publications/global_report/2009.
4. Ma, Z.; Lienhardt, C.; McIlleron, H.; Nunn, A.; Wang, X. Lancet. 2010, 375, 2100-2109.
5. Zaleskis, R. Eur. Respirat. Dis. 2006, 47-49.
6. Russell, D. G.; Barry 3rd, C. E.; Flynn, J. L. Science. 2010, 328, 852-856.
7. Velayati. A.; Farnia, P.; Masjedi, M.; Ibrahim, T.; Tabarsi, P.; Haroun, R.; et al. Eur. Resp. J. 2009, 34, 1202-1203.
8. Velayati, A.; Masjedi, M.; Farnia, P.; Tabarsi, P.; Ghanavi, J.; ZiaZarifi, A.; et al. CHEST. 2009, 136, 420-425.
9. Gomez, J.; MdKinney, J. Tuberculosis. 2004, 84, 29-44.
10. Hasan, S.; Daugelat, S.; Rao, P. S. S.; Schreiber, M. PLoS Comput. Biol. 2006, 2, e61.
11. Sassetti, C.; Dana, H.; Rubin, E. Mol. Miccrobiol. 2003, 48, 77-84.
12. Fox, B.; Bzik, D. Nature. 2002, 415, 926-930.
13. Krungkrai, S.; Aoki, S.; Palacpac, N.; Sato, D.; Mitamura, T.; Kungkrai, J.; et al. Mol. Biochem. Parasitol. 2004, 134, 245-255.
14. Boshoff, H.; Barry 3rd, C. E. Nature Rev. Microbiol. 2005, 3, 70-80.
15. Pando, R.; Aguilar, L.; Infante, E.; Cataldi, A.; Bigi, F.; Martin, C.; et al. Tuberculosis. 2006, 86, 203-210.
16. Zhang, Y.; Schramm, V. L. JACS. 2010, 132, 8787-8794.
17. Abdo, M.; Zhang, Y.; Schramm, V. L.; Knapp, S. Org. Let. 2010, 12, 2982-2985.
18. Zhang, Y.; Luo, M.; Schramm, V. L. J. Am. Chem. Soc. 2009, 131, 4685-4694.
19. Javaid, Z. Z.; el Kouni, M. H.; Ilzsch, M. H. Biochem. Pharmacol. 1999, 58, 1457-1465.
20. Temmink, O.; Bruin, M.; Turksma, A.; Cricca, S.; Laan, A.; Peters, G. IJBCB. 2007, 39, 565-575.
21. Ichikawa, W. Gastric Cancer. 2006, 9, 145-155.
22. Witte, J. F.; Bray, K. E.; Thornburg, C. K.; McClard, R. W. Bioorg. Med. Chem. Let. 2006, 16, 6112-6115.
23. Argyrou, A.; Jin, L.; Siconilfi-Baez, L.; Angeletti, R. H.; Blanchard, J. S. Biochemistry. 2006, 45, 13947-13953.
24. Schroeder, E. K.; Basso, L. A.; Santos, D. S.; Souza, O. N. Biophys. J. 2005, 89, 876-884.
25. Taylor, E. A.; Clinch, K.; Kelly, P. M.; Li, L.; Evans, G. B.; Tyler, P. C.; et al. J. Am. Chem. Soc. 2007, 129, 6984-6985.

26. Mannich, C.; Krösche, W. Archiv der Pharmazie. 1912, 250, 647-667.

27. *Enzymatic activity assay* – All chemicals were purchased from Sigma Aldrich. Effect of each inhibitor on *Mt*OPRT activity was measured by direct monitoring OA consumption. The assay was performed in quartz cuvettes with UV-visible Shimadzu spectrophotometer UV2550 equipped with a temperature-controlled cuvette holder. Reaction mixture (500 µL) contained Tris HCl 50 mM $MgCl_2$ 20 mM pH 8.0, OA 50 µM, PRPP 500 µM and *Mt*OPRT 26 nM. Reaction was started by the addition of enzyme, and followed a linear progress curve of absorbance change at 295 nm up to 60 sec at 25°C. The extinction coefficient of this conversion was 3950 $M^{-1}cm^{-1}$. [42] Inhibitors were then added to reaction mixture at final concentration of 100 µM and enzyme activity was measured as before. All enzymatic activity and further assays were performed in duplicate or triplicate. Selection of inhibitors for further assays was based on observed activity difference in absence and presence of inhibitor at 100 µM, and set to a 60% inhibitory activity cutoff.

28. Wiley, R. H.; Kraus, H. J. Org. Chem. 1956, 21, 757-758.

29. *Time-dependency* – Evaluation of time-dependency of observed inhibitory activity was evaluated at same enzymatic assay conditions described above. Reaction was started by addition of *Mt*OPRT 26 nM previous incubated with inhibitor compounds at final concentration of 1 µM in the reaction mixture. Inhibitory activity was evaluated at distinct *Mt*OPRT and inhibitor compound incubation times, up to 30 minutes.

30. *Inhibition assay* – Inhibition assays were conducted in final volume 500 µL reactions, at 25°C, monitoring OA consumption at 295 nm for 60 sec, where one substrate concentration was held constant at saturation (5 times its K_M value, OA 50 µM and PRPP 500 µM) while the second substrate was varied (PRPP: 25-500 µM, OA: 12-75 µM), in absence and presence of varied concentrations of each inhibitor (**6**: 0.4-10 µM, **13**: 0.2-12 µM, **14**: 4-100 µM, **15**: 16-150 µM), in Tris HCl 50 mM $MgCl_2$ 20 mM, with 26 nM *Mt*OPRT. Double reciprocal data were fitted to **Eq. (1)** and **Eq. (2)** that describes competitive and uncompetitive inhibition mechanisms respectively (v, V, A, and I correspond to the steady-state reaction rate; reaction V_{max}; substrate A and inhibitor I concentrations. K is varied substrate K_M value; K_i is the dissociation constant of inhibitor I). All measurements were performed in duplicate or triplicate with at least five varied substrate and inhibitor concentrations.

$$v = VA/[K(1 + I/K_i) + A] \qquad \textbf{Eq. (1)}$$

$$v = VA/[A(1 + I/K_i) + K] \qquad \textbf{Eq. (2)}$$

31. Copeland, R. A. Evaluation of Enzyme Inhibitors in Drug Discovery; John Wiley & Sons: 2005, Chapter 3.

32. *Binding assays* – Inhibitor binding to *Mt*OPRT were evaluated by isothermal titration calorimetry (ITC) with iTC_{200} Microcalorimeter (Microcal, Inc., Northampton, MA). Reference cell (200 µL) was loaded with Millie-Q water during all assays. The injection syringe (39.7 µL) was filled with inhibitors **6** and **13** 400 µM; ligand binding isotherms were measured by direct titration (ligand into macromolecule). Titration first injection (0.5 µL) was not used in data analysis and was followed by 13 injections of 2.26 µL plus 12 injections of 1.13 µL each, spaced by 180 sec, into *Mt*OPRT 60 µM incubated with PRPP 500 µM (sample cell). *Mt*OPRT and ligand solutions contained $MgCl_2$ 20mM in buffer Gly-Gly 100 mM pH 8.0, in substitution of Tris HCl 50 mM due to high enthalpy of ionization of Tris. [43] Control titrations (ligand into buffer) were performed in order to subtract the heats of dilution and mixing for each experiment prior to data analysis. Thermodynamic constants were derived from **Eq. (3)**, where ΔH is the enthalpy of process given by the ITC experiment, ΔG is the Gibbs free energy change, ΔS is the entropy change, *T* is the temperature of the experiment in Kelvin, *R* is the gas constant (1.987 cal K^{-1} mol^{-1}), and K_a is the association constant. The dissociation constant, K_d, was calculated by the inverse of K_a. All data were evaluated utilizing the Origin 7 SR4 software (Microcal, Inc., Northampton, MA). Entropy values are depicted as $-T\Delta S$.

$$\Delta G = \Delta H - T\Delta S = RT \ln K_a \qquad \textbf{Eq. (3)}$$

33. O'Brien, R.; Haq, I. In Biocalorimetry 2 Applications of calorimetry in the biological sciences; Ladbury, J. E.; Doyle, M. L. USA: John Wiley & Sons; 2004; pp 3-34.

34. Rebholz, K. L.; Northrop, D. B. Met. Enzymol. 1995, 249, 211-239.

35. Sinha, S. C.; Smith, J. L. Cur. Op. Struct. Biol. 2001, 11, 733-739.

36. Wang, G.; Lundegaard, C.; Jensen, K.; Grubmeyer, C. Biochemistry. 1999, 38, 275-283.

37. Scapin, G.; Grubmeyer, C.; Sacchettini, J. C. Biochemistry. 1994, 33, 1287-1294.

38. Scapin, G.; Ozturk, D. H.; Charles, G.; Sacchettini, J. C. Biochemistry. 1995, 34, 10744-10754.

39. González-Segura, L.; Witte, J. F.; McClard, R. W.; Hurley, T. D. Biochemistry. 2007, 46, 14075-14086.

40. Freire, E. Drug Discov. Today. 2008, 13, 869-874.

41. Roselin, L. S.; Lin, M. S.; Lin, P. H.; Chang, Y.; Chen, W. Y. Biotechnol. J. 2010, 5, 85-98.

42. Krungkrai, S.; DelFraino, B.; Smiley, J.; Prapunwattana, P.; Mitamura, T.; Horii, T.; et al. Biochemistry. 2005, 5, 1643-1652.

43. Fukada, H.; Takahashi, K. Proteins: Structure, Function, and Genetics. 1998, 33, 159-166.

Figure legends

Fig. 1. OPRT catalyzed conversion of OA and PRPP into PP_i and an *N*-glycosidic bond of OMP, in the presence of Mg^{2+}.

Fig. 2. Commercially available chemical compounds tested *in vitro* as possible *Mt*OPRT inhibitors.

Fig. 3. Mono-Iso Ordered Bi Bi kinetic mechanism of *Mt*OPRT. Substrates bind to enzyme's active site in an ordered fashion, followed by a non chemical rate-limiting step (conformational change from *E* to *E*′ form) prior to catalysis, with ordered product release.

Fig. 4. Thermodynamic discrimination profiles of lead-like compounds **6** and **13**.

Schemes legends

Scheme 1. Reactants and conditions: (*i*) $NHR^1(R^2)$, $OH(CH_2O)_nH$ (*n* = 8-100), MeOH, 100°C, 2-18 h.

Scheme 2. Reactants and conditions: (*i*) R^1-2-Ph(CHO), EtOH, reflux, 16-24 h. (*ii*) $NHR^1(R^2)$, $OH(CH_2O)nH$ (*n* = 8-100), MeOH, 100°C, 2-3 h.

Table 1. Observed inhibitory activity, and inhibitory constants, of pyridinone-based compounds over *Mt*OPRT catalyzed reaction.

Compound	*Observed inhibitory activity*[a]	K_i *OA (μM)*	*Inhibition mode*	K_i *PRPP (μM)*	*Inhibition mode*
1	none	--	--	--	--
2	18%	--	--	--	--
3	none	--	--	--	--
4	none	--	--	--	--
5	15%	--	--	--	--
6	90%	0.25 ± 0.03	competitive	8.21 ± 0.35	uncompetitive
7	15%	--	--	--	--
8	10%	--	--	--	--
9	2%	--	--	--	--
10	2.2%	--	--	--	--
11	7.5%	--	--	--	--
12	4%	--	--	--	--
13	95%	0.19 ± 0.01	competitive	6.5 ± 0.21	uncompetitive
14	60%	7.40 ± 0.62	competitive	140.06 ± 9.15	uncompetitive
15	71%	6.20 ± 0.45	competitive	135 ± 6.64	uncompetitive
16	40%	--	--	--	--

[a] Initial screening of possible inhibitors at 100 μM final concentrations in the assay mixtures. [(27)]

Figure01
Click here to download high resolution image

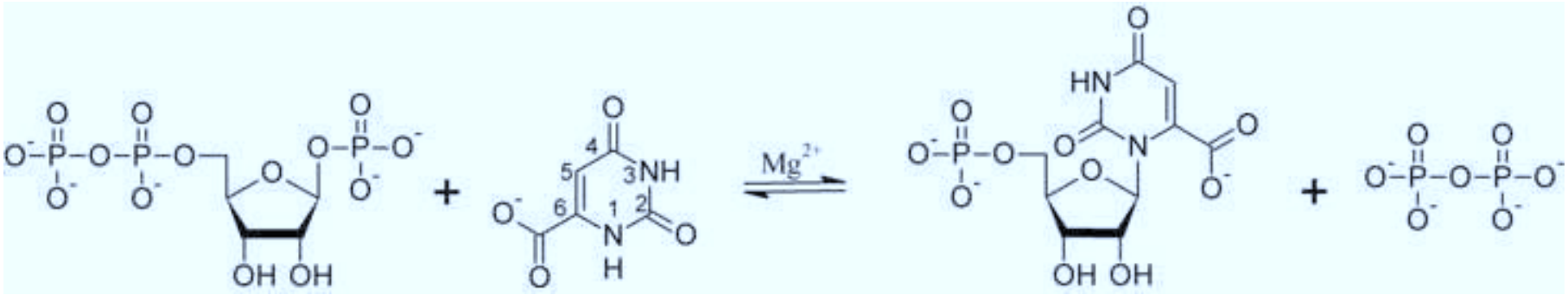

Figure02
Click here to download high resolution image

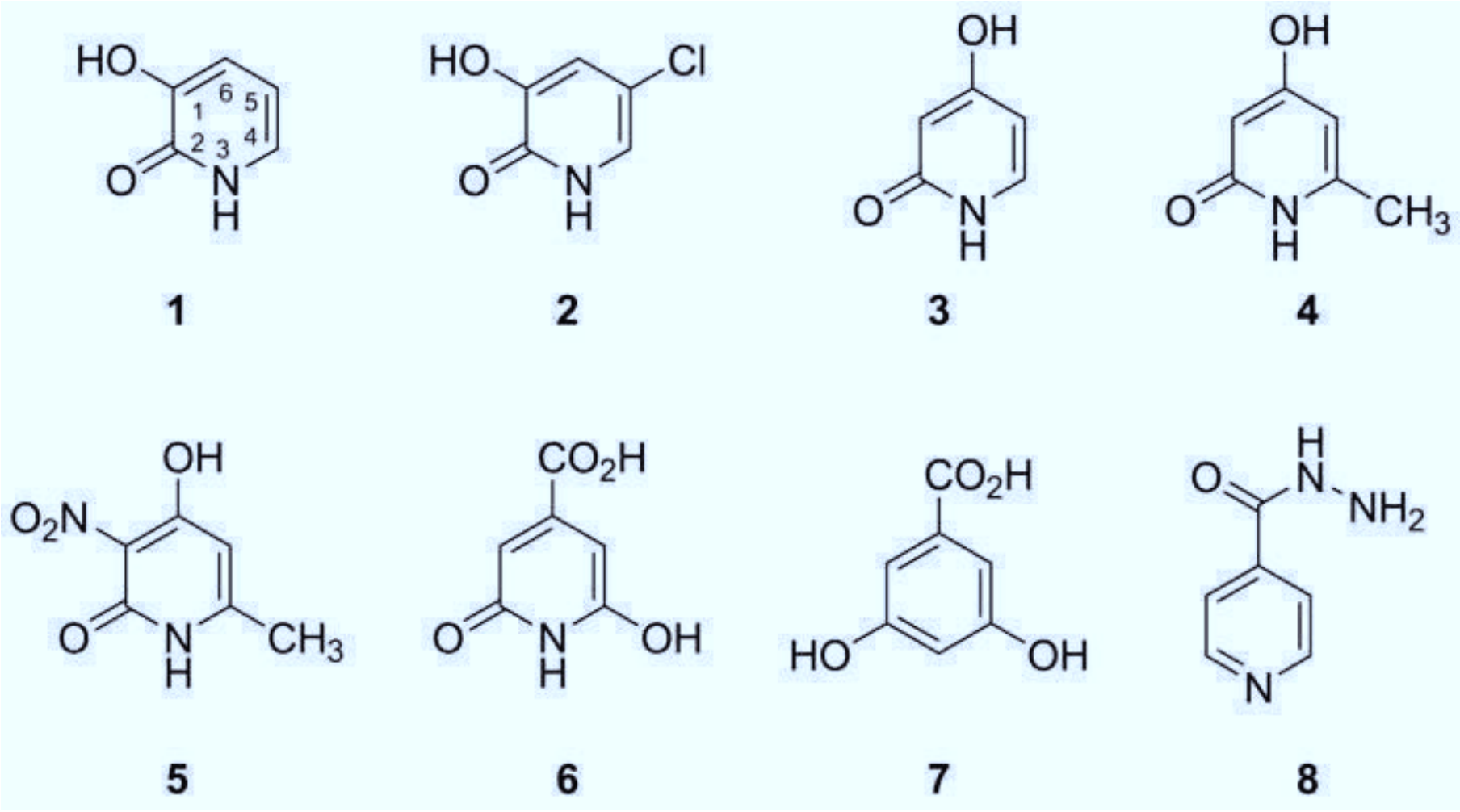

Figure03
Click here to download high resolution image

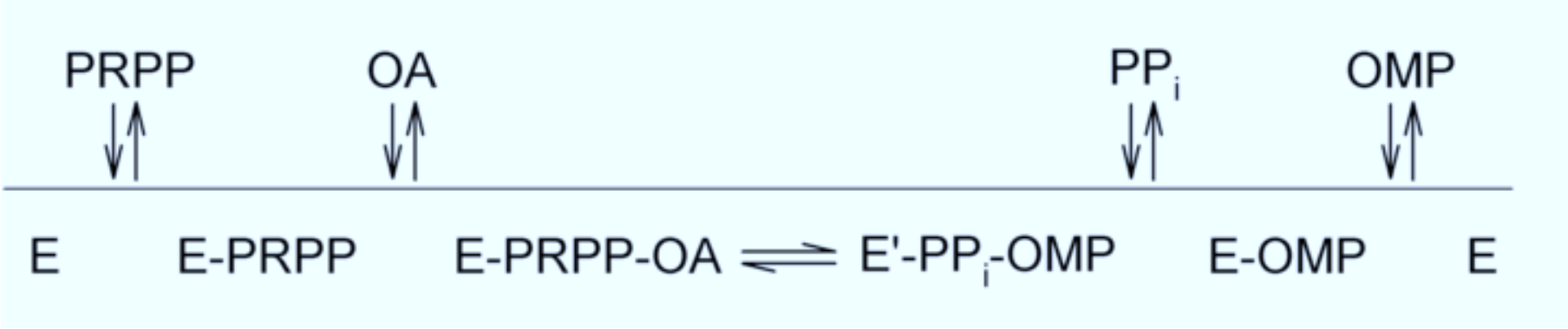

Figure04
Click here to download high resolution image

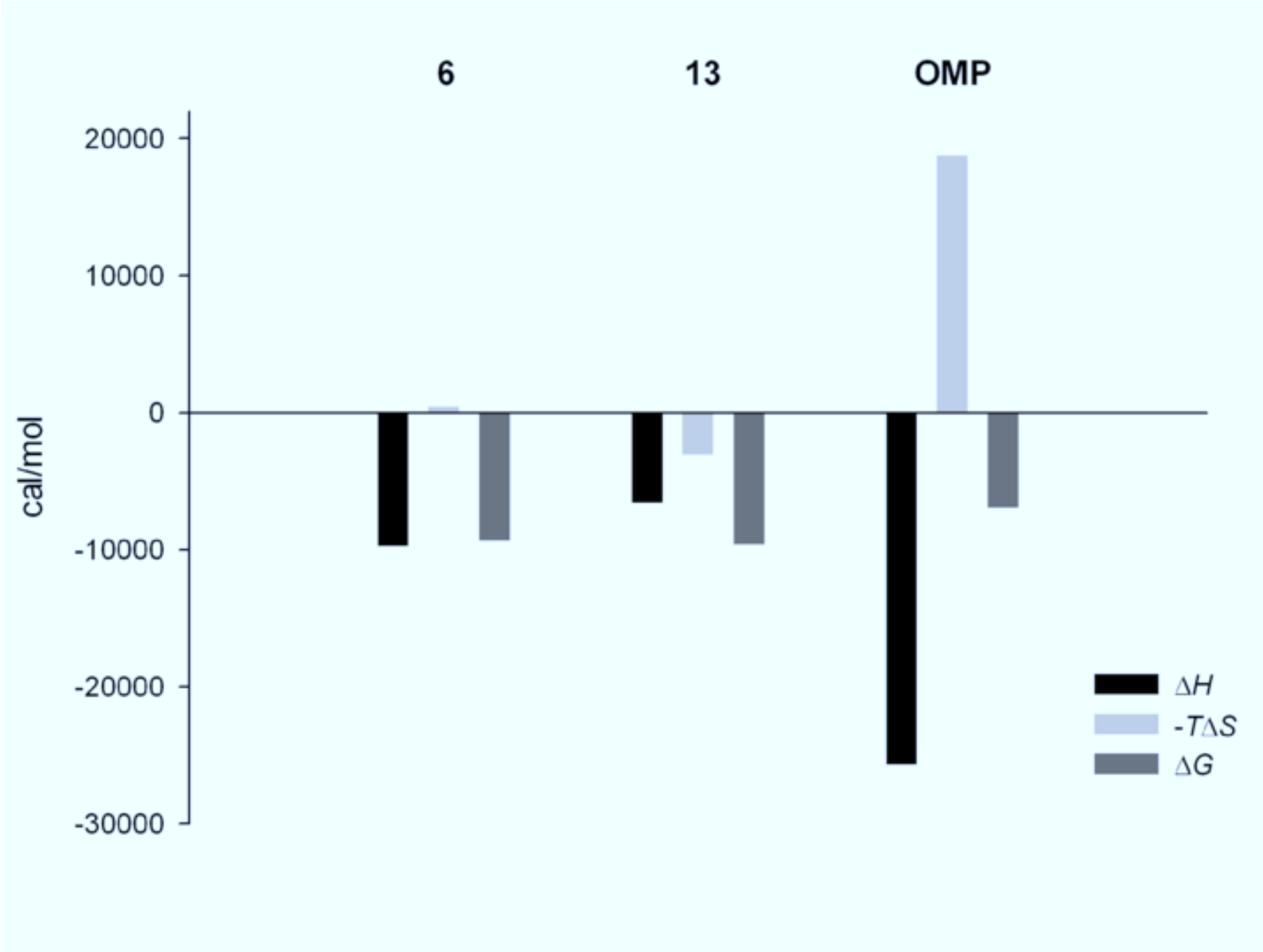

Scheme01
Click here to download high resolution image

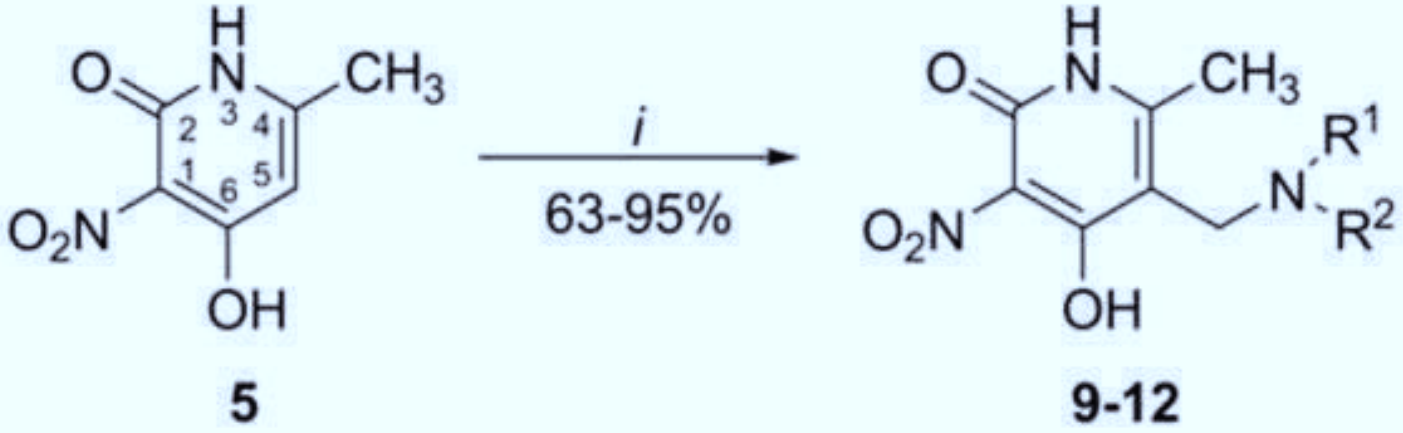

5 **9-12**

Entry	R^1	R^2	*Yield (%)*
9	CH_3	CH_3	95
10	H	CH_2CH_2OH	75
11	H	$CH_2CH(OH)CH_2OH$	63
12	H	$(CH_3)C(CH_2OH)CH_2OH$	82

Scheme02

Click here to download high resolution image

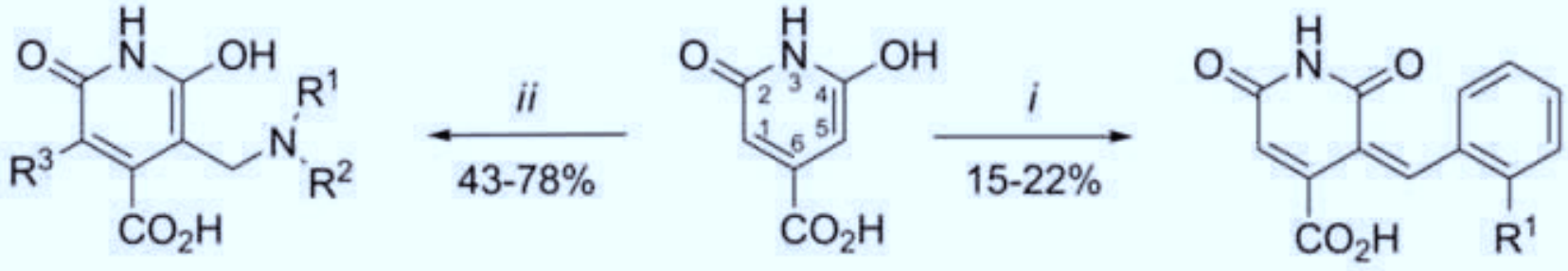

Entry	R^1	R^2	R^3	*Yield (%)*
13	H	--	--	22
14	OH	--	--	15
15	H	CH_2CH_2OH	H	43
16	CH_3	CH_3	$CH_2N(CH_3)_2$	78

SupplementaryMaterial_Breda

Click here to download Supplementary Material: Breda_et_al_supplementary.docx

Supplementary data

Fig. I. Double-reciprocal plot of inhibition assays for compounds **6** (A, B), **13** (C, D), **14** (E, F) and **15** (G, H). Pattern of intersecting lines at y-axis are prognostic of competitive inhibition towards OA and parallel lines indicate uncompetitive inhibition towards PRPP. Substrate OA was varied from 12-75 μM in presence of PRPP 500 μM (A, C, E, G), substrate PRPP was varied from 25-500 μM in presence of OA 100 μM. Each inhibitor variation range is depicted in the plots.

Fig. II. Ligand binding assays. Binding isotherms of **6** (A) and **13** (B) ITC data were fitted to sequential binding sites model.

Fig. I

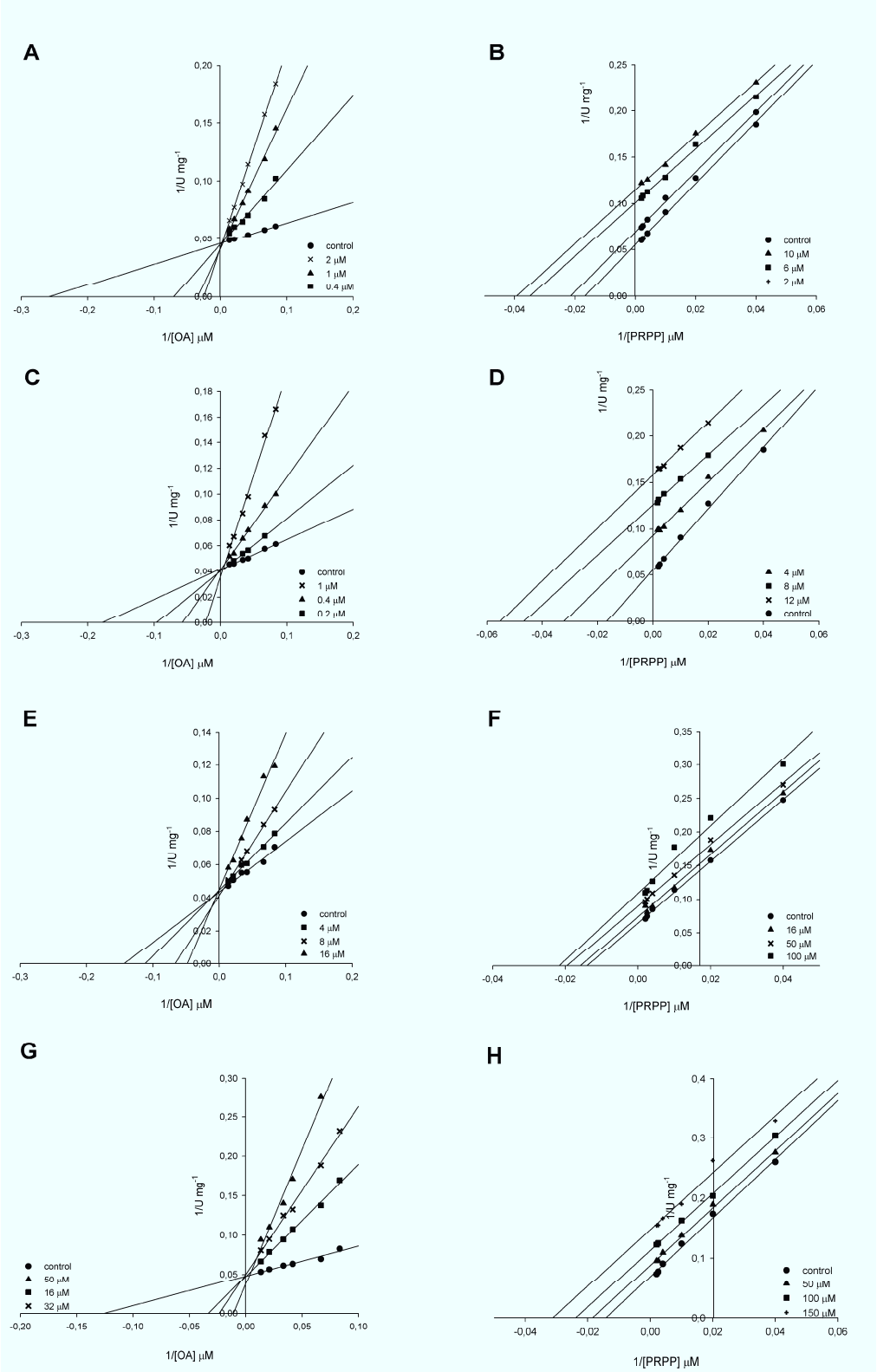
A
1/U mg-1
1/[OA] μM
control
2 μM
1 μM
B
1/U mg-1
1/[PRPP] μM
control
10 μM
6 μM
C
1/U mg-1
1/[OA] μM
control
1 μM
0.4 μM
D
1/U mg-1
1/[PRPP] μM
4 μM
8 μM
12 μM
control
E
1/U mg-1
1/[OA] μM
control
4 μM
8 μM
16 μM
F
1/U mg-1
1/[PRPP] μM
control
16 μM
50 μM
100 μM
G
1/U mg-1
1/[OA] μM
control
16 μM
32 μM
H
1/U mg-1
1/[PRPP] μM
control
100 μM
150 μM

Fig. II

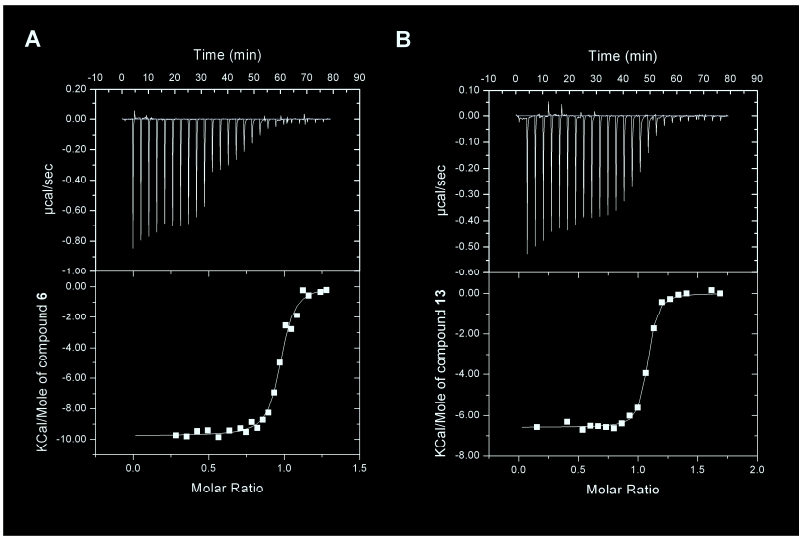
A
Time (min)
µcal/sec
KCal/Mole of compound 6
Molar Ratio
B
Time (min)
µcal/sec
KCal/Mole of compound 13
Molar Ratio

Capítulo 4

DETERMINAÇÃO DA ESTRUTURA TERCIÁRIA E QUATERNÁRIA DA ENZIMA OPRT DE *Mycobacterium tuberculosis* ATRAVÉS DE CRISTALOGRAFIA POR DIFRAÇÃO DE RAIOS X

Determinação da estrutura terciária e quaternária da enzima OPRT de *Mycobacterium tuberculosis* através de cristalografia por difração de raios x

A cristalografia por difração de raios X é a metodologia experimental considerada mais confiável para a determinação da estrutura terciária e quaternária de proteínas e tem relevância amplamente reconhecida no processo de desenvolvimento de novos fármacos de ação específica pela sua capacidade de resolução dos parâmetros estruturais relacionados à seletividade de substrato apresentada pelas enzimas (50).

As enzimas OPRT de *Saccharomyces cerevisiae* (51), *Salmonella typhimurium* (52, 53), *Escherichia coli* (54) e *Streptococcus mutans* (55) já tiveram sua estrutura resolvida experimentalmente, assim como a porção N-terminal da isoforma humana da enzima UMP sintase, que apresenta atividade OPRT (37); além das enzimas homólogas identificadas em *Aeropyrum pernix*, *Streptococcus pyogenes*, *Bacillus antracis*, *Francisella tularensis* e *Vibrio cholerae*, sendo que estas últimas têm suas estruturas resolvidas disponíveis no banco de dados PDB (*Protein Data Bank*) (56), embora seus artigos científicos correspondentes ainda não tenham sido publicados[1]. Concordando com as características que definem a família de enzimas PRTases do tipo I (40), estas enzimas apresentam baixa conservação de suas estruturas primárias (**Figura 8**) e grande conservação de suas estruturas terciárias e quaternárias (compostas por dímero de subunidades idênticas). A determinação do estado oligomérico, através de cromatografia líquida por exclusão de tamanho, da enzima de MTB indica que ela se apresenta como dímero em solução, independente da sua concentração (Capítulo 2), conforme o esperado de acordo com as demais enzimas OPRT já caracterizadas.

[1] Os códigos de acesso no PDB das estruturas citadas são respectivamente: 2PRY, 2PRZ e 2PS1; 1STO, 2LHO e 1OPR; 1ORO; 3DEZ; 2WNS; 2YZK; 2AEE; 3M3H; 3MJD; e 3N2L.

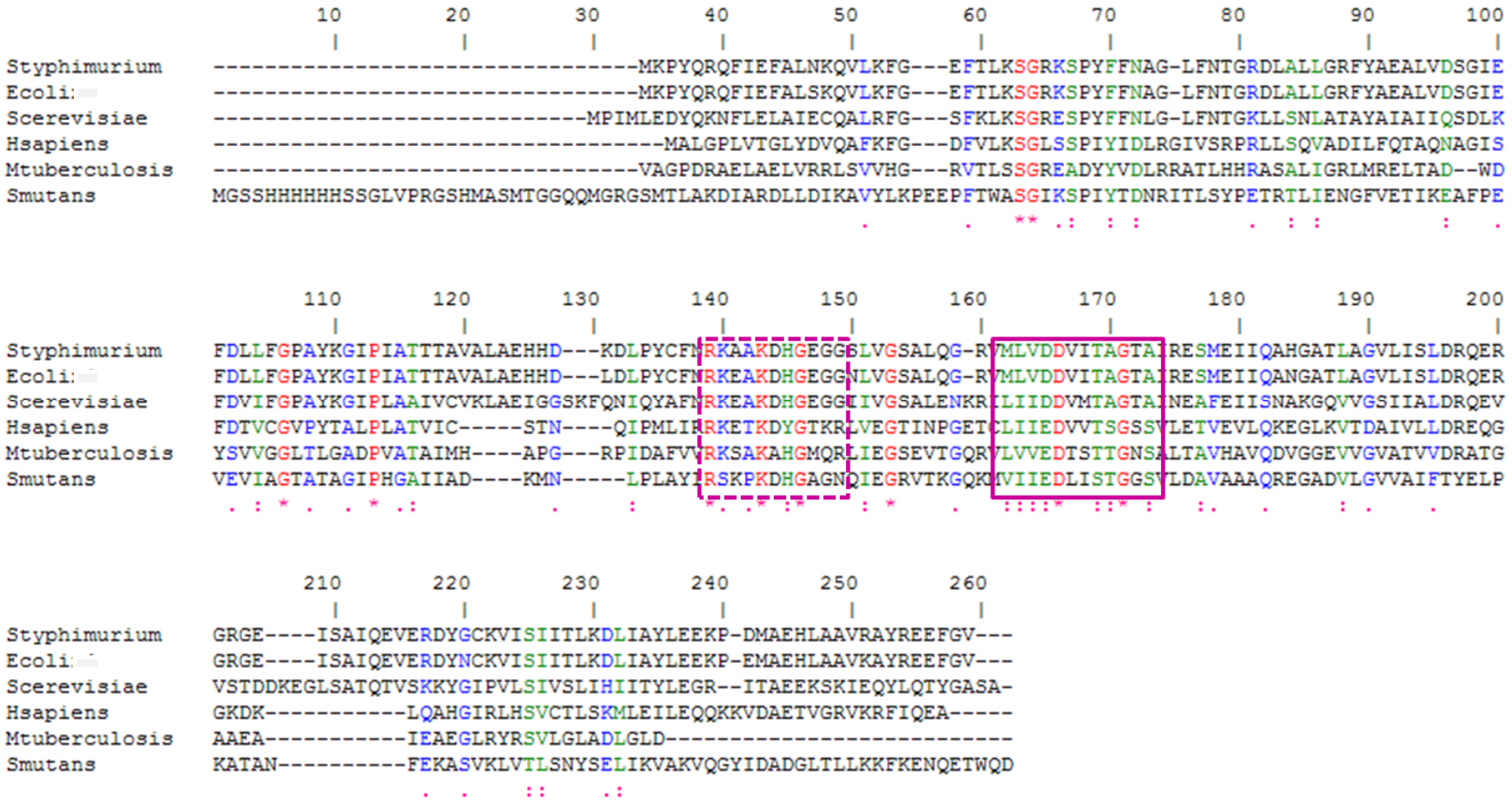

Figura 8. Alinhamento par-a-par das sequências de aminoácidos das enzimas OPRT de *S. typhimurium*, *E. coli*, *S. cerevisiae*, *H. sapiens* (porção N-terminal da enzima UMP sintase), MTB e *S. mutans* (sequências obtidas a partir do PDB, exceto para MTB, obtida do TubercuList), mostrando a não conservação das suas estruturas primárias, salvo pelo sítio de ligação ao PRPP (retângulo em linha cheia) e pelos aminoácidos que compõem o *loop* catalítico (retângulo em linha tracejada) – ver Capítulo 02.

Atualmente, existem 733 estruturas cristalográficas de proteínas codificadas no genoma de MTB depositadas no PDB, sendo a sua maioria (149 estruturas) determinada pelo TBSGC (*Tuberculosis Structural Genomics Consortium*) (57). O processo de determinação da estrutura de macromoléculas biológicas através da cristalografia por difração de raios X envolve quatro etapas principais: a obtenção de cristais com qualidade suficiente para a difração; a obtenção de dados; a determinação da estrutura; e por fim o refinamento e validação do modelo proposto (50), sendo a primeira a etapa limitante do processo, uma vez que características inerentes a cada proteína (como a sua organização estrutural, presença de ligantes ou metais divalentes, arranjo de sua estrutura quaternária, solubilidade, homogeneidade, entre outros) afetam o processo de obtenção de cristais (58).

Para a determinação da estrutura tridimensional da enzima OPRT de MTB foi utilizada a metodologia de difusão de vapor por *hanging-drop* (59), onde a solução da proteína recombinante homogênea 50 µM em tampão Gly-Gly 100 mM $MgCl_2$ 20 mM pH 8.0 foi misturada ao tampão presente no reservatório da placa (24 poços – 400 µL cada) em proporção 50/50 (vol/vol), em volume final de 2 µL. As gotas resultantes foram depositadas em lamínulas utilizadas para selar cada poço da placa, com a gotícula voltada para o interior do poço. Cada reservatório da placa de triagem foi selado e mantido a 20°C.

Neste processo de triagem foram utilizados os kits comerciais *Crystal Screen*, *Crystal Screen 2*, *PEG/Ion* e *Index* (Hampton Research Corp.), contendo 50, 48, 48 e 96 condições distintas de tampões, concentração de sais, pH, e presença de agentes crioprotetores como polietileno glicol. Diversas condições testadas tiveram como resultado a obtenção de microcristais que embora não sejam adequados para as etapas seguintes do processo de cristalografia são um indicativo de que a subunidade da macromolécula apresenta ordenamento estrutural ou simetria

suficiente para a viabilidade do processo de cristalização (59). A melhor condição de cristalização da enzima OPRT de MTB foi identificada na triagem realizada com *PEG/Ion*, em presença de tampão formiato de magnésio diidratado 0.2 M, 20% (w/vol) polietileno glicol, pH 7.0, utilizando a forma apo da enzima (na ausência de ligantes), conforme mostra a **Figura 9**, onde cristais foram observados cerca de 60 dias após a montagem do experimento de triagem.

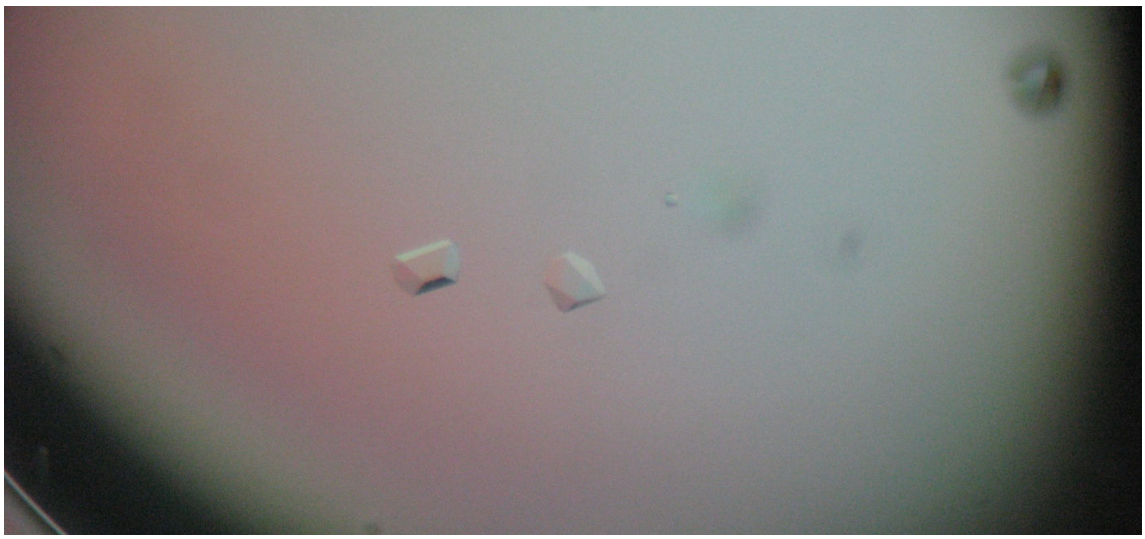

Figura 9. Cristais da enzima OPRT de MTB, obtidos pelo processo de difusão de vapor por *hanging-drop*, obtidos em tampão formiato de magnésio diidratado, que serão submetidos ao processo de difração de raios X.

Os cristais obtidos nesta condição serão também submetidos ao processo de *soaking* (60) para a obtenção da proteína ligada a seus substratos naturais (Capítulo 2) e aos inibidores identificados (Capítulo 3), permitindo a obtenção da estrutura tridimensional da OPRT de MTB na forma apo e na presença de ligantes, resultados que complementarão os resultados já obtidos (Capítulos 2 e 3), favorecendo principalmente o processo de desenvolvimento de inibidores específicos mais potentes. A estrutura terciária e quaternária da OPRT de MTB será resolvida no decorrer do primeiro semestre de 2011; a difração dos cristais gerados, tanto na forma enzimática apo quanto complexada a seus ligantes, será realizada no

Laboratório Nacional de Luz Sincrotron (LNLS, Campinas – SP), e o processamento de dados, refinamento e validação do modelo proposto serão realizados em parceria com o Laboratório de Bioquímica Estrutural – PUCRS, coordenado pelo Prof. Dr. Walter Filgueira de Azedo Jr.

Capítulo 5

NOCAUTE GÊNICO DA SEQÜÊNCIA DE DNA CORRESPONDENTE AO GENE *pyrE* DE *Mycobacterium tuberculosis*

Nocaute gênico da sequência de DNA correspondente ao gene *pyrE* de *Mycobacterium tuberculosis*

O metabolismo de nucleotídeos de purinas e pirimidinas é uma rota metabólica essencial para a viabilidade de microorganismos, e a via de síntese *de novo* de nucleotídeos de pirimidina já foi demonstrada experimentalmente como sendo essencial para a virulência de *Toxoplasma gondii*, onde a interrupção desta via resultou no desenvolvimento de cepas avirulentas e dependentes nutricionais de uracil (auxotrófos) (23). O mesmo estudo demonstrou que uma única injeção intramuscular destas cepas foi capaz de induzir resposta imune de longo prazo em *Mus musculus*; que se tornaram resistentes a infecções posteriores com cepas tipo-selvagem de *T. gondii* (23).

Micobactérias, incluindo o MTB apresentam enzimas da via de síntese *de novo* e de salvamento de nucleotídeos de purinas e pirimidinas, e a sua dependência de cada uma destas rotas metabólicas ainda não é clara (Capítulo 2). A obtenção de cepas de MTB com a deleção do gene *pyrE*, responsável pela codificação da enzima OPRT, pode resultar na inviabilidade da micobactéria caso o produto deste gene seja essencial, demonstrando a dependência da síntese *de novo* para a sobrevivência do bacilo; ou ainda, pode resultar em cepas com capacidade de infecção atenuada, como descrito acima, dependentes nutricionais de uracil, passíveis de serem utilizadas como amostras vacinais contra a TB.

A enzima OPRT foi escolhida como alvo para a obtenção de possíveis cepas atenuadas, pois codifica a quinta reação da via de síntese *de novo* de pirimidinas (**Figura 1** – **Capítulo 1**), gerando OMP, sendo esta a última etapa desta via em que não ocorre a intervenção da enzima UPRT (uracil fosforibosiltransferase), responsável pelo salvamento de bases livres de uracil, convertendo-as diretamente em UMP. A OPRT de MTB é ainda a enzima da rota codificada pelo gene de menor

extensão (540 pb), cerca de metade do número de pares de bases dos demais genes que codificam as enzimas responsáveis pela catálise das etapas anteriores à síntese de OMP (**Figura 5** – **Capítulo 1** e **Figura 10**).

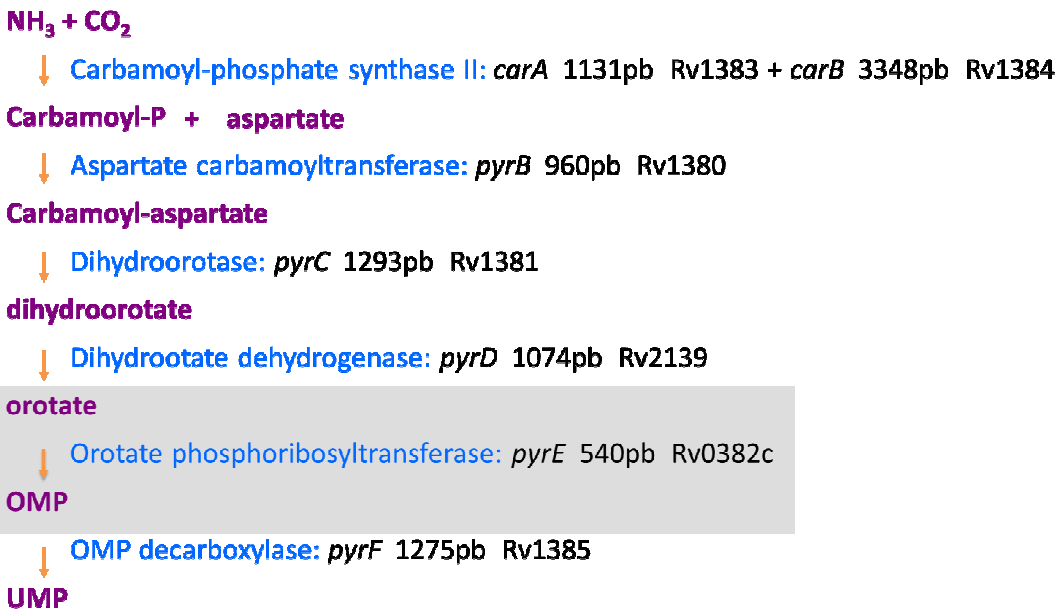

Figura 10. Via de síntese *de novo* de nucleotídeos de pirimidina, destacando as enzimas responsáveis pela catálise de cada etapa (azul), seus genes correspondentes em MTB e seu número de pares de base. A reação catalisada pela enzima OPRT está destacada pelo retângulo cinza.

A hipótese de trabalho se baseia na não essencialidade do gene *pyrE* e na obtenção de cepas incapazes de sintetizar nucleotídeos de pirimidina a partir de precursores simples, dependendo do salvamento de bases livres de uracil pela reação catalisada pela enzima UPRT para a obtenção de todos os nucleotídeos de pirimidina derivados de OMP. A interrupção desta rota metabólica poderá gerar cepas atenuadas, com capacidade de infecção reduzida, afetando o MTB nas formas ativas da TB, bem como o processo de reativação da doença, uma vez a disponibilidade de uracil no meio (proveniente de processos catabólicos ou apoptóticos do organismo hospedeiro) em que se o MTB se encontra pode ser limitado, visto que mamíferos realizam o salvamento de pirimidinas a partir de uridina

circulante, e não uracil, estando a uridina presente em concentrações plasmáticas entre 3 a 5 μM (61) ou 3 a 8 μM (62), variando conforme o tecido e tipo celular avaliado.

O objetivo dos experimentos apresentados neste capítulo é a realização do nocaute gênico do gene *pyrE* de MTB H37Rv através de estratégia de duas etapas desenvolvida por Parish e Stocker (63), que permite a substituição de uma sequência específica do DNA genômico por uma cópia contendo mutações definidas (substituição gênica por recombinação homóloga). Esta metodologia viabiliza a geração de uma provável cepa atenuada de MTB, dependente auxotrófico de uracil, e capaz de induzir resposta imune de longo prazo contra a TB.

Sequências de DNA de 1000 pares de bases (1 kb) localizadas nas regiões flanqueadoras 5' e 3' do gene *pyrE* foram amplificadas separadamente a partir do DNA genômico total de MTB através de reação em cadeia da polimerase (PCR). Para a amplificação da região flanqueadora 5' do gene *pyrE* foram utilizados os oligonucleotídeos iniciadores oprt1 (5'-gtctgcaggttgtgacctggtcgcattctc-3') e oprt2 (5'-ccaagcttagccaactctgcgcggtcagg-3') contendo sítios de restrição para as enzimas *Pst*I e *Hind*III (sublinhadas). A amplificação da região adjacente à porção 3' do gene *pyrE* foi realizada utilizando os oligonucleotídeos iniciadores oprt3 (5'-ccaagcttctgggcctggccgatctgggggc-3') e oprt4 (5'-ccggtaccactcatcgcgaggtccacaacg-3') contendo sítios de restrição para as enzimas *Hind*III e *Kpn*I (sublinhadas). A reação de amplificação foi realizada em presença de DMSO (dimetilsulfóxido) 10%, empregando 45 ciclos de desnaturação a 98°C (45 segundos), anelamento a 55°C (45 segundos) e extensão a 72°C (2 minutos). O produto da reação de PCR foi visualizado em gel de agarose 1%, extraído e purificado do gel utilizando kit comercial QIAquick gel extraction (QIAGEN). Os fragmentos amplificados (aqui denominados fragmento oprtUP e oprtDOWN) foram clonados separadamente em

vetor de clonagem pCR-Blunt (Invitrogen). A identidade e integridade das sequências amplificadas foram confirmadas através de digestões com as enzimas de restrição apropriadas (New England BioLabs) e pelo sequenciamento automático de DNA.

Cada um dos fragmentos amplificados foi digerido com as enzimas de restrição apropriadas (oprtUP: *Pst*I e *Hind*III; oprtDOWN: *Hind*III e *Kpn*I), gerando extremidades coesivas. Em seguida, estes dois fragmentos foram ligados simultaneamente ao vetor p2NIL (4753 pb) previamente digerido com *Pst*I e *Kpn*I, gerando uma região de inserção no vetor igual a 2 kb pela complementaridade das extremidades coesivas da porção 3' do fragmento oprtUP e 5' do fragmento oprtDOWN, ambos com sítio de restrição para *Hind*III.

O plasmídeo resultante foi transformado em células competentes de *E. coli* DH10B propagadas em meio de cultivo LB (Luria-Bertani) contendo canamicina 50 μg mL^{-1}. Colônias isoladas obtidas após a incubação das placas de cultura em estufa a 37°C por 16 horas foram transferidas para 5 mL de meio LB líquido contendo canamicina 50 μg mL^{-1}; esta cultura foi mantida em agitador orbital a 180 rpm por 16 horas a 37°C. O DNA plasmidial contido nestas células foi extraído com kit comercial QIAprep Spin Miniprep (QIAGEN) e os clones contendo a ligação dos fragmentos oprtUP e oprtDOWN foram identificados através da digestão com as enzimas de restrição *Pst*I e *Kpn*I (**Figura 11**). O processo de clonagem dos fragmentos oprtUP e oprtDOWN no vetor p2NIL tem como resultado um vetor plasmidial contendo a sequencia de DNA de 2 kb de extensão, complementar às sequências localizadas nas regiões adjacentes à porção 5' e à porção 3' do gene *pyrE*, na qual a região codificante deste gene é ausente.

Um segundo vetor plasmidial, pGOAL19, de 10435 pb, foi clivado com a enzima de restrição *Pac*I para liberação do fragmento de 7939 pb contendo as

marcas de seleção – *hyg*, *lacZ* e de contra seleção – *sacB*. A construção final no vetor p2NIL (p2NIL::oprtUP-DOWN) foi também clivada com *Pac*I a fim de gerar extremidades coesivas complementares ao fragmento liberado do vetor pGOAL19. Os dois vetores foram ligados gerando o plasmídeo suicida (não replicativo, contendo marcas de seleção e de contra seleção) final de aproximadamente 14 kb (**Figura 12**).

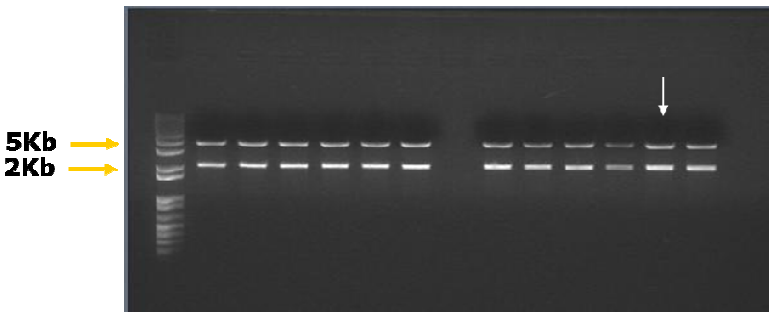

Figura 11. Gel de agarose 1% mostrando a liberação do inserto de 2 kb correspondente aos fragmentos oprtUP e oprtDOWN ligados, após a digestão com as enzimas de restrição *Pst*I e *Kpn*I, e o fragmento de aproximadamente 5 kb corresponde ao vetor p2NIL linearizado. A seta branca indica o clone selecionado para a reação de ligação ao vetor pGOAL19.

O produto da reação de ligação foi transformado em células eletrocompetentes de *E. coli* DH10B e isolado em placas contendo meio de cultivo LB, higromicina 100 µg mL^{-1} e X-Gal (5-bromo-4-cloro-3-indolil-β-D-tiogalactopiranosídeo) 50 µg mL^{-1}. As células de *E. coli* contendo a construção plasmidial final p2NIL-pGOAL19 são capazes de utilizar X-Gal presente no meio como fonte de carbono, degradando-a em um produto de coloração azul que permite a seleção dos clones verdadeiros por inspeção visual (**Figura 13**). Colônias azuis isoladas foram selecionadas e propagadas em 5 mL de meio LB líquido contendo canamicina 20 µg mL^{-1} e higromicina 100 µg mL^{-1}. As culturas foram mantidas em agitador orbital a 180 rpm por 16 horas a 37°C e o DNA plasmidial contido nestas células foi extraído com kit comercial QIAprep Spin Miniprep (QIAGEN).

Reações de digestão com as enzimas de restrição *Pst*I e *Eco*RI foram realizadas para a seleção dos vetores plasmidiais contendo o fragmento derivado do vetor pGOAL19 inserido no sentido direto de ligação dos fragmentos oprtUP e oprtDOWN. O clone selecionado foi então inserido novamente em células eletrocompetentes de *E. coli* DH10B, isolado em placas contendo meio de cultivo LB, higromicina 100 µg mL^{-1} e X-Gal 50 µg mL^{-1} e propagado em 100 mL de LB líquido contendo canamicina 20 µg mL^{-1} e higromicina 100 µg mL^{-1} para extração de grande quantidade de DNA plasmidial (Midiprep – QIAgen).

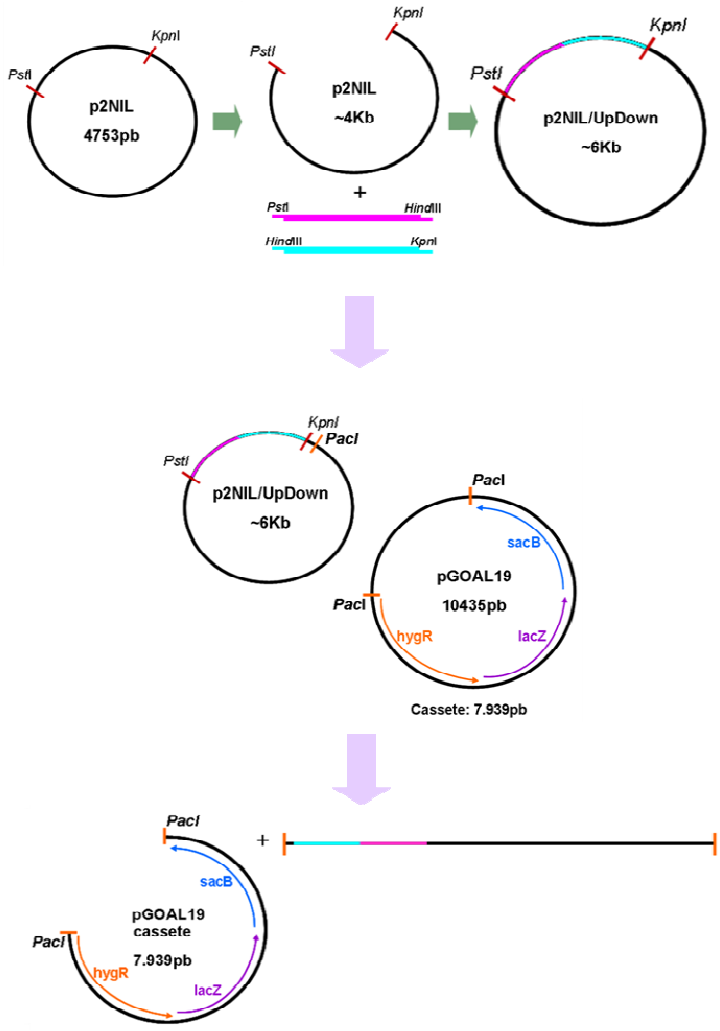

Figura 12. Representação esquemática da metodologia empregada para a construção do vetor suicida contendo as regiões adjacentes ao gene *pyrE* (fragmento oprtUP em cor de rosa e fragmento oprtDOWN em azul) ligadas ao plasmídeos p2NIL e as marcas de seleção derivadas do vetor pGOAL19.

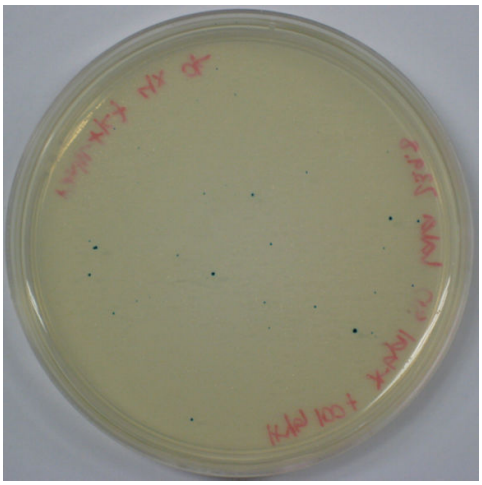

Figura 13. Culturas de células competentes DH10B de *E. coli* contendo o plasmídeo suicida final (colônias azuis).

O vetor suicida contendo a sequência nocauteada do gene *pyrE* será inserido em células de MTB H37Rv através de pulso elétrico. Estas células serão expostas à radiação UV para indução do sistema procariótico de reparo de DNA e da enzima RecA (pela formação de dímeros de pirimidina) para a mediação do evento de recombinação homóloga (64). As células serão então propagadas em placas de cultura 7H10, higromicina 100 µg mL^{-1}, canamicina 20 µg mL^{-1} e X-Gal 50 µg mL^{-1}. Através do repique das células em placa de cultura, ocorre o estímulo de um evento de *crossing-over* entre o DNA genômico de MTB e a sequência contida no vetor suicida, com a inserção de todo o vetor plasmidial no genoma da micobactéria, gerando colônias azuis (positivas para o evento de recombinação) e colônias brancas (negativas para o evento de recombinação e portadoras do gene tipo-selvagem). Colônias azuis isoladas serão selecionadas e repicadas em placas de cultura contendo X-Gal 50 µg mL^{-1} e sacarose 2%. Com a indução do segundo evento de *crossing-over*, as marcas de seleção contidas no vetor serão perdidas, e o alelo tipo-selvagem é substituído pela sequência contendo a deleção da região codificante do gene *pyrE*, gerando colônias brancas, incapazes de degradar X-Gal.

As colônias brancas (positivas para o segundo evento de recombinação) serão separadas visualmente das colônias negativas para o segundo evento de recombinação (azuis), e serão propagadas novamente em placas de cultura contendo canamicina 20 μg mL^{-1} para a seleção de cepas sensíveis ao antibiótico e descarte de cepas com eventuais mutações espontâneas que confiram resitência à canamicina (**Figura 14**). Estes experimentos serão realizados em duplicatas, com placas positivas e negativas para a suplementação com uracil, permitindo a identificação da dependência nutricional dos clones selecionados (65).

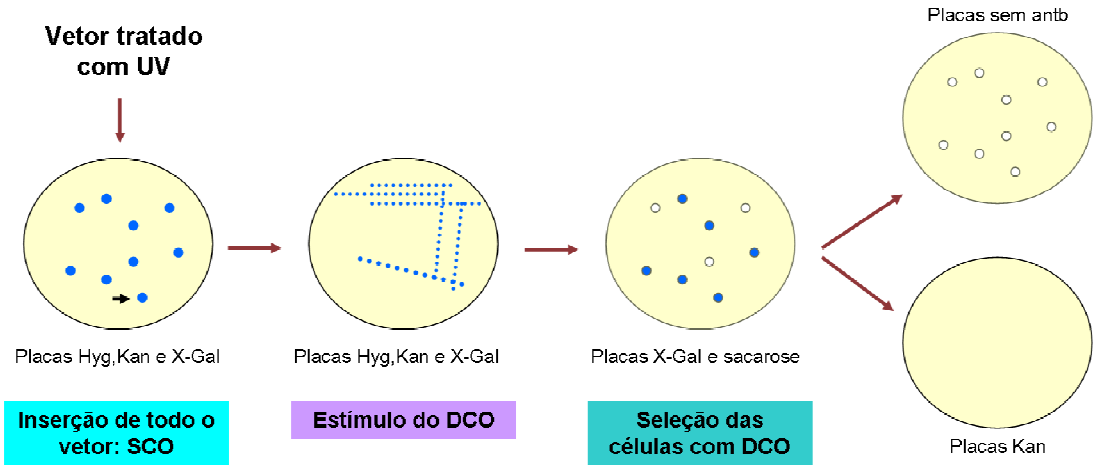

Figura 14. Representação esquemática das etapas de recombinação genética, com a deleção da região codificante do gene *pyrE*. O intervalo de tempo entre cada experimento representado é de 4 a 5 semanas devido ao lento crescimento do MTB.

Os mutantes auxotróficos serão avaliados quanto a sua capacidade de infecção em modelo animal. Uma cepa de MTB H37Rv incapaz de realizar a síntese *de novo* de nucleotídeos de pirimidina poderá constituir uma cepa atenuada, de acordo com a hipótese de trabalho, com a possibilidade de vir a ser utilizada como amostra vacinal na profilaxia da TB.

Capítulo 6

VIRTUAL SCRENING OF DRUGS: SCORE FUNCTIONS, DOCKING, AND DRUG DESIGN

Artigo publicado – *Current Computer-Aided Drug Design*, 2008, 4(4):265-272.

Virtual Screening of Drugs: Score Functions, Docking, and Drug Design

Ardala Breda[1,2], Luiz A. Basso[1,2], Diogenes S. Santos[*,1,2] and Walter F. de Azevedo Jr.[*,1]

[1]*Faculdade de Biociências, Pontifícia Universidade Católica do Rio Grande do Sul, Porto Alegre, RS, Brazil*

[2]*Centro de Pesquisas em Biologia Molecular e Funcional, Instituto de Pesquisas Biomédicas, Pontifícia Universidade Católica do Rio Grande do Sul, Av. Ipiranga, 6681 Prédio 92A, TECNOPUC, Partenon, CEP 90619-900, Porto Alegre, RS, Brazil.*

Abstract: The computational approach for new drug design and/or identification, was initially proposed in mid 70's. The virtual screening of chemical libraries against a biological target has proven its reliability on structure-based drug design, for instance, for many HIV virus protein inhibitors and for the development of Cyclin-Dependent Kinase inhibitors. Target-based virtual screening, allied to docking studies, enables searches on larger data set of probable ligands, with less costs than the traditional experimental screening. The increasing availability of small molecules databases and its free online distribution is now allowing not only pharmaceutical industries, but independent research labs as well, to apply this methodology on early stages of drug discovery. When the protein target structure is available, and a chemical virtual library is accessible, following questions need to be answered: how the target and the ligand interact and how these interactions may be evaluated? Several docking algorithms for the identification of the molecular features responsible for binding specificity are available. While such algorithms are very robust and accurate, the scoring functions remain more questionable in the sense of what parameters should be considered when defining protein-ligand binding affinity when ranking candidates pointed-out by the virtual screening to the next step on drug testing. Aside conformational and chemical information, pharmacokinetics properties should be considered as well when selecting potential new drugs. Along with structural well-match, appropriate molecular features that define desired kinetics characteristics should be consistently addressed for usefulness of virtual screening results. The present review is focused on these questions and their implication for virtual screening.

Keywords: Virtual screening, drug design, protein targets, filtering methods.

Pharmaceutical industry has a continuing need for novel and improved drugs. During the 1980's, *in vitro* technologies of high-throughput screening (HTS) became a keystone for pharmaceutical research [1], but this traditional way for the selection of potential active compounds not necessarily led to attractive candidates for drug development [2].

Even so, such advance on experimental methodologies was of major impact since the biological screening and preclinical testing stand for approximately 14% of total expenditures on drugs research and development [1]. Besides the incontestable contribution of HTS techniques, active compounds identification remains extensively time consuming. So, computational approaches complementary to HTS were developed, among those, the virtual screening (VS) became one of the most popular.

This alternative approach to the physical screening of large libraries of chemicals against a biological target was proposed in mid 70's. Here, the complementarities between target and ligand are assessed computationally to be experimentally test those potential drugs predicted to bound with high affinity to the target. Such methodology is based on the assumption that computational simulations of receptors structures and of the chemical forces that govern their interactions with their ligands could enable ligand design and discovery [3].

*Address correspondence to these authors at the Faculdade de Biociências, Pontifícia Universidade Católica do Rio Grande do Sul, Porto Alegre, RS, Brazil; E-mail: diogenes@pucrs.br or Walter.junior@pucrs.br

Taken together, both these experimental HTS and theoretical VS methodologies may benefit the early stages of drug discovery and development, turning it into a knowledge-based process that can avoid investments on drugs that do not present suitable properties and that will fail on later stages of clinical tests.

This review focuses on the VS method and on its principal characteristic of allowing access to a large number of possible new ligands that would be impracticable to test *in vitro*.

The main origin of VS is the structure-based compound screening or docking and the chemical-similarity searching based on small molecules [1]. This approach is more cost-effective to drug discovery since it applies high-performance computing to analyze chemical databases [4], selecting more promising compounds for experimental assays.

The VS is an automatic evaluation of virtual libraries of chemical compounds, using bioinformatics tools. There are two approaches for VS methods; the first one, named target-based VS (TBVS) or receptor-based, exploits the molecular recognition between the ligand and a target protein when structural information about the target is available, and selects chemical that has high affinity for the target's active site [4, 5]. Here, structural information may be an experimentally determined structure, by nuclear magnetic resonance (NMR) or X-ray diffraction, or even a structure determined theoretically by molecular modeling when suitable templates for the target protein are known and satisfy high identities premises [6]. TBVS allows the identification of

1573-4099/08 $55.00+.00

structurally novel ligands that may present interaction modes similar to the already known ligands or even new interaction pattern with different parts of the target's active site.

The second VS approach is the ligand-based VS (LBVS), or similarity-based VS, where there is no structural information about the target and the screening focuses on physical and chemical searches among the ligands [4], through pharmacophore pattern matching or based on similarity searching using descriptors that may be one-dimensional, two-dimensional or three dimensional (3D) [7], for example, the well-known Lipinski's rule of 5, where linear descriptors are applied to select only chemical that do not violate any of the rules for drugs solubility and permeability estimation [8], or even approaches that use 3D grids around a query molecule to assign location-specific properties that will be used on searches through chemical databases [7]. LBVS are more limited than TBVS since it is biased by the properties of the already known ligands for a given target [4].

LBVS will be briefly discussed in next paragraphs; TBVS will be discussed in this article, being the main focus of it.

LIGAND-BASED VIRTUAL SCREENING

On LBVS, one or more compounds that are known to bind to the target protein are used as a structural query and the screening procedure will extract compound from a database according to the stipulated similarity criterion [7]. Characteristics of known ligands may be used to derive a consensus generic structure where the spatial arrangement of atoms or functional groups that interact with the target or that are responsible for the biological activity are retained [9]. This consensus structure is named a pharmacophore, and its chemical and physical properties are used to search for novel ligands on databases. Aside from analyzing just the atoms pointed out by the pharmacophore partial structure template, the complete structure of the ligands can be considered in the quantitative structure-activity relationships (QSAR) methods. Through superimposing the ligand structures, QSAR methods can make accurate prediction of the relative conformation and alignment of the ligands as they are bound in the native protein, generating models that can be exploited for computational assessment of potential candidate molecules [7, 10, 11].

It is of general knowledge that most frequently there are no high resolution structures of the target proteins as well as classes of targets whose structure determination can be challenging, such as membrane proteins. For such cases, where TBVS can not be applied, ligand predictive approaches are required, both when only a small number of ligands have been discovered for a target and there is a need for augmentation of this initial set when many existing ligands are known but they share side-effects or biological properties that limit their biological utility [11].

Exploiting databases through ligand properties may lead to biased searching [4], as pointed out before; and the compound databases reflect only a tiny portion of the universe of compounds that can be synthesized [7]. The combinatory library design, or the structure based *de novo* design [7] explores these questions.

One example is the SOSA approach [12] that exploits smaller libraries of drug molecules known to be safe and to have bioavailability in humans. It applies combinatorial chemistry for altering these initial drug sets, highlighting already existing side-effects and suppressing their original main effects. This hit optimization is one example of taking advantages of the biased chemical databases, not being limited by it. Another advantage of this method is that original chemicals in the database have already being clinically tested, what improves the probability of the new designed drugs to not fail preclinical tests.

Successful applications of LBVS included the identification of novel glycogen synthase kinase-3 inhibitors [13], integrin α4β1 antagonists [14] and urotensin II receptor antagonists [15].

TARGET-BASED VIRTUAL SCREENING

TBVS relies on 3D structures of protein targets and on 3D databases of chemicals. This methodology uses virtual filtering of the all available ligands in a suitable database, followed by docking and scoring functions to identify potential lead candidates to a target by predicting their binding modes (docking) and affinity (scoring) [4].

DATABASES

The genome projects provided a data explosion regarding various bioinformatics fields, such as the number of organism's complete or partial genomes published, genomic target identification, and new proteins annotation, detection of protein homology relationships among species and exponential growth of structural databanks especially after 90's. This growth on both the number of nucleotide sequences deposited at the National Center for Biotechnology Information (NCBI) GenBank [16] and at protein structures deposited at Protein Data Bank (PDB) [17], as shown in Fig. (**1**) and Fig. (**2**), along with improvements and spreading of VS techniques allowed its increasing application on current pharmaceutical researches for drug identification and optimization.

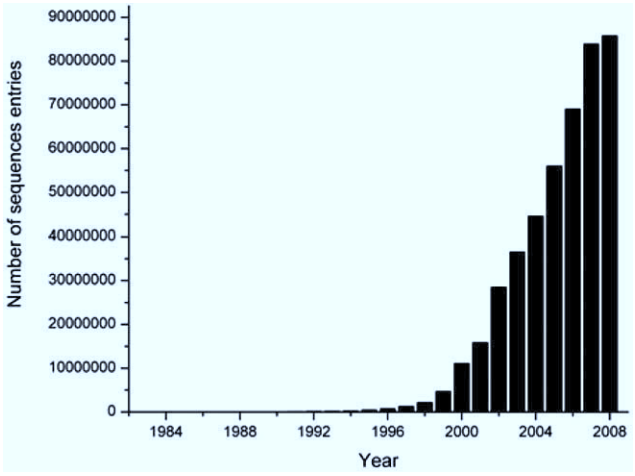

Fig. (1). Total number of nucleotide sequences deposited at the Genbank database, at February 2008.

Although there is still a larger number of nucleotide sequences when compared to available solved structures, the theoretical methods for protein structure prediction (being homology molecular modeling the most popular and with the most promising results [18], in concert with threading [19]

and *de novo* structure prediction [20]), allow the use of VS techniques to a much higher number of proteins than the experimentally solved ones.

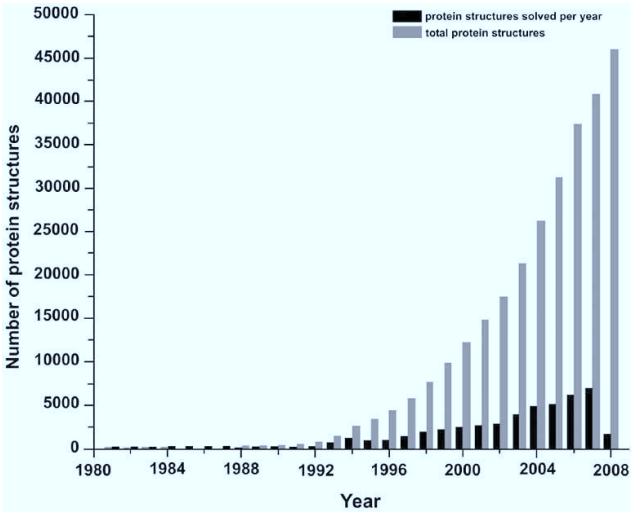

Fig. (2). Total number of protein structures deposited at the PDB at March 25, 2008.

Also, the now availability of free ligand 3D structures databases has enable a larger number of research groups, both in private industry and on the academic field to carry out studies on VS. Some of the most used ligand databases are listed in Table **1**. The Available Chemicals Directory Screening Compounds (ACD-SC) combined databases [21] contain over than 5.5 million compounds suitable as 3D models. ChemNavigator [22] contains over 10 million purchasable drug-like compounds but it is not entirely free or ready for docking experiments. A smaller collection of ligands structures is found at Ligand.Info [23], a compilation of publicly available databases with 1.2 million molecules. The PubChem, a public molecular information repository, maintained by NCBI, consists of chemical compounds, substances and bioassay databases. The PubChem System generates a binary substructure fingerprint for chemical structures. These fingerprints are used by PubChem for similarity searching [24, 25]. However, neither of these databases contains molecules ready for application of docking algorithm, and generally they require an extended prior work on archive preparation. To use these libraries in docking screens, molecular properties such as protonation, charge, stereochemistry, accessible conformations and salvation must be calculated, characteristics that can even change upon ligand binding to the target [3]. ZINC is a free library of approximately 4.6 million molecules 3D structures ready for use with most popular docking programs, each of which links to its vendor web site, ready for purchase [26].

VS WORKFLOW

There is no simple guide for VS procedures, since it depends on the system under study and on researcher expertise about protein target, knowledge about possible already identified ligands, and on the programs offered. Although, there are some basic principles that can be applied to any TBVS workflow, regarding the following problems: (1) Construction: how feasible structures can be systematically assembled? (2) Docking: how does the ligand interact with the target? (3) Scoring: how the binding affinity can be estimated? [27]. Fig. (**3**) shows a basic TBVS workflow. Each of the box contents are depicted along the article.

Table 1. Some of the Most Used Databases of Ligand Structures, and their Websites

Ligand Databases	
Databases	**Website**
ACD-SC	http://cds.dl.ac.uk/cds/datasets/orgchem/isis/acd.html
ChemNavigator	http://www.chemnavigator.com
Ligand.Info	http://ligand.info
PubChem	http://pubchem.ncbi.nlm.nih.gov
ZINC	http://zinc.docking.org

SYSTEM CONSTRUCTION – FILTERING METHODS

The atomic coordinates of the desired target structure can be obtained from PDB for example, a much simpler task than ligand selection. For initial selection of suitable ligands, general filters can be applied to the chosen ligand 3D database. Compound filtering primary purpose was not the identification of molecules that have a desired activity, but the enrichment of libraries with molecules with preferred properties, or the elimination of undesired ones, mainly the properties that are not compatible with the drug development requirements [1]. When considered at the early steps of the workflow, filtering can avoid computer-time expenses downsize the chemical space for follow up docking experiments. Most of all, it can eliminate compounds known to present characteristics that unable drug development, by removal of the compounds with reactive or undesired functional groups.

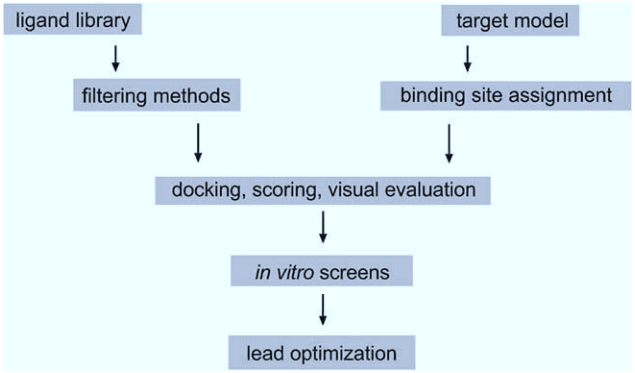

Fig. (3). A basic TBVS workflow. Although each step in a VS approach will depend on known information about the target and ligands, as well as on researchers' expertise, these steps are present in general. (Adapted from [4]).

These "rule-based" filters have much in common to LBVS, since at this step, we are dealing mostly with ligand properties, biased in some degree by target pre knowledge. Applied filters can deal with different drug desired properties, such as: drug solubility and absorption, bioavailability, drug-like character, blood-brain barrier penetration and ADMET. A suitable pharmacokinetic profile for a drug is a

complex function of properties such as dissolution, intestinal absorption, cellular permeability, binding to plasma proteins, turnover by metabolic enzymes and clearance mechanisms, drug distribution and deposition. All of these properties are influenced by drug's physical characteristics, i.e., molecular weight, lipophilicity, hydrogen bond donors and acceptors [26]; being all related in some degree to the above listed general filters.

Solubility and Absorption. The well known Lipinski's rule of 5 states that compounds with more than 5 hydrogen bond donors, 10 hydrogen bond acceptors, molecular weight greater than 500 Dalton (Da) and calculated Log P greater than 5 were prone to poor absorption [8]. Log P is the logarithm of the octanol/water partition coefficient, and describes the solubility of a compound in octanol (hydrophobic solvent) relative to its solubility in water (polar solvent) [1]. Statistical analyses of today's marketed drugs show that the molecular weight decreases on passing through each of the clinical phases, as an increase in molecular weight will have a tendency to lead to lower permeability, lower solubility, increased number of metabolized moieties and toxic pharmacophores. The same analyses point out that the most lipophilic compounds tend to be discontinued from development [28].

Along with the Log P, the polar molecular surface area (PSA) descriptor can also predict absorptions characteristics. Molecules with PSA smaller than 140Å^2 and Log P between 0 and 4 usually have favored absorption, as calculated experimentally from various data sets [1]. The Food and Drug Administration (FDA) implemented a biopharmaceutical classification system (BCS) to waive clinical studies of generic high-permeability/high-solubility drugs. The BCS preclude PSA and Log P as the best measurement of absorption properties of compound libraries in drug discovery would provide information about whether a compound is solubility or permeability limited instead of highlighting potential absorption or solubility as the rule of 5 [29]. The authors claimed that surface areas data analysis related to the nonpolar part of the molecule result in good predictions of solubility; whereas surface area related to polar parts of the molecule resulted on good predictions of permeability. They also claim attention to the fact that the total number of hydrogen bond donors and acceptor must be taken carefully since hydrogen bonds to the surrounding water net may difficult permeability, but if this donors and acceptor atoms are located at molecular interfaces they may enhance the drug stability, beneficiating its solubility.

Bioavailability. A study from the GlaxoSmithKline Laboratories of 1100 compounds database indicated that molecules with reduced molecular flexibility, as measured by the number of rotatable bonds (10 or fewer), low PSA (under 140Å^2) and low total hydrogen bond count (sum of donors and acceptors), as well as molecular weight under 500 Da, as molecular properties that may influence oral bioavailability [30]. Authors pointed out the success of molecular weight in predicting oral availability as a consequence of a lower rotatable bonds and PSA observed on smaller compounds, but not as a threshold *per se*. Rotatable bonds were defined as any single bond, not in a ring, bound to a nonterminal heavy atom, except for the C-N bonds because of its rotational energy barrier [30].

Drug-like character. What defines if a drug-like molecule is still very subjective. Intuitive and simple guidelines to identify drug candidates are yet an open field. Some knowledge-based analyses showed that some core structures are recurrent among the marketed drugs; and sets of fragments and chemical substitutions in drug-like molecules have been identified and are capable of differentiating drug-like from synthetic databases. Pharmacophore design and genetic algorithms have being used for such characteristic assignment [1]. Pharmacophore models are 3D representation of one single mode of action, or one binding mode of ligands that attach to the same target [31], so defining a pharmacophore model from known protein-ligand complexes or from the maximum common set of chemical features among ligands can help defining the drug-likeness of sets of compounds in a database. The chemical features used in the pharmacophore generation algorithm may represent chemical functionality but not molecular topology [31], what enable these resulting pharmacophore models to find potentially active ligands in a database that although are drug-like, may present completely new structures.

Blood-brain barrier penetration. Drugs that act at the central nervous system need to cross the blood-brain barrier to reach their target; by contrast, drugs with peripheral targets should have little or no brain penetration to avoid side effects [32]. QSAR analysis indicates compounds with molecular mass lower than 450Da and PSA smaller than 90-100Å^2 as capable of crossing the blood brain barrier [33].

ADMET. Absorption, distribution, metabolism, excretion and toxicity (together called ADMET data) were now considered as early as possible in the drug discovery process since late 90's, where studies indicated that poor pharmacokinetics and toxicity were important causes of late-stage failures in drug development. ADMET properties are applied on early stages in the design of new compounds both to reduce the risk of late-stage attrition on optimizing the screening and on testing most promising compounds [32]. The most important part of any *in silico* approach is the quality of the underlying data used to develop the models, what also applies to ADMET computational predictions, and unfortunately the data sets are very limited, what may bias new compound design, especially in regards to toxicity [32]. There are many *in silico* approaches for predicting ADMET properties of compounds from their chemical structure, ranging from data-based approaches such as QSAR, similarity searches, and three dimensional QSAR, to structure-based methods such as ligand-based docking and pharmacophore modeling [34]. The predictive ADMET models allow chemists and drug-design scientists to concentrate on compounds with the highest chances of meeting such pharmacokinetics criteria, contributing to the reduction of late-stage attrition. These models are under constant refinement but the difficulty in modeling these properties does not rely on the modeling but on accessing large enough successful data [32, 34].

Another task on ADMET predictions is the evaluation of predictors' accuracy, mainly to avoid filtering out series of compounds as a consequence of wrongly estimative of any of the above properties. The reliability of the predicted physicochemical properties became an even greater issue since the European Union requires a clear assessment of the developed QSAR models before they can be used in the registra-

tion, evaluation and authorization of chemical (REACH) system [35]. Tetko *et al.* presented in their review an evaluation method of predictors based on molecular similarity and on physicochemical properties similarities [35].

DOCKING ALGORITHMS

In VS screens, large libraries of organic drug-like molecules are docked into the receptor or target protein and than ranked by the calculated binding affinity. Although false-positives are a known problem for this methodology, docking algorithms are precise enough to predict genuinely novel ligands binding modes, what allied with the ready obtaining of target and with the ligand databases balance false-positive results. VS, as the correlated experimental technique of HTS, tolerate these false-positives as long as interesting ligands are found and large scale screening continues to be manageable [3].

The docking algorithms deal with ligand conformation prediction and orientation within the target active site. Besides very accurate, some issues like induced fit, target and ligand conformational changes upon binding [36], and protein-water interactions still remain to be solved.

Docking can be divided into steps: the process begins with ligand posing or orientation into the active site by the docking algorithms, next step is sampling degrees of freedom with sufficient accuracy to identify the ligand conformation that best matches target structure and fast enough to allow evaluation of thousands of compounds in a docking run [9].

Both target and ligand can be represented in different ways; structure representation is divided into atomic (more computer time-consuming, used in conjunction with potential energy functions), surface (most used in protein-protein docking) and potential energy grid schemes (support two types of potentials: electrostatics and van der Waals) [37].

Ligand flexibility can be addressed by systematic methods (incremental construction [27], conformational search – all degrees of freedom are explored), random or stochastic methods (genetic algorithm, Monte Carlo techniques – random changes are applied to a single ligand or a set of ligands) and by simulation methods (molecular dynamics, energy minimization – searches for the local minima on the energy surface). See reference [9] for more detailed explanation.

When choosing which docking software to use, some factors can be considered: capability for iterative parameters and protocols refinements, adaptability to extra scoring functions, filtering methods, validation studies, friendly user interface, file formats and upgrading possibilities [4] and where it applies for protein-ligand, protein-protein, and protein-nucleic acid docking, VS experiments and structure-based design. Some of the most used docking programs are listed in Table **2**. A list of other docking algorithms can be found at http://www.bio.vu.nl/nvtb/Docking.html.

Next we presented a brief description of Table **2** docking algorithms. For extensively description refer to each programs reference.

Autodock. An automated molecular docking software distributed to academics and non-profit research institutes free-of-charge since 1990. It offers a variety of search algorithms, including Monte Carlo simulated annealing, a genetic algorithm, and a hybrid local search genetic algorithm, also known as the Lamarckian genetic algorithm. AutoDock use a linear free energy model of molecular mechanics terms including van der Waals non-bonded interactions, directional hydrogen bonding, screened Coulombic electrostatics, and an atomic solvation parameter-based desolvation free energy term. There is also an empirical term that estimates the loss of torsional entropy of the ligand upon binding [38].

Table 2. Some of the Most Used Docking Programs, their Websites and Corresponding Fees*

Docking Programs	Website	Fees
AutoDock	http://autodock.scripps.edu/	no (academics) yes (profits)
DOCK	http://dock.compbio.ucsf.edu/	no (academics) yes (profits)
FlexX	http://biosolveit.de/FlexX http://www.tripos.com	yes
FRED	http://www.eyesopen.com/products/ applications/fred.html	yes
Glide	http://philscience.com/schrodinger/ Glide.htm	yes
GOLD	http://www.ccdc.cam.ac.uk.products/ life_sciences/gold	yes
ICM	http://www.molsoft.com/docking.html	yes

*See references [38-44] for each of the docking programs listed.

Dock. Conceived at 80's and still very popular, it generates many possible orientation of the candidate ligand within the target active site (described by spheres, where their centers correspond to the potential locations for the ligand atoms) by exhaustive search and fragment docking [27, 39].

FlexX. Ligand is treated by an incremental construction algorithm. Only ligand can be flexible. Possible interactions are described in a geometry database, and a torsion angle database is used to generate ligand conformers [27, 40].

FRED. The program exhaustively examines all possible poses within the protein active site, filtering for shape complementarities and pharmacophoric features before scoring. FRED use systematic and nonstochastic docking approaches, and allow customizing and consensus scoring functions [41].

Glide. The program applies a hierarchical protocol through a sequence of steps for searching the best dockings. Protein-ligand conformational space is explored by the use of grids of site points and rotation of the ligand around such points. Initial simpler scoring functions are applied to reject incorrect dockings, and become more sophisticated as the search progresses [42, 45].

GOLD. Genetic algorithms and stochastic methods are applied for determination of ligand best conformation and orientation, as well as the complex configuration. Ligand is treated as a flexible molecule and target as a partially-flexible one. Energy functions are derived from crystallographic data [27, 43].

ICM. The docking module allows an automatic preparation of a molecule for a flexible docking. It also allows the browsing of docking solutions, binding site analysis, visualization of grid potentials, adjustment of grid potential areas, and configurable preferences for ligand size and score thresholds [44].

Cummings *et al.* [45] compared different automated docking programs regarding only docking algorithms performing VS searches on a small database against a number of targets. Programs selected were DOCK [39], GOLD [43], Glide [42] and DOCKVISION [46]. No rescoring of the original docking results was performed. Results evaluation concern total number of actives (true positives) and total number of negatives (false positives) found by each of the programs, and the total number of targets for which hits were founded. Authors highlighted that although Glide gave the most consistent levels of success, when coarsely compared all methods presented similar results.

SCORING FUNCTIONS

The docking programs are usually successful in generating multiple poses that include binding modes similar to crystalloghaphically determined protein-ligand bound complexes. But at the same time, the scoring functions are less successful in correctly identifying the binding mode or predicting binding affinity [47].

All ligand conformations generated at the docking step must than be evaluated in terms of ligand target binding affinity by a scoring function in the scoring step, as a crucial aspect of VS. Free-energy simulation techniques for the prediction of binding affinity are still not very accurate [4, 9]. There are three groups of scoring functions: force-field based methods, empirical scoring functions and knowledge-based potentials [9, 48]. Table **3** lists some scoring functions grouped by type.

Table 3. Scoring Functions Grouped by their Binding Affinity Energy Evaluation Methods

Scoring Functions
Force-Field Scoring Functions
AutoDock [37]
G-Score [40]
D-Score [40]
Empirical Scoring Functions
LigScore [49]
PLP [50]
LUDI [51]
F-Score [52]
Chem-Score [53]
X-Score [54]
Knowledge-Based Potentials
PMF [55]
DrugScore [56]

Force-field scoring functions. Make use of classical molecular mechanics for energy function calculations. The binding free energy of protein-ligand complexes are estimated by the sum of van der Waals (by Lennard-Jones potential function) and electrostatics interactions. Solvation is considered as a distance-dependent dielectric function. Non-polar contributions are assumed to be proportional to the solvent-accessible surface area. Non-bonded interactions are treated with the introduction of a cut-off distance [9]. The method requires energy minimization prior to energy evaluations [48]. Various force-field scoring functions are based on different sets of parameters, although they are functionally similar.

Empirical scoring functions. The binding free energy is estimated based on weighted structural parameters by fitting the scoring functions to experimental determined binding constants of a set of complexes [48]. These scoring functions may be highly biased by the selected training set of ligand-protein complexes. The advantage of these functions is that their terms, although similar to force-field functions, are often simple to evaluate. More complex functions addresses solvation and desolvation effects, but still provide only incomplete descriptions of these effects on protein-ligand binding [9].

Knowledge-based scoring functions. Here, binding affinity is considered as a sum of the ligand and protein atoms interactions. As the empirical scoring functions, these potentials are derived from experimental structures, where interatomic distances are converted into distance-dependent interactions free energies [48]. These functions are designed to reproduce experimental structures rather than binding energies. Due to its simplicity, knowledge-based scoring functions permit efficient screening of large compound databases [9].

Given imperfections of current scoring functions, consensus scoring has been proposed, where the combination of different score would balance errors on single scores, improving identification of true ligands [9]. Teramoto & Fukunishi, 2007 [48] tested consensus scoring with combination of the scoring functions listed in Table **3**. Their findings suggested that none consensus score perform better than the best scoring function among those used in each combination.

Since major weakness of docking programs lie not in sampling methods (docking step) but in scoring functions, Wang *et al.* [57] performed comparative analyses of the same 11 scoring functions listed above. The data set selected was first submitted to an exhaustive conformational sampling with AutoDock [37], and than each of the scoring functions was applied. Authors pointed that the only two scoring functions that stand alone (not implemented on a docking program), X-Score and DrugScore, presented best results as their scoring functions lead to a faster convergence to the global minimum in conformational sampling. Results also suggested that given an adequate conformational sampling, the performance of every scoring function is acceptable for molecular docking tasks.

An ideal algorithm should be high-quality both at conformational sampling and scoring [48]; improvements on precision of scoring functions should focus on inclusion of solvation and entropy contributions to binding free energy

[9], what makes than more computationally expensive although more accurate, and may limit its applicability on VS.

DRUG-DESIGN

About 30 years ago, X-ray crystallography emerged in drug discovery, and a radical change in drug design then initiated where knowledge of the 3D structures of target proteins was incorporated into the design process. A decade ago HTS and VS started to gain attention in the same field [58].

The target-based approach to drug discovery has two main points: first, the resolution by experimental or theoretical methodologies of the structure of biological targets with an activity that has a causative role on the onset or on the progression of human diseases. Second, the identification of therapeutic agents that appropriately modulates the activity of this target, with limited or no adverse effects [59].

These two points are exactly the main field covered by TBVS, where selection of potential effective drugs from large databases should improve drug discovery and also subsequent drug design by lead optimization.

Examples of successful VS approaches in drug development are the antiretroviral drugs based on HIV protease inhibitors [60] as well as kinase inhibitors [61]. Not only human proteins have been used as targets for VS; structure determination of proteins in parasite organisms such as *Mycobacterium tuberculosis* (MTB) and *Plasmodium falciparum* lead to recent inhibitors identification for MTB's thymidine monophosphate kinase [62] and chorismate mutase [63] and *P. falciparum* enoyl-acyl carrier protein reductase [64]. Other examples of successful applications of TBVS can also be found in [4].

FINAL CONSIDERATIONS

VS approaches fulfill the current and always crescent need of pharmaceutical industries for novel and more effective hits identification in much lesser time scales and with better cost-benefits. It may be soon to evaluate its productivity since 10 to 15 years are generally required for new drugs discovery and development [59] but its contribution to compounds research, hit identification and lead optimization is unquestionable.

Human expertise is one of the key points in this methodology for its false positive and false negative hits still remain as a major concern. Knowledge about the target or previously known ligands can only improve VS results although some bias can be introduced in the discovery process [65], even so, biased compound identification can pave the way to lead optimization. Furthermore, development of new empirical scoring functions [66] will help to speed up the VS approaches.

As both experimental target structures' determination, ligand filtering and VS evolve as parallel fields even newer approaches already emerges, as the VS of target libraries instead of ligand libraries [67] where same principle applies backswords, and most likely target could be predicted for given ligands.

Clearly, computational developments in this area of bioinformatics became more and more relevant for drug discovery and development researches, both in academic and industry laboratories. VS tend to be a routine tool on today's and near future marketed drugs.

ACKNOWLEDGEMENTS

This work was supported by grants from CNPq, CAPES and Instituto do Milenio (CNPq-MCT). WFA, DSS and LAB are senior researchers of CNPq (Conselho Nacional de Pesquisas, Brazil).

ABBREVIATIONS

3D	=	Three dimensional
ACD-SC	=	Available Chemicals Directory Screening Compounds
ADMET	=	Absorption, distribution, metabolism, excretion and toxicity
BCS	=	Biopharmaceutical classification system
Da	=	Dalton
FDA	=	Food and Drug Administration
HTS	=	High throughput screening
LBVS	=	Ligand-based virtual screening
NCBI	=	National Center for Biotechnology Information
NMR	=	Nuclear magnetic resonance
PDB	=	Protein Data Bank
PSA	=	Polar molecular surface area
QSAR	=	Quantitative structure-activity relationships
REACH	=	Registration evaluation and authorization of chemical
TBVS	=	Target-based virtual screening
VS	=	Virtual screening

REFERENCES

[1] Bajorath, J. *Nat. Rev. Drug Discov.*, **2002**, *1*, 882-894.
[2] Kassel, D.B. *Curr. Opin. Chem. Biol.*, **2004**, *8*, 339-345.
[3] Shoichet, B.K. *Nature*, **2004**, 432,862-865.
[4] Ghosh, S.; Nie, A.; An, J.; Huang, Z. *Curr. Opin. Chem. Biol.*, **2006**, *10*, 194-202.
[5] Oprea, T.I.; Matter, H. *Curr. Opin. Chem. Biol.*, **2004**, *8*, 349-358.
[6] Martí-Renom, M.A.; Stuart, A.C.; Fiser, A.; Sánchez, R.; Melo, F.; Šali, A. *Annu. Rev. Biophys. Biomol. Struct.,* **2000**, *29*, 291-325.
[7] Lengauer, T.; Lemmen, C.; Rarey, M.; Zimmermann, M. *Drug Discov. Today*, **2004**, *9*, 27-34.
[8] Lipinski, C.A.; Lombardo, F.; Dominy, B.W.; Feeney, P.J. *Adv. Drug Deliv. Rev.*, **1997**, *23*, 3-25.
[9] Kitchen, D.B.; Decornez, H.; Furr, F.R.; Bajorath J. *Nat. Rev. Drug Discov.*, **2004**, *3*, 935-949.
[10] Eckert, H.; Bajorath, J. *Drug Discov. Today*, **2007**, *12*, 225-233.
[11] Jain, A.N. *J. Med. Chem.*, **2004**, *47*, 947-961.
[12] Wermuth, C.G. *Drug Discov. Today*, **2006**, *11*, 160-164.
[13] Naerum, L.; Norskov-Lauritsen, L.; Olesen, P.H. *Angew. Chem. Int. Ed. Engl.,* **1999**, *38*, 2894-2896.
[14] Singh, J.; Vlijmen, H.; Liao, Y.; Lee, W.C.; Cornebise, M.; Harris, M.; Shu, I.; Gill, A.; Cuervo, H.J.; Abraham, W.M.; Adams, S.P. *J. Med. Chem.*, **2002**, *45*, 2988-2993.
[15] Flohr, S.; Kurz, M.; Kostenis, E.; Brkovich, A.; Fournier, A.; Klabundle T. *J. Med. Chem.*, **2002**, *45*, 1799-1805.
[16] Benson, D.A.; Karsch-Mizrachi, I.; Lipman, D.J.; Ostell, J.; Wheeler, D.L. *Nucleic Acids Res.*, **2007**, *35*, D21-D25.

[17] Berman, H.M.; Westbrook, J.; Feng, Z.; Gilliland, G.; Bhat, T.N.; Weissig, H.; Shindyalov, I.N.; Bourne, P.E. *Nucleic Acids Res.*, **2000**, *28*, 235-242.
[18] Moult, J.; Fidelis, K.; Hubbard, T.; Tramontano, A. *Proteins*, **2005**, *61*, 3-7.
[19] David, R.; Korenberg, M.J.; Hunter, I.W. *Pharmacogenomics*, **2000**, *1*, 445-455.
[20] Hardin, C; Pogonorev, T.V.; Luthey-Schulten, Z. *Curr. Opin. Struct. Biol.*, **2002**, *12*, 176-181.
[21] Available Chemicals Directory Screening Compounds (ACD-SC) http://cds.dl.ac.uk/cds/datasets/orgchem/isis/acd.html
[22] ChemNavigator – San Diego, California. http://chemnavigator.com.
[23] von Grotthuss, G.; Koczyk, M.; Pas, J.; Wyrwicz, L.S.; Rychlweski, L. *Comb. Chem. High Throughput Screen.*, **2004**, *7*, 757-761.
[24] Lazo, J.S. *Mol. Interv.,* **2006**, *6*, 240-243.
[25] Xie, X.Q.; Chen, J.Z. *J. Chem. Inf. Model.,* **2008**, *48*, 465-475.
[26] Irwin, J.J.; Shoichet, B.K. *J. Chem. Inf. Model.*, **2005**, *45*, 177-182.
[27] Schneider, G.; Böhm H.J. *Drug Discov. Today,* **2002**, *7*, 64-70.
[28] Wenlock, M.C.; Austin, R.P.; Barton, P.; Davis, A.M.; Leeson, P.D. *J. Med. Chem.*, **2003**, *46*, 1250-1256.
[29] Bergström, C.A.S.; Strafford, M.; Lazorova, L.; Avdeef, A.; Luthman, K.; Artursson, P. *J. Med. Chem.,* **2003**, *46*, 558-570.
[30] Veber, D.F.; Johnson, S.R.; Cheng, H.Y.; Smith, B.R.; Ward, K.W.; Kopple, K.D. *J. Med. Chem.*, **2002**, *45*, 2615-2623.
[31] Wolber, G.; Langer, T. *J. Chem. Inf. Model.*, **2005**, *45*, 160-169.
[32] van de Waterbeemd, H.; Gifford, E. *Nat. Rev. Drug Discov.*, **2003**, *2*, 192-204.
[33] van de Waterbeemd, H.; Camenish, G.; Folkers, G.; Chretien, J.R.; Raevsky, O. *J. Drug Target*, **1998**, *6*, 151-165.
[34] Yamashita, F.; Hashida, M. *Drug Metab. Pharmacokinet.*, **2004**, *19*, 327-338.
[35] Tetko, I.V.; Bruneau, P.; Mewes, H.W.; Rohrer, D.C.; Poda, G.I. *Drug Discov. Today,* **2006**, *11*, 700-707.
[36] Perola, E.; Charifson P.S. *J. Med. Chem.*, **2004**, *47*, 2499-2510.
[37] Halperin, I.; Ma, B.; Wolfson, H.; Nussinov, R. *Proteins*, **2002**, *47*, 409-443.
[38] Morris, G.M.; Goodsell, D.S.; Halliday, R.S.; Huey, R.; Hart, W.E.; Belew, R.K.; Olson, A.J. *J. Comput. Chem.*, **1998**, *19*, 1639-1662.
[39] Ewing, T.J.; Makino, S.; Skillman, A.G.; Kuntz, I.D. *J. Comput. Aided Mol. Des.*, **2001**, *15*, 411-428.
[40] Kramer, B.; Metz, G.; Rarey, M.; Lengauer, T. *Med. Chem. Res.*, **1999**, *9*, 463-478.
[41] McGann, M.R.; Almond, H.R.; Nichols, A.; Grant, J.A.; Brwn, F.K. *Biopolymers*, **2003**, *68*, 76-90.
[42] Friesner, R.A.; Banks, J.L.; Murphy, R.B.; Hagren, T.A.; Klicic, A.A.; Mainz, D.T.; Repasky, M.P.; Knoll, M.S.; Perry, J.K.; Shaw, D.E.; Francis, P.; Shenkin, P.S. *J. Med. Chem.*, **2004**, *47*, 1739-1749.
[43] Jones, G.; Willet, P.; Glen, R.C.; Leach, A.R. & Taylor, R.D. *J. Mol. Biol.*, **1997**, *267*, 727-748.
[44] Abagyan, R.A.; Totrov, M.M.; Kuznetsov, D.A. *J. Comput. Chem.*, **1994**, *15*, 488-506.
[45] Cummings, M.D.; DesJarlais, RL; Gibbs, AC; Mohan, V.; Jaeger, E.P. *J. Med. Chem.*, **2005**, *48*, 962-976.
[46] Hart, T.N.; Read, R.J. *Proteins*, **1992**, *13*, 206-222.
[47] Warren, G.L.; Andrews, C.W.; Capelli, A.M.; Clarke, B.; LaLonde, J.; Lambert, M.H.; Lindvall, M.; Nevins, N.; Semus, S.F.; Senger, S.; Tedesco, G.; Wall, I.D.; Woolven, J.M.; Peishoff, C.E.; Head, M.S. *J. Med. Chem.*, **2006**, *49*, 5912-5931.
[48] Teramoto, R.; Fukunishi, H. *J. Chem. Inf. Model.*, **2007**, *47*, 526-534.
[49] Krammer, A.; Kirchhhoff, P.D.; Jiang, X.; Venkatachalam, C.M.; Waldman, M. *J. Mol. Graph. Model.*, **2005**, *23*, 395-407.
[50] Verkivker, G.M.; Bouzida, D.; Gehlaar, D.K.; Rejto, P.A.; Arthurs, S.; Colson, A.B.; Freer, S.T.; Larson, V.; Luty, B.A.; Marone T.; Rose, P.W. *J. Comput. Aided Mol. Des.*, **2000**, *14*, 731-751.
[51] Böhm, H.J. *J. Comput. Aided Mol. Des.*, **1992**, *6*, 593-606.
[52] Rarey, M.; Kramer, B.; Lengauer, T.; Klebe, G. *J. Mol. Biol.*, **1996**, *261*, 470-489.
[53] Eldridge, M.D.; Murray, C.W.; Auton, T.R.; Paolini, G.V.; Mee, R.P. *J. Comput. Aided Mol. Des.*, **1997**, *11*, 425-445.
[54] Wang, R.; Lai, L.; Wang, S. *J. Comput. Aided Mol. Des.*, **2002**, *16*, 11-26.
[55] Muegge, I.; Martin, Y.C. *J. Med. Chem.*, **1999**, *42*, 791-804.
[56] Gohlke, H.; Hendlich, M.; Klebe, G. *J. Mol. Biol.*, **2000**, *295*, 337-356.
[57] Wang, R.; Lu, Y.; Wang, S. *J. Med. Chem.,* **2003**, *46*, 2287-2303.
[58] Blundel, T.L.; Sibanda, B.L.; Montalvão, R.W.; Brewerton, S.; Chelliah, V.; Worth, C.L.; Harmer, N.J.; Davies, O.; Burke, D. *Philos. Trans. R. Soc. Lond. B. Biol. Sci.*, **2006**, *361*, 413-423.
[59] Hajduck, P.J.; Greer, J. *Nat. Rev. Drug Discov.*, **2007**, *6*, 211-219.
[60] Chang, M.W.; Lindstrom, W.; Olson, A.J.; Belew, R.K. *J. Chem. Inf. Model.*, **2007**, *47*, 1258-1262.
[61] Yu, H.; Wang, Z.; Zhang, L.; Zhang, J.; Huang, Q. *Chem. Biol. Drug Des.*, **2007**, *69*, 204-211.
[62] Gopalakrishnan, B.; Aparna, V.; Jeevan, J.; Ravi, M.; Desiraju, G.R. *J. Chem. Inf. Model.*, **2005**, *45*, 1101-1108.
[63] Agrawal, H.; Kumar, A.; Bal, N.C.; Siddiqi, M.I.; Arora, A. *Bioorg. Med. Chem. Lett.*, **2007**, *17*, 3053-3058.
[64] Nicola, G.; Smith, C.A.; Lucumi, E.; Kuo, M.R.; Karagyozov, L.; Fidock, D.A.; Sacchettini, J.C.; Abagyan, R. *Biochem. Biophys. Res. Commun.*, **2007**, *338*, 686-691.
[65] Jansen, J.M.; Martin, E.J. *Curr. Opin. Chem. Biol.*, **2004**, *8*, 359-364.
[66] Caceres, R.A.; Timmers, L.F.S.; Dias, R.; Basso, L.A.; Santos, D.S.; de Azevedo Jr., W.F. *Bioorg. Med. Chem.*, **2008** (doi:10.1016/j.bmc.2008.04.044).
[67] Rognan, D. *J. Physiol. Paris*, **2006**, *99*, 232-244.

Received: March 17, 2008 **Revised: April 2, 2008** **Accepted: April 12, 2008**

Capítulo 7

CONSIDERAÇÕES FINAIS

A TB é uma doença crônica causada principalmente pelo MTB, de impacto global, considerada emergencial para a saúde pública, e que requer novos e maiores esforços no desenvolvimento de alternativas para o seu tratamento e profilaxia, principalmente quando considerado o surgimento de cepas resistentes às drogas utilizadas no tratamento preconizado pela OMS; o aumento do número de pessoas infectadas (incluindo populações de risco, como pacientes soropositivos e imunodeprimidos); e o grande número de pessoas infectadas com a forma latente da TB, que constituem um grande reservatório da doença (2). As vias de metabolismo de nucleotídeos são consideradas fontes promissoras de potenciais alvos moleculares para o desenvolvimento de drogas de ação específica, que podem idealmente ter ação sobre a forma ativa e a forma latente da TB.

A clonagem, amplificação e caracterização do produto do gene *pyrE* de MTB H37Rv como uma enzima funcional responsável pela conversão de OA e PRPP em OMP e PP_i permitiu a sua correta notação como uma orotato fosforibosiltransferase (OPRT, EC 2.4.2.10), pertencente à família de PRTases do tipo I, que catalisam a transferência do grupamento fosforibosil para bases nitrogenadas em presença de metais divalentes (40) (Mg^{2+} para a enzima de MTB).

A determinação de um protocolo de purificação através de HPLC permitiu a obtenção da forma homogênea e ativa da enzima, com rendimento superior a protocolos já publicados, inclusive quando comparado ao uso de técnicas de cromatografia líquida de afinidade. O protocolo desenvolvido resulta em uma forma homogênea e também estável da enzima, sem perda significativa de atividade quando armazenada em ultrafreezer (-80°C), em presença de glicerol 5%, por até 10 meses, e adequada para a realização dos ensaios posteriores utilizados para a sua caracterização molecular, cinética e termodinâmica.

A caracterização molecular da enzima através do sequenciamento da sua estrutura primária e a determinação da sua estrutura quaternária por cromatografia líquida de exclusão de tamanho permitiu a identificação da forma ativa da enzima como um dímero composto por duas subunidades iguais, cuja forma em solução não é afetada pela variação da sua concentração.

Os ensaios espectrofotométricos de atividade e de inibição pelos produtos da reação, juntamente com os resultados obtidos pelos ensaios de ligação realizados através de titulação isotérmica por microcalorimetria permitiram a identificação do mecanismo cinético da reação catalisada e a determinação das constantes cinéticas e termodinâmicas associadas às reações direta e inversa da enzima. A enzima OPRT de MTB segue um mecanismo de reação Mono-Iso Ordenado Bi Bi, que a distingue das demais enzimas homólogas já caracterizadas até o momento. Embora as formas homólogas da enzima também sigam mecanismos cinéticos sequenciais, a presença de uma etapa de isomerização ainda não havia sido descrita para uma OPRT, e se reflete na menor eficiência catalítica e diferente afinidade pelos substratos de reação da enzima OPRT de MTB quando esta é comparada às suas homólogas.

Os resultados dos ensaios de titulação isotérmica por microcalorimetria permitiram não apenas a determinação das constantes termodinâmicas dos ligantes da enzima, mas também a identificação dos eventos moleculares envolvidos com a formação dos complexos enzima-ligante, como a formação de pontes de hidrogênio e de contatos hidrofóbicos favoráveis entre o sítio ativo da enzima e seus ligantes (refletida na entalpia favorável da ligação), e na ocorrência de rearranjo da estrutura tridimensional da enzima com a presença dos ligantes em seu sítio ativo (entropia desfavorável) – resultado corroborado pelos dados estruturais disponíveis para

formas homólogas da OPRT; em processos exotérmicos espontâneos (energia livre de Gibbs favorável).

Estes resultados, apresentados no Capítulo 02, foram compilados em um artigo científico submetido ao *Journal of Biological Chemistry*, revista internacional indexada de alto impacto. Estes dados permitem que características exclusivas da enzima de OPRT de MTB sejam exploradas no desenvolvimento de inibidores de ação específica e alta afinidade de ligação, onde a caracterização de alvos moleculares específicos é considerada a primeira etapa no processo de desenvolvimento de um novo fármaco de ação seletiva (13).

As drogas atualmente disponíveis para o tratamento da TB não são consideradas completamente eficazes (6) e não apresentam atividade bactericida e esterilizante contra as formas MDR-TB e XDR-TB (12, 11), salientando, portanto a necessidade de desenvolvimento de novas e mais efetivas drogas para o controle e profilaxia da TB (1), capazes de reduzir o tempo de tratamento e que apresentem menos efeitos colaterais e interações medicamentosas, aumentando a adesão dos pacientes (66, 67).

O uso de informações derivadas da caracterização de um alvo específico; como a identificação das etapas químicas e não químicas presentes no mecanismo cinético de reação de uma enzima; já foi descrito no desenvolvimento de inibidores seletivos da enzima inosina monofosfato desidrogenase (68).

O mecanismo cinético da reação, as constantes de afinidade pelos substratos e os dados de perfil termodinâmico da formação dos complexos enzima-ligante para a enzima OPRT de MTB foram utilizados para a proposição de compostos químicos análogos de OA, com potencial atividade inibitória, considerando ainda as propriedades físico-químicas associadas ao maior sucesso de drogas nos ensaios

clínicos de fase I e II, conhecidas como 'Regras de Lipinski' (69, 70), e 'Regras de Veber' (71)[ii].

Ensaios de inibição da atividade enzimática permitiram a identificação de um composto comercial com atividade inibitória, escolhido como molécula inicial para a realização de substituição de grupamentos (derivatização química) para o aprimoramento dos potenciais inibidores.

A determinação das constantes de inibição e do perfil de inibição através de ensaio espectrofotométrico indicou que os compostos testados apresentavam inibição do tipo competitiva em relação ao OA e do tipo incompetitiva em relação ao PRPP. Como os compostos testados tiveram suas estruturas baseadas na estrutura do OA, e este substrato da OPRT só é capaz de se ligar ao sítio ativo da enzima na presença de PRPP, os resultados encontrados nos ensaios de inibição indicam que os inibidores identificados não possuem afinidade pela enzima na sua forma livre, possuindo afinidade pelo complexo enzima-PRPP, competindo então com o substrato OA pela ligação à enzima, formando o complexo ternário enzima-PRPP-inibidor, sem atividade catalítica. Estes resultados são corroborados pelo mecanismo cinético da enzima, e indicam que uma vez que a OPRT de MTB tenha sido inibida por um destes compostos, ocorrerá o acúmulo dos substratos naturais da enzima, e a maior concentração de PRPP levará ao aumento da concentração de complexos enzima-PRPP, o que aumenta a afinidade de inibidores incompetitivos pela enzima. Inibidores incompetitivos são, portanto desejados pela indústria farmacêutica no processo de desenvolvimento de novas drogas, uma vez que sua ação inibitória não

[ii] As 'Regras de Lipinski' propõem que compostos que apresentam melhor absorção e permeabilidade gastrointestinal apresentam menos de 5 grupamentos doadores de hidrogênio, menos de 5 grupamentos aceptores de hidrogênio, massa molecular abaixo de 500 Daltons e baixa lipofilicidade (expressa como LogP inferior a 5). Estas regras são aplicadas a compostos que permeiem membranas através de difusão livre, não mediada por proteínas transportadoras, e embora a violação de uma destas regras não seja um indicativo direto de baixa absorção e biodisponibilidade oral, esta probabilidade aumenta com o número de violações observadas para cada molécula (75). Veber postulou que a flexibilidade da molécula está também relacionada à sua biodisponibilidade oral, refletida em um número menor ou igual a 10 rotâmeros e até 12 grupamentos doadores e aceptores de hidrogênio (71).

é revertida pelo acúmulo de substratos naturais da enzima (72). A formação do complexo ternário $E \cdot PRPP \cdot I$, além de inibir a síntese de nucleotídeos de pirimidina a partir de precursores simples, ainda sequestra moléculas de PRPP no meio celular, afetando outras vias metabólicas como a síntese de nucleotídeos de purinas.

Os compostos inibidores testados apresentaram valores de K_i na faixa de μM em relação ao substrato PRPP e na faixa de nM em relação ao substrato OA. No entanto, apenas o composto **13** apresentou valores de K_i menores que o composto inicial **6**, indicando que a adição de um grupamento benzil na posição 1 do orotato, em substituição ao átomo N1 que faria ligação glicosídica com a porção fosforibosil do PRPP, aumenta a afinidade da molécula pelo sítio ativo da enzima.

Os perfis de discriminação termodinâmica dos compostos **6** e **13** mostram que a ligação dos inibidores ao complexo enzima-PRPP é um processo espontâneo que ocorre pela formação de pontes de hidrogênio e contatos de van der Waals favoráveis. A entropia desfavorável observada na ligação do composto **6** pode ser atribuída às alterações conformacionais induzidas na estrutura tridimensional da enzima, correspondendo à etapa de isomerização presente no mecanismo cinético da OPRT de MTB, assim como é observado na ligação dos seus substratos naturais. A ligação do composto inibidor **13**, derivado do composto **6** apresenta entropia de ligação favorável, característica que, aliada à entalpia de ligação também favorável, corresponde ao perfil termodinâmico mais positivo para moléculas inibitórias de alta afinidade (73). A energia livre de Gibbs do composto **13** é maior que o valor observado para o composto **6**, e está diretamente relacionada à diferença observada nas suas afinidades de ligação. A entropia favorável é ainda acompanhada pela diminuição da entalpia, devido à liberação de moléculas de água pela ligação do grupamento benzil ao sítio ativo da enzima, grupamento substituinte que é ausente

no composto **6**, juntamente com a indução de alterações conformacionais na enzima (74) (fechamento do sítio ativo da enzima pelo *loop* catalítico).

Os melhores valores de K_i do composto **13** quando comparado ao composto **6** podem ser explicados, portanto, pela otimização da sua entropia de ligação através do aumento da sua hidrofobicidade, refletida pela alteração dos seus valores de coeficientes de partição entre a fase aquosa e a fase orgânica, LogP (que considera apenas as formas neutras da molécula) e LogD (que considera as formas ionizadas da moléculas em decorrência da variação de pH), que passam de 0.714 para 0.938 (LogP), e de -3.92 para -2.58 (LogD, pH 8.0), estando mais próximos dos valores considerados ótimos para compostos com boa biodisponibilidade oral e absorção gastrointestinal (75)[iii].

Os resultados correspondentes aos primeiros inibidores de ação seletiva contra a enzima OPRT de MTB, apresentados no Capítulo 03, foram compilados em um artigo científico submetido ao *Bioorganic and Medicinal Chemistry Letters*, revista internacional indexada de alto impacto. Estes dados serão o ponto de partida para a realização de novas substituições químicas, utilizando como molécula base o composto **13**, com o intuito de otimizar sua hidrofobicidade (valores de LogP e LogD) e aumentar a sua afinidade pela enzima, reduzindo ainda mais seus valores de K_i.

O efeito dos inibidores identificados, assim como a próxima geração de inibidores seletivos da OPRT de MTB que serão derivados do composto **13**, será avaliado *in vivo* através de ensaios celulares para a determinação da concentração mínima inibitória (MIC) e de ensaios em modelo animal.

A resolução experimental através de cristalografia por difração de raios X da estrutura tridimensional da enzima OPRT de MTB, na sua forma apo e associada a

[iii] Valores ótimos de LogP para compostos com boa absorção gastrointestinal variam entre 0 e 3, sendo observada baixa permeabilidade celular em valores abaixo de zero (compostos mais polares), e baixa solubilidade em água em valores acima de 3 (compostos mais apolares). Valores ótimos de LogD variam entre 1 e 3, correspondendo a compostos com boa solubilidade e permeabilidade celular (75).

seus ligantes (Capítulo 4) permitirá a identificação dos resíduos de aminoácidos envolvidos na ligação de substratos, produtos e inibidores ao sítio ativo da enzima, assim como os resíduos de aminoácidos envolvidos com a catálise da reação, e na formação da sua estrutura quaternária.

Os resultados obtidos com a conclusão dos experimentos de nocaute gênico da sequência de DNA responsável pela codificação da enzima OPRT de MTB (Capítulo 5), proporcionará maior entendimento sobre o metabolismo de nucleotídeos em MTB, indicando a sua maior ou menor dependência das vias de síntese *de novo* ou de salvamento de bases livres. A obtenção de uma cepa auxotrófica para uracil poderá viabilizar o desenvolvimento de uma amostra atenuada com potencial uso na profilaxia da TB, podendo aumentar a eficácia das vacinas utilizadas atualmente, baseadas em MTB BCG, cuja eficácia é altamente variável (26). Em conjunto, estes resultados complementarão a determinação do papel da enzima OPRT na sobrevivência e/ou persistência do MTB. O metabolismo necessário para a sua sobrevivência durante o estado latente ainda é pouco compreendido; no entanto, evidências experimentais indicam que a síntese de nucleotídeos é mantida mesmo durante a latência (19). Desta forma, um inibidor específico de enzimas pertencentes às rotas de síntese de nucleotídeos, como a OPRT, tem potencial para ser efetivo tanto contra a forma ativa como contra a forma latente da TB.

Referências

1. World Health Organization. Global Tuberculosis Control - Epidemiology, Strategy, Financing. [Online]. 2009 [citado 2010]. Disponível em: www.who.int/tb/publications/global_report/2009.

2. World Health Organization. Global tuberculosis control: a short update to the 2009 report Switzerland: WHO Press; 2010.

3. Corbett E, Watt C, Walker N, Maher D, Williams B, Ravaglione M, et al. The growing burden of tuberculosis: global trends and interactions woth the HIV epidemic. Arch Intern Med. 2003; 163(9):1009-1021.

4. Ministério da Saúde do Brasil. Ministério da Saúde. [Online]. 2008 [citado 2010]. Disponível em: http://portal.saude.gov.br/saude/visualizar_texto.cfm?idtxt=21445.

5. Pablos-Mendez A, Gowda D, Frieden T. Controlling multidrug-resistant tuberculosis and access to expensive drugs: a rational framework. Bull World Health Organ. 2002; 80(6):489-495.

6. Zaleskis R. Adverse effects of anti-tuberculosis chemotherapy. Eur Resp Dis. 2006:47-49.

7. World Health Organization. XDR-TB - Extensive Drug Resistant TB. [Online].; 2006 [cited 2010]. Disponível em: http://who.int/mediacentre/news/notes/2006/np23/index.html.

8. Wise J. Southern Africa is moving swiftly to combat the threat of XDT-TB. Bull World Health Organ. 2006; 84(12):924-925.

9. Velayati A, Masjedi M, Farnia P, Tabarsi P, Ghanavi J, ZiaZarifi A, et al. Emergence of new forms of totally drug-resistant tuberculosis bacilli. CHEST. 2009 Novembro 16; 136:420-425.

10. Velayati A, Farnia P, Masjedi M, Ibrahim T, Tabarsi P, Haroun R, et al. Totally drug-resistant tuberculosis strains: evidence of adaptation at hte cellular level. Eur Resp J. 2009 Novembro 01; 34(5):1202-1203.

11. Russell DG, Barry 3rd CE, Flynn JL. Tuberculosis: What we don't know ca, and does, hurt us. Science. 2010 Maio 14; 328:852-856.

12. Ma Z, Lienhardt C, McIlleron H, Nunn A, Wang X. Global tuberculosis drug development pipeline: the need and the reality. Lancet. 2010 Junho 12; 375:2100-2109.

13. Hasan S, Daugelat S, Rao PSS, Schreiber M. Prioritizing genomic drug targets in pathogens: Application to *Mycobacterium tuberculosis*. PLoS Comput Biol. 2006; 2(6):e61.

14. Malathi V, Ramakrishnan T. Byosynthesis of nucleic acid purines in *Mycobacterium tuberculosis* H37Rv. Biochem J. 1966; 98(2):594-597.

15. Eisenreich W, Dandekar T, Heesemann J, Goebel W. Carbon metabolism of intracellular bacterial pathogens and possible links to virulence. Nature Rev Microbiol. 2010; 8:401-412.

16. Niederweis M. Nutrient acquisition by mycobacteria. Microbiology. 2008; 154:679-692.

17. Davis J, Ramakrishnan L. The role of the granuloma in expansion and dissemination of early tuberculosis infection. Cell. 2009; 136:38-49.

18. Raupach B, Kaufmann S. Immune responces to intracellular bacteria. Cur Opin Immunol. 2001; 13:417-428.

19. Boshoff H, Barry C3. Tuberculosis - metabolism and respiration in the absence of growth. Nature Rev Microbiol. 2005; 3:70-80.

20. Hanekom W, Abel B, Scriba T. Immunological protection against tuberculosis. SAMJ. 2007; 97(10):973-977.

21. Russell D. Who put the tubercle in the tuberculosis? Nature Rev Microbiol. 2007; 5:39-47.

22. Saunders B, Britton W. Life and death in the granuloma: immunopathology of tuberculosis. Immunol Cell Biol. 2007; 85:103-111.

23. Fox BA, Bzik JD. *De novo* pyrimidine biosynthesis is required for virulence of *Toxoplasma gondii*. Nature. 2002 Fevereiro 22; 415:926-930.

24. Krungkrai S, Aoki S, Palacpac N, Sato D, Mitamura T, Kungkrai J, et al. Human malaria parasite orotate phosphoribosyltransferase: funcional expression, characterization of kinetic reaction mechanism and inhibition profile. Mol Biochem Parasitol. 2004; 134:245-255.

25. Kant S, Maurya AK, Kushwaha R, Nag VL, Prasad R. Multi-drug resistant tuberculosis: An iatrogenic problem. BioSci Trends. 2010; 4(2):48-55.

26. Pando R, Aguilar L, Infante E, Cataldi A, Bigi F, Martin C, et al. The use of mutant mycobacteria as new vaccines to prevent tuberculosis. Tuberculosis. 2006; 86:203-210.

27. Voet D, Voet J. Biochemistry. 2ª ed. EUA: Wiley; 1995.

28. Nelson D, Cox M. Lehninger Principles of Biochemistry. 4ª ed. EUA: Freeman; 2005.

29. Campbell M. Bioquímica. 3ª ed. Porto Alegre: Artmed; 2000.

30. Kilstrup M, Hammer K, Jensen PR, Martinussen J. Nucleotide metabolsim and its control in lactic acid bacteria. FEMS Microbiol Rev. 2005; 29(3):555-590.

31. Smith C, Marks A, Lieberman M. Mark's Basic Medical Biochemistry. 2ª ed. EUA: Lippincott Williams & Wilkins; 2005.

32. Tozzi M, Camici M, Mascia L, Sgarrella F, Ipata P. Pentose phosphates in nucleoside interconversion and catabolism. FEBS J. 2006; 273(6):1089-1101.

33. Ducati RG, Breda A, Basso LA, Santos DS. Purine salvage pathway in *Mycobacterium tuberculosis*. Cur Med Chem. 2010; *in press*.

34. O'Donovan G, Neuhard J. Pyrimidine metabolism in microorganisms. Bacteriol Rev. 1970; 34(3):278-343.

35. Shambaugh III GE. Pyrimidine biosynthesis. Am J Clin Nutr. 1979; 32:1290-1297.

36. Jones ME. Pyrimidine nucleotide biosynthesis in animals; genes, enzymes, and regulation of UMP biosynthesis. Annu Rev Biochem 1980; 49:253-279.

37. Yablonski MJ, Pasek DA, Han BD, Jones ME, Traut T. Intrinsic activity and stability of bifunctional human UMP synthase and its two separate catalytic domains, Orotate phosphoribosyltransferase and Orotidine-5'-phosphate decarboxylase. J Biol Chem. 1996; 271(18):10704-10708.

38. Villela AD, Sánchez-Quitian ZA, Ducati RG, Santos DS, Basso LA. Pyrimidine salvage pathway in *Mycobacterium tuberculosis*. Cur Med Chem J. 2010; *in press*.

39. Bhatia MB, Vinitsky A, Grubmeyer C. Kinetic mechanism of orotate phosphoribosyltransferase from *Salmonella Typhimurium*. Biochemistry. 1990; 29(46):10480-10487.

40. Sinha SC, Smith JL. The PRT protein family. Cur Opin Struct Biol. 2001; 11:733-739.

41. Wang G, Cahill S, Liu X, Girvin M, Grubmeyer C. Motional dynamics of the catalytic loop in OMP synthase. Biochemistry. 1999; 38:284-295.

42. Wang G, Lundegaard C, Jensen K, Grubmeyer C. Kinetic mechanism of OMP synthase: a slow physical step following transfer limits catalytic rate. Biochemistry. 1999; 38:275-283.

43. Zhang Y, Schramm VL. Pyrophosphate interactions at the transition states of *Plasmodium falciparum* and human orotate phosphoribosyltransferase. JACS.

2010; 132:8787-8794.

44. Abdo M, Zhang Y, Schramm VL, Knapp S. Electrophilic aromatic selenylation: New OPRT inhibitors. Org Lett. 2010; 12(13):2982-2985.

45. Zhang Y, Luo M, Schramm VL. Transition states of *Plasmodium falciparum* and human orotate phosphoribosyltransferases. JACS. 2009; 131:4685-4694.

46. Javaid ZZ, el Kouni MH, Ilzsch MH. Pyrimidine nucleobase ligands of orotate phosphoribosyltransferase from *Toxoplasma gondii*. Biochem Pharmacol. 1999; 58:1457-1465.

47. Temmink O, Bruin M, Turksma A, Cricca S, Laan A, Peters G. Activity and substrate specificity of pyrimidine phosphorylases and their role in flouropyrimidine sensitivity in colon cancer cell lines. IJBCB. 2007; 39(3):565-575.

48. Ichikawa W. Prediction of clinical outcome of fluoropyrimidine-based chemotherapy for gastric cancer patients, in terms if the 5-fluoruracil metabolic pathway. Gastric Cancer. 2006; 9:145-155.

49. Sibley L. No more free lunch. Nature. 2002; 415:843-844.

50. Deschamps JR. X-ray crystallography of chemical compounds. Life Sci. 2010; 86:585-589.

51. González-Segura L, Witte JF, McClard RW, Hurley TD. Ternary complex formation and induced asymmetry in orotate phosphoribosyltransferase. Biochemistry. 2007; 46:14075-14086.

52. Scapin G, Grubmeyer C, Sacchettini JC. Crystal strcture of orotate phosphoribosyltransferase. Biochemistry. 1994; 33(6):1287-1294.

53. Scapin G, Ozturk DH, Charles G, Sacchettini JC. The crystal structure of the orotate phosphoribosyltransferase complexed with orotate and α-D-5-phosphoribosyl-1-pyrophosphate. Biochemistry. 1995; 34(34):10744-10754.

54. Henriksen A, Aghajari N, Jensen KF, Gajhede M. A flexible loop at the dimer interface is a part of the active site of the monomer of the *Escheria coli* orotate phosphoribosyltransferase. Biochemistry. 1996; 35(12):3803-3809.

55. Liu CP, Xu R, Gao ZQ, Xu JH, Hou HF, Li LQ, et al. Structure of orotate phosphoribosyltransferase from caries pathogen *Streptococcus mutans*. Acta Crystallogr. 2010; F66:498-502.

56. Berman HM, Westbrook J, Feng Z, Gilliland G, Bhat TN, Weissig H, et al. The Protein Data Bank. Nucleic Acids Res. 2000; 28:235-242.

57. Ioerger TR, Sacchettini JC. Structural genomics approach to drug discovery for Mycobacterium tuberculosis. Cur Opin Microbiol. 2009; 12:318-325.

58. Ochi T, Bolanos-Garcia VM, Stojanoff V, Moreno A. Perspectives on protein crystallisation. Prog Biophys Mol Biol. 2009; 101:56-63.

59. Smyth MS, J MJH. X-ray crystallography. J Clin Pathol: Mol Pathol. 2000; 53(1):8-14.

60. Hassell AM, An G, Bledsoe RK, Bynum JM, Carter III HL, Deng SJJ, et al. Crystallization of protein-ligand complexes. Acta Crystallogr. 2007; D63:72-79.

61. Pizzorno G, Cao D, Leffert JJ, Russel RL, Zhang D, Handschumacher RE. Homeostatic control of uridine and the role of uridine phosphorylase: a biological and clinical update. Biochim Biophys Acta. 2002 Julho 18; 1587(2-3):133-144.

62. Connolly GP, Duley JA. Uridine and its nucleotides: biological actions, therapeutics potentials. TiPS. 1999; 20(5):218-225.

63. Parish T, Stoker NG. Use of flexible cassette method to generate a double unmarked *Mycobacterium tuberculosis* tlyA plcABC mutant by gene replacement. Microbiology. 2000; 146:1969-1975.

64. Kowalczykowski SC, Dixon DA, Eggleston AK, Lauder SD, Rehrauer WM. Biochemistry of homologous recombination in *Escherichia coli*. Microbiol Rev. 1994; 58(3):401-465.

65. Gordhan BG, Parish T. Gene replacement using pretreated DNA. Em Parish T, Stoker NG. Methods in Molecular Medicine: *Mycobacterium tuberculosis* protocols. Totowa, NJ: Humana Press Inc; 2001. p. 77-92.

66. Spigelman M, Woosley R, Gheuens J. New iniciative speeds tuberculosis drug development: novel drug regimens become possible in years, not decades. Int J Tuberc Lung Dis. 2010; 14(6):663-664.

67. Donald PR. The treatment of tuberculosis in childhood. SAMJ. 2007; 97(10):992-994.

68. Umejiego NN, Li C, Riera T, Hedstrom L, B S. *Cryptosporidium parvum* IMP dehydrogenase: identification of functional, structural, and dynamic properties that can be exploited for drug design. J Biol Chem. 2004; 279(39):40320-40327.

69. Lipinski CA, Lombardo F, Dominy BW, Feeney PJ. Experimental and computational approaches to estimate solubility and permeability in drug discovery and development settings. Adv Drug Deliv Rev. 1997; 23:3-25.

70. Hopkins AL, Groom CR. The druggable genome. Nature Rev Drug Discov. 2002;

1:727-730.

71. Veber DF, Johnson SR, Cheng HY, Smith BR, Ward KW, Kopple KD. Molecular Properties That Influence the Oral Bioavailability of Drug Candidates. J Med Chem. 2002; 45(12):2615-2623.

72. Copeland R. Evaluation of enzyme inhibitors in drug discovery: Wiley-Interscience; 2005.

73. Freire E. Do enthalpy and entropy distinguish first in class from best in class? Drug Discov Today. 2008; 13(19-20):869-874.

74. Roselin LS, Lin MS, Lin PH, Chang Y, Chen WY. Recent trends and some applications of isothermal titration calorimetry in biotechnology. Biotechnol J. 2010; 5:85-98.

75. Kerns EH, Di L. Drug-like properties: Concepts, structure design and methods from ADME to toxicity optimization. 1ª ed. San diego: Elsevier; 2008.

Anexos

A. CARTA DE SUBMISSÃO AO JBC
CARTA DE SUBMISSÃO AO BMCL
B. Artigo publicado – THE CONSERVED LYSINE69 RESIDUE PLAYS A CATALYTIC ROLE IN *Mycobacterium tuberculosis* SHIKIMATE DEHYDROGENASE
C. Artigo aceito para publicação – PURINE SALVAGE PATHWAY IN *Mycobacterium tuberculosis*
D. Artigo aceito para publicação – UMP KINASE FROM *Mycobacterium tuberculosis*: MODE OF ACTION AND ALLOSTERIC INTERACTIONS, AND THEIR LIKELY ROLE IN PYRIMIDINE METABOLISM REGULATION
E. Artigo submetido para publicação – RECOMBINANT *Escherichia coli* GMP REDUCTASE: KINETIC, CATALYTIC AND CHEMICAL MECHANISMS, AND THERMODYNAMICS OF ENZYME-LIGAND BINARY COMPLEX FORMATION.

Anexo A

Carta de submissão ao *The Journal of Biological Chemistry*

Carta de submissão ao *Bioorganic and Medicinal Chemistry Letters*

From: jbc@asbmb.org [mailto:jbc@asbmb.org]
Sent: Mon 2/14/2011 12:37 PM
To: Luiz Augusto Basso
Subject: JBC/2011/230839 Manuscript Submission

MS ID#: JBC/2011/230839
MS TITLE: MOLECULAR, KINETIC AND THERMODYNAMIC CHARACTERIZATION OF Mycobacterium tuberculosis OROTATE PHOSPHORYBOSILTRANSFERASE

Dear Dr. Basso:

This is an automatic message acknowledging your online submission to The Journal of Biological Chemistry.
Thank you for your submission.
Sincerely,

Editorial Staff
The Journal of Biological Chemistry

Sent on: February 14, 2011

MS ID#: JBC/2011/230839
MS TITLE: Molecular, kinetic and thermodynamic characterization of Mycobacterium tuberculosis orotate phosphorybosiltransferase

Dear Dr. Basso:

We have received your manuscript entitled:

"Molecular, kinetic and thermodynamic characterization of Mycobacterium tuberculosis orotate phosphorybosiltransferase".

It has been given the number JBC/2011/230839 and has been assigned to:

Dr. Guengerich
Associate Editor
Journal of Biological Chemistry
E-mail: ktrisler@asbmb.org

Dear Dr Souto,

Your submission entitled "PYRIDINONE-BASED INHIBITORS OF Mycobacterium tuberculosis OROTATE PHOSPHORIBOSYLTRANSFERASE" has been received by Bioorganic & Medicinal Chemistry Letters

You may check on the progress of your manuscript by logging on to the Elsevier Editorial System as an author. The URL is http://ees.elsevier.com/bmcl/.

Your username is: Andre_Arigony
If you can't remember your password please click the "Send Password" link on the Login page.

Your manuscript will be given a reference number once an Editor has been assigned.

Bioorganic and Medicinal Chemistry Letters operates a rapid publication policy allowing papers to be posted on ScienceDirect immediately following acceptance of the manuscript. This will be a huge advantage to authors, allowing timely dissemination of your work. If you feel that this service is not appropriate for your paper, please contact bmcl-eo@elsevier.com

Thank you for submitting your work to Bioorganic & Medicinal Chemistry Letters.

Kind regards,

Bioorganic & Medicinal Chemistry Letters

For further assistance, please visit our customer support site at http://support.elsevier.com Here you can search for solutions on a range of topics, find answers to frequently asked questions and learn more about EES via interactive tutorials. You will also find our 24/7 support contact details should you need any further assistance from one of our customer support representatives.

Ms. Ref. No.: BMCL-D-11-00173
Title: PYRIDINONE-BASED INHIBITORS OF Mycobacterium tuberculosis OROTATE PHOSPHORIBOSYLTRANSFERASE
Bioorganic & Medicinal Chemistry Letters

Dear Dr Souto,

Your submission entitled "PYRIDINONE-BASED INHIBITORS OF Mycobacterium tuberculosis OROTATE PHOSPHORIBOSYLTRANSFERASE" has been been assigned the following manuscript number: BMCL-D-11-00173.

You may check on the progress of your manuscript by logging on to the Elsevier Editorial System as an author. The URL is http://ees.elsevier.com/bmcl/.

Your username is: Andre_Arigony
If you can't remember your password please click the "Send Password" link on the Login page.

Thank you for submitting your work to Bioorganic & Medicinal Chemistry Letters.

Kind regards,

Mary Leitel
Journal Manager
Bioorganic & Medicinal Chemistry Letters

For guidelines on how to track your manuscript in EES please go the following address: http://support.elsevier.com/app/answers/detail/a_id/89

Anexo B

THE CONSERVED LYSINE69 RESIDUE PLAYS A CATALYTIC ROLE IN *Mycobacterium tuberculosis* SHIKIMATE DEHYDROGENASE

Valnês S Rodrigues Junior, Ardala Breda, Diógenes S Santos, Luiz A Basso

Artigo publicado
BMC Research Notes, 2009, 2:227

BMC Research Notes

Short Report

The conserved Lysine69 residue plays a catalytic role in *Mycobacterium tuberculosis* shikimate dehydrogenase

Valnês S Rodrigues Junior[1], Ardala Breda[1,2], Diógenes S Santos*[1] and Luiz A Basso*[1]

Addresses: [1]Centro de Pesquisas em Biologia Molecular e Funcional (CPBMF), Instituto Nacional de Ciência e Tecnologia em Tuberculose (INCT-TB), Pontifícia Universidade Católica do Rio Grande do Sul (PUCRS); Porto Alegre, Brazil and [2]Programa de Pós-Graduação em Biologia Celular e Molecular, Pontifícia Universidade Católica do Rio Grande do Sul (PUCRS); Porto Alegre - RS, Brazil

E-mail: Valnês S Rodrigues Junior - valnesjunior@yahoo.com.br; Ardala Breda - ardalabreda@hotmail.com; Diógenes S Santos* - diogenes@pucrs.br; Luiz A Basso* - luiz.basso@pucrs.br
*Corresponding author

Published: 16 November 2009

BMC Research Notes 2009, **2**:227 doi: 10.1186/1756-0500-2-227

Received: 22 May 2009
Accepted: 16 November 2009

This article is available from: http://www.biomedcentral.com/1756-0500/2/227

Abstract

Background: The shikimate pathway is an attractive target for the development of antitubercular agents because it is essential in *Mycobacterium tuberculosis*, the causative agent of tuberculosis, but absent in humans. *M. tuberculosis aroE*-encoded shikimate dehydrogenase catalyzes the forth reaction in the shikimate pathway. Structural and functional studies indicate that Lysine69 may be involved in catalysis and/or substrate binding in *M. tuberculosis* shikimate dehydrogenase. Investigation of the kinetic properties of mutant enzymes can bring important insights about the role of amino acid residues for *M. tuberculosis* shikimate dehydrogenase.

Findings: We have performed site-directed mutagenesis, steady-state kinetics, equilibrium binding measurements and molecular modeling for both the wild-type *M. tuberculosis* shikimate dehydrogenase and the K69A mutant enzymes. The apparent steady-state kinetic parameters for the *M. tuberculosis* shikimate dehydrogenase were determined; the catalytic constant value for the wild-type enzyme (50 s^{-1}) is 68-fold larger than that for the mutant K69A (0.73 s^{-1}). There was a modest increase in the Michaelis-Menten constant for DHS (K69A = 76 μM; wild-type = 29 μM) and NADPH (K69A = 30 μM; wild-type = 11 μM). The equilibrium dissociation constants for wild-type and K69A mutant enzymes are 32 (± 4) μM and 134 (± 21), respectively.

Conclusion: Our results show that the residue Lysine69 plays a catalytic role and is not involved in substrate binding for the *M. tuberculosis* shikimate dehydrogenase. These efforts on *M. tuberculosis* shikimate dehydrogenase catalytic mechanism determination should help the rational design of specific inhibitors, aiming at the development of antitubercular drugs.

Background

Tuberculosis (TB) remains a major global health concern. It has been estimated that one-third of the world population is infected with *Mycobacterium tuberculosis*, the causative agent of TB, and that 30 million people died from this disease in the last decade [1]. The epidemic of the human immunodeficiency virus, the increase in the homeless population, and the decline in health care structures and national surveillance are contributing factors to TB resurgence. Inappropriate treatment regimens and patient noncompliance in completing the therapies are associated with the

emergence of multi-drug resistant TB (MDR-TB), defined as strains of *M. tuberculosis* resistant to at least isoniazid and rifampicin, two pivotal drugs used in the standard treatment of TB [2]. It has been reported the emergence of extensively drug-resistant (XDR) TB cases, defined as cases in persons with TB whose isolates are MDR as well as resistant to any one of the fluoroquinolone drugs and to at least one of the three injectable second-line drugs [3]. XDR-TB is widespread raising the prospect of virtually incurable TB worldwide [3]. There is thus an urgent need for new drugs to improve the treatment of MDR- and XDR-TB, and to provide more effective drugs to shorten the duration of TB treatment. Enzyme inhibitors make up roughly 25% of the drugs marketed [4], and are thus important promising drug targets.

The shikimate pathway is an attractive target for the development of herbicides and antimicrobial agents because it is essential in algae, higher plants, bacteria, and fungi, but absent from mammals [5]. The mycobacterial shikimate pathway leads to the biosynthesis of precursors of aromatic amino acids, naphthoquinones, menaquinones, and mycobactins [6], and is essential for *M. tuberculosis* viability [7]. Shikimate dehydrogenase (SD; EC 1.1.1.25), the fourth enzyme of this pathway, catalyzes the NADPH-dependent reduction of 3-dehydroshikimate (DHS) to shikimate (SHK, Fig. 1). We have previously reported production, characterization, and determination of kinetic and chemical mechanisms of *aroE*-encoded SD from *M. tuberculosis* H37Rv strain (*Mtb*SD) [8-10]. Multiple sequence alignment, comparative homology modeling, and pH-rate profiles suggested that the Lysine69 in the DHS/SHK binding site of *Mtb*SD plays a role in substrate binding and/or catalysis [10,11]. Here we describe site-directed mutagenesis, steady-state kinetics, fluorimetric measurements and structural analyses to probe the role of Lys69 in *Mtb*SD and provide insight into the molecular basis of DHS/SHK recognition and/or catalysis.

Methods

Site-directed mutagenesis

A previously constructed pET-23a(+)::*aroE* recombinant vector [8] was used as a template for PCR-based mutagenesis using the Quick Change site-directed mutagenesis kit (Stratagene, La Jolla, CA). The synthetic oligonucleotides employed were as follows: 5′-ggtgtttcggtgaccatgccgggc**gcg**ttcgccgccctgcggttcg-3′ (forward) and 5′-cgaaccgcagggcggcgaa**cgc**gcccggcatggtcaccgaaacacc-3′ (reverse) (in bold is the codon for alanine). *Pfu*Turbo® DNA polymerase and standard PCR amplification program were employed. The PCR product was treated with *Dpn*I endonuclease that specifically digests the methylated DNA template, and selects for the mutation-containing synthesized DNA.

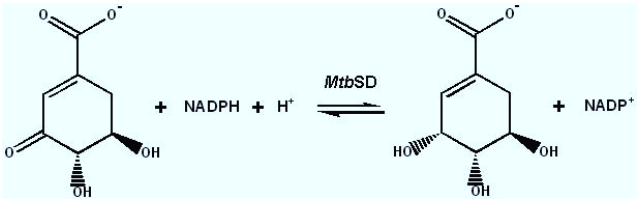

Figure 1
The shikimate dehydrogenase-catalyzed reaction.

Expression, release and purification of recombinant MtbSD

The recombinant plasmid was introduced into *E. coli* C41 (DE3) host cells (Novagen, Madison, WI) by electroporation. Single colonies were used to inoculate 2 L of LB medium containing 50 μg mL^{-1} ampicillin, and 1 mM isopropyl β-D-thiogalactopyranoside was added to cultures reaching an OD_{600} of 0.4 - 0.6, and grown for 24 h at 37°C at 180 rpm. Cells (5 g) were harvested by centrifugation at 14,900 *g* for 30 min at 4°C, and stored at -20°C. The freeze-thaw method was used to release the proteins in the soluble fraction [8]. The purification protocol was as previously described [12]. Samples of the purification steps were analyzed by SDS-PAGE [13] and protein content by the Bradford's method [14].

Enzyme activity assays and determination of kinetic parameters

Steady-state kinetics measurements of homogeneous *Mtb*SD K69A mutant activity were carried out for the forward direction at 25°C in 100 mM potassium phosphate buffer, pH 7.3, by monitoring the decrease in absorbance at 340 nm (ε = 6220 M^{-1} cm^{-1} for NADPH) accompanying the conversion of NADPH and DHS to $NADP^+$ and SHK. The K69A activity was measured at varying final concentrations of DHS (20-300 μM) and NADPH at constant saturating level (200 μM); and varying NADPH concentrations (20-250 μM) and DHS at constant saturating level (250 μM; Fig. 2B and 2D). The wild-type SD activity was measured at various DHS concentrations (10-100 μM) and NADPH at constant saturating level (200 μM); and various NADPH concentrations (5-50 μM) and DHS at constant saturating level (250 μM; Fig. 2A and 2C). All measurements were in duplicate. Steady-state kinetic constants were obtained by non-linear regression analysis of the kinetic data fitted to the Michaelis-Menten equation ($v = V_{max} \times [S]/K_m + [S]$) using the SigmaPlot software (SPSS, Inc).

Fluorescence spectroscopy

Fluorescence titration was performed in a Shimadzu spectrofluorophotometer RF-5301PC at 25°C by making

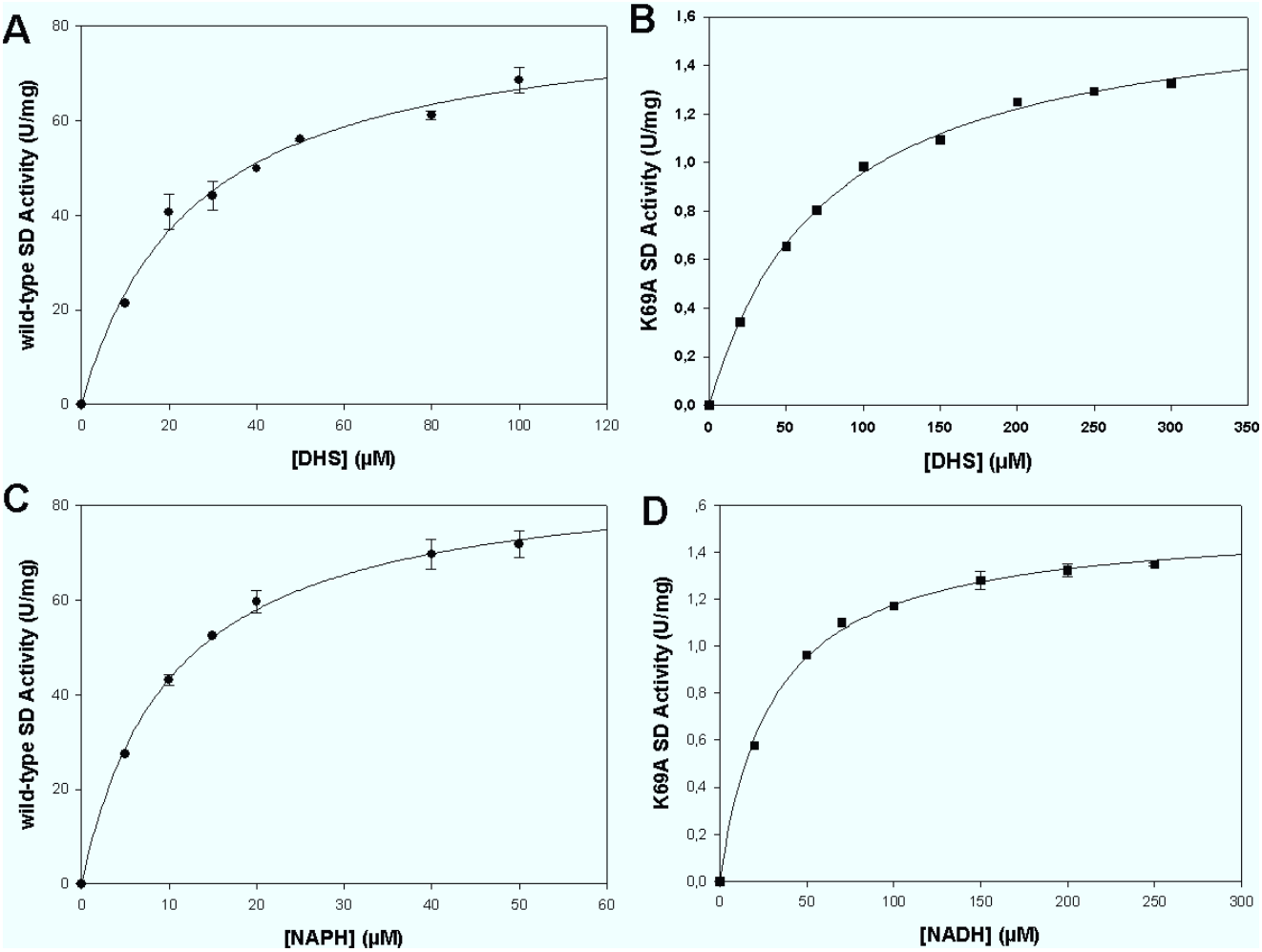

Figure 2
Steady-state kinetic measurements for wild-type (A and C) and K69A (B and D) *Mtb*SD in the forward direction. A and B: DHS concentrations were varied while NADPH concentration was maintained at a fixed saturating level. C and D: NADPH concentrations were varied while DHS concentration was maintained at a fixed saturating level.

microliter additions of DHS substrate stock solutions to 2 mL of 1 μM of *Mtb*SD in 100 mM potassium phosphate buffer pH 7.3. The binding of DHS to *Mtb*SD causes a quench in the intrinsic protein fluorescence (λ_{exc} = 300 nm; 310 ≤ λ_{em} ≤ 450 nm; maximum λ_{em} at 340 nm), which allowed monitoring of *Mtb*SD-DHS binary complex formation at equilibrium. To assess the DHS inner-filter effect in the fluorimeter, two cuvettes were placed in series so that the contents of the first cuvette acted as a filter of the excitation light and the light emitted from the second cuvette detected. DHS was added to the first cuvette, while the second cuvette contained the protein. In this manner, DHS inner-filter effect on protein fluorescence could be assessed. The results were plotted to a rectangular hyperbola by using the nonlinear regression function of SigmaPlot 2004 (SPSS, Inc.).

MtbSD K69A structural analysis

The wild-type *Mtb*SD three-dimensional (3D) model was built previously by comparative homology modeling using *Escherichia coli* SD as template (**PDB ID**: 1NYT) [10], however, a more recent 3D structure for *Thermus thermophilus* SD (**PDB ID**: 2EV9), solved by X-ray crystallography at 1.90 Å in complex with shikimate [15], was used as a template for *Mtb*SD K69A mutant modeling, as well as to evaluate DHS/SHK substrate binding mode to *Mtb*SD. *T. thermophilus* SD shows higher primary structure identity to *Mtb*SD (~30% identity and 13% strong similarity) than *E. coli* SD (26% identity and 15% strong similarity), and the presence of both enzyme's cofactor and substrate bound at its active site makes such structure a more suitable template for *Mtb*SD comparative homology modeling.

Target and template pair-wise sequence alignment required small gaps inclusion on both *M. tuberculosis* and *T. thermophilus* SD primary sequences. *Mtb*SD K69A model was built by restrained-based homology modeling implemented in MODELLER9v1 [16], with the standard protocol of the comparative protein structure modeling methodology, by satisfaction of spatial restrains [17,18]. Atomic coordinates of SHK heteroatoms were copied from template structure into the *Mtb*SD K69A model. The best model was selected according to MODELLER objective function [19] and subjected to energy minimization for amino acid side chain and main chain rearrangements with GROMACS package [20] using the 43a1 force-field. The system was submitted to an initial steepest descent energy minimization *in vacuo* with a maximum number of 400 minimization steps, followed by a maximum of 3000 steps of conjugate gradient energy minimization.

The program PROCHECK and VERIFY 3D were employed to, respectively, analyze stereochemical quality and validate the 3D profile of the model, as previously described [10]. Structural correspondence between *Mtb*SD K69A model and *T. thermophilus* was evaluated by their root-mean square deviation (RMSD). H-bond interactions were evaluated with LIGPLOT v4.4.2 [21], considering an atomic distance cut off of 3.9 Å (program default values).

Findings and Discussion

Site-directed mutagenesis, protein expression and purification

Total sequencing of *aroE* mutant DNA into pET-23a(+) vector confirmed that the mutation was introduced into the expected site and that no unwanted mutations were introduced by the PCR amplification step. The recombinant *Mtb*SD protein purification protocol resulted in a protein yield of 13%, according to the previous protocol [12].

Steady-state kinetic parameters

The apparent steady-state kinetic parameters for K69A (Fig. 2B and 2D) and wild-type *Mtb*SD (Fig. 2A and 2C) are given in Table 1. It is noteworthy that the catalytic constant (k_{cat}) value for wild-type *Mtb*SD (50 s^{-1}) is 68-fold larger than K69A (0.73 s^{-1}), whereas there was a modest increase in the K_m values for DHS (K69A = 76 μM; wild-type *Mtb*SD = 29 μM) and NADPH (K69A = 30 μM; wild-type *Mtb*SD = 11 μM). The apparent second-order rate constant (k_{cat}/K_m) values for DHS (K69A = 9.6×10^3 $M^{-1}s^{-1}$; wild-type *Mtb*SD = 1.7×10^6 $M^{-1}s^{-1}$) and NADPH (K69A = 24×10^3 $M^{-1}s^{-1}$; wild-type *Mtb*SD = 4.5×10^6 $M^{-1}s^{-1}$) indicate that the mutant has a lower specificity constant for both substrates. A comparison of k_{cat}/K_m values is an appropriate method to assess the effect(s) of a mutation on substrate(s) binding and catalysis since it includes the activation energies and the binding energies [22]. A change of 12.8 kJ mol^{-1} can be calculated when we compare the values of k_{cat}/K_m of DHS reduction for wild-type and K69A *Mtb*SD. These results indicate that the conserved Lys69 residue in *Mtb*SD plays a critical role in catalysis, but plays no role in substrate binding. Moreover, the fact that the K69A *Mtb*SD mutant protein still binds DHS and NADPH with only slightly larger K_m values as compared to wild-type enzyme indicates that the mutant protein is properly folded giving more confidence that the results are not an artifact generated by the mutation. Linearity of each measurement and dose dependence when adding different volumes of the enzyme solution were confirmed for all enzyme activity assays (data not shown).

Table 1: Apparent steady-state kinetic parameters and equilibrium binding constants for wild type and K69A mutant *Mtb*SD

Parameter	Wild-type	K69A
V_{max} (U mg^{-1})[a]	110 ± 2	1.61 ± 0.03
K_m DHS (μM)[a]	29 ± 2	76 ± 4
K_m NADPH (μM)[a]	11.0 ± 0.6	30 ± 2
k_{cat} (s^{-1})[a]	50 ± 1	0.73 ± 0.01
k_{cat}/K_m DHS (M^{-1} s^{-1})[a]	1.7 (± 0.1) × 10^6	9.6 (± 0.5) × 10^3
k_{cat}/K_m NADPH (M^{-1} s^{-1})[a]	4.5 (± 0.2) × 10^6	24 (± 2) × 10^3
K_d DHS (μM)[b]	32 ± 4	134 ± 21

[a] steady-state kinetic parameters.
[b] spectroscopic measurements of intrinsic protein fluorescence (equilibrium binding).

Equilibrium binding

Spectrofluorimetric assays were carried out to determine the equilibrium dissociation constant for *Mtb*SD-DHS binary complex formation (Fig. 3). The change in the intrinsic protein fluorescence at varying DHS concentrations (2-450 μM) yielded equilibrium dissociation constant (K_d) values of 32 (± 4) μM for wild-type *Mtb*SD and 134 (± 21) μM for K69A mutant (Table 1). Interestingly, measurements of changes in nucleotide fluorescence upon NADPH binding to wild-type *Mtb*SD (λ_{exc} = 370 nm; 380 ≤ λ_{em} ≤ 600 nm; maximum λ_{em} at 445 nm) did not show any saturation, which indicates a very large K_d value. This is consistent with a steady-state ordered bi-bi mechanism with DHS binding first followed by NADPH binding to *Mtb*SD active site [10]. Moreover, these experiments confirmed our proposal that the Lys69 residue plays a minor role, if any, in substrate binding.

Structural analysis

Two crystallographic structures of SD in complex with both its coenzyme and SHK (*Aquifex aeolicus*, **PDB ID**: 2HK9[23] and *T. thermophilus*, **PDB ID**: 2EV9[15], solved by X-ray diffraction at 2.20 Å and 1.90 Å resolution, respectively) are available in the Protein Data Bank

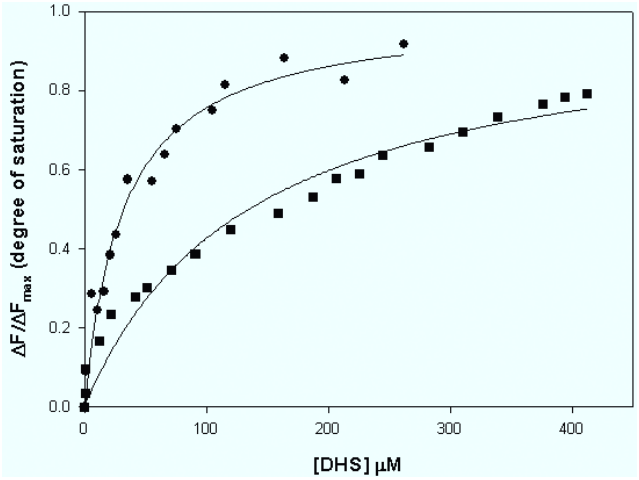

Figure 3
Spectroscopic measurements of intrinsic protein fluorescence for wild-type (black circles) and K69A (black squares) *Mtb*SD upon DHS binding at varying concentrations.

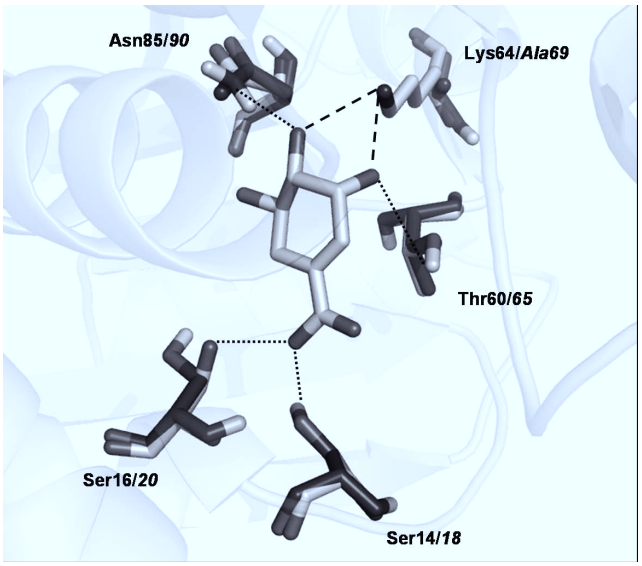

Figure 4
***Mtb*SD K69A model superimposed on experimentally solved *T. thermophilus* SD structure**. Amino acid side chains involved in SHK binding and SHK molecule are shown as sticks. *T. thermophilus* and *Mtb*SD K69A amino acids are colored, respectively, in light gray (residue number in **bold**) and dark gray (residue number in *italics*). H-bonds are shown as dotted lines; dashed lines represent H-bonds between Lys**64**/*69*, missing in *Mtb*SD K69A model.

(PDB). *T. thermophilus* SD structure was chosen as template for comparative homology modeling of *Mtb*SD K69A and for SHK binding analysis because of larger primary sequence identity to *Mtb*SD (~30% identity and 13% strong similarity) as compared to *A. aeolicus* (24% identity and 16% strong similarity), and lower requirement for inclusion of gaps in primary sequence comparisons.

Analysis of the 3D structures of SDs in complex with $NADP^+$ and SHK suggest that Lys64 in *T. termophilus* [15] and Lys70 in *A. aeolicus* [23] interact with C3 of DHS and act as an acid-base catalytic group. Corresponding Lys residue is also suggested to be catalytically active in *Staphylococcus epidermidis* [24], *Haemophilus influenzae* [25] and *Arabidopsis thaliana* [26] SDs.

No significant changes were observed on protein's overall tertiary structure and in DHS/SHK binding site after energy minimization of the *Mtb*SD K69A model. The RMSD deviation from template of only 0.55 Å, 99% of amino acids within allowed regions of the Ramachandran's plots and PROCHECK parameters indicate that the K69A model satisfies all stereochemical requirements. Considering only substrate binding site amino acids, *Mtb*SD K69A RMSD values reduced to 0.12 Å when compared to template. Such minor structural variations indicate a strong conservation of the amino acid arrangement at the enzyme's substrate binding site, not only at their α-carbon position but also in regard to their χ rotational angles, where only *Mtb*SD residue Ser20 (Ser16 on template) shows variation on its rotational angle χ_1 (2.02 Å for Oγ atom), although not affecting H-bonding to SHK. (Fig. 4).

H-bonding pattern between MtbSD and SHK

LIGPLOT analysis showed that the pattern of H-bonding to SHK is conserved in *T. thermophilus* SD and *Mtb*SD K69A (Table 2). Gln243 residue in *M. tuberculosis* (corresponding to Gln235 in *T. thermophilus* SD) also makes a hydrophobic contact to C5 of SHK, as observed on template's structure. No significant amino acid

Table 2: Hydrogen bonding pattern of SD enzyme and SHK substrate. *T. thermophilus* values are shown in bold, *Mtb*SD K69A corresponding values are shown in *italics*.

SD residue	SD Atom	SHK atom	H bond distance (Å)
Ser14/*Ser18*	**Oγ**	**O2**	**2.62**/*2.55*
Ser16/*Ser20*	**Oγ**	**O2**	**2.72**/*2.73*
Thr60/*Thr65*	**Oγ 1**	**O11**	**3.28**/*3.22*
Lys64/*Lys69*	**Nζ**	**O11**	**2.80**/–
Lys64/*Lys69*	**Nζ**	**O12**	**3.10**/–
Asn85/*Asn90*	**Nδ 2**	**O12**	**3.15**/*2.93*

Atom numbering as [24]*.
* O2 corresponds to carboxyl negative oxygen atom, O11 to hydroxyl oxygen bound to C3, O12 to hydroxyl oxygen bound to C4, and O7 to hydroxyl oxygen bound to C5, as depicted in Fig. 1.

rearrangements were observed for *Mtb*SD K69A. Not surprisingly, the noticeable change is the loss of two H-bonds with the SHK molecule in K69A mutant. It could be argued that the loss of two H-bonds in K69A *Mtb*SD mutant would demonstrate the role of Lys69 in DHS/SHK binding. The energies of hydrogen bonds have been variously estimated to be between 12 and 38 kJ mol^{-1} [22]. Spectrofluorimetric measurements showed a reduction of 3.5 kJ mol^{-1} in binding energy of DHS to K69A *Mtb*SD as compared to the wild-type enzyme.

Conclusion

Based on double isotope effects and pH-rate profiles, we have previously proposed that the chemical mechanism for *Mtb*SD involves hydride transfer and solvent proton transfer in a concerted manner, and that an amino acid residue with an apparent pK_a value of 8.9 is involved in catalysis [10]. Here we demonstrate that the *Mtb*SD Lys69 is important for catalysis and is likely involved in stabilization of the developing negative charge at the hydride-accepting C-3 carbonyl oxygen of DHS for the forward reaction, acting as an acid-base catalytic group that donates a proton to DHS carbonyl group during reduction, playing a minor role, if any, in substrate binding.

In bacteria, four subclasses of SD have been identified, distinguished by their phylogeny and biochemical activity [27]. In agreement with our results, mutagenesis studies showed that the corresponding residues Lys67 in *Haemophilus influenzae* SD [25] and Lys385 in *Arabidopsis thaliana* dehydroquinate dehydratase-SD [26] play a critical role in catalysis and no role in substrate binding. Interestingly, site-directed mutagenesis of *Escherichia coli* YdiB (a bifunctional enzyme that catalyzes the reversible reductions of 3-dehydroquinate to quinate and 3-dehydroshikimate to shikimate using as co-substrate either NADH or NADPH) has shown that the conserved Lys71 residue plays a primary role in substrate binding in the Michaelis complex and, although it contributes to some extent to transition state stabilization, plays no essential role in catalysis [28].

It should be pointed out that mechanistic analysis should always be a top priority for new enzyme-targeted drug programs since effective enzyme inhibitors take advantage of enzyme chemistry to achieve inhibition [29]. Accordingly, we hope that the results here presented will pave the way for the target-based rational design of novel effective antitubercular agents. The design of inhibitors of *Mtb*SD enzyme activity may contemplate derivatization of C-3 of DHS with functional groups that make strong interactions with the Lys69 side chain. It would appear to be unlikely that a mutation of Lys69 residue would be selected for to afford drug resistance because here is shown that this amino acid residue plays a critical role in *Mtb*SD enzyme activity. However, an important additional point to be considered when selecting a particular enzyme as a successful drug target is to determine a flux control coefficient, which measures the sensitivity of flux to a change in enzyme concentration. An enzyme is likely a good target if the flux control coefficient is high, whereas it is less likely a good target if the flux control coefficient is close to zero (virtually all the activity must be eliminated by an inhibitor to have the desired chemotherapeutic effect). Bifunctional dehydroquinate dehydratase-shikimate dehydrogenases in plants are responsible for preferential routing of carbon to aromatic amino acid synthesis [30]. However, how shikimate dehydrogenase affects the shikimate pathway flux in *M. tuberculosi*s is still unknown. Therefore, strategies for drug design contemplating derivatization of C-3 of DHS should also take into account whether shikimate dehydrogenase has a low flux control coefficient because mutation of Lys69 would be one way of gaining resistance to this enzyme's inhibitors.

List of abbreviations used

TB: tuberculosis; MDR: multi-drug resistant; XDR: extensively drug-resistant; *Mtb*SD: shikimate dehydrogenase from *M. tuberculosis*; DHS: 3-dehydroshikimate; SHK: shikimate; K_m: Michaelis-Menten constant; RMSD: root-mean square deviation; k_{cat}: catalytic constant; K_d: equilibrium dissociation constant.

Competing interests

The authors declare that they have no competing interests.

Author's contributions

VSRJ performed most of the experiments and drafted the manuscript. AB performed the structural analysis and helped to write the manuscript. The study was conceived and coordinated by DSS and LAB, who have also helped to draft the manuscript. All authors read and approved the final version of the manuscript.

Acknowledgements

This work was supported by National Institute of Science and Technology on Tuberculosis (Decit/SCTIE/MS-MCT-CNPq-FNDCT-CAPES) and Millennium Initiative Program (CNPq), Brazil, to D.S.S. and L.A.B. D.S.S. and L.A.B. also acknowledge grants awarded by FINEP. D.S.S. (304051/1975-06) and L.A.B. (520182/99-5) are research career awardees from the National Council for Scientific and Technological Development of Brazil (CNPq). We are grateful to Professor John W. Frost, Department of Chemistry of Michigan State University, for his generous gift of 3-dehydroshikimate.

References

1. Dye C, Scheele S, Dolin P, Pathania V and Raviglione MC: **Global burden of tuberculosis: estimated incidence, prevalence, and mortality by country.** *JAMA* 1999, **282:**677–686.
2. Basso LA and Blanchard JS: **Resistance to antitubercular drugs.** *Adv Exp Med Biol* 1998, **456:**115–144.
3. Dorman SE and Chaisson RE: **From magic bullets back to the Magic Mountain: the rise of extensively drug-resistant tuberculosis.** *Nat Med* 2007, **13:**295–298.
4. Robertson JG: **Mechanistic basis of enzyme-targeted drugs.** *Biochemistry* 2005, **44:**5561–5571.
5. Bentley R: **The shikimate pathway - a metabolic tree with many branches.** *Crit Rev Biochem Mol Biol* 1990, **25:**307–384.
6. Ducati RG, Basso LA and Santos DS: **Mycobacterial shikimate pathway enzymes as targets for drug design.** *Curr Drug Targets* 2007, **8:**423–435.
7. Parish T and Stoker NG: **The common aromatic amino acid biosynthesis pathway is essential in *Mycobacterium tuberculosis*.** *Microbiology* 2002, **148:**3069–3077.
8. Magalhães MLB, Pereira CP, Basso LA and Santos DS: **Cloning and expression of functional shikimate dehydrogenase (EC 1.1.1.25) from *Mycobacterium tuberculosis* H37Rv.** *Prot Expr Purif* 2002, **26:**59–64.
9. Fonseca IO, Magalhães MLB, Oliveira JS, Silva RG, Mendes MA, Palma MS, Santos DS and Basso LA: **Functional shikimate dehydrogenase from *Mycobacterium tuberculosis* H37Rv: purification and characterization.** *Prot Expr Purif* 2006, **46:**429–437.
10. Fonseca IO, Silva RG, Fernandes CL, de Souza ON, Basso LA and Santos DS: **Kinetic and chemical mechanisms of shikimate dehydrogenase from *Mycobacterium tuberculosis*.** *Arch Biochem Biophys* 2007, **457:**123–133.
11. Arcuri HA, Borges JC, Fonseca IO, Pereira JH, Neto JR, Basso LA, Santos DS and de Azevedo WF Jr: **Structural studies of shikimate 5-dehydrogenase from *Mycobacterium tuberculosis*.** *Proteins* 2008, **72:**720–730.
12. Rodrigues-Junior VS, Basso LA and Santos DS: **Homogeneous recombinant *Mycobacterium tuberculosis* shikimate dehydrogenase production: an essential step towards target-based drug design.** *Int J Biol Macromol* 2009, **45:**200–205.
13. Laemmli UK: **Cleavage of structural proteins during the assembly of the head of bacteriophage T4.** *Nature* 1970, **227:**680–685.
14. Bradford MM, McRorie RA and Williams WL: **A rapid and sensitive method for the quantification of microgram quantities of protein utilizing the principle of protein-dye binding.** *Anal Biochem* 1976, **72:**248–254.
15. Bagautdinov B and Kunishima N: **Crystal structures of shikimate dehydrogenase AroE from *Thermus thermophilus* HB8 and its cofactor and substrate complexes: insights into the enzymatic mechanism.** *J Mol Biol* 2007, **373:**424–438.
16. Šali A and Blundell TL: **Comparative Protein Modelling by Satisfaction of Spatial Restraints.** *J Mol Biol* 1993, **234:**779–815.
17. Martí-Renom MA, Stuart AC, Fiser A, Sánchez R, Melo F and Šali A: **Comparative Protein Structure Modeling of Genes and Genomes.** *Annu Rev Biophys Biomol Struct* 2000, **29:**291–325.
18. Šali A and Overington JP: **Derivation of rules for comparative protein modelling from a database of protein structure alignments - Modeling mutations and homologous proteins.** *Protein Science* 1994, **3:**1582–1596.
19. Shen MY and Šali A: **Statistical potential for assessment and prediction of protein structures.** *Protein Science* 2006, **15:**2507–2524.
20. Spoel van der D, Lindahl E, Hess B, Groenhof G, Mark AE and Berendsen HJC: **GROMACS: fast, flexible, and free.** *J Comp Chem* 2005, **26:**1701–1718.
21. Wallace AC, Laskowski RA and Thornton JM: **LIGPLOT: a program to generate schematic diagrams of protein-ligand interactions.** *Prot Eng* 1995, **8:**127–134.
22. Fersht A: **Structure and Mechanism in Protein Science.** W. H. Freeman and Company, New York; first1999.
23. Gan J, Wu Y, Prabakaran P, Gu Y, Li Y, Andrykovitch M, Liu H, Gong Y, Yan H and Ji X: **Structural and biochemical analyses of shikimate dehydrogenase AroE from *Aquiflex aeolicus*: implications for the catalytic mechanism.** *Biochemistry* 2007, **46:**9513–9522.
24. Han C, Hu T, Wu D, Qu S, Zhou J, Ding J, Shen X, Qu D and Jiang H: **X-ray crystallographic and enzymatic analyses of shikimate dehydrogenases from *Staphylococcus epidermidis*.** *FEBS J* 2009, **276:**1125–1139.
25. Singh S, Korolev S, Koroleva O, Zarembinski T, Collart F, Joachimiak A and Christendat D: **Crystal structure of a novel shikimate dehydrogenase from *Haemophilus influenzae*.** *J Biol Chem* 2005, **280:**17101–17108.
26. Singh SA and Christendat D: **Structure of *Arabidopsis* dehydroquinate dehydratase-shikimate dehydrogenase and implications for metabolic channeling in the shikimate pathway.** *Biochemistry* 2006, **45:**7787–7796.
27. Singh S, Stavrinides J, Christendat D and Guttman DS: **A phylogenomic analysis of the shikimate dehydrogenases reveals broadscale functional diversification and identifies one functionally distinct subclass.** *Mol Biol Evol* 2008, **25:**2221–2232.
28. Lindner HA, Nadeau G, Matte A, Michel G, Ménard R and Cygler M: **Site-directed mutagenesis of the active site region in the quinate/shikimate 5-dehydrogenase YdiB of *Escherichia coli*.** *J Biol Chem* 2005, **280:**7162–7169.
29. Robertson JG: **Enzymes as a special class of therapeutic target: clinical drugs and modes of action.** *Curr Opin Struct Biol* 2007, **17:**674–679.
30. Moore B: **Bifunctional and moonlighting enzymes: lighting the way to regulatory control.** *Trends Plant Sci* 2004, **9:**221–228.

Anexo C

PURINE SALVAGE PATHWAY IN *Mycobacterium tuberculosis*

Rodrigo Gay Ducati, Ardala Breda, Luiz Augusto Basso, Diógenes Santiago Santos

Artigo *in press*
Current Medicinal Chemistry Journal, 2010

De: walter@azevedolab.net <walter@azevedolab.net>

Assunto: HT-SBJ-CMC-0007

Para: rodrigoducati@yahoo.com.br

Data: Quarta-feira, 11 de Agosto de 2010, 13:16

Dear authors,

I am glad to inform that your review entitled "Purine Salvage Pathway in Mycobacterium tuberculosis" has been accepted for publication in Current Medicinal Chemistry.

Kind regards,

Walter F. de Azevedo Jr., guest editor CMC

Purine Salvage Pathway in *Mycobacterium tuberculosis*

R.G. Ducati[1], A. Breda[1,2], L.A. Basso*[,1,2] and D.S. Santos*[,1,2]

[1]*Instituto Nacional de Ciência e Tecnologia em Tuberculose (INCT-TB), Centro de Pesquisas em Biologia Molecular e Funcional (CPBMF), Pontifícia Universidade Católica do Rio Grande do Sul (PUCRS), Porto Alegre, RS, Brazil;* [2]*Programa de Pós-Graduação em Biologia Celular e Molecular (PPGBCM), Faculdade de Biociências, PUCRS, Porto Alegre, RS, Brazil*

Abstract: Millions of deaths worldwide are caused by the aetiological agent of tuberculosis, *Mycobacterium tuberculosis*. The increasing prevalence of this disease, the emergence of drug-resistant strains, and the devastating effect of human immunodeficiency virus co-infection have led to an urgent need for the development of new and more efficient antimycobacterial drugs. The modern approach to the development of new chemical compounds against complex diseases, especially the neglected endemic ones, such as tuberculosis, is based on the use of defined molecular targets. Among the advantages, this approach allows (i) the search and identification of lead compounds with defined molecular mechanisms against a defined target (e.g. enzymes from defined pathways), (ii) the analysis of a great number of compounds with a favorable cost/benefit ratio, and (iii) the development of compounds with selective toxicity. The present review describes the enzymes of the purine salvage pathway in *M. tuberculosis* as attractive targets for the development of new antimycobacterial agents. Enzyme kinetics and structural data have been included to provide a thorough knowledge on which to base the search for compounds with biological activity. We have focused on the mycobacterial homologues of this pathway as potential targets for the development new antitubercular agents.

Keywords: Crystallographic structures, enzyme kinetics, *Mycobacterium tuberculosis*, nucleotide metabolism, purine salvage pathway, rational drug design, selective toxicity, tuberculosis.

1. INTRODUCTION

Infectious diseases stand as a global concern along centuries of human history, claiming for millions of lives every year. Tuberculosis (TB) pictures as a main player among these, since approximately one third of the world's population is infected with *Mycobacterium tuberculosis* (MTB), the aetiological agent of human TB [1], which is responsible for more human deaths than any other single infectious agent. Approximately 95% of TB cases occur in developing nations, which account for 98% of the deaths worldwide [2, 3]. These statistics are inevitable, as a reflection of financial constraints of countries where very few resources are available to ensure proper treatment and where human immunodeficiency virus (HIV) infection is common, which wanes immunity, thereby reactivating the contained, but not eradicated, mycobacterial infection, both forging a deadly synergy [4, 5]. The demographical concentration of TB deaths among developing nations and higher mortality rates among ages ranging from 25 to 54 years, the most economically fruitful years of life, causes substantial losses in productivity and contributes to the impoverishment of third-world countries [6]. Several countries have been reaching treatment success's substantially below average due, in part, to the complications caused by the HIV/AIDS epidemic and the widespread emergence and dissemination of multidrug-resistant (MDR) and extensively drug-resistant (XDR) strains [7, 8].

Among the existing therapeutic agents, isoniazid and rifampicin stand as the most effective first-line antimycobacterial drugs [9] prescribed. However, drug-resistant TB is more difficult and expensive to treat, and more likely to be fatal, thus leading to the use of second-line drugs, which are less effective and more toxic [10, 11]. The emergence of MDR/XDR-TB strains has become a worldwide concern, leading to a requirement for the development of new antimicrobial agents, which, in turn, demands the identification of suitable drug targets. The modern approach to the development of new chemical compounds against complex diseases, especially the neglected endemic ones, such as TB, is based on the use of defined molecular targets. Among the advantages, this approach allows (i) the search and identification of lead compounds with defined molecular mechanisms against a defined target (e.g. enzymes from defined pathways), (ii) the analysis of a great number of compounds with a favorable cost/benefit ratio, and (iii) the development of compounds with selective toxicity.

There is an urgent need for the development of new and more efficient antimycobacterial agents. However, little interest has been shown by the pharmaceutical industry, which has not been necessarily attributed to the high investment needed to develop a new anti-TB compound, but to the small financial return awaited, since most TB cases occur in developing countries [2].

2. THE PURINE SALVAGE PATHWAY

In most organisms, nucleic acids undergo active turnover through catabolic processes to form free purine bases [12]. Purine nucleotides may be derived from preformed purine bases and nucleosides by the so-called salvage pathways, or they may be formed *de novo* from simpler precursors. The ribose 5'-phosphate moiety is derived from 5'-phospho-α-D-ribose 1'-diphosphate (PRPP), which takes part in both *de novo* and salvage pathways of purine and pyrimidine nucleotides, and acts as a common regulator [13].

In the purine salvage pathway, adenine, guanine and hypoxanthine nucleobases are reconverted to their corresponding nucleotides (AMP, GMP and IMP, respectively). In contrast, the *de novo* pathway leads to the formation of inosine 5'-monophosphate (IMP), which then diverges into separate sets of anabolic reactions that synthesize adenosine 5'-monophosphate (AMP) and guanosine 5'-monophosphate (GMP) [14].

Purine metabolism is conserved among eukaryote and prokaryote organisms, including MTB. Although *de novo* and salvage pathways have not been extensively detailed in MTB, it is known that the bacillus expresses enzymes of both pathways [15], thereby not being a purine auxotroph like other obligatory intracellular parasites such as *Toxoplasma gondii* [13], *Plasmodium falciparum* [16] and *Leishmania donovani* [13]. Whether MTB will sway between *de novo* or salvage pathways is still an unclear question. Since mycobacteria is able to suffice its metabolic needs for nucleotides from simpler substrates, a high energy demanding process, while is also capable of scavenging free nitrogenous bases from the medium, over passing up to 11 chemical steps, it seems that under conditions of low energy availability or rapid multiplication, the salvage pathway should be the main source of maintaining the nucleotide pool.

*Address correspondence to these authors at the Instituto Nacional de Ciência e Tecnologia em Tuberculose (INCT-TB), Centro de Pesquisas em Biologia Molecular e Funcional (CPBMF), Pontifícia Universidade Católica do Rio Grande do Sul (PUCRS), Av. Ipiranga 6681/Prédio 92-A, 90619-900, Porto Alegre, RS, Brazil; Tel/Fax: +55-51-33203629; E-mails: luiz.basso@pucrs.br and diogenes@pucrs.br

0929-8673/11 $58.00+.00

MTB adapts its own metabolism under distinct stages of TB infection, in response to microenvironments such as necrotic or caseous regions that are remote from the cavity surface of host lungs, where the availability of oxygen, nutrients and drugs is likely to be restricted. The metabolism required for sustaining mycobacterial survival during TB persistence and latency is still poorly understood. Transcriptional profiling has shown that a ribonucleotide reductase (RR; EC 1.17.4.1) encoded by *nrdZ* is up-regulated on latent bacillus, which indicates that a pool of deoxyribonucleotides is required either for maintenance of chromosomal integrity or for the process of DNA repair and replication that is expected to occur during TB reactivation [17].

The purine salvage pathway in MTB is a yet little explored possibility for drug development, and chemical agents with novel mechanisms of action are needed to combat emerging MDR/XDR-TB strains. The selective activity of 2-methyladenosine (methyl-Ado; an adenosine analogue) against MTB has provided proof of concept for the use of nucleoside analogs as antimycobacterial agents [18]. A thorough understanding of the enzymes involved in purine salvage and metabolism could lead to identification of nucleoside analogs that potently and selectively inhibit MTB viability [19].

Although data on purine metabolism is relatively scarce in MTB, it is believed that the purine salvage pathway is used when the bacillus uptakes hypoxanthine, guanine, and adenine from the external medium, which are subsequently converted to, respectively, IMP, GMP, and AMP [20]. Several homologues to enzymes of the purine salvage pathway have been identified in the genome sequence of MTB H37Rv [21]. Purine bases, nucleosides, and nucleotides can be interconverted through the activities of adenosine deaminase (EC 3.5.4.4, *add*, Rv3313c), adenosine kinase (EC 2.7.1.20, *adoK*, Rv2202c), 5'-nucleotidase (EC 3.1.3.5, Rv2232), hypoxanthine-guanine phosphoribosyltransferase (EC 2.4.2.8, *htp*, Rv3624c), adenine phosphoribosyltransferase (EC 2.4.2.7, *apt*, Rv2584c), purine nucleoside phosphorylase (EC 2.4.2.1, *deoD*, Rv3307), purine nucleosidase (EC 3.2.2.1, *iunH*, Rv3393), inosine monophosphate dehydrogenase (EC 1.1.1.205, *guaB2*, Rv3411c), adenylosuccinate synthase (EC 6.3.4.4, *purA*, Rv0357c), adenylosuccinate lyase (EC 4.3.2.2, *purB*, Rv0777), guanylate kinase (EC 2.7.4.8, *gmk*, Rv1389), adenylate kinase (EC 2.7.4.3, *adk*, Rv0733), and guanosine monophosphate synthase (EC 6.3.5.2, *guaA*, Rv3396c) (Fig. **1**).

Singular features of this pathogen such as enzymes either of essential metabolic pathways exclusive to the microorganism [22] or of purine and pyrimidine [23] salvage pathways with unique characteristics as compared to the human host, can be explored to direct efforts towards selective target drug development. Although intermediates of the purine salvage pathway seem to be alike for both prokaryotic and eukaryotic organisms, differences can occasionally be found in the primary structure and properties of homologous enzymes. Nucleotide metabolic pathways are a good source of new targets for antibacterial drugs, as the enzymes/pathways involved are often different from their human counterparts. The purine salvage pathway is one of the promising pathways for the development of novel nucleoside analogs with anti-TB activity [13].

Nucleoside analogs are prodrugs resembling natural nucleosides that usually must be metabolized intracellularly to active compounds. They are thus an important class of drugs used in the treatment of viral infections and cancer that may prove to be particularly useful in treating drug-resistant TB, since their mechanism of action is likely to be different from those of existing therapies [18]. These antimetabolites comprise a class of drugs that inhibit DNA synthesis either directly or through inhibition of DNA precursor synthesis of *de novo* or salvage pathways [24].

A better understanding of the characteristics of the enzymes involved in purine salvage in MTB should aid in the rational design of purine analogs that can selectively inhibit MTB replication and survival. Ideally, this class of compounds should be active against strains of MTB that are resistant to the agents currently used to treat this disease and may, hopefully, also target latent disease.

Here we describe the enzymes of the purine salvage pathway that have been identified in the MTB genome (Fig. **1**), their main characteristics, the state-of-art of ongoing researches on each enzyme, the resemblance to their human counterparts, and a brief discussion of features that might be explored for identification or development of specific inhibitors.

3. PURINE SALVAGE ENZYMES

3.1. Adenosine Deaminase (EC 3.5.4.4)

(other designations: ADD and adenosine aminohydrolase)

Encoded by the *add* gene (MTB Rv3313c, 1098 bp, 366 aa, 39743.10 Da, and Isoelectric point (pI) = 5.36), adenosine deaminase (ADD) plays an important role in the purine salvage pathway, catalyzing the irreversible hydrolytic deamination of (deoxy)adenosine to generate (deoxy)inosine (Fig. **2**). There are nearly one hundred compounds capable of binding to ADD, being some substrates and most inhibitors that display different types of inhibition [25-27]. This enzyme belongs to the superfamily of metallo-dependent hydrolases (also called amidohydrolase superfamily), a large group of proteins (which includes AMP and adenine deaminases, among others) that show conservation in their three-dimensional fold and in details of their active sites. The vast majority of the members have a conserved metal binding site (zinc metalloenzyme), involving three histidines and one aspartic acid residue. In the common reaction mechanism, the metal ion (or ions) deprotonates a water molecule for a nucleophilic attack on the substrate [12, 28, 29].

Enzyme activity for the human homologue has been observed in all human tissues, owing to at least three isoforms [30]. In humans, rare genetic defects have been described for this gene and associated to specific diseases. Deficiency in this enzyme causes a form of severe combined immunodeficiency disease (SCID), where there is a dysfunction of both B and T lymphocytes with impaired cellular immunity and decreased production of immunoglobulins. This condition is invariably fatal at an early age due to overwhelming infection. In case an appropriate donor is available, SCID patients can be treated with bone marrow transplantation. Gene therapy, in combination with replacement enzyme infusion has been employed as an alternative attempt to treat this disorder [12, 14]. The enzyme's coding DNA sequence is conserved in cells of chimpanzee, dog, cow, mouse, rat, chicken, zebrafish, *Caenorhabditis elegans*, *Schizosaccharomyces pombe*, *Saccharomyces cerevisiae*, *Kluyveromyces lactis*, and *P. falciparum*. The prokaryotic homologue has also been extensively studied. The synthesis of the *E. coli* enzyme, which is inhibited by conformycin (K_i = 30 nM), is induced by adenine and hypoxanthine [31]. In *Salmonella typhimurium*, however, it is apparently synthesized constitutively, and in low amounts [32].

A number of studies have been reported for ADD from various sources, including X-ray crystallography for the complex with 6-hydroxyl-1,6-dihydropurine ribonucleoside, a nearly ideal transition-state analogue [28]. However, there has been no publication regarding MTB ADD (MtADD). Our group has PCR-amplified and pET23a(+)-cloned the MTB *add* gene. The mycobacterial recombinant enzyme was expressed in its insoluble form in all electrocompetent *E. coli* commercial variants available for heterologous expression tested to date. Although homogeneous MtADD could be obtained through a sequence of anion exchange, gel filtration, and hydrophobic interaction chromatographic steps, protein solubiliza-

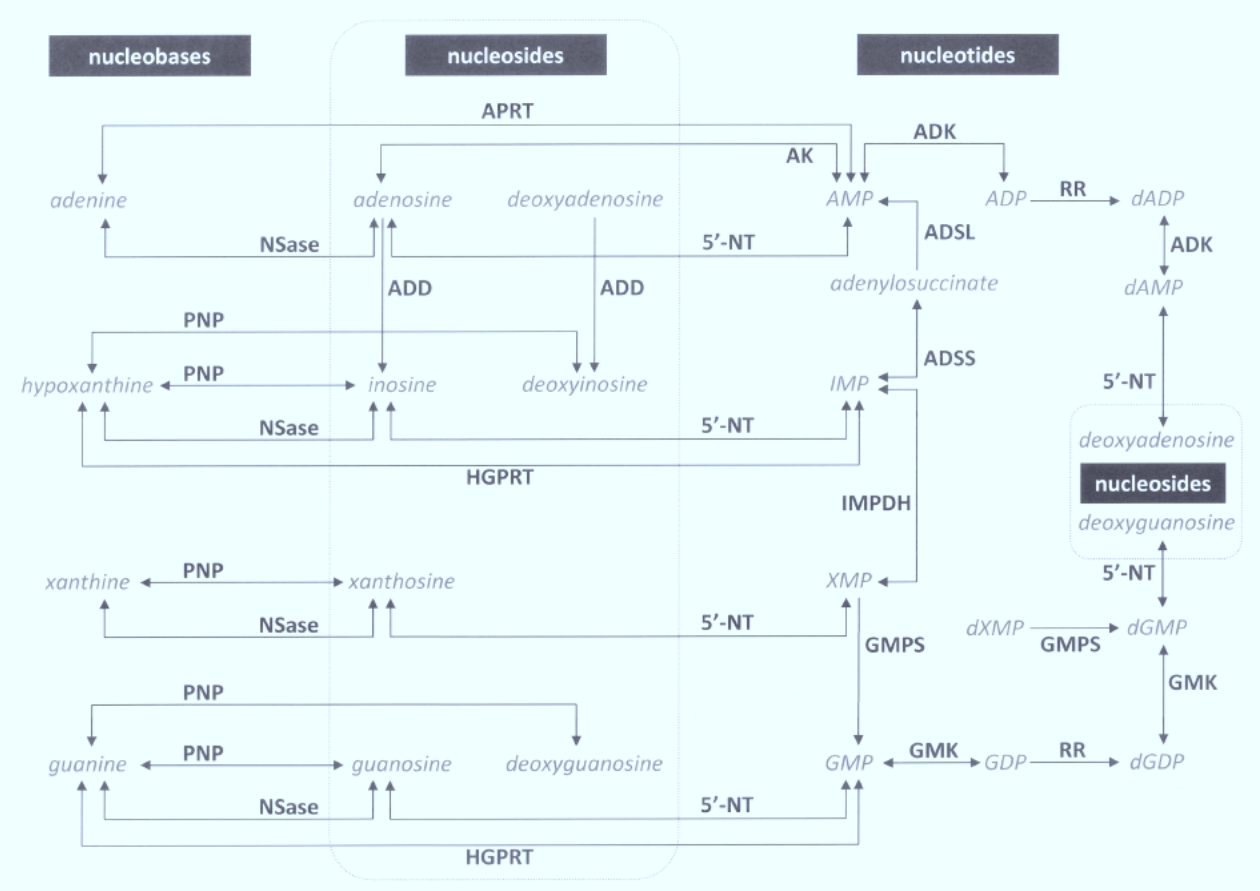

Fig. (1). Overview of the purine salvage pathway enzymes identified in the *M. tuberculosis* H37Rv genome sequence. For enzymes' and intermediates' abbreviations refer to text.

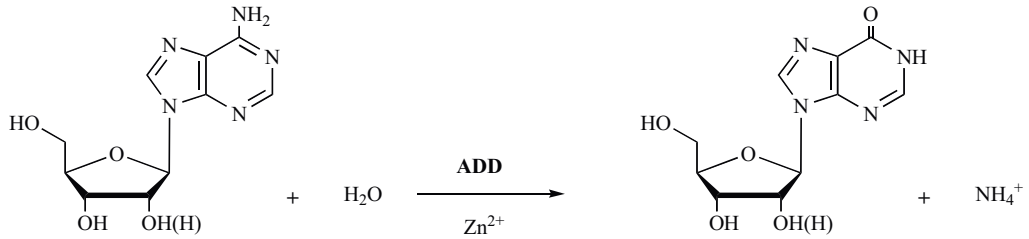

(deoxy)adenosine **(deoxy)inosine**

Fig. (2). Adenosine deaminase catalyses the irreversible hydrolytic deamination of (deoxy)adenosine to generate (deoxy)inosine.

tion processes resulted in protein with no activity so far. Soluble and active MtADD protein expression is underway (unpublished data).

3.2. *Adenosine Kinase* (EC 2.7.1.20)

(other designations: AK and ATP:adenosine 5'-phosphotransferase)

Encoded by the *adoK* (previously named *cbhK*) gene (MTB Rv2202c, 975 bp, 325 aa, 34439.90 Da, and pI = 4.51), adenosine kinase (AK) catalyses the phosphorylation of adenosine to AMP (Fig. **3**), an important step in the purine salvage pathway, using adenosine 5'-triphosphate (ATP) as a phosphate donor, and releasing adenosine 5'-diphosphate (ADP). Enzyme activity of most AKs is dependent on Mg^{2+}. In agreement with previous observations with the human homologue [33-35], deoxyadenosine is a poor substrate for MTB AK (MtAK) [36]. AK belongs to the phosphofructokinase B family of carbohydrate and nucleoside kinases, a family of structurally related enzymes which includes ribokinase and fructokinase, among others [37]. AK is found in most eukaryotes, fungi, plants, and parasites, but it is seldom found in bacteria [36]. MtAK shows greater homology to ribokinases than to other AKs. Not surprisingly, it was previously classified as a hypothetical sugar kinase. AK activity has been biochemically proven in MTB [18], being the first bacterial homologue to be characterized.

In 1994, the Tuberculosis Antimicrobial Acquisition and Coordinating Facility was established by the National Institute of Allergy and Infectious Diseases, as an attempt to support research and design new drugs to combat TB [38]. Many purine analogues with selective activity against MTB were identified. Methyl-Ado was one of the compounds whose MtAK-phosphorylation yielded an active form with highest index of potency and selectivity [39], being active against MTB drug-resistant strains and against mycobacteria incubated under latency simulating conditions. It is important to note that the high selectivity for MTB attributed to this com-

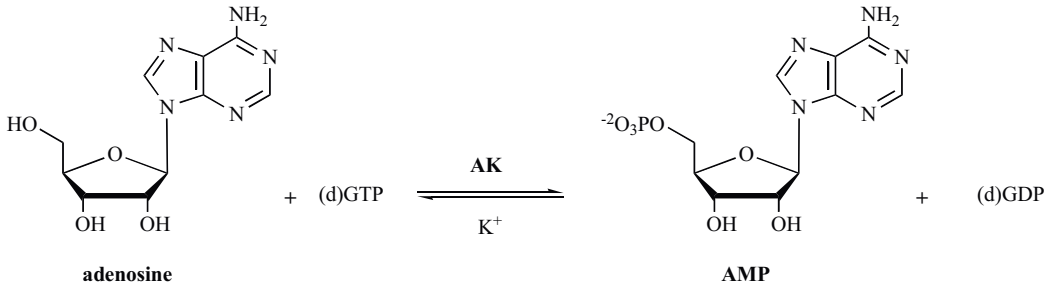

Fig. (3). Adenosine kinase catalyses the phosphorylation of adenosine to AMP using GTP (or dGTP) as phosphate donor.

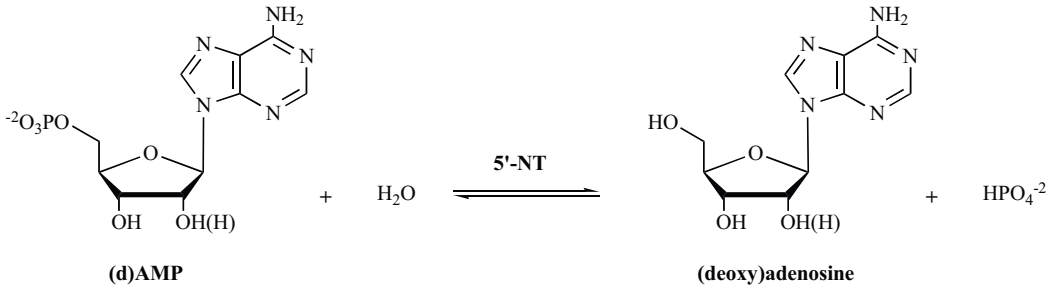

Fig. (4). 5'-Nucleotidase catalyzes the hydrolytic dephosphorylation of (deoxy)ribonucleoside monophosphates to the corresponding (deoxy)nucleosides.

pound is due to its extremely low cytotoxic level to human cells. In humans, clinically useful antimetabolites, such as base or nucleoside analogues, are metabolized to biologically active nucleotides. The primary target of methyl-Ado appears to be an enzyme involved in protein synthesis. Although the enzyme responsible for this activity has not yet been identified, it is known that the primary enzyme involved in the activation of methyl-Ado in MTB is AK.

The mycobacterial homologue exhibits several physicochemical and three-dimensional features considerably different as compared to AKs from other sources [19]. The differences between human and mycobacterial enzyme homologues justify selective activation of methyl-Ado by the latter. Differently to AKs from various sources, and similarly to other ribokinases, MtAK catalytic activity is stimulated in the presence of monovalent metal ions (ionic requirement) such as K^+ [40, 41]. Formerly thought to be a tetramer, MtAK's native form is actually a dimer formed by an extended β-sheet [42, 43], somewhat different from the monomeric form of human AK [44-46]. High resolution structures for MtAK have been determined (PDB accession codes 2PKM, 2PKF, 2PKK, and 2PKN), and demonstrate that the active site of the enzyme is in an open conformation in absence of ligands (apo form), and upon adenosine binding a LID domain undergoes a large conformational change to close the active site of this protein. In the closed conformation, the LID forms direct interactions with the substrate and residues of the active site [42]. The human and mycobacterial enzymes also share differences with respect to their respective preferences for phosphate donors [18, 47], as the mycobacterial enzyme activity was shown to be higher with guanosine 5'-triphosphate (GTP) and deoxy(d)GTP than with ATP. Furthermore, the considerably higher rate of methyl-Ado phosphorylation by MtAK is also responsible for the selective activity of this compound against mycobacteria [19]. Although it has recently been questioned whether MtAK functions as an adenosine kinase in *M. tuberculosis* cellular setting [48], the biological role of MtAK still awaits further experimental evidence such as gene replacement studies. At any rate, methyl-Ado selective activity against MtAK has provided proof of concept for the use of nucleoside analogues as antimycobacterial agents [36]. From a drug development point of view, the fact that MtAK differs in substrate, inhibitor, and phosphate donor specificities from the human homologue is of particular importance, because these results indicate that mycobacterial and human enzymes are different enough to allow selective activation of adenosine analogs, such as methyl-Ado. AK is not required for the *in vitro* growth of MTB, which would suggest that inhibitors of this enzyme are not candidates for drug development. However, it is possible that this enzyme does have a critical role in the growth of MTB in a human cell. If this turns out to be the case, then these inhibitors may also be considered as leads for further drug development. Moreover, it has been suggested that MtAK may be utilized for selective phosphorylation of nucleoside analogs to metabolites active against MTB [36].

3.3. *5'-Nucleotidase* (EC 3.1.3.5)

(other designations: 5'-NT)

5'-nucleotidases (5'-NT) are a family of enzymes that catalyze the hydrolytic dephosphorylation of (deoxy)ribonucleoside monophosphates to the corresponding nucleosides (Fig. **4**) and regulate cellular nucleotide and nucleoside levels. Since cellular nucleotides are derived either from *de novo* synthesis or salvage pathways, this enzyme is critically positioned at the interface of both processes and may determine the fate of extra and intracellular nucleotides.

Unlike the well studied AK, many of the catabolic nucleotidases have only recently been cloned and characterized. 5'-NTs and nucleoside kinases catalyze reverse reactions, forming substrate cycles in which phosphorylation and dephosphorylation of nucleosides create a dynamic balance between pathways to rapidly respond to changes in metabolic conditions by increasing or decreasing the concentration of a particular nucleotide. Thereby, aside from maintaining (deoxy)ribonucleotide pools, substrate cycles that are formed with the kinase and nucleotidase activities are also likely to regulate the activation of nucleoside analogues [49]. A few studies have suggested that since 5'-NTs can dephosphorylate the monophosphate forms of many nucleoside analogues that are administered in cancer and viral infection treatments, increased levels of nucleotidase activity can inhibit their activation, possibly playing a role in resistance to these compounds [24]. The expression of this enzyme has been observed in bacteria, plant and vertebrate cells. However, it is not clear whether it is indeed present in MTB (Mt5'-NT; MTB Rv2232, 876 bp, 291 aa, 30662.20 Da, and pI = 7.14). Although there are significant differences with respect to the range of substrate hydrolyzed and substrate specificity, 5'-

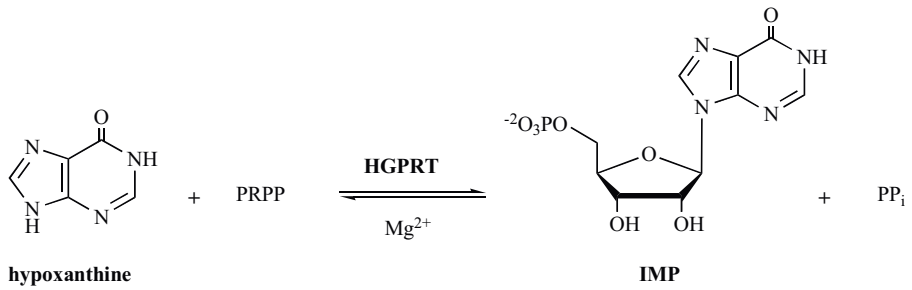

Fig. (5). Hypoxanthine-guanine phosphoribosyltransferase catalyzes the reversible transfer of the 5'-phosphoribosyl moiety from PRPP to 6-oxopurines (hypoxanthine depicted here) to form the corresponding ribonucleotides and PP_i.

mononucleotides appear to be the most commonly hydrolyzed. Its physiological function is possibly disparate among various organisms and tissues, and probably extends beyond its catalytic activity. Notwithstanding their source, 5'-NTs are usually present as two main biochemical forms: membrane-bound and soluble [24, 50]. Polyphenolic substances that display antitumor activity (with no general cytotoxic effects observed) and inhibit 5'-NT activity from different sources have been isolated from plants [51-53].

Our group has PCR-amplified and pET23a(+)-cloned the MTB Rv2232 gene, that has been assigned *in silico* to encode a 5'-NT enzyme in MTB. The identity of the cloned sequence was confirmed by automated nucleotide sequencing and the recombinant encoded protein was expressed in its soluble form in electrocompetent *E. coli* BL21(DE3) host cells. Availability of homogeneous Mt5'-NT will allow measurements of enzyme-catalyzed chemical reactions to provide experimental evidence whether or not the Rv2232 DNA sequence codes for a mycobacterial 5'-NT activity (unpublished data).

3.4. Phosphoribosyltransferase Family Enzymes

The family of phosphoribosyltransferase (PRTase) enzymes show a common catalytic reaction of pyrophosphate (PP_i) displacement from PRPP by a nitrogen-containing nucleophile, such as ammonia, adenine, guanine, hypoxanthine, xanthine, orotate or uracil, producing a β-substituted ribose 5-phosphate and PP_i [54, 55]. These enzymes take part in key steps of purine, pyrimidine, and pyridine (nicotinamide) nucleotide synthesis or salvage, as well as in aromatic amino acids (histidine and tryptophan) biosynthesis, being present in eukaryotic and prokaryotic organisms [56].

Although PRTase proteins show remarkable tertiary and quaternary structure conservation [57, 58], a PRPP conserved binding motif of 12 amino acids (MLVDDVITAGTA), shared with PRPP synthetases, is only observed among PRTase family members involved in nucleotide synthesis or salvage pathways [55], being the main primary structure unifying characteristic for this group of enzymes, typifying the 'type I PRTases'.

Crystallographic structures of type I PRTases have revealed a conserved nucleotide binding Rossmann fold, where a common CORE of five parallel β-sheets are surrounded by α-helices at one side, and an α/β motif at the other [55-57]. At the C-terminal portion of this α/β motif, an 11-amino-acid long conserved flexible loop (RKEAKDHGEGG) is involved in binding and partial solvent occlusion of the nitrogenous base substrate [57, 58]. The readers may refer to a mini-review by Sinha and Smith for a more in-depth discussion on the three-dimensional structures of type I PRTases [55].

Other shared features of type I PRTases are: catalytic role of conserved lysine residues [54], sequential kinetic mechanisms - either random or ordered [57], homodimeric assembly of their tertiary structures [55], loop closure upon substrate binding on adjacent subunit binding site [56, 58-60], and absolute requirement for magnesium divalent ion for catalysis, where Mg^{2+}-PRPP has already being proved to be the true substrate for some PRTases [61].

In purine nucleotide metabolism, PRTase enzymes are involved in the first step of *de novo* synthesis (glutamine phosphoribosylpyrophosphate amidotransferase, E.C. 2.4.2.14) [62]; and two other enzymes are responsible for nucleobases salvage pathway, hypoxanthine-guanine phosphoribosyltransferase and adenine phosphoribosyltransferase, which catalyze nucleotide formation in a single catalytic step from the corresponding free nitrogenous bases available from catabolism. The pivotal role that these enzymes play in the purine salvage pathway denote their potential as chemotherapeutic targets for parasitic diseases, since all four purine nucleobases (xanthine, hypoxanthine, guanine, and adenine) are incorporated into the nucleotide pool via the PRTase reactions [13], and their characterization might reveal insightful data on metabolic balance between host and parasites [20].

3.4.1. Hypoxanthine-Guanine Phosphoribosyltransferase (EC 2.4.2.8)

(other designations: HGPRT, hypoxanthine phosphoribosyltransferase, guanine phosphoribosyltransferase, hypoxanthine-guanine-xanthine phosphoribosyltransferase, IMP diphosphorylase, IMP pyrophosphorylase, and transphosphoribosyltransferase; named according to substrate specificity)

Encoded by the *hpt* gene (MTB Rv3624c, 651 bp, 217 aa, 23603.70 Da, and pI = 4.72), hypoxanthine-guanine phosphoribosyltransferase (HGPRT) catalyzes the Mg^{2+}-dependent reversible transfer of the 5'-phosphoribosyl moiety from PRPP to the N9 position of 6-oxopurines (guanine, hypoxanthine, and xanthine) to form the corresponding ribonucleotides, GMP, IMP, and xanthosine 5'-monophosphate (XMP), and PP_i [20] (Fig. **5**). We have previously described PCR amplification, cloning, DNA sequencing, heterologous protein expression in electrocompetent *E. coli* BL21(DE3) host cells, purification to homogeneity, and biochemical characterization of a predicted MTB HGPRT (MtHGPRT) [20]. Correct assignment to the structural gene encoding MtHGPRT was probed by measurement of the biological activity of the recombinant enzyme by steady-state kinetics. Apparent steady-state kinetic constants and substrate specificities for homogeneous MtHGPRT were determined for hypoxanthine, guanine, xanthine, and PRPP (Table **1**). The recombinant enzyme-catalyzed chemical reaction obeys Michaelis-Menten kinetics for all substrates tested; however, no activity with xanthine as substrate could be detected, indicating that the recombinant MtHGPRT protein does not utilize xanthine. The k_{cat}/K_M ratios indicate that MtHGPRT has a slightly higher preference for hypoxanthine ($18 \pm 7 \times 10^3$ $M^{-1}s^{-1}$) than for guanine ($5.6 \pm 1.5 \times 10^3$ $M^{-1}s^{-1}$) as co-substrate [20].

Transition-state analogues, known as immucillin 5'-phosphates, were shown to be tight-binding inhibitors of HGPRT enzyme activity. Crystallographic structures and structural analyses of these inhibitors in complex with human HGPRT (PDB accession code 1BZY) [63] and with the *P. falciparum* homologue (PDB accession

Table 1. Apparent Steady-State Kinetic Constants for the MtHGPRT Forward Reaction*

Substrate pair	K_M (μM)	V_{max} (U mg^{-1})	k_{cat} (s^{-1})	k_{cat}/K_M (M^{-1}s^{-1})
Guanine	25 ± 6	0.37 ± 0.03	0.14 ± 0.01	5.6 (± 1.5) x 10^3
PRPP	360 ± 26	0.0376 ± 0.006	0.139 ± 0.002	386 ± 29
Hypoxanthine	50 ± 18	2.4 ± 0.4	0.9 ± 0.1	18 (± 7) x 10^3
PRPP	2039 ± 201	2.6 ± 0.1	0.97 ± 0.05	476 ± 52

*Adapted from [20].

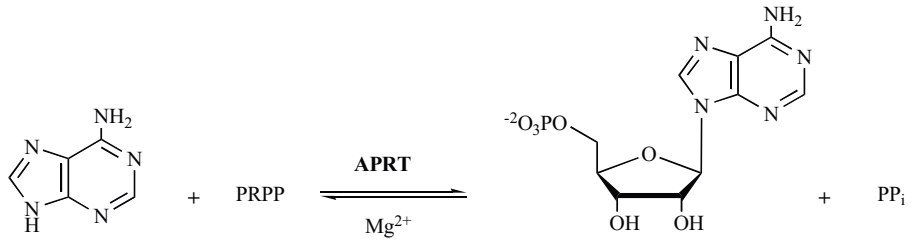

Fig. (6). Adenine phosphoribosyltransferase catalyzes the reversible transfer of the 5'-phosphoribosyl moiety from PRPP to adenine to form AMP and PP_i.

code 1CJB) [64] have shown an almost identical binding mode, which suggests that it may be difficult to design specific parasite HGPRT inhibitors [65, 66], even though chlorine substituted at 6-position, and nitrogen substituted at 8-position (6-chloroguanine, 8-azaguanine, and 8-azahypoxanthine) exhibited high selectivity towards parasite HGPRT [66]. More recently, acyclic nucleoside phosphonates, 2-(phosphoalkoxy)alkyl derivates of purine and pyrimidine bases, have been shown to be potent and highly selective inhibitors of malarial HGPRT, with K_i values in the μM range [65].

Human HGPRT, encoded by the *hgprt1* gene and located at chromosome Xq26.1, presented 218 amino acids and a molecular mass of 24448 Da (GenBank accession number: NP_000185.1). As for MtHGPRT, the human homologue also shows no activity with xanthine as co-substrate [67]. This characteristic lack of xanthine metabolism in humans and its presence in some parasites can be exploited to develop antiparasitic drugs, since xanthine analogues may selectively inhibit the parasitic PRTase, not interfering with host purine salvage pathway [13]. However, specific inhibitor development for MtHGPRT should exploit features other than xanthine usage, as low sequence identity (24.9%, assigned by pairwised amino acids sequence alignment [68]) may indicate non conservation of key catalytic residues, distinct steady-state kinetic constants and mechanism. Human HGPRT follows a sequential ordered mechanism: Mg^{2+}-PRPP binds first followed by 6-oxopurine base binding. After the phosphoribosyl transfer, PP_i dissociates from the complex and the nucleoside monophosphate is released in the rate-limiting step [69]. Although MtHGPRT true steady-state kinetic constants and the enzyme kinetic mechanism have not been shown yet, these efforts are currently underway in our research group. These results should provide experimental data on which to base the rational design of MtHGPRT inhibitors.

3.4.2. Adenine Phosphoribosyltransferase (EC 2.4.2.7)

(other designations: APRT, AMP diphosphorylase, AMP pyrophosphorylase, and transphosphoribosidase)

Encoded by the *apt* gene (MTB Rv2584c, 672 bp, 223 aa, 23155.60 Da, and pI = 10.13), adenine phosphoribosyltransferase (APRT) is specific for 6-aminopurine nucleobases, catalyzing the Mg^{2+}-dependent reversible transfer of the 5'-phosphoribosyl moiety from PRPP to adenine, resulting in the formation of AMP and PP_i [70] (Fig. **6**). Several parasites deficient in APRT activity employ adenine deaminase (EC 3.5.4.2) to deaminate adenine to hypoxantine, which is substrate for HGPRT. On the other hand, parasites that do have APRT activity usually lack adenine deaminase activity [13], as observed for MTB.

Compared to other purine and pyrimidine PRTases, studies of APRT are so far scarce. The crystallographic structures available on public databases indicate APRT as a well characterized member of type I PRTases, but presenting a unique purine binding pocket that slightly opens to accommodate the larger AMP ligand [70, 71]. APRT crystallographic data (PDB accession codes 1L1Q, 1L1R, 1G2P and 1G2Q) suggest that loop closure upon substrate binding occurs in the same subunit, and not over the adjacent subunit, distinguishing such enzymes amongst the type I PRTases [72, 73]. Since structural analyses of orotate phosphoribosyltransferase (OPRT; EC 2.4.2.10) and APRT show a single metal binding site [74] whereas HGPRT crystallographic data suggest a second Mg^{2+} binding site [59, 63-65], APRT is considered more similar to OPRT homologues, a type I PRTase that catalyzes the fifth step of *de novo* synthesis of pyrimidine nucleotides, than to other purine PRTases. APRT enzymes can be further subdivided into short- and long-APRTs based on their amino acid sequences. Short-APRT enzymes present primary structure of 120 to 180 amino acids and include human, yeast, *E. coli*, and *Giardia* genus APRTs [72]. Long-APRT enzymes have a C-terminal extension of 50 amino acids, which is comprised of approximately 230 amino acids, and is found in all *Leishmania* genus and *Trypanossoma brucei* homologues [72]. The enzyme from the MTB H37Rv laboratorial strain belongs to the long-APRT group, while the ones from most of the remaining MTB strains are classified as short-APRTs. This C-terminal extension, initially attributed only to *Leishmania*, expands the dimer interface by wrapping around the adjacent subunit and double the total buried solvent-accessible surface area upon dimer formation [71].

Human APRT, encoded by the *aprt* gene and located at chromosome 16q24, has two isoforms, one with 134 amino acids and other with 180 amino acids (GenBank accession number NP_001025189.1 and NP_000476.1), as a result of distinct splicing processes. Its crystallographic structure (PDB accession code 1ORE) analysis led to the proposal of two conserved amino acids in the active sites of APRTs that are involved in 6-aminopurine recognition over different purines: Leu/Ile159 and Ala131 (numbered according to 1ORE structure) [74]. MTB APRT (MtAPRT) presents 29% and 42% identity to human short and long APRT isoforms, respectively, when the 50 amino acid C-terminal extension is disregarded; and both Leu159 and Ala131 are conserved within its

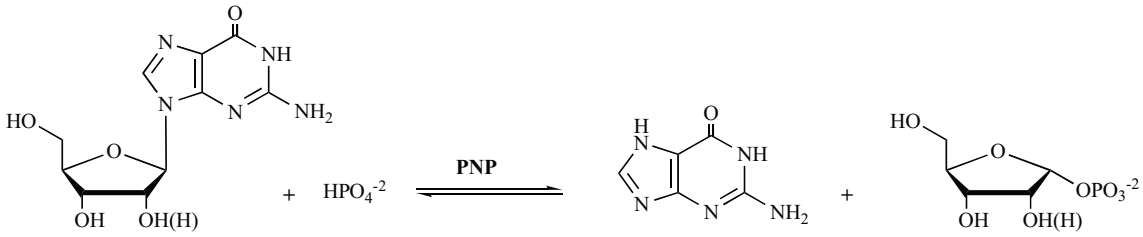

(deoxy)guanosine **guanine** **α-(deoxy)ribose 1-phosphate**

Fig. (7). Purine nucleoside phosphorylase catalyzes the reversible phosphorolysis of purine (deoxy)ribonucleosides to generate α-(deoxy)ribose 1-phosphate and the corresponding purine bases.

primary sequence. Further attempts to fully characterize MtAPRT should be accomplished to highlight which mycobaterial features might be exploited for inhibitor development to ensure that no significant interactions are made with the human APRT isoforms. Amongst PRTase enzymes that bind 6-oxopurines, positions 159 and 131 are occupied by a lysine and an aspartic acid, respectively. Both these charged amino acids are believed to direct hydrogen bond to the nitrogenous base, defining enzymes' specificity [74]. However, double knockout experiments of HGPRT and xanthine phosphoribosyltransferase (EC 2.4.2.22) enzymes in *L. donovani* parasites have shown that besides presenting dramatically diminished infecting capability, such parasites still persisted in culture when no purine source other than hypoxanthine was supplemented. These data reveal that, under conditions of high expression and in the absence of other PRTases, APRT is able to use this 6-oxopurine base as substrate to further synthesize purine nucleotides, since *Leishmania* genus rely solely on salvage pathways for purine and pyrimidine synthesis [75]. Taken together, these results imply that mechanisms other than conserved amino acid residues at positions 131 and 159 are related to 6-amino and 6-oxopurine recognition, and further investigations are necessary to fully describe and distinguish HGPRTs and APRTs, enabling specific inhibitor development that might even take advantage of what can possibly represent a substrate interchange between them. We have recently PCR-amplified, pET23a(+)-cloned the MTB *apt* gene. The mycobacterial recombinant enzyme was expressed in its insoluble form in all electrocompetent *E. coli* commercial variants available for heterologous expression tested to date. Attempts for soluble protein expression for further purification to homogeneity and biochemical characterization of the predicted MtAPRT are currently underway (unpublished data).

3.5. Purine Nucleoside Phosphorylase (EC 2.4.2.1)

(other designations: PNP, inosine phosphorylase, nucleoside phosphorylase, and purine-nucleoside:orthophosphate ribosyltransferase)

Encoded by the *deoD* (alternatively named *punA*) gene (MTB Rv3307, 807 bp, 268 aa, 27539.4 Da, and pI = 5.75), purine nucleoside phosphorylase (PNP) is primarily assigned as a purine nucleoside salvage enzyme, although it is also involved in pyrimidine and pyridine metabolism [76]. It catalyzes the reversible phosphorolysis of the *N*-glycosidic bond of β-purine (deoxy)ribonucleosides to generate α-(deoxy)ribose 1-phosphate and the corresponding purine bases [77, 78] (Fig. **7**). Structurally, PNP enzymes are subdivided according to their quaternary structures into homotrimeric and homohexameric, which implies distinct substrate specificities. Homotrimeric PNPs are highly specific for 6-oxopurines, their nucleosides (inosine, deoxyinosine, guanosine, and deoxyguanosine), and some analogues, whereas homohexameric PNPs additionally accept 6-aminopurine (adenine), their nucleosides and many analogues as substrates [79]. Among homotrimeric PNPs, the rates of phosphorolysis and/or synthesis of adenosine, when detectable, are negligible or extremely low [80, 81]. Readers are suggested to refer to reference [79] for an authoritative review on PNP structural properties.

MTB PNP (MtPNP) has been shown to be trimeric [82], like mammalian PNP, which distinguishes the mycobacterial homologue from the hexameric prokaryotic enzymes [83, 84]. MtPNP has been numbered among the top 100% persistence targets by the TB Structural Genomics Consortium (www.webtb.org). However, the physiological role of PNP in MTB remains to be demonstrated. We have reported cloning, expression, purification, and studies on slow-onset inhibition by a transition-state analogue, immucillin-H (ImmH), including a detailed analysis of ImmH component parts (dissection by parts) and their effects on MtPNP enzyme activity [82]. We have also determined MtPNP structure in complex with ImmH (PDB accession codes 1G2O and 1I80) [85], indicating that mimicry of transition-state features is the dominant force for ImmH tight binding [86]. On evaluation of size and charge distribution effects in transition-state analogues that inhibit MtPNP, it has been demonstrated that over-the-barrier transition-state analogues (DADMe-Immucillin compounds) have increased affinity for mycobacterial enzyme, which resulted from more favorable ion-pair formation between the cationic mimic of the oxocarbenium ion and the anionic phosphate nucleophile [87]. More recently, we have solved the X-ray crystallographic structure of MtPNP in complex with inorganic phosphate and discussed structural changes resulting from ImmH binding [88].

The human PNP (HsPNP) counterpart is encoded by the *np* gene, also assigned as *pnp1*, located at chromosome 14q13.1, which codifies a 289 amino acid transcript (GenBank accession number NC_000014.8). HsPNP is also classified as a homotrimeric PNP. Pairwise amino acid sequence alignment of the mycobaterial and human homologues indicates a 34.81% identity and 18.43% strong similarity between them. Besides their similarity, it should be pointed out that the design of inhibitors with higher affinity for MtPNP than for HsPNP is a feasible goal since it has been shown that they appear to have slightly different transition states [87] and structural features [89-91] that may be exploited to achieve specificity [85, 92-100]. In addition, it has recently been shown that even though bovine and HsPNP homologues share 87% sequence identity and have full conservation of active site residues, inhibitors with differential specificity can still be designed [101].

Although MtPNP has been clearly classified among the homotrimeric enzymes, there was no experimental data probing MtPNP specificity for adenosine. MtPNP substrate specificity was determined by measurements of initial velocity employing different substrates, including 6-aminopurine, as well as determination of true steady-state kinetic parameters, product inhibition, substrates and products binding studies (spectrofluorimetry and surface plasmon resonance), pH-rate profiles, temperature effects, and solvent kinetic isotope effects to provide enzyme kinetic and chemical mechanisms [102]. MtPNP was more specific to guanosine N7 methyl analogues, 2-amino-6-mercapto-7-methylpurine ribonucleoside (MESG) and 7-methylguanosine [103], than any natural nucleoside tested, which is largely due to increased catalytic constant values, since K_M values were of similar magnitude [102]. HsPNP has been shown to be more specific for natural substrates, such as

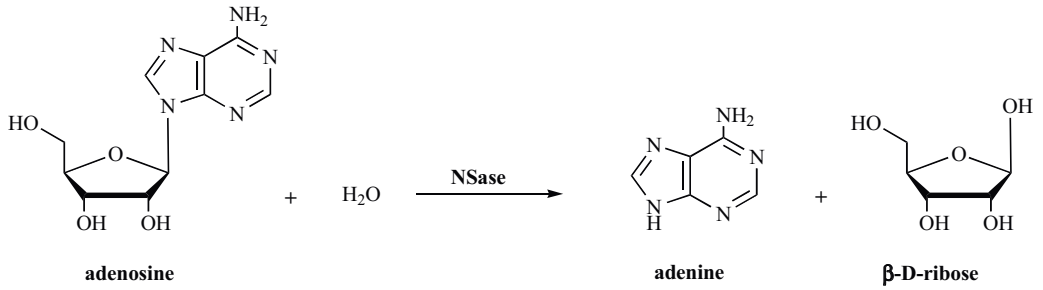

Fig. (8). Purine nucleosidase catalyzes the irreversible hydrolysis of all of the commonly occurring purine and pyrimidine nucleosides into β-D-ribose and the corresponding base.

inosine and guanosine, than to MESG [100]. In addition, the HsPNP K_M value for MESG (358 μM; [100]) is approximately 12-fold larger than that for MtPNP [102]. These differences imply that enzyme inhibitors more specific for MtPNP may be designed based on the chemical functional group substitutions of MESG, in particular the sulfur at the sixth position of the purine base. Our results also indicate that the rate of phosphorolysis of adenosine by MtPNP is undetectable or, at the most, negligible [102]; in agreement with homotrimeric PNP enzymes that are not able to catalyze the phosphorolysis of 6-aminopurine nucleosides to an appreciable extent. A comparison between the three-dimensional structures of ternary complexes of MtPNP and bovine spleen PNP in complex with a transition-state analogue (ImmH) and inorganic phosphate showed that the contacts in their catalytic sites are similar, but not identical [85]. Tyr188 (numbered after MtPNP amino acid sequence) had been identified as the only residue that interacts directly with the bound ImmH inhibitor that is not conserved in the mammalian PNPs [85], which shed some light on another structural feature that could be exploited to design specific inhibitors for MtPNP.

We have suggested that inhibition of MtPNP could potentially lead to the accumulation of dGTP through deoxycytidine kinase (EC 2.7.1.74) activity, which can use deoxyguanosine as substrate, synthesizing dGMP that is further converted to dGTP. For instance, dGTP inhibits the enzyme RR, restraining DNA and RNA synthesis [104, 105]. Owing to the accumulation of guanine nucleotides and of hyperphosphorylated guanosine moieties, MtPNP might, thereby, play a role in the MTB latent state in response to nutritional stress [82]. Hence, we have carried out gene replacement experiments to produce a MTB mutant strain defective in functional PNP. Surprisingly, *deoD*-encoded MtPNP appears to play an essential role in survival of MTB grown in rich medium, since a knockout strain could not be generated due to the unexpected essentiality of the *deoD* gene (unpublished results). This result underscores the need for demonstrating protein function by experimental approaches instead of assigning function to a particular gene product based only on comparative data. These data also suggest that purine salvage metabolism is probably rather more complex in MTB than previously thought. More recently, crystals diffracting at 2.15 Å were obtained for the MtPNP, sulfate, and deoxyguanosine ternary complex [91], which should provide further insight into the mode of action of this enzyme.

3.6. Purine Nucleosidase (EC 3.2.2.1)

(other designations: NSase, purine nucleoside hydrolase, purine ribonucleosidase, and riboside hydrolase)

Encoded by the *iunH* gene (MTB Rv3393, 927 bp, 308 aa, 32937.50 Da, and pI = 5.15), purine nucleosidase (NSase), also known as purine nucleoside hydrolase, catalyzes the irreversible hydrolysis of all of the commonly occurring purine and pyrimidine nucleosides (*N*-glycosidic bond cleavage) to β-D-ribose and the associated base [106] (Fig. **8**). Deoxyribonucleosides are not substrates for this enzyme, notwithstanding their source. NSases have been isolated or the respective encoding genes identified from a number of sources, including bacteria [107-109], parasitic protozoans [110-114], and yeast [115]. Since parasitic protozoans lack the *de novo* pathway to synthesize purine nucleosides, they rely on NSase to supply purine nucleosides by salvaging them from the host [111]. Protozoan NSases may be divided into three subclasses according to the substrate preference: the first class is devoted to the preferential usage of inosine and uridine; the second to inosine, adenosine, and guanosine; and the third to inosine and guanosine [116]. The *E. coli* genome also contains genes for three NSases, which have been classified based on their substrate specificity: *rihA* and *rihB* are pyrimidine-specific, whereas *rihC* hydrolyzes both purine and pyrimidine ribonucleosides [109]. It has been shown that the features of the transition state structure determined by kinetic isotope effects of uridine hydrolysis catalyzed by the *E. coli rihC*-encoded enzyme are activation of the heterocyclic base by protonation of/or hydrogen bonding to O2, an extensively broken C1'-N1 glycosidic bond, decreased C1'–O4' bond distance due to oxocarbenium ion formation in the ribose ring, C3'-exo ribose ring conformation, and almost no bond formation to the attacking nucleophile [117]. The *E. coli* NSase proposed transition state is similar to that of *Crithidia fasciculata* NSase [118].

Apparently, NSase from MTB (MtNSase) has a substrate preference for inosine and uridine. Since humans lack this enzyme, relying on a different set of enzymatic reactions to supply their nucleoside requirements, the mycobacterial enzyme appears to represent one of the most attractive target amongst the purine salvage pathway enzymes for the rational design of drugs to treat human TB, with no, or little, side effects to the human host, according to the principle of selective toxicity. We have recently PCR-amplified and pET23a(+)-cloned the MTB *iunH* gene. The mycobacterial recombinant enzyme was expressed in its soluble form in electrocompetent *E. coli* C41(DE3) host cells. Homogeneous MtNSase could be obtained through a sequence of anion exchange and gel filtration chromatographic steps. Kinetic and structural studies are currently underway (unpublished data).

3.7. Inosine Monophosphate Dehydrogenase (EC 1.1.1.205)

(other designations: IMPDH, IMP dehydrogenase, inosine dehydrogenase, inosinic acid dehydrogenase, inosinate dehydrogenase, and IMP oxidoreductase)

Encoded by the *guaB2* gene (MTB Rv3411c, 1590 bp, 529 aa, 54866.90 Da, and pI = 6.33), inosine monophosphate dehydrogenase (IMPDH) catalyzes the oxidation of IMP to XMP with concomitant conversion of oxidized nicotinamide adenine dinucleotide (NAD^+) to the reduced form of nicotinamide adenine dinucleotide (NADH) [119] (Fig. **9**). IMPDH has already been described in eukaryotes and prokaryotes organisms, with great degree of conservation. Formerly classified as EC 1.2.1.14, IMPDH is a key enzyme of guanine nucleotide synthesis whose activity is strictly dependent on the presence of monovalent cations [120, 121], and classified as an IMPDH/GMPR family member. Its quaternary structure corre-

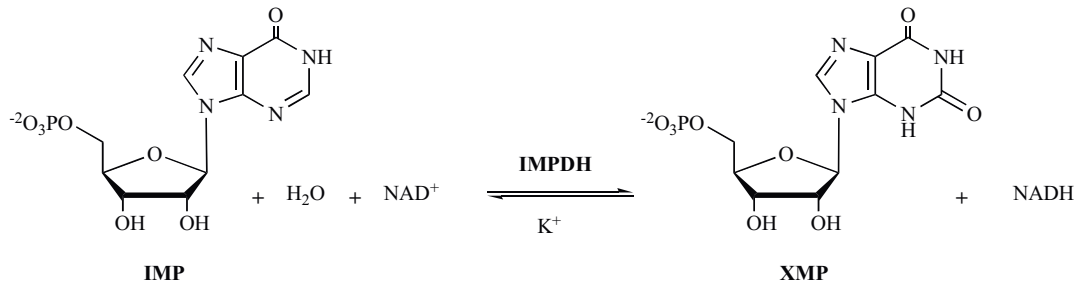

Fig. (9). Inosine monophosphate dehydrogenase catalyzes the NAD^+-dependent oxidation of IMP to XMP, with concomitant formation of NADH.

sponds to a homotetramer of approximately 55 kDa per subunit, with a β/α barrel CORE domain that comprises the substrate binding sites, and a smaller subdomain composed by two tandem cystathione-β-synthase (CBS) dimer domains [122] (PDB accession codes and a thorough review on IMPDH structural features the readers will find in reference [122]). IMPDH has received considerable interest in recent years as an important target enzyme for anticancer, antiviral, antiparasitic, and immunosuppressive chemotherapy [119, 122]. Inhibition of IMPDH causes an overall reduction in guanine nucleotide pools and, since GTP is a cofactor in the conversion of IMP to AMP, adenylate pools are also diminished. Subsequent interruption of DNA and RNA synthesis results in cytotoxicity [119]. As previously described, MTB IMPDH (MtIMPDH) is encoded by the *guaB2* gene. IMPDH activity was also hypothetically attributed to the *guaB1* (Rv1843c) and *guaB3* genes (Rv3410c). However, only *guaB2* gene has been experimentally identified by mass spectrometry proteomic assays [123]. Since it has been suggested that the IMPDH gene is present in a double copy in many species [122], including human homologues [124, 125], IMPDH activity for the products of MTB *guaB1* and *guaB3* genes cannot be discarded, even though they codify slightly shorter amino acid sequences (479 and 376 amino acids, respectively) and enzymes' activity were inferred solely by sequence homology.

Human IMPDH homologues, encoded by two separated genes, *impdh1* and *impdh2*, and located at chromosomes 7q31.3 and 3p21.2, correspond to IMPDH type I (Genbank accession number: NC_000007.13) and type II (Genbank accession number: NC_000003.11), respectively. The two isoforms have 84% sequence identity and show similar kinetic properties [126]. It was found that type I IMPDH was prevalent in normal human leukocytes and lymphocytes, while type II predominated in tumor cells and rapidly proliferating cells [119, 124]. Both are rate limiting enzymes of guanine nucleotide synthesis and are, therefore, involved in the regulation of cell growth [124]. MtIMPDH and human IMPDH type I and II (514 amino acid residues) share amino acid sequence identity of 37.92% and 37.99%, respectively.

Structural data indicate that IMPDH enzymes undergo major conformation rearrangements upon catalysis: during initial substrate binding the enzyme adopts an open configuration, while a catalytic cysteine residue mediates a nucleophilic attack to IMP C2 atom, followed by hydride transfer to NAD^+, generating NADH. When NADH departs from the active site, a mobile flap closes and docks into the vacant dinucleotide binding site. Hydrolysis of the covalent bond between cysteine and the purine ring then releases XMP [122, 127, 128]. Such conformational alterations, along with kinetic data, suggest a random substrate binding followed by an ordered product release [125, 129]. Several NAD^+/NADH binding site IMPDH inhibitors take advantage of the vacant dinucleotide binding site, arresting the enzyme on a dead-end conformation, preventing XMP release [129]. One example that recently reached the market is the mycophenolic acid (MPA) prodrug mycophenolate mofetil, CellCept®, introduced as an immunosuppressant [130]. Although showing positive results in phase I trials on the inhibition of myeloma cell proliferation [131], MPA dose-limiting gastrointestinal toxicity limits its potential for autoimmune disorders [132]. To overcome such drawbacks, MPA quinolone derivatives were developed aiming at human type II IMPDH selectivity [130]. Since its action is based on IMPDH structural features, MPA exhibits some species selectivity as an IMPDH inhibitor. Mammalian IMPDHs are very sensitive to MPA, while microbial IMPDHs are much less so. This selectivity was explained by the conformational difference between the human and bacterial enzyme homologues in the reaction intermediate formed, in which recently formed XMP is still covalently bound to IMPDH. Depending on the position of the flap in the dinucleotide binding site, there are two conformations of such reaction intermediate; while human IMPDH seems to prefer the open conformation, according to available crystallographic data, the bacterial enzymes prefer the closed one, diminishing its susceptibility to MPA binding [119]. IMPDH inhibitors may also compete for the IMP binding site; examples of marketed drugs include ribavirin (Rebetol®), a broad-spectrum antiviral agent and relatively weak IMPDH inhibitor, which is now used in combination with interpheron-alpha for the treatment of hepatitis C and HIV virus infections [133, 134]. Mizoribine (Bredinin®) is also a IMPDH inhibitor that must be phosphorylated to its monophosphate form prior to substrate site binding, inducing a closed conformation of IMPDH [133, 134]. Ribavirin is incorporated via its triphosphate form into the viral RNA genome by the action of the viral RNA-dependent RNA polymerase. Incorporation of this non-natural nucleotide into the viral RNA forces the RNA virus into a lethal accumulation of errors. This is further amplified by the reduction of GTP pools caused by the inhibition of IMPDH by ribavirin monophosphate, since the decrease in cellular GTP pools is likely to increase the frequency of RNA incorporation of ribavirin triphosphate, a GTP analog [119]. For this same reason, MPA and nucleoside analogue inhibitors combined therapy proved to be a valid way of controlling HIV infection, targeting viral replication [135]. Experimental evidence demonstrated that MPA induces IMPDH aggregate formation concomitant with its inhibition, both *in vivo* and *in vitro*, through protein conformational change leading to perinuclear linear arrays up to 2000 kDa [134]. The same researchers also showed that when intracellular GTP pools are re-established, aggregate formation is reversed, and IMPDH activity restored; both these findings are due to GTP binding to IMPDH CBS domain, implying a possible role of intracellular energy sensor for IMPDH [134]. The CBS domain is a conserved protein domain present in the proteome of archaebacteria, prokaryotes, and eukaryotes, usually in tandem repeats [136]. Mutations in CBS domains are related to several human hereditary diseases (homocystinuria, retinitis pigmentosa, hypertrophic cardiomyopathy, and myotonia congenital), but their function and how they affect the structural and/or functional properties of enzymes they are part of are yet to be determined. CBS domains have been proposed to affect multimerization and sorting of proteins, channel gating, and ligand binding, along with intracellular metabolite sensor activity [136]. A recent report suggested that the CBS domain of IMPDH is involved in coordinating the activities of the enzymes of purine nucleotide metabolism (IMPDH, adenylo-

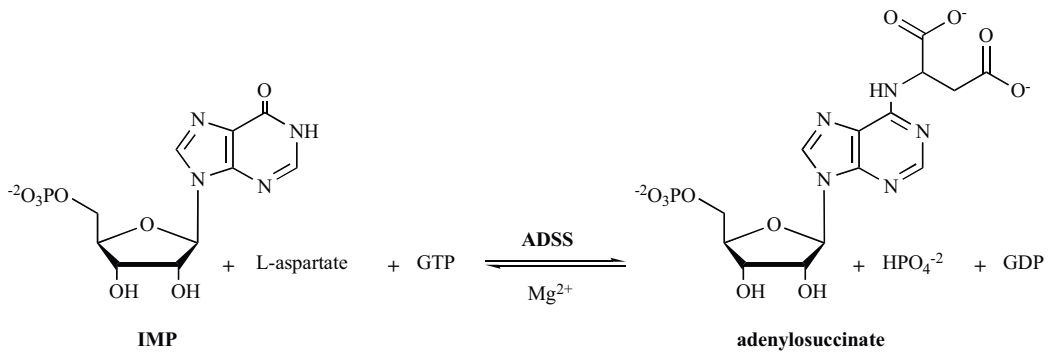

Fig. (10). Adenylosuccinate synthase catalyzes the first committed step in the conversion of IMP to AMP. IMP and L-aspartate are conjugated in a two-step reaction accompanied by the hydrolysis of GTP to GDP. Initially, the γ-phosphate group of GTP is transferred to IMP. Aspartate then displaces the phosphate group to form the product, adenylosuccinate.

succinate synthase and GMP reductase) and is essential for maintaining the normal ATP and GTP pool sizes in *E. coli* [137]. These authors also attributed a possible allosteric IMPDH activity role to CBS domains [137].

Amino acid sequence alignments of MtIMPDH against non-redundant protein sequence data base of the National Center for Biotechnology and Information (NCBI) indicates that the mycobacterial enzyme shows the well conserved tandem CBS pair of domains. This structural conservation, along with previously described results concerning IMPDH activity and CBS domains probable cellular energetic sensor role indicate that this enzyme may play a key role in the biology of MTB. Reports that guanine nucleotide starvation induced quiescent phenotype in *S. cerevisiae* due to nutrient limitation [138] and of an attenuated strain of *Streptococcus suis* obtained after IMPDH gene knockout [139] can also indicate that the IMPDH enzyme, through its CBS domains, might act as a sensor of energetic availability and metabolic status changes, like latency entry and rescue in MTB, in addition to MTB virulence. Both structural and amino acid residue conservation features should be explored on MTB highly specific inhibitor development, since it has been shown that even 84% identity between human isoforms do not prevent IMPDH selective inhibition [140, 141]. We have recently PCR-amplified and pET23a(+)-cloned the MTB *guaB2* gene. The mycobacterial recombinant enzyme was expressed in its soluble form in electrocompetent *E. coli* C41(DE3) host cells. Homogeneous MtIMPDH could be obtained by a purification protocol including of affinity and gel filtration chromatographic steps. Correct assignment to the structural gene encoding MtHGPRT was confirmed by measurement of the biological activity of the recombinant enzyme by steady-state kinetics (unpublished data). MtIMPDH apparent and true kinetic parameters, as well as its metal requirement and kinetic mechanism are currently underway. Cloning and characterization of protein encoded by MTB *guaB1* and *guaB3* genes have yet to be pursued.

3.8. Adenylosuccinate Synthase (EC 6.3.4.4)

(other designations: ADSS and IMP:L-aspartate ligase (GDP-forming))

Encoded by the *purA* gene (MTB Rv0357c, 1299 bp, 432 aa, 46822.40 Da, and pI = 6.72), adenylosuccinate synthase (ADSS) catalyzes the first committed step in the conversion of IMP to AMP. IMP and L-aspartate are conjugated in a two-step reaction accompanied by the hydrolysis of GTP to guanosine 5'-diphosphate (GDP) in the presence of Mg^{2+}. Initially, the γ-phosphate group of GTP is transferred to the O6 of IMP, to give 6-phosphoryl IMP. Aspartate then displaces the phosphate group to form the product, adenylosuccinate (Fig. **10**) [142].

This three-substrate enzyme is present in a broad range of organisms and cell types, with exception of mature erythrocytes [143]. Mammalian cells present two isoforms of the enzyme, the basic and acidic isozymes [144], whereas bacteria possess a single form. The regulation of this enzyme, which is involved in maintenance of ATP/GTP ratios in the cell, can be effected by the products of its catalyzed reaction (GDP and adenylosuccinate) and by the end products of the pathway (AMP and GMP) [145]. According to its protein sequence, MTB ADSS (MtADSS) is expected to be highly similar to many bacterial homologues. The enzyme from *E. coli*, and perhaps from other sources, undergoes significant conformational changes upon IMP binding, which organizes the catalytic machinery of the active site [143, 146]. Indeed, IMP binding may play an important physiological role in the regulation of ADSS activity by stabilizing the assembly of inactive monomers into active dimers [147]. Based on the consensus oligomeric state of homologues from other sources, where it is essential [142, 143, 148], the enzyme from MtADSS is very likely to be active as a homodimer. Some inhibitors have been considered for ADSS; one of the most studied, hadacidin, a competitive inhibitor with respect to aspartate, coordinates the active site Mg^{2+} with its *N*-formyl group and packs against the base moiety of IMP [149-152]. We have recently PCR-amplified and pET23a(+)-cloned the MTB *purA* gene. The mycobacterial recombinant enzyme was expressed in its insoluble form in electrocompetent *E. coli* BL21(DE3). Efforts to improve protein solubility or to express ADSS in the soluble form are currently underway (unpublished data).

3.9. Adenylosuccinate Lyase (EC 4.3.2.2)

(other designations: ADSL, adenylosuccinase, and succino AMP-lyase)

Encoded by the *purB* gene (MTB Rv0777, 1419 bp, 473 aa, 51008.30 Da, and pI = 6.33), adenylosuccinate lyase (ADSL) catalyses two steps in the purine pathway: the conversion of succinylaminoimidazolecarboxiamide ribonucleotide (SAICAR) into aminoimidazolecarboxiamide ribonucleotide (AICAR) in the *de novo* pathway; and the conversion of adenylosuccinate (also named succinyladenosine monophosphate) into AMP and fumarate through β-elimination in the purine salvage pathway (Fig. **11**) [153]. ADLS belongs to the fumarase superfamily of enzymes, which catalyze reactions with fumarate as one of the products, with high conservation of protein's tertiary structure without corresponding primary structure conservation [154, 155]. Structural dissimilarities between SAICAR and adenylosuccinate indicated which groups make no specific contact to the enzyme's active site, since no major ADSL rearrangements occur due to binding of both substrates [153, 156]. Further evidence that no enzyme structural modification is necessary for both substrate binding arose from *P. falciparum* ADSL studies, in which it was demonstrated that the homogeneous form of the enzyme was capable of catalyzing the ADSL *de novo* reaction *in vitro*, even though such pathway is absent in this parasite [153].

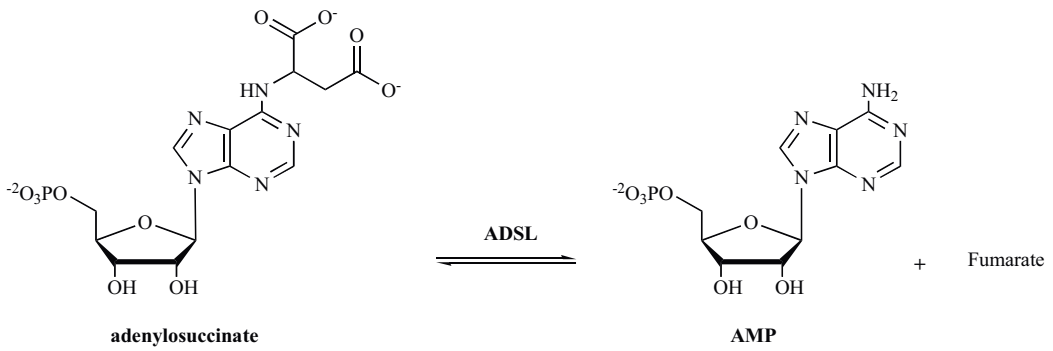

Fig. (11). In the purine salvage pathway, adenylosuccinate lyase catalyses the conversion of adenylosuccinate into AMP and fumarate through a β-elimination.

MTB ADSL (MtADSL) primary structure pairwise alignment to human and *Bacillus subtilis* (one of the best characterized ADSL enzymes) homologues indicate 29.13% and 23.95% identity, respectively. *B. subtilis* ADSL (GenBank accession code NC_000964.3) is a homotetramer comprised by 431 amino acids per subunit, also coded by a *purB* gene [157, 158]. Human ADSL, encoded by the *adsl* gene (also denoted as *amps*) and located at chromosome 22q13.1-13.2 (GenBank accession code NC_000022.10) has each subunit composed by 484 amino acids with 54,889 Da. Crystallographic structures have already been solved for the human homologue bound to AMP (PDB accession code 2J91) and to adenylosuccinate, fumarate, and AMP (PDB accession code 2VD6). Defects in ADSL are the cause of adenylosuccinate deficiency characterized by the accumulation in the body fluids of succinylaminoimidazolecarboxamide riboside and succinyladenosine, associated with autism, psychomotor retardation, and, in some cases, growth retardation associated with muscle wasting and epilepsy [153]. Several point mutations, such as P75A, D397Y, R401H, and S413P, are associated with defective enzyme [157] and are located outside the ADSL active site, most probably rendering structurally unstable enzymes [158]. Besides not being attributed to a single cause, severity of adenylosuccinate deficiency clinical phenotype correlates with ADSL activity level [159, 160].

Together, the reactions catalyzed by ADSS and ADSL form the purine nucleotide cycle [155], and regulate cellular metabolism by controlling fumarate, a citric acid cycle intermediate, and free AMP levels [156]. ADSL enzymes are homotetramers with approximately 52 kDa per subunit, where three subunits contribute with amino acids to the active site located on such interface [161], with histidine residues from two distinct subunits taking part on catalysis [153, 157]. The β-elimination of fumarate on both ADSL catalyzed reactions proceed through a general base-general acid mechanism, in which His68 and His141 in *B. subtilis* and *Thermotoga maritima* are involved [156, 157, 162]. The enzyme mechanism is uni-bi mechanism with either steady-state [163, 164] or rapid equilibrium [153] ordered product release, where fumarate departs first from the ADSL active site. Site-directed mutagenesis experiments and crystallographic data of *E. coli* ADSL indicate, however, that His141, and not His68, is the general acid, and a serine residue, located in a mobile loop that closes the ADSL catalytic site upon substrate binding, is the general base [165]. All these residues are conserved in the MtADSL homologue, corresponding to His76, His147, and Ser277, and are also observed among all ADSL homologues described [156]. A third fully conserved histidine residue, corresponding to MtADSL His95, was implicated in substrate binding and proper orientation for catalysis by site-directed mutagenesis and crystallographic data analysis [158].

Metabolic adaptations to environmental energetic status are related to the shift between the *de novo* and salvage pathways of purine synthesis. It has already been shown that pathogenic mycobacteria are able to change purine salvage enzyme expression, owing to purine base supplementation [166]. Further experiments in *E. coli* demonstrated that all genes involved in IMP synthesis are repressed upon hypoxanthine supplementation, and that such gene expression, along with genes of GMP synthesis, are regulated by a common PurR repressor, encoded by the *purR* gene. The PurR repressor is know to bind PUR box-like sequences (gaaaacgtttnc) found in the promoter region of purine related genes, as well as downstream from transcriptional start region of the *purR* own gene [167]. *E. coli purB* gene differs in its regulation patterns by upregulating under limiting adenine conditions, even with hypoxanthine or guanine excess [168], indicating that the *purB* gene is regulated by the purine pool and *purR* [169]. No homologue to *purR* gene has been observed in the MTB genome, nor were PUR box-like sequences identified in the *purB* gene, indicating that MtADSL might be responsive only to purine pools, which corroborates the free AMP level regulation activity attributed to the purine nucleotide cycle [155]. Aside from a role in energetic sensing, ADSL from *B. subtilis* has been shown to act as a regulatory factor of glutamil-tRNA synthetase, an enzyme involved in protein biosynthesis, which is a high energy demanding process [170]. ADSL may, thus, couple purine and protein biosynthesis, regulating AMP biosynthesis and maintaining cellular ATP/AMP ratio [171].

ADSL crystallographic data could not provide unequivocal evidence of amino acid residues involved in substrate binding specificity, especially for being a single substrate enzyme, thus requiring enzyme co-crystallization with possible inhibitors to allow active site inspection [172]; however, ADSL homologues have broad-substrate specificity [173], which limit the information that can be extracted from structural data to further develop specific inhibitors. A non-cleavable substrate analog, adenosine phosphonobutyric acid, 2'(3'), 5'-diphosphate (APBADP), was shown to be a competitive inhibitor of *B. subtilis* ADSL with K_i values of 0.18 ± 0.04 μM and 0.16 ± 0.04 μM when tested against adenylosuccinate and SAICAR substrates, respectively. For human ADSL, these values were 0.09 ± 0.04 μM and 0.21 ± 0.08 μM, respectively [174]. APBADP structure presents two extra phosphate groups, in the ribose ring and in the four-carbon chain [174]; these additional groups impair ADSL to properly arrange the molecule for catalysis [153]. Structural comparison between both ADSL natural substrates to identify conserved chemical groups, knowledge of potential amino acid residues involved in catalysis, and stereochemical restrains might be exploited for ADSL specific inhibitors development. We have recently PCR-amplified, pET23a(+)-cloned the MTB *purB* gene. The mycobacterial recombinant enzyme was expressed in its soluble form in electrocompetent *E. coli* BL21(DE3) host cells. Availability of homogeneous MtADSL, currently underway, will enable to assign ADSL activity to this mycobacterial enzyme (unpublished data).

3.10. Nucleoside Monophosphate Kinases

Nucleotide triphosphates (NTP) are DNA and RNA precursors and critical regulators in diverse cellular pathways. An essential

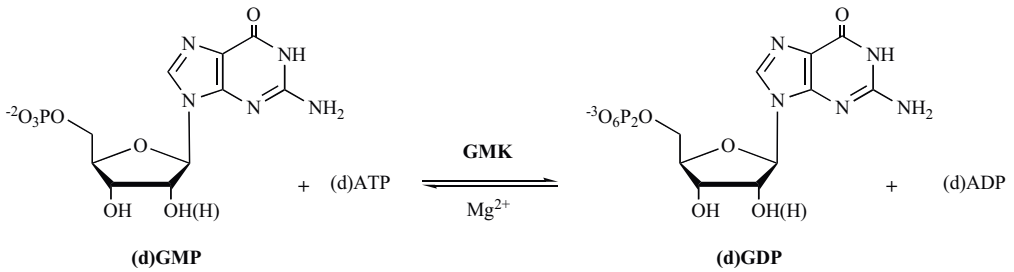

Fig. (12). Guanylate kinase catalyzes the reversible transfer of a phosphate from ATP to GMP, yielding ADP and GDP.

step for their synthesis relies on the conversion of nucleoside monophosphates (NMP) to nucleoside diphosphates (NDP), a process that involves the reversible transfer of the γ-phosphoryl group of ATP to an NMP acceptor by NMP kinases. Two purine NMP kinases are responsible for these activities in MTB: guanylate kinase and adenylate kinase. Based on the structures solved to date (PDB accession codes and a in-depth review on NMP structural features the readers will find in reference [175]), all purine NMP kinases consist of a CORE domain with the LID domain and the NMP-binding domain attached to it [175]. Even though prokaryotic NMP kinases share a similar modular architecture with their eukaryotic counterparts, in many cases they display singular features that are solely observed in bacteria or bacterial groups. Since unique enzymological properties can be studied to explore potential antibacterial targets, this group of enzymes might also be worth the effort.

3.10.1. Guanylate Kinase *(EC 2.7.4.8)*

(other designations: GMK, GMP kinase, and ATP:(d)GMP phosphotransferase)

Encoded by the *gmk* gene (MTB Rv1389, 627 bp, 208 aa, 22063.10 Da, and pI = 7.58), guanylate kinase, also known as guanosine monophosphate kinase (GMK), is an essential enzyme that recycles GMP (and, indirectly, cGMP) by catalyzing the reversible transfer of a phosphate group from ATP to GMP, yielding ADP and GDP (Fig. **12**). dGMP can also act as an acceptor, and dATP can act as a donor; Mg^{2+} is a critical component of catalysis, whose binding to GMK is enhanced by the presence of both substrates [176]. This enzyme plays an essential role in the biosynthesis of GTP. It also has a medicinal importance as it activates guanosine analog prodrugs, like some antiviral and anticancer agents, such as mercaptopurine, thioguanine, acyclovir, ganciclovir, and carbovir, among others [177-179].

As is evident from the structure (PDB accession code 1LVG), mouse GMK has a clamp-like cavity, where the two lobes of the protein close through an approximately 1 nm conformational change upon binding the substrates [180]; most of this conformational motion is induced by the binding of GMP. The substrates drive this conformational change through several direct and indirect (via water molecules) interactions that bring the LID and NMP-binding domain together and towards the CORE region, the structure closing in a vise-like motion [180, 181]. In this configuration, the CORE is catalytically active towards phosphoryl transfer, which relies on a residue sequence (the P-loop) that is conserved in kinases [182]. Using a nanotechnology approach based on controlled mechanical stress to bias conformational states in favor of GMK open (without substrates) conformation, it could be observed that the binding affinity for GMP is considerably reduced, whereas ATP binding constant and the catalytic rate remain essentially unaffected. Since the binding of GMP does not control, allosterically or cooperatively, the binding of ATP to the enzyme, it must allosterically control catalysis itself or, at least, the ATP hydrolysis step. The concept of using mechanical stress to control the conformation of a protein can be applied to virtually any protein to study the fundamental mechanisms of allostery from a new perspective [183].

Based on the crystal structure, MTB GMK (MtGMK) is a monomeric enzyme that displays a low catalytic efficiency (as previously mentioned) in relation to eukaryotic homologues, an unusual specificity for ATP as a phosphate donor, and carries two redox-sensitive cysteines in the central CORE domain. Although MtGMK has a modular domain structure as most NMP kinases, the unusual CORE domain conformation and the partially open LID and GMP-binding domains (which are the same in the apo, GMP-bound, and GDP-bound forms) relative to the CORE of the mycobacterial enzyme point to considerable differences to the eukaryotic homologues [184], which could be explored towards development of drugs with selective activity. We have PCR-amplified and pET23a(+)-cloned the MTB *gmk* gene. Efforts to produce the recombinant protein in electrocompetent *E. coli* commercial variants available for heterologous expression is currently underway (unpublished data).

3.10.2. *Adenylate Kinase* (EC 2.7.4.3)

(other designations: ADK, ATP:AMP phosphotransferase, adenylokinase, and myokinase)

Encoded by the *adk* gene (MTB Rv0733, 546 bp, 181 aa, 20092.80 Da, and pI = 4.76), adenylate kinase (ADK) catalyzes the reversible Mg^{2+}-dependent high-energy phosphoryl transfer from ATP to AMP, releasing two ADP molecules, thereby regulating the adenine nucleotide composition within the cell [185]; it also accepts dAMP (Fig. **13**). This small ubiquitous enzyme is essential in intracellular nucleotide metabolism, and has been found to act as both a NMP and NDP kinase, suggesting that it may have a role in RNA and DNA biosynthesis [186].

The ADK family has been classified into two groups based on the polypeptide chain length, in which the long variants present a longer LID domain [187]. Several isoforms have been identified in eukaryotes, with diverse size and cell, tissue, and organ distribution [188, 189]. Eukaryotic cytosolic enzymes belong to a short type of ADK, while the bacterial, yeast, and mitochondrial enzymes generally belong to the long type. In the enzyme from MTB (MtADK), a representative of a new proposed subfamily of short bacterial ADK variants [187], the LID is reduced to a small irregular loop; the rest of the primary structure, overall fold, and side chains that are involved in catalysis and nucleotide binding are, however, conserved in all variants [190, 191]. This monomeric enzyme, which is essential for bacterial survival, displays an unexpectedly high thermal stability [187] and a compact and rigid structure [187, 192], possibly due to the considerably short LID domain, and a noticeably low catalytic activity, which could be related to its singular structural and dynamic features [193] or to a functional role in its slow growing phenotype or even latent state survival process [187]. MtADK crystal structure in complex with two ADP molecules and Mg^{2+} (PDB accession code 2CDN) revealed significant conformational changes of the LID and NMP-binding domain upon substrate binding. The ternary complex represents the state of the enzyme at the start of ATP synthesis reaction, and is consistent with the direct nucleophilic attack of a terminal oxygen from the acceptor ADP molecule on the β-phosphate from the donor substrate, and hints to

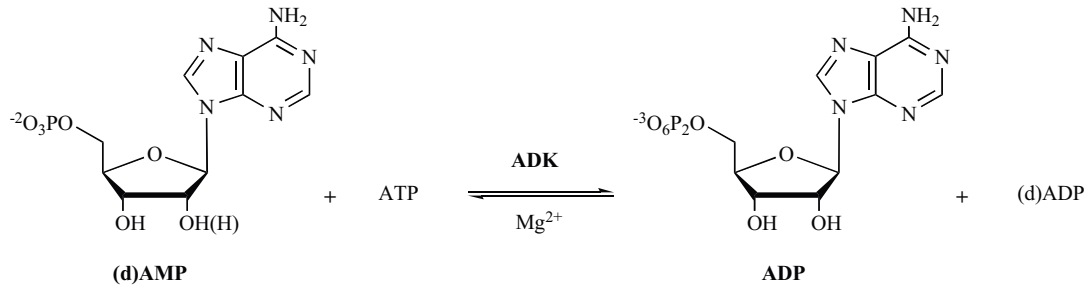

Fig. (13). Adenylate kinase catalyzes the reversible phosphoryl transfer from ATP to AMP, releasing two ADP molecules.

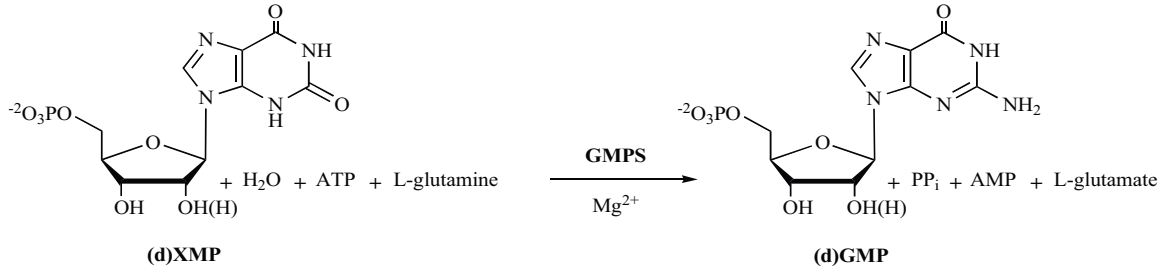

Fig. (14). Guanosine monophosphate synthase catalyses the irreversible conversion of XMP into GMP though a reaction that requires ATP and involves the transfer of an amino group from L-glutamine to the C2 of XMP via an adenyl-XMP intermediate.

an associative mechanism for phosphoryl transfer [192]. MtADK seems to display structural and catalytic features considerably different from the ones observed in the eukaryotic and prokaryotic homologues [187, 194], an essential fact for selective drug target design with little or no effect on eukaryotic isoforms.

3.11. Guanosine Monophosphate Synthase (EC 6.3.5.2)

(other designations: GMPS, GMP synthase (glutamine-hydrolyzing), GMP synthetase, glutamine amidotransferase, guanylate synthetase, XMP aminase, xanthosine 5'-phosphate amidotransferase, and xanthosine-5'-phosphate-ammonia ligase)

Encoded by the *guaA* gene (MTB Rv3396c, 1578 bp, 525 aa, 56027.60 Da, and pI =5.23), guanosine monophosphate synthase (GMPS) catalyses the biosynthesis GMP from XMP and L-glutamine in the presence of H_2O, ATP, and Mg^{2+}, yielding GMP, PP_i, AMP, and L-glutamate [195]; the enzyme also accepts dXMP (Fig. **14**). The irreversible transfer of an amino group from glutamine to the C2 atom of XMP via an adenyl-XMP intermediate characterizes the G-type family of glutamine amidotransferases (GAT) that utilize glutamine as the main ammonia source [196]. Guanine nucleotide products are not only essential for DNA and RNA synthesis, but also provide GTP for a number of essential cellular processes [197]. Both prokaryotic and eukaryotic GMPS homologues show a tertiary structure composed by two distinct domains, a GAT domain at its N-terminal portion, where glutamine is hydrolised to glutamate and ammonia, and an ATP pyrophosphatase (ATPPase) C-terminal domain, where the adenyl-XMP intermediate is formed [196]. Ammonia is channeled between these two domains in a substrate-protective environment, ensuring an efficient catalysis. The presence of two separate although connected domains, further classifies GMPS as a Class I amidotransferase [198, 197]. Even though it has already been shown that the glutaminase activity might be independent from XMP or ATP binding to ATPPase domain, GMPS only achieves maximum activity upon binding of both substrates to the C-terminal domain [196], highlighting both active sites concerted action [198, 197].

The human counterpart corresponds to a 693 amino acid protein, codified by the *umps* gene, located at the chromosome 3q24 (GenBank accession code NM_003875); even being considered a particularly interesting target for anticancer and immunosupprecive therapies [199], literature relating to human and other GMPS homologues are considerably scarse. Unlike *P. falciparum*, that presents a homodimeric quaternary structure, human GMPS seems to be a monomer in solution [196].

Despite differences on quaternary organization, all GMPS noted to date exhibit a conserved cysteine residue on their GAT domain, involved in the hydrolysis of glutamine, which corresponds to Cys93 in MTB GMPS (MtGMPS) [199, 200]. Acivicin has been identified as a selective inhibitor of human GMPS glutaminase activity, abolishing GAT function while preserving ATPPase mediated XMP amination in the presence of Mg^{2+}, ATP, and XMP, indicating that these ligands might be necessary for the cysteine residue to become a reactive nucleophile. Thereby, acivicin totally inhibit GMPS activity when glutamine is the sole ammonia source, by forming an imino-thioesther linkage to the conserved active site cysteine residue [199, 201]. Notwithstanding such catalytic residue absolute conservation, and perhaps a conserved catalytic mechanism, a comparative analysis of GMPS conding genes across prokaryotes and eukaryotes indicated mammalian orthologs as a clearly diverged branch [202], a positive indicative that high specific inhibitors towards pathogens may be identified.

MtGMPS might be an interesting target for drug development due to its role in GMP synthesis. It is important to point that disruption of the *guaA* gene from *Francisella tularensis*, the causative agent of tularemia, has already been shown to result in attenuated strain guanine auxotrophs, unable to replicate within macrophages, presenting decreased numbers over infection time [203]; the corresponding gene is also essential for survival and infectivity of *Borrelia burgdorferi*, the infectious agent of Lyme borreliosis [204]. We have recently PCR-amplified and pET23a(+)-cloned the MTB *guaA* gene. The mycobacterial recombinant enzyme was expressed in its soluble form in electrocompetent *E. coli* BL21(DE3) host cells. Homogeneous dimeric MtGMPS could be obtained through a sequence of anion exchange, gel filtration, and hydrophobic interaction chromatographic steps. Kinetic and structural studies are currently underway (unpublished data).

4. SUMMARY

The current situation imposed by human TB demands urgent development of new and more effectivet drugs to combat mycobacterial drug-resistance and, hopefully, latency. Enzymes from the purine salvage pathway seem to be attractive molecular targets on which to base the development of inhibitors to be used against this infectious disease, since purine analogues were already found to be toxic for bacterial cell growth. Although some of these enzyme activities are shared between MTB and the human host, it is possible to develop inhibitors with selective activity against the pathogen's enzymes by exploiting differences in their functional and structural features.

ACKNOWLEDGEMENTS

This work was supported by funds of Millennium Initiative Program and National Institute of Science and Technology on Tuberculosis (INCT-TB), MCT-CNPq, Ministry of Health - Department of Science and Technology (DECIT) - Secretary of Health Policy (Brazil) to L.A.B. and D.S.S. L.A.B. (CNPq, 520182/99-5) and D.S.S. (CNPq, 304051/1975-06) are Research Career Awardees of the National Research Council of Brazil (CNPq). R.G.D. is a postdoctoral fellow of CNPq. A.B. acknowledges a scholarship awarded by BNDES.

ABBREVIATIONS

5'-NT	=	5'-nucleotidase
ADD	=	adenosine deaminase
ADK	=	adenylate kinase
ADP	=	adenosine 5'-diphosphate
ADSL	=	adenylosuccinate lyase
ADSS	=	adenylosuccinate synthase
AICAR	=	aminoimidazolecarboxiamide ribonucleotide
AK	=	adenosine kinase
AMP	=	adenosine 5'-monophosphate
APBADP	=	adenosine phosphonobutyric acid, 2'(3'), 5'-diphosphate
APRT	=	adenine phosphoribosyltransferase
ATP	=	adenosine 5'-triphosphate
ATPPase	=	ATP pyrophosphatase
CBS	=	cystathione-β-synthase
d	=	deoxy
GAT	=	glutamine amidotransferase
GDP	=	guanosine 5'-diphosphate
GMK	=	guanosine monophosphate kinase
GMP	=	guanosine 5'-monophosphate
GMPS	=	guanosine monophosphate synthase
GTP	=	guanosine 5'-triphosphate
HGPRT	=	hypoxanthine-guanine phosphoribosyltransferase
HIV	=	human immunodeficiency virus
HsPNP	=	human purine nucleoside phosphorylase
ImmH	=	immucillin-H
IMP	=	inosine 5'-monophosphate
IMPDH	=	inosine monophosphate dehydrogenase
MDR	=	multidrug-resistant
MESG	=	2-amino-6-mercapto-7-methylpurine ribonucleoside
methyl-Ado	=	2-methyladenosine
MPA	=	mycophenolic acid
Mt5'-NT	=	*M. tuberculosis* 5'-nucleotidase
MtADD	=	*M. tuberculosis* adenosine deaminase
MtADK	=	*M. tuberculosis* adenylate kinase
MtADSL	=	*M. tuberculosis* adenylosuccinate lyase
MtADSS	=	*M. tuberculosis* adenylosuccinate synthase
MtAK	=	*M. tuberculosis* adenosine kinase
MtAPRT	=	*M. tuberculosis* adenine phosphoribosyltransferase
MTB	=	*Mycobacterium tuberculosis*
MtGMK	=	*M. tuberculosis* guanosine monophosphate kinase
MtGMPS	=	*M. tuberculosis* guanosine monophosphate synthase
MtHGPRT	=	*M. tuberculosis* hypoxanthine-guanine phosphoribosyltransferase
MtIMPDH	=	*M. tuberculosis* inosine monophosphate dehydrogenase
MtNSase	=	*M. tuberculosis* purine nucleosidase
MtPNP	=	*M. tuberculosis* purine nucleoside phosphorylase
NAD^+	=	oxidized nicotinamide adenine dinucleotide
NADH	=	reduced form of nicotinamide adenine dinucleotide
NCBI	=	National Center for Biotechnology and Information
NDP	=	nucleoside diphosphate
NMP	=	nucleoside monophosphate
NSase	=	purine nucleosidase
NTP	=	nucleotide triphosphate
OPRT	=	orotate phosphoribosyltransferase
pI	=	isoelectric point
PNP	=	purine nucleoside phosphorylase
PP_i	=	pyrophosphate
PRPP	=	5'-phospho-α-D-ribose 1'-diphosphate
PRTase	=	phosphoribosyltransferase
RR	=	ribonucleotide reductase
SAICAR	=	succinylaminoimidazolecarboxiamide ribonucleotide
SCID	=	severe combined immunodeficiency disease
TB	=	tuberculosis
XDR	=	extensively drug-resistant
XMP	=	xanthosine 5'-monophosphate

REFERENCES

[1] World Health Organization, Global Tuberculosis Control, A short update to the 2009 report, **2009**.
[2] Ruffino-Netto, A. Tuberculosis: the negleted calamity. *Rev. Soc. Bras. Med. Trop.*, **2002**, *35*(1), 51-58.
[3] Lienhardt, C.; Ogden, J.A. Tuberculosis control in resource-poor countries:

have we reached the limits of the universal paradigm? *Trop. Med. Int. Health*, **2004**, *9*(7), 833-841.
[4] Ducati, R.G.; Ruffino-Netto, A.; Basso, L.A.; Santos, D.S. The resumption of consumption - a review on tuberculosis. *Mem. Inst. Oswaldo Cruz*, **2006**, *101*(7), 697-714.
[5] Young, D.B. Blueprint for the white plague. *Nature*, **1998**, *393*(6685), 515-516.
[6] Murray, C.J.L. In *Tuberculosis: Pathogenesis, Protection, and Control*; Bloom, B.R. Ed.; ASM: Washington, **1994**; pp. 583-622.
[7] Bloom, B.R.; Murray, C.J. Tuberculosis: commentary on a reemergent killer. *Science*, **1992**, *257*(5073), 1055-1064.
[8] Dorman, S.E.; Chaisson, R.E. From magic bullets back to the magic mountain: the rise of extensively drug-resistant tuberculosis. *Nat. Med.*, **2007**, *13*(3), 295-298.
[9] Basso, L.A.; Blanchard, J.S. Resistance to antitubercular drugs. *Adv. Exp. Med. Biol.*, **1998**, *456*, 115-144.
[10] World Health Organization. World Health Organization press release. Drug resistant tuberculosis levels ten times higher in Eastern Europe and Central Asia. *Saudi Med. J.*, **2004**, *25*(8), 1139-1140.
[11] Stokstad, E. Infectious disease. Drug-resistant TB on the rise. *Science*, **2000**, *287*(5462), 2391.
[12] Voet, D.; Voet, J.G. In *Biochemistry*; John Wiley & Sons: New Jersey, **2004**; pp. 1069-1104.
[13] el Kouni, M.H. Potential chemotherapeutic targets in the purine metabolism of parasites. *Pharmacol. Ther.*, **2003**, *99*(3), 283-309.
[14] Smith, C.; Marks, A.D.; Lieberman, M. In *Mark's Basic Medical Biochemistry - A Clinical Approach*; Lippincott Williams & Wilkins: Maryland, **2005**; pp. 747-761.
[15] Malathi, V.G.; Ramakrishnan, T. Biosynthesis of nucleic acid purines in *Mycobacterium tuberculosis* H37Rv. *Biochem. J.*, **1966**, *98*(2), 594-597.
[16] Downie, M.J.; Kirk, K.; Mamoun, C.B. Purine salvage pathways in the intraerythrocytic malaria parasite *Plasmodium falciparum*. *Eukaryot. Cell*, **2008**, *7*(8), 1231-1237.
[17] Boshoff, H.I.M.; Barry, C.E. 3rd. Tuberculosis - metabolism and respiration in the absence of growth. *Nat. Rev. Microbiol.*, **2005**, *3*(1), 70-80.
[18] Long, M.C.; Escuyer, V.; Parker, W.B. Identification and characterization of a unique adenosine kinase from *Mycobacterium tuberculosis*. *J. Bacteriol.*, **2003**, *185*(22), 6548-6555.
[19] Parker, W.B.; Long M.C. Purine metabolism in *Mycobacterium tuberculosis* as a target for drug development. *Curr. Pharm. Des.*, **2007**, *13*(6), 599-608.
[20] Biazus, G.; Schneider, C.Z.; Palma, M.S.; Basso, L.A.; Santos D.S. Hypoxanthine-guanine phosphoribosyltransferase from *Mycobacterium tuberculosis* H37Rv: cloning, expression, and biochemical characterization. *Protein Expr. Purif.*, **2009**, *66*(2), 185-190.
[21] Cole, S.T.; Brosch, R.; Parkhill, J.; Garnier, T.; Churcher, C.; Harris, D.; Gordon, S.V.; Eiglmeier, K.; Gas, S.; Barry, C.E. 3rd; Tekaia, F.; Badcock, K.; Basham, D.; Brown, D.; Chillingworth, T.; Connor, R.; Davies, R.; Devlin, K.; Feltwell, T.; Gentles, S.; Hamlin, N.; Holroyd, S.; Hornsby, T.; Jagels, K.; Krogh, A.; McLean, J.; Moule, S.; Murphy, L.; Oliver, K.; Osborne, J.; Quail, M.A.; Rajandream, M.A.; Rogers, J.; Rutter, S.; Seeger, K.; Skelton, J.; Squares, R.; Squares, S.; Sulston, J.E.; Taylor, K.; Whitehead, S.; Barrell, B.G. Deciphering the biology of *Mycobacterium tuberculosis* from the complete genome sequence. *Nature*, **1998**, *393*(6685), 537-544.
[22] Ducati, R.G.; Basso, L.A.; Santos, D.S. Mycobacterial shikimate pathway enzymes as targets for drug design. *Curr. Drug Targets*, **2007**, *8*(3), 423-435.
[23] Villela, A.D.; Sánchez-Quitian, Z.A.; Ducati, R.G.; Santos, D.S.; Basso, L.A. Pyrimidine salvage pathway in *Mycobacterium tuberculosis*. *Curr. Med. Chem.*, **2010**, volume and page numbers of this issue.
[24] Hunsucker, S.A.; Mitchell, B.S.; Spychala, J. The 5'-nucleotidases as regulators of nucleotide and drug metabolism. *Pharmacol. Ther.*, **2005,** *107*(1), 1-30.
[25] Schaefer, H.J. In *Drug Design*; Ariens, E.J. Ed.; Academic Press: New York, **1971**; pp. 129-159.
[26] Agarwal, R.P. Inhibitors of adenosine deaminase. *Pharmacol. Ther.*; **1982**, *17*(3), 399-429.
[27] Centelles, J.J.; Franco, R.; Bozal, J. Purification and partial characterization of brain adenosine deaminase: inhibition by purine compounds and by drugs. *J. Neurosci. Res.*, **1988**, *19*(2), 258-267.
[28] Wilson, D.K.; Rudolph, F.B.; Quiocho, F.A. Atomic structure of adenosine deaminase complexed with a transition-state analog: understanding catalysis and immunodeficiency mutations. *Science*, **1991**, *252*(5010), 1278-1284.
[29] Wilson, D.K.; Quiocho, F.A. A pre-transition-state mimic of an enzyme: X-ray structure of adenosine deaminase with bound 1-deazaadenosine and zinc-activated water. *Biochemistry*, **1993**, *32*(7), 1689-1694.
[30] Hershfield, M.S. Genotype is an important determinant of phenotype in adenosine deaminase deficiency. *Curr. Opin. Immunol.*, **2003**, *15*(5), 571-577.
[31] Nygaard, P. Adenosine deaminase from *Escherichia coli*. *Methods Enzymol.*, **1978**, *51*, 508-512.
[32] Nygaard, P. In *Metabolism of Nucleotides, Nucleosides, and Nucleobases in Microorganisms*; Munch-Petersen, A. Ed.; Academic Press: London, **1983**; pp. 27-93.
[33] Hurley, M.C.; Lin, B.; Fox, I.H. Regulation of deoxyadenosine and nucleoside analog phosphorylation by human placental adenosine kinase. *J. Biol. Chem.*, **1985**, *260*(29), 15675-15681.
[34] Schnebli, H.P.; Hill, D.L.; Bennett, L.L. Jr. Purification and properties of adenosine kinase from human tumor cells of type H. Ep. No. 2. *J. Biol. Chem.*, **1967**, *242*(9), 1997-2004.
[35] Miller, R.L.; Adamczyk, D.L.; Miller, W.H.; Koszalka, G.W.; Rideout, J.L.; Beacham, L.M. 3rd; Chao, E.Y.; Haggerty, J.J.; Krenitsky, T.A.; Elion, G.B. Adenosine kinase from rabbit liver. II. Substrate and inhibitor specificity. *J. Biol. Chem.*, **1979**, *254*(7), 2346-2352.
[36] Long, M.C.; Shaddix, S.C.; Moukha-Chafiq, O.; Maddry, J.A.; Nagy, L.; Parker, W.B. Structure-activity relationship for adenosine kinase from *Mycobacterium tuberculosis* II. Modifications to the ribofuranosyl moiety. *Biochem. Pharmacol.*, **2008**, *75*(8), 1588-1600.
[37] Spychala, J.; Datta, N.S.; Takabayashi, K.; Datta, M.; Fox, I.H.; Gribbin, T.; Mitchell, B.S. Cloning of human adenosine kinase cDNA: sequence similarity to microbial ribokinases and fructokinases. *Proc. Natl. Acad. Sci. USA*, **1996**, *93*(3), 1232-1237.
[38] Orme, I. Search for new drugs for treatment of tuberculosis. *Antimicrob. Agents Chemother.*, **2001**, *45*(7), 1943-1946.
[39] Barrow, E.W.; Westbrook, L.; Bansal, N.; Suling, W.J.; Maddry, J.A.; Parker, W.B.; Barrow, W.W. Antimycobacterial activity of 2-methyladenosine. *J. Antimicrob. Chemother.*, **2003**, *52*(5), 801-808.
[40] Park. J.; Gupta, R.S. Adenosine kinase and ribokinase - the RK family of proteins. *Cell. Mol. Life Sci.*, **2008**, *65*(18), 2875-2896.
[41] Andersson, C.E.; Mowbray, S.L. Activation of ribokinase by monovalent cations. *J. Mol. Biol.*, **2002**, *315*(3), 409-419.
[42] Reddy, M.C.; Palaninathan, S.K.; Shetty, N.D.; Owen, J.L.; Watson, M.D.; Sacchettini, J.C. High resolution crystal structures of *Mycobacterium tuberculosis* adenosine kinase: insights into the mechanism and specificity of this novel prokaryotic enzyme. *J. Biol. Chem.*, **2007**, *282*(37), 27334-27342.
[43] Wang, Y.; Long, M.C.; Ranganathan, S.; Escuyer, V.; Parker, W.B.; Li, R. Overexpression, purification and crystallographic analysis of a unique adenosine kinase from *Mycobacterium tuberculosis*. *Acta Crystallogr. Sect. F Struct. Biol. Cryst. Commun.*, **2005**, *61*(Pt 6), 553-557.
[44] Mathews, I.I.; Erion, M.D.; Ealick, S.E. Structure of human adenosine kinase at 1.5 Å resolution. *Biochemistry*, **1998**, *37*(45), 15607-15620.
[45] Andres, C.M.; Fox, I.H. Purification and properties of human placental adenosine kinase. *J. Biol. Chem.*, **1979**, *254*(22), 11388-11393.
[46] Yamada, Y.; Goto, H.; Ogasawara, N. Adenosine kinase from human liver. *Biochim. Biophys. Acta*, **1981**, *660*(1), 36-43.
[47] Palella, T.D.; Andres, C.M.; Fox, I.H. Human placental adenosine kinase. Kinetic mechanism and inhibition. *J. Biol. Chem.*, **1980**, *255*(11), 5264-5269.
[48] Park, J.; Singh, B.; Gupta, R.S. Mycobacterial adenosine kinase is not a typical adenosine kinase. *FEBS Lett.*, **2009**, *583*(13), 2231-2236.
[49] Bianchi, V.; Pontis, E.; Reichard, P. Interrelations between substrate cycles and *de novo* synthesis of pyrimidine deoxyribonucleoside triphosphates in 3T6 cells. *Proc. Natl. Acad. Sci. USA*, **1986**, *83*(4), 986-990.
[50] Zimmermann, H. 5'-Nucleotidase: molecular structure and functional aspects. *Biochem. J.*, **1992**, *285*(Pt 2), 345-365.
[51] Uchino, K.; Matsuo, T.; Iwamoto, M.; Tonosaki, Y.; Fukuchi, A. New 5'-nucleotidase inhibitors, NPF-86IA, NPF-86IB, NPF-86IIA, and NPF-86IIB from *Areca catechu*; Part I. Isolation and biological properties. *Planta Med.*, **1988**, *54*(5), 419-422.
[52] Iwamoto, M.; Matsuo, T.; Uchino, K.; Tonosaki, Y.; Fukuchi, A. New 5'-nucleotidase inhibitors, NPF-86IA, NPF-86IB, NPF-86IIA, and NPF-86IIB from *Areca catechu*; Part II. Anti-tumor effects. *Planta Med.*, **1988**, *54*(5), 422-425.
[53] Toukairin, T.; Uchino, K.; Iwamoto, M.; Murakami, S.; Tatebayashi, T.; Ogawara, H.; Tonosaki, Y. New polyphenolic 5'-nucleotidase inhibitors isolated from the wine grape "Koshu" and their biological effects. *Chem. Pharm. Bull. (Tokyo)*, **1991**, *39*(6), 1480-1483.
[54] Ozturk, D.H.; Dorfman, R.H.; Scapin, G.; Sacchettini, J.C.; Grubmeyer, C. Locations and functional roles of conserved lysine residues in *Salmonella typhimurium* orotate phosphoribosyltransferase. *Biochemistry*, **1995**, *34*(34), 10755-10763.
[55] Sinha, S.C.; Smith, J.L. The PRT protein family. *Curr. Opin. Struct. Biol.*, **2001**, *11*(6), 733-739.
[56] Henriksen, A.; Aghajari, N.; Jensen, K.F.; Gadjede, M. A flexible loop at the dimer interface is a part of the active site of the adjacent monomer of *Escherichia coli* orotate phosphoribosyltransferase. *Biochemistry*, **1996**, *35*(12), 3803-3809.
[57] Wang, G.P.; Lundegaard, C.; Jensen, K.F.; Grubmeyer, C. Kinetic mechanism of OMP synthase: a slow physical step following group transfer limits catalytic rate. *Biochemistry*, **1999**, *38*(1), 275-283.
[58] Wang, G.P.; Cahill, S.M.; Liu, X.; Girvin, M.E.; Grubmeyer, C. Motional dynamics of the catalytic loop in OMP synthase. *Biochemistry*, **1999**, *38*(1), 284-295.
[59] Schumacher, M.A.; Carter, D.; Ross, D.S.; Ullman, B.; Brennan, R.G. Crystal structures of *Toxoplasma gondii* HGXPRTase reveal the catalytic role of a long flexible loop. *Nat. Struct. Biol.*, **1996**, *3*(10), 881-887.
[60] Smith, J.L. Forming and inhibiting PRT active sites. *Nat. Struct. Biol.*, **1999**, *6*(6), 502-504.
[61] Bhatia, M.B.; Grubmeyer, C. The role of divalent magnesium in activating the reaction catalyzed by orotate phosphoribosyltransferase. *Arch. Biochem. Biophys.*, **1993**, *303*(2), 321-325.
[62] Krahn, J.M.; Kim, J.H.; Burns, M.R.; Parry, R.J.; Zalkin, H.; Smith, J.L.

Coupled formation of an amidotransferase interdomain ammonia channel and a phosphoribosyltransferase active site. *Biochemistry*, **1997**, *36*(37), 11061-11068.

[63] Shi, W.; Li, C.M.; Tyler, P.C.; Furneaux, R.H.; Grubmeyer, C.; Schramm, V.L.; Almo, S.C. The 2.0 Å structure of human hypoxanthine-guanine phosphoribosyltransferase in complex with transition-state analog inhibitor. *Nat. Struct. Biol.*, **1999**, *6*(6), 588-593.

[64] Shi, W.; Li, C.M.; Tyler, P.C.; Furneaux, R.H.; Cahill, S.M.; Girvin, M.E.; Grubmeyer, C.; Schramm, V.L.; Almo, S.C. The 2.0 Å structure of malarial purine phosphoribosyltransferase in complex with transition-state analog inhibitor. *Biochemistry*, **1999**, *38*(31), 9872-9880.

[65] Keough, D.T.; Hocková, D.; Holý, A.; Naesens, L.M.; Skinner-Adams, T.S.; Jersey, J.; Guddat, L.W. Inhibition of hypoxanthine-guanine phosphoribosyltransferase by acyclic nucleoside phosphonates: a new class of antimalarial therapeutics. *J. Med. Chem.*, **2009**, *52*(14), 4391-4399.

[66] Keough, D.T.; Skinner-Adams, T.; Jones, M.K.; Ng, A.L.; Brereton, I.M.; Guddat, L.W.; de Jersey, J. Lead compounds for antimalarial chemotherapy: purine base analogs discriminate between human and *P. falciparum* 6-oxopurine phosphoribosyltransferase. *J. Med. Chem.*, **2006**, *49*(25), 7479-7486.

[67] Keough, D.T.; Ng, A.L.; Winzor, D.J.; Emmerson, B.T.; de Jersey, J. Purification and characterization of *Plasmodium falciparum* hypoxanthine-guanine-xanthine phosphoribosyltransferase and comparison with the human enzyme. *Mol. Biochem. Parasitol.*, **1999**, *98*(1), 29-41.

[68] Thompson, J.D.; Higgins, D.G.; Gibson, T.J. CLUSTAL W: improving the sensitivity of progressive multiple sequence alignment through sequence weighting, position-specific gap penalties and weight matrix choice. *Nucleic Acids Res.*, **1994**, *22*(22), 4673-4680.

[69] Xu, Y.; Eads, J.; Sacchettini, J.C.; Grubmeyer, C. Kinetic mechanism of human hypoxanthine-guanine phosphoribosyltyransferase: rapid phosphoribosyl transfer chemistry. *Biochemistry*, **1997**, *36*(12), 3700-3712.

[70] Bashor, C.; Denu, J.M.; Brennan, R.G.; Ullman, B. Kinetic mechanism of adenine phosphoribosyltransferase from *Leishmania donovani*. *Biochemistry*, **2002**, *41*(12), 4020-4031.

[71] Phillips, C.L.; Ullman, B.; Brennan, R.G.; Hill, C.P. Crystal structure of adenine phosphoribosyltransferase from *Leishmania donovani*. *EMBO J.*, **1999**, *18*(13), 3533-3545.

[72] Shi, W.; Sarver, A.E.; Wang, C.C.; Tanaka, K.S.E.; Almo, S.C.; Schramm, V.L. Closed site complexes of adenine phosphoribosyltransferase from *Giardia lamblia* reveal a mechanism of ribosyl migration. *J. Biol. Chem.*, **2002**, *277*(42), 39981-39988.

[73] Shi, W.; Tanaka, K.S.E.; Crother, T.R.; Taylor, M.W.; Almo, S.C.; Schramm, V.L. Structural analysis of adenine phosphoribosyltransferase from *Saccharomyces cerevisiae*. *Biochemistry*, **2001**, *40*(36), 10800-10809.

[74] Silva, M.; Silva, C.H.; Iulek, J.; Thiemann, O.H. Three-dimensional structure of human adenine phosphoribosyltransferase and its relation to DHA-urolithiasis. *Biochemistry*, **2004**, *43*(24), 7663-7671.

[75] Boitz, J.M.; Ullman, B. Amplification of adenine phosphoribosyltransferase suppresses the conditionally lethal growth and virulence phenotype of *Leishmania donovani* mutants lacking both hypoxanthine-guanine and xanthine phosphoribosyltransferase. *J. Biol. Chem.*, **2010**, e-pub, Manuscript M110.125393, April 2.

[76] Mascia, L.; Cappiello, M.; Cherri, S.; Ipata, P.L. *In vitro* recycling of α-D-ribose-1-phosphate for the salvage of purine bases. *Biochim. Biophys. Acta*, **2000**, *1474*(1), 70-74.

[77] Porter, D.J. Purine nucleoside phosphorylase. Kinetic mechanism of the enzyme from calf spleen. *J. Biol. Chem.*, **1992**, *267*(11), 7342-7351.

[78] Kalckar, H.M. Differential spectrophotometry of purine compounds by means of specific enzymes: I. Determination of hydroxypurine compounds. *J. Biol. Chem.*, **1947**, *167*(2), 429-443.

[79] Bzowska, A.; Kulikowska, E.; Shugar, D. Purine nucleoside phosphorylases: properties, functions, and clinical aspects. *Pharmacol. Ther.*, **2000**, *88*(3), 349-425.

[80] Zimmerman, T.P.; Gersten, N.B.; Ross, A.F.; Miech, R.P. Adenine as substrate for purine nucleoside phosphorylase. *Can. J. Biochem.*, **1971**, *49*(9), 1050-1054.

[81] Stoecker, J.D.; Poirot, A.F.; Smith, R.M.; Parks, R.E. Jr.; Ealick, S.E.; Takabayashi, K.; Erion, M.D. Purine nucleoside phosphorylase. 3. Reversal of purine base specificity by site-directed mutagenesis. *Biochemistry*, **1997**, *36*(39), 11749-11756.

[82] Basso, L.A.; Santos, D.S.; Shi, W.; Furneaux, R.H.; Tyler, P.C.; Schramm, V.L.; Blanchard, J.S. Purine nucleoside phosphorylase from *Mycobacterium tuberculosis*. Analysis of inhibition by a transition-state analogue and dissection by parts. *Biochemistry*, **2001**, *40*(28), 8196-8203.

[83] Jensen, K.F.; Nygaard, P. Purine nucleoside phosphorylase from *Escherichia coli* and *Salmonella typhimurium*. Purification and some properties. *Eur. J. Biochem.*, **1975**, *51*(1), 253-265.

[84] Jensen, K.F. Two purine nucleoside phosphorylases in *Bacillus subtilis*. Purification and some properties of the adenosine-specific phosphorylase. *Biochim. Biophys. Acta*, **1978**, *525*(2), 346-356.

[85] Shi, W.; Basso, L.A.; Santos, D.S.; Tyler, P.C.; Furneaux, R.H.; Blanchard, J.S.; Almo, S.C.; Schramm, V.L. Structures of purine nucleoside phosphorylase from *Mycobacterium tuberculosis* in complexes with Immucillin-H and its pieces. *Biochemistry*, **2001,** *40*(28), 8204-8215.

[86] Sauve, A.A.; Cahill, S.M.; Zech, S.G.; Basso, L.A.; Lewandowicz, A.; Santos, D.S.; Grubmeyer, C.; Evans, G.B.; Furneaux, R.H.; Tyler, P.C.; McDermott, A.; Girvin, M.E.; Schramm, V.L. Ionic states of substrates and transition state analogues at the catalytic sites of *N*-Ribosyltransferases. *Biochemistry*, **2003,** *42*(19), 5694-5705.

[87] Lewandowicz, A.; Shi, W.; Evans, G.B.; Tyler, P.C.; Furneaux, R.H.; Basso, L.A.; Santos, D.S.; Almo, S.C.; Schramm, V.L. Over-the-barrier transition state analogues and crystal structure with *Mycobacterium tuberculosis* purine nucleoside phosphorylase. *Biochemistry*, **2003,** *42*(20), 6057-6066.

[88] Nolasco, D.O.; Canduri, F.; Pereira, J.H.; Cortinóz, J.R.; Palma, M.S.; Oliveira, J.S.; Basso, L.A.; de Azevedo W.F. Jr.; Santos, D.S. Crystallographic structure of PNP from *Mycobacterium tuberculosis* at 1.9 Å resolution. *Biochem. Biophys. Res. Commun.*, **2004**, *324*(2), 789-794.

[89] Timmers, L.F.; Caceres, R.A.; Vivan, A.L.; Gava, L.M.; Dias, R.; Ducati, R.G.; Basso, L.A.; Santos, D.S.; de Azevedo, W.F. Jr. Structural studies of human purine nucleoside phosphorylase: towards a new specific empirical scoring function. *Arch. Biochem. Biophys.*, **2008**, *479*(1), 28-38.

[90] Caceres, R.A.; Timmers, L.F.; Pauli, I.; Gava, L.M.; Ducati, R.G.; Basso, L.A.; Santos, D.S.; de Azevedo, W.F. Jr. Crystal structure and molecular dynamics studies of human purine nucleoside phosphorylase complexed with 7-deazaguanine. *J. Struct. Biol.*, **2010**, *169*(3), 379-388.

[91] Ducati, R.G.; Basso, L.A.; Santos, D.S.; de Azevedo, W.F. Jr. Crystallographic and docking studies of purine nucleoside phosphorylase from *Mycobacterium tuberculosis*. *Bioorg. Med. Chem.*, **2010**, *18*(13), 4769-4774.

[92] de Azevedo, W.F.Jr.; Canduri, F.; dos Santos, D.M.; Silva, R.G.; de Oliveira, J.S.; de Carvalho, L.P.; Basso, L.A.; Mendes, M.A.; Palma, M.S.; Santos, D.S. Crystal structure of human purine nucleoside phosphorylase at 2.3 Å resolution. *Biochem. Biophys. Res. Commun.*, **2003**, *308*(3), 545-552.

[93] de Azevedo, W.F.Jr.; Canduri, F.; Marangoni dos Santos, D.; Pereira, J.H.; Dias, M.V.; Silva, R.G.; Mendes, M.A.; Basso, L.A.; Palma, M.S.; Santos, D.S. Structural basis for inhibition of human PNP by immucillin-H. *Biochem. Biophys. Res. Commun.*, **2003**, *309*(4), 917-922.

[94] de Azevedo, W.F.Jr.; dos Santos, G.C.; dos Santos, D.M.; Olivieri, J.R.; Canduri, F.; Silva, R.G.; Basso, L.A.; Renard, G.; da Fonseca, I.O.; Mendes, M.A.; Palma, M.S.; Santos, D.S. Docking and small angle X-ray scattering studies of purine nucleoside phosphorylase. *Biochem. Biophys. Res. Commun.*, **2003**, *309*(4), 923-928.

[95] de Azevedo, W.F.Jr.; Canduri, F.; dos Santos, D.M.; Pereira, J.H.; Bertacine Dias, M.V.; Silva, R.G.; Mendes, M.A.; Basso, L.A.; Palma, M.S.; Santos, D.S. Crystal structure of human PNP complexed with guanine. *Biochem. Biophys. Res. Commun.*, **2003**, *312*(3), 767-772.

[96] Canduri, F.; dos Santos, D.M.; Silva, R.G.; Mendes, M.A.; Basso, L.A.; Palma, M.S.; de Azevedo, W.F.; Santos, D.S. Structures of human purine nucleoside phosphorylase complexed with inosine and ddI. *Biochem. Biophys. Res. Commun*., **2004**, *313*(4), 907-914.

[97] Canduri, F.; Fadel, V.; Dias, M.V.; Basso, L.A.; Palma, M.S.; Santos, D.S.; de Azevedo, W.F. Jr. Crystal structure of human PNP complexed with hypoxanthine and sulfate ion. *Biochem. Biophys. Res. Commun.*, **2005**, *326*(2), 335-338.

[98] Canduri, F.; Fadel, V.; Basso, L.A.; Palma, M.S.; Santos, D.S.; de Azevedo, W.F. Jr. New catalytic mechanism for human purine nucleoside phosphorylase. *Biochem. Biophys. Res. Commun.*, **2005**, *327*(3), 646-649.

[99] dos Santos, D.M.; Canduri, F.; Pereira, J.H.; Vinicius Bertanice Dias, M.; Silva, R.G.; Mendes, M.A.; Palma, M.S.; Basso, L.A.; de Azevedo, W.F. Jr.; Santos, D.S. Crystal structure of human purine nucleoside phosphorylase complexed with acyclovir. *Biochem. Biophys. Res. Commun.*, **2003**, *308*(3), 553-559.

[100] Silva, R.G.; Pereira, J.H.; Canduri, F.; de Azevedo, W.F. Jr.; Basso, L.A.; Santos, D.S. Kinetics and crystal structure of human purine nucleoside phosphorylase in complex with 7-methyl-6-thio-guanosine. *Arch. Biochem. Biophys.*, **2005**, *442*(1), 49-58.

[101] Taylor Ringia, E.A.; Tyler, P.C.; Evans, G.B.; Furneaux, R.H.; Murkin, A.S.; Schramm, V.L. Transition state analogue discrimination by related purine nucleoside phosphorylases. *J. Am. Chem. Soc.*, **2006**, *128*(22), 7126-7127.

[102] Ducati, R.G.; Santos, D.S.; Basso, L.A. Substrate specificity and kinetic mechanism of purine nuceloside phosphorylase from *Mycobaterium tuberculosis*. *Arch. Biochem. Biophys.*, **2009**, *486*(2), 155-164.

[103] Kulikowska, E.; Bzowska, A.; Wierzchowski, J.; Shugar, D. Properties of two unusual, and fluorescent, substrates of purine-nucleoside phosphorylase: 7-methylguanosine and 7-methylinosine. *Biochim. Biophys. Acta*, **1986**, *874*(3), 355-363.

[104] Mitchell, B.S.; Mejias, E.; Daddona, P.E.; Kelley, W.N. Purinergic immunodeficiency diseases: selective toxicity of deoxyribonucleosides for T cells. *Proc. Natl. Acad. Sci. USA*, **1978**, *75*(10), 5011-5014.

[105] Thelander, L.; Reichard, P. Reduction of ribonucleotides. *Annu. Rev. Biochem.*, **1979**, *48*, 133-158.

[106] Versées, W.; Steyaert, J. Catalysis by nucleoside hydrolases. *Curr. Opin. Struct. Biol.*, **2003**, *13*(6), 731-738.

[107] Takagi, Y.; Horecker, B.L. Purification and properties of a bacterial riboside hydrolase. *J. Biol. Chem.*, **1957**, *225*(1), 77-86.

[108] Terada, M.; Tatibana, M.; Hayaishi, O. Purification and properties of nucleoside hydrolase from *Pseudomonas fluorescens*. *J. Biol. Chem.*, **1967**, *242*(23), 5578-5585.

[109] Petersen, C.; Møller, L.B. The RihA, RihB, and RihC ribonucleoside hydrolases of *Escherichia coli*. *J. Biol. Chem.*, **2001**, *276*(2), 884-894.

[110] Estupiñán, B.; Schramm, V.L. Guanosine-inosine-preferring nucleoside *N*-

glycohydrolase from *Crithidia fasciculata*. *J. Biol. Chem.*, **1994**, *269*(37), 23068-23073.

[111] Parkin, D.W.; Horenstein, B.A.; Abdulah, D.R.; Estupiñán, B.; Schramm, V.L. Nucleoside hydrolase from *Crithidia fasciculata*. Metabolic role, purification, specificity, and kinetic mechanism. *J. Biol. Chem.*, **1991**, *266*(31), 20658-20665.

[112] Gopaul, D.N.; Meyer, S.L.; Degano, M.; Sacchettini, J.C.; Schramm, V.L. Inosine-uridine nucleoside hydrolase from *Crithidia fasciculata*. Genetic characterization, crystallization, and identification of histidine 241 as a catalytic site residue. *Biochemistry*, **1996**, *35*(19), 5963-5970.

[113] Pellé, R.; Schramm, V.L.; Parkin, D.W. Molecular cloning and expression of a purine-specific *N*-ribohydrolase from *Trypanosoma brucei brucei*. Sequence, expression, and molecular analysis. *J. Biol. Chem.*, **1998**, *273*(4), 2118-2126.

[114] Shi, W.; Schramm, V.L.; Almo, S.C. Nucleoside hydrolase from *Leishmania major*. Cloning, expression, catalytic properties, transition state inhibitors, and the 2.5 Å crystal structure. *J. Biol. Chem.*, **1999**, *274*(30), 21114-21120.

[115] Magni, G.; Fioretti, E.; Ipata, P.L.; Natalini, P. Bakers' yeast uridine nucleosidase. Purification, composition, and physical and enzymic properties. *J. Biol. Chem.*, **1975**, *250*, 9-13.

[116] Versées, W.; Decanniere, K.; Pellé, R.; Depoorter, J.; Brosens, E.; Parkin, D.W.; Steyaert, J. Structure and function of a novel purine specific nucleoside hydrolase from *Trypanosoma vivax*. *J. Mol. Biol.*, **2001**, *307*(5), 1363-1379.

[117] Hunt, C.; Gillani, N.; Farone, A.; Rezaei, M.; Kline, P.C. Kinetic isotope effects of nucleoside hydrolase from *Escherichia coli*. *Biochim. Biophys. Acta*, **2005**, *1751*(2), 140-149.

[118] Horenstein, B.A.; Parkin, D.W.; Estupiñán, B.; Schramm, V.L. Transition-state analysis of nucleoside hydrolase from *Crithidia fasciculate*. *Biochemistry*, **1991**, *30*(44), 10788-10795.

[119] Shu, Q.; Nair, V. Inosine monophosphate dehydrogenase (IMPDH) as a target in drug discovery. *Med. Res. Rev.*, **2008**, *28*(2), 219-232.

[120] Kerr, K.M.; Cahoon, M.; Bosco, D.A.; Hedstrom, L. Monovalent cation activation in *Escherichia coli* inosine 5'-monophosphate dehydrogenase. *Arch. Biochem. Biophys.*, **2000**, *375*(1), 131-137.

[121] Xiang, B.; Taylor, J.C.; Markham, G.D. Monovalent cation activation and kinetic mechanism of inosine 5'-monophosphate dehydrogenase. *J. Biol. Chem.*, **1996**, *271*(3), 1435-1440.

[122] Sintchak, M.D.; Nimmesgern, E. The structure of inosine 5'-monophosphate dehydrogenase and the design of novel inhibitors. *Immunopharmacology*, **2000**, *47*(2-3), 163-184.

[123] Rosenkrands, I.; King, A.; Weldingh, K.; Moniatte, M.; Moertz, E.; Andersen, P. Towards the proteome of *Mycobacterium tuberculosis*. *Electrophoresis*, **2000**, *21*(17), 3740-3756.

[124] Zimmermann, A.; Gu, J.J.; Spychala, J.; Mitchell, B.S. Inosine monophosphate dehydrogenase expression: transcriptional regulation of the type I and type II genes. *Adv. Enzyme Regul.*, **1996**, *36*, 75-84.

[125] Wang, W.; Hedstrom, L. Kinetic mechanism of human inosine 5'-monophosphate dehydrogenase type II: random addition of substrates and ordered release of products. *Biochemistry*, **1997**, *36*(28), 8479-8483.

[126] Natsumeda, Y.; Ohno, S.; Kawasaki, H.; Konno, Y.; Weber, G.; Suzuki, K. Two distinct cDNAs for human IMP dehydrogenase. *J. Biol. Chem.*, **1990**, *265*(9), 5292-5295.

[127] Riera, T.V.; Wang, W.; Josephine, H.R.; Hedstrom, L. A kinetic alignment of orthologous inosine 5'-monophosphate dehydrogenase. *Biochemistry*, **2008**, *47*(33), 8689-8696.

[128] Prosise, G.L.; Luecke, H. Crystal structures of *Tritrichomonas foetus* inosine monophosphate dehydrogenase in complex with substrate cofactor and analogs: a structural basis for the random-in ordered-out kinetic mechanism. *J. Mol. Biol.*, **2003**, *326*(2), 517-527.

[129] Umejiego, N.N.; Li, C.; Riera, T.; Hedstrom, L; Striepen, B. *Cryptosporidium parvum* IMP dehydrogenase: identification of functional, structural, and dynamic properties that can be exploited for drug design. *J. Biol. Chem.*, **2004**, *279*(39), 40320-40327.

[130] Watterson, S.H.; Carlsen, M.; Dhar, T.G.; Shen, Z.; Pitts, W.J.; Guo, J.; Gu, H.H.; Norris, D.; Chorba, J.; Chen, P.; Cheney, D.; Witmer, M.; Fleener, C.A.; Rouleau, K.; Townsend, R.; Hollenbaugh, D.L.; Iwanowicz, E.J. Novel inhibitors of IMPDH: a highly potent and selective quinolone-based series. *Bioorg. Med. Chem. Lett.*, **2003**, *13*(3), 543-546.

[131] Takebe, N.; Cheng, X.; Wu, S.; Bauer, K.; Goloubeva, O.G.; Fenton, R.G.; Heyman, M.; Rapoport, A.P.; Badros, A.; Shaughnessy, J.; Ross, D.; Meisenberg, B.; Tricot, G. Phase I clinical trial of the inosine monophosphate dehydrogenase inhibitor mycophenolate mofetil (Cellcept) in advanced multiple myeloma patients. *Clin. Cancer Res.*, **2004**, *10*(24), 8301-8308.

[132] Iwanowicz, E.J.; Watterson, S.H.; Liu, C.; Gu, H.H.; Mitt, T.; Leftheris, K.; Barrish, J.C.; Fleener, C.A.; Rouleau, K.; Sherbina, N.Z.; Hollenbaugh, D.L. Novel guanidine-based inhibitors of inosine monophosphate dehydrogenase. *Bioorg. Med. Chem. Lett.*, **2002**, *12*(20), 2931-2934.

[133] Köhler, G.A.; Gong, X.; Bentink, S.; Theiss, S.; Pagani, G.M.; Agabian, N.; Hedstrom, L. The functional basis of mycophenolic acid resistance in *Candida albicans* IMP dehydrogenase. *J. Biol. Chem.*, **2005**, *280*(12), 11295-11302.

[134] Ji, Y.; Gu, J.; Makhov, A.M.; Griffith, J.D.; Mitchell, B.S. Regulation of the interaction of inosine monophosphate dehydrogenase with mycophenolic acid by GTP. *J. Biol. Chem.*, **2006**, *281*(1), 206-212.

[135] Borroto-Esoda, K.; Myrick, F.; Feng, J.; Jeffrey, J.; Phillip Furman, P. *In vitro* combination of amdoxovir and the inosine monophosphate dehydrogenase inhibitors mycophenolic acid and ribavirin demonstrates potent activity against wild-type and drug-resistant variants of human immunodeficiency virus type 1. *Antimicrob. Agents Chemother.*, **2004**, *48*(11), 4387-4394.

[136] Ignoul, S.; Eggermont, J. CBS domains: structure, function, and pathology in human proteins. *Am. J. Physiol. Cell. Physiol.*, **2005**, *289*(6), C1369-C1378.

[137] Pimkin, M.; Markham, G.D. The CBS subdomain of inosine 5'-monophosphate dehydrogenase regulates purine nucleotide turnover. *Mol. Microbiol.*, **2008**, *68*(2), 342-359.

[138] Sagot, I.; Schaeffer, J.; Daignan-Fornier, B. Guanylic nucleotide starvation affects *Saccharomyces cerevisiae* mother-daughter separation and may be a signal for entry into quiescence. *BMC Cell Biol.*, **2005**, *6*(1), 24-36.

[139] Zhang, X.H.; He, K.W.; Duan, Z.T.; Zhou, J.M.; Yu, Z.Y.; Ni, Y.X.; Lu, C.P. Identification and characterization of inosine 5-monophosphate dehydrogenase in *Streptococcus suis* type 2. *Microb. Pathog.*, **2009**, *47*(5), 267-273.

[140] Prosise, G.L.; Wu, J.Z.; Luecke, H. Crystal structure of *Tritrichomonas foetus* inosine monophosphate dehydrogenase in complex with the inhibitor ribavirin monophosphate reveals a catalysis-dependent ion-binding site. *J. Biol. Chem.*, **2002**, *277*(52), 50654-50659.

[141] Colby, T.D.; Vanderveen, K.; Strickler, M.D.; Markham, G.D.; Goldstein, B.M. Crystal structure of human type II inosine monophosphate dehydrogenase: implications for ligand binding and drug design. *Proc. Natl. Acad. Sci. USA*, **1999**, *96*(7), 3531-3536.

[142] Stayton, M.M.; Rudolph, F.B.; Fromm, H.J. Regulation, genetics, and properties of adenylosuccinate synthetase: a review. *Curr. Top. Cell. Regul.*, **1983**, *22*, 103-141.

[143] Honzatko, R.B.; Fromm, H.J. Structure-function studies of adenylosuccinate synthetase from *Escherichia coli*. *Arch. Biochem. Biophys.*, **1999**, *370*(1), 1-8.

[144] Lowenstein, J.M. Ammonia production in muscle and other tissues: the purine nucleotide cycle. *Physiol. Rev.*, **1972**, *52*(2), 382-414.

[145] Borza, T.; Iancu, C.V.; Pike, E.; Honzatko, R.B.; Fromm, H. J. Variations in the response of mouse isozymes of adenylosuccinate synthetase to inhibitors of physiological relevance. *J. Biol. Chem.*, **2003**, *278*(9), 6673-6679.

[146] Hou, Z.; Wang, W.; Fromm, H.J.; Honzatko, R.B. IMP alone organizes the active site of adenylosuccinate synthetase from *Escherichia coli*. *J. Biol. Chem.*, **2002**, *277*(8), 5970-5976.

[147] Wang, W.; Gorrell, A.; Honzatko, R.B.; Fromm, H.J. A study of *Escherichia coli* adenylosuccinate synthetase association states and the interface residues of the homodimer. *J Biol Chem.*, **1997**, *272*(11), 7078-7084.

[148] Honzatko, R.B.; Stayton, M.M.; Fromm, H.J. Adenylosuccinate synthetase: recent developments. *Adv. Enzymol. Relat. Areas Mol. Biol.*, **1999**, *73*, 57-102.

[149] Poland, B.W.; Fromm, H.J.; Honzatko, R.B. Crystal structures of adenylosuccinate synthetase from *Escherichia coli* complexed with GDP, IMP hadacidin, NO^{3-}, and Mg^{2+}. *J. Mol. Biol.*, **1996**, *264*(5), 1013-1027.

[150] Poland, B.W.; Bruns, C.; Fromm, H.J.; Honzatko, R.B. Entrapment of 6-thiophosphoryl-IMP in the active site of crystalline adenylosuccinate synthetase from *Escherichia coli*. *J. Biol. Chem.*, **1997**, *272*(24), 15200-15205.

[151] Choe, J.Y.; Poland, B.W.; Fromm, H.J.; Honzatko, R.B. Mechanistic implications from crystalline complexes of wild-type and mutant adenylosuccinate synthetases from *Escherichia coli*. *Biochemistry*, **1999**, *38*(21), 6953-6961.

[152] Iancu, C.V.; Borza, T.; Fromm, H.J.; Honzatko, R.B. IMP, GTP, and 6-phosphoryl-IMP complexes of recombinant mouse muscle adenylosuccinate synthetase. *J. Biol. Chem.*, **2002**, *277*(30), 26779-26787.

[153] Bulusu, V.; Srinivasan, B.; Bopanna, M.P.; Balaram, H. Elucidation of the substrate specificity, kinetic and catalytic mechanism of adenylosuccinate lyase from *Plasmodium falciparum*. *Biochim. Biophys. Acta*, **2009**, *1794*(4), 642-654.

[154] Spiegel, E.K.; Colman, R.F.; Patterson, D. Adenylosuccinate lyase deficiency. *Mol. Genet. Metab.*, **2006**, *89*(1-2), 19-31.

[155] Van den Berghe, G.; Vincent, M.F.; Jaeken, J. Inborn errors of the purine nucleotide cycle: adenylosuccinase deficiency. *J. Inher. Metab. Dis.*, **1997**, *20*(2), 193-202.

[156] Toth, E.A.; Yeates, T.O. The structure of adenylosuccinate lyase, an enzyme with dual activity in the *de novo* purine biosynthetic pathway. *Structure*, **2000**, *8*(2), 163-174.

[157] Lee, T.T.; Worby, C.; Bao, Z.Q.; Dixon, J.E.; Colman, R.F. His68 and His141 are critical contributors to the intersubunit catalytic site of adenylosuccinate lyase of *Bacillus subtilis*. *Biochemistry*, **1999**, *38*(1), 22-32.

[158] Brosius, J.L.; Colman, R.F. A key role in catalysis for His89 of adenylosuccinate lyase of *Bacillus subtilis*. *Biochemistry*, **2000**, *39*(44), 13336-13343.

[159] Kmoch, S.; Hartmannová, H.; Stibůrková, B.; Krijt, J.; Zikánová, M.; Šebesta, I. Human adenylosuccinate lyase (ADSL), cloning and characterization of full-length cDNA and its isoforms, gene structure and molecular basis for ADSL deficiency in six patients. *Hum. Mol. Genet.*, **2000**, *9*(10), 1501-1513.

[160] Zikanova, M.; Skopova, V.; Hnizda, A.; Krijt, J.; Kmoch, S. Biochemical and structural analysis of 14 mutant ADSL enzyme complexes and correlation to phenotypic heterogeneity of adenylosuccinate lyase deficiency. *Hum. Mutat.*, **2010**, *31*(4), 445-455.

[161] Brosius, J.L.; Colman, R.F. Three subunits contribute amino acids to the active site of tetrameric adenylosuccinate lyase: Lys268 and Glu275 are re-

quired. *Biochemistry*, **2002**, *41*(7), 2217-2226.
[162] Sivendran, S.; Segall, M.L.; Rancy, P.C.; Colman, R.F. Effect of Asp69 and Arg310 on the pK of His68, a key catalytic residue of adenylosuccinate lyase. *Protein Sci.*, **2007**, *16*(8), 1700-1707.
[163] Stone, R.L.; Zalkin, H.; Dixon, J.E. Expression, purification, and kinetic characterization of recombinant human adenylosuccinate lyase. *J. Biol. Chem.*, **1993**, *268*(26), 19710-19716.
[164] Bridger, W.A.; Cohen, L.H. The kinetics of adenylosuccinate lyase. *J. Biol. Chem.*, **1968**, *243*(6), 644-650.
[165] Tsai, M.; Koo, J.; Yip, P.; Colman, R.F.; Segall, M.L.; Howell, P.L. Substrate and product complexes of *Escherichia coli* adenylosuccinate lyase provide new insights into enzymatic mechanism. *J. Mol. Biol.*, **2007**, *370*(3), 541-554.
[166] Wheeler, P.R. Enzymes for purine synthesis and scavenging in pathogenic mycobacteria and their distribution in *Mycobaterium leprae*. *J. Gen. Microbiol.*, **1987**, *133*(11), 3013-3018.
[167] Meng, L.M.; Kilstrup, M.; Nygaard, P. Autoregulation of PurR repressor synthesis and involvement of *purR* in the regulation of *purB*, *purC*, *purL*, *purMN* and *guaBA* expression in *Escherichia coli*. *Eur. J. Biochem*., **1990**, *187*(2), 373-379.
[168] Wolfe, S.A.; Smith, J.M. Separate regulation of *purA* and *purB* loci of *Escherichia coli* K-12. *J. Bacteriol.*, **1985**, *162*(2), 822-825.
[169] He, B.; Smith, J.M.; Zalkin, H. *Escherichia coli purB* gene: cloning, nucleotide sequence, and regulation by *purR*. *J. Bacteriol.*, **1992**, *174*(1), 130-136.
[170] Gendron, N.; Breton, R.; Champagne, N.; Lapointe, J. Adenylosuccinate lyase of *Bacillus subtilis* regulates the activity of the glutamyl-tRNA synthetase. *Proc. Natl. Acad. Sci. USA*, **1992**, *89*(12), 5389-5392.
[171] Toth, E.A.; Worby, C.; Dixon, J.E.; Goedken, E.R.; Marqusee, S.; Yeates, T.O. The crystal structure of adenylosuccinate lyase from *Pyrobaculum aerophilum* reveals an intracellular protein with three disulfide bonds. *J. Mol. Biol.*, **2000**, *301*(2), 433-450.
[172] Redinbo, M.R.; Eide, S.M.; Stone, R.L.; Dixon, J.E.; Yeates, T.O. Crystallization and preliminary structural analysis of *Bacillus subtilis* adenylosuccinate lyase, an enzyme implicated in infantile autism. *Protein Sci.*, **1996**, *5*(4), 786-788.
[173] Spector, T.; Jones, T.E.; Elion, G.B. Specificity of adenylosuccinate synthetase and adenylosuccinate lyase from *Leishmania donovani*. Selective amination of an antiprotozoal agent. *J. Biol. Chem.*, **1979**, *254*(17), 8422-8426.
[174] Sivendran, S.; Colman, R.F. Effect of a new non-cleavable substrate analog on wild-type and serine mutants in the signature sequence of adenylosuccinate lyase of *Bacillus subtilis* and *Homo sapiens*. *Proteins Sci.*, **2008**, *17*(7), 1162-1174.
[175] Yan, H.; Tsai, M.D. Nucleoside monophosphate kinases: structure, mechanism, and substrate specificity. *Adv. Enzymol. Relat. Areas Mol. Biol.*, **1999**, *73*, 103-134.
[176] Prinz, H.; Lavie, A.; Scheidig, A.J.; Spangenberg, O.; Konrad, M. Binding of nucleotides to guanylate kinase, $p21^{ras}$, and nucleoside-diphosphate kinase studied by nano-electrospray mass spectrometry. *J. Biol. Chem.*, **1999**, *274*(50), 35337-35342.
[177] Boehme, R.E. Phosphorylation of the antiviral precursor 9-(1,3-dihydroxy-2-propoxymethyl)guanine monophosphate by guanylate kinase isozymes. *J. Biol. Chem.*, **1984**, *259*(20), 12346-12349.
[178] Miller, W.H.; Daluge, S.M.; Garvey, E.P.; Hopkins, S.; Reardon, J.E.; Boyd, F.L.; Miller, R.L. Phosphorylation of carbovir enantiomers by cellular enzymes determines the stereoselectivity of antiviral activity. *J. Biol. Chem.*, **1992**, *267*(29), 21220-21224.
[179] Miller, W.H.; Miller, R.L. Phosphorylation of acyclovir (acycloguanosine) monophosphate by GMP kinase. *J Biol Chem.*, **1980**, *255*(15), 7204-7207.
[180] Sekulic, N.; Shuvalova, L.; Spangenberg, O.; Konrad, M.; Lavie, A. Structural characterization of the closed conformation of mouse guanylate kinase. *J. Biol. Chem.*, **2002**, *277*(33), 30236-30243.
[181] Blaszczyk, J.; Li, Y.; Yan, H.; Ji, X. Crystal structure of unligated guanylate kinase from yeast reveals GMP-induced conformational changes. *J. Mol. Biol.*, **2001**, *307*(1), 247-257.
[182] Dreusike, D.; Schulz, G.E. The glycine-rich loop of adenylate kinase forms a giant anion hole. *FEBS Lett.*, **1986**, *208*(2), 301-304.
[183] Choi, B.; Zocchi, G. Guanylate kinase, induced fit, and the allosteric spring probe. *Biophys. J.*, **2007**, *92*(5), 1651-1658.
[184] Hible, G.; Christova, P.; Renault, L.; Seclaman, E.; Thompson, A.; Girard, E.; Munier-Lehmann, H.; Cherfils, J. Unique GMP-binding site in *Mycobacterium tuberculosis* guanosine monophosphate kinase. *Proteins*, **2006**, *62*(2), 489-500.
[185] Noda, L.H. In *The Enzymes*; Boyer, P.D. Ed.; Academic Press: New York, **1973**; Vol. *8*, pp. 279-305.
[186] Meena, L.S.; Chopra, P.; Bedwal, R.S.; Singh, Y. Nucleoside diphosphate kinase-like activity in adenylate kinase of *Mycobacterium tuberculosis*. *Biotechnol. Appl. Biochem.*, **2003**, *38*(Pt 2), 169-174.
[187] Munier-Lehmann, H.; Burlacu-Miron, S.; Craescu, C.T.; Mantsch, H.H.; Schultz, C.P. A new subfamily of short bacterial adenylate kinases with the *Mycobacterium tuberculosis* enzyme as a model: a predictive and experimental study. *Proteins*, **1999**, *36*(2), 238-248.
[188] Nakazawa, A.; Yamada, M.; Tanaka, H.; Shahjahan, M.; Tanabe, T. In *Isozymes: structure, function, and use in biology and medicine*; Wiley-Liss: New York, **1990**; pp. 495-514.
[189] Schulz, G.E.; Schiltz, E.; Tomasselli, A.G.; Frank, R.; Brune, M.; Wittinghofer, A.; Schirmer, R.H. Structural relationships in the adenylate kinase family. *Eur. J. Biochem.*, **1986**, *161*(1), 127-132.
[190] Bârzu, O.; Gilles, A.-M. In *Annals de l' Institut Pasteur lactualites*; Elsevier: Paris, **1993**; Vol. *4*, pp. 121-132.
[191] Tsai, M.D.; Yan, H. Mechanism of adenylate kinase: site-directed mutagenesis versus X-ray and NMR. *Biochemistry*, **1991**, *30*(28), 6806-6818.
[192] Bellinzoni, M.; Haouz, A.; Graña, M.; Munier-Lehmann, H.; Shepard, W.; Alzari, P.M. The crystal structure of *Mycobacterium tuberculosis* adenylate kinase in complex with two molecules of ADP and Mg^{2+} supports an associative mechanism for phosphoryl transfer. *Protein Sci.*, **2006**, *15*(6), 1489-1493.
[193] Miron, S.; Munier-Lehmann, H.; Craescu, C.T. Structural and dynamic studies on ligand-free adenylate kinase from *Mycobacterium tuberculosis* revealed a closed conformation that can be related to the reduced catalytic activity. *Biochemistry*, **2004**, *43*(1), 67-77.
[194] Miron, S.; Munier-Lehmann, H.; Craescu, C.T. ^{1}H, ^{13}C and ^{15}N resonance assignment and secondary structure of *Mycobacterium tuberculosis* adenylate kinase. *J. Biomol. NMR*, **2001**, *19*(1), 89-90.
[195] Maruoka, S.; Horita, S.; Lee, W.C.; Nagata, K.; Tanokura, M. Crystal structure of the ATPPase subunit and its substrate-dependent association with the GATase subunit: a novel regulatory mechanism for a two-subunit-type GMP synthetase from *Pyrococcus horikoshii* OT3. *J. Mol. Biol.*, **2010**, *395*(2), 417-429.
[196] Bhat, J.Y.; Shastri, B.G.; Balaram, H. Kinetic and biochemical characterization of *Plasmodium falciparum* GMP synthetase. *Biochem. J.*, **2008**, *409*(1), 263-273.
[197] Abbott, J.L.; Newell, J.M.; Lightcap, C.M.; Olanich, M.E.; Loughlin, D.T.; Weller, M.A.; Lam, G.; Pollack, S.; Patton, W.A. The effects of removing the GAT domain from *E. coli* GMP synthetase. *Protein J.*, **2006**, *25*(7-8), 483-491.
[198] Tesmer, J.J.; Klem, T.J.; Deras, M.L.; Davisson, V.J.; Smith, J.L. The crystal structure of GMP synthetase reveals a novel catalytic triad and is a structural paradigm for two enzyme families. *Nat. Struct. Biol.*, **1996**, *3*(1), 74-86.
[199] Nakamura, J.; Straub, K.; Wu, J.; Lou, L. The glutamine hydrolysis function of human GMP synthetase. Identification of an essential active site cysteine. *J. Biol. Chem.*, **1995**, *270*(40), 23450-23455.
[200] Truitt, C.D.; Hermodson, M.A.; Zalkin, H. Amino acid sequence of a peptide containing an essential cysteine residue of *Escherichia coli* GMP synthetase. *J. Biol. Chem.*, **1978**, *253*(23), 8470-8473.
[201] Chittur, S.V.; Klem, T.J.; Shafer, C.M.; Davisson, V.J. Mechanism for acivicin inactivation of triad glutamine amidotransferases. *Biochemistry*, **2001**, *40*(4), 876-887.
[202] Rodriguez-Suarez, R.; Xu, D.; Veillette, K.; Davison, J.; Sillaots, S.; Kauffman, S.; Hu, W.; Bowman, J.; Martel, N.; Trosok, S.; Wang, H.; Zhang, L.; Huang, L.Y.; Li, Y.; Rahkhoodaee, F.; Ransom, T.; Gauvin, D.; Douglas, C.; Youngman, P.; Becker, J.; Jiang, B.; Roemer, T. Mechanism-of-action determination of GMP synthase inhibitors and target validation in *Candida albicans* and *Aspergillus fumigatus*. *Chem. Biol.*, **2007**, *14*(10), 1163-1175.
[203] Santiago, A.E.; Cole, L.E.; Franco, A.; Vogel, S.N.; Levine, M.M.; Barry, E.M. Characterization of rationally attenuated *Francisella tularensis* vaccine strains that harbor deletions in the *guaA* and *guaB* genes. *Vaccine*, **2009**, *27*(18), 2426-2436.
[204] Jewett, M.W.; Lawrence, K.A.; Bestor, A.; Byram, R.; Gherardini, F.; Rosa, P.A. GuaA and GuaB are essential for *Borrelia burgdorferi* survival in the tick-mouse infection cycle. *J Bacteriol.*, **2009**, *191*(20), 6231-6241.

Anexo D

UMP KINASE FROM *Mycobacterium tuberculosis*: MODE OF ACTION AND ALLOSTERIC INTERACTIONS, AND THEIR LIKELY ROLE IN PYRIMIDINE METABOLISM REGULATION

Diana C Rostirolla, Ardala Breda, Leonardo A Rosado, Mario S Palma, Luiz Augusto Basso, Diógenes Santiago Santos

Artigo publicado
Archives of Biochemistry and Biophysics, 2011, 505:202-212.

Archives of Biochemistry and Biophysics 505 (2011) 202–212

Contents lists available at ScienceDirect

Archives of Biochemistry and Biophysics

journal homepage: www.elsevier.com/locate/yabbi

UMP kinase from *Mycobacterium tuberculosis*: Mode of action and allosteric interactions, and their likely role in pyrimidine metabolism regulation ☆

Diana C. Rostirolla [a,b], Ardala Breda [a,b], Leonardo A. Rosado [a,c], Mario S. Palma [d], Luiz A. Basso [a,b,*], Diógenes S. Santos [a,b,*]

[a] *Centro de Pesquisas em Biologia Molecular e Funcional (CPBMF), Instituto Nacional de Ciência e Tecnologia em Tuberculose (INCT-TB), Pontifícia Universidade Católica do Rio Grande do Sul (PUCRS), Av. Ipiranga 6681 – Tecnopuc – Prédio 92-A, Porto Alegre 90619-900, RS, Brazil*

[b] *Programa de Pós-Graduação em Biologia Celular e Molecular, Pontifícia Universidade Católica do Rio Grande do Sul (PUCRS), Porto Alegre, RS, Brazil*

[c] *Programa de Pós-Graduação em Medicina e Ciências da Saúde, PUCRS, Av. Ipiranga 6681, Porto Alegre 90619-900, RS, Brazil*

[d] *Laboratório de Biologia Estrutural e Zooquímica, Centro de Estudos de Insetos Sociais, Departamento de Biologia, Instituto de Biociências de Rio Claro, Universidade Estadual Paulista (UNESP), Rio Claro, SP, Brazil*

ARTICLE INFO

Article history:
Received 25 July 2010
and in revised form 21 October 2010
Available online 28 October 2010

Keywords:
UMPK
Cooperative kinetics
Allosteric regulation
Pyrimidine metabolism
Thermodynamic binding parameters
Antitubercular drug target

ABSTRACT

The *pyrH*-encoded uridine 5′-monophosphate kinase (UMPK) is involved in both *de novo* and salvage synthesis of DNA and RNA precursors. Here we describe *Mycobacterium tuberculosis* UMPK (*Mt*UMPK) cloning and expression in *Escherichia coli*. N-terminal amino acid sequencing and electrospray ionization mass spectrometry analyses confirmed the identity of homogeneous *Mt*UMPK. *Mt*UMPK catalyzed the phosphorylation of UMP to UDP, using ATP–Mg^{2+} as phosphate donor. Size exclusion chromatography showed that the protein is a homotetramer. Kinetic studies revealed that *Mt*UMPK exhibits cooperative kinetics towards ATP and undergoes allosteric regulation. GTP and UTP are, respectively, positive and negative effectors, maintaining the balance of purine versus pyrimidine synthesis. Initial velocity studies and substrate(s) binding measured by isothermal titration calorimetry suggested that catalysis proceeds by a sequential ordered mechanism, in which ATP binds first followed by UMP binding, and release of products is random. As *Mt*UMPK does not resemble its eukaryotic counterparts, specific inhibitors could be designed to be tested as antitubercular agents.

Introduction

Human tuberculosis (TB),[1] mainly caused by *Mycobacterium tuberculosis*, is a major cause of illness and death worldwide. *M. tuberculosis* is a remarkably successful pathogen that latently infects one third of the world population [1] and, despite the availability of effective chemotherapy and moderately protective vaccine, the tubercle bacillus continues to claim more lives than any other single infectious agent [2]. Increasing HIV–TB co-infections [2], the emergence of multidrug-resistant (MDR), extensively drug-resistant (XDR) [3], and, more recently, of totally drug-resistant strains (TDR) [4] have highlighted the need for the development of new therapeutic strategies to combat TB. Strategies based on the discovery of new targets for antimycobacterial agent development include elucidation of

☆ This work was supported by the National Institute of Science and Technology on Tuberculosis (DECIT/SCTIE/MS-MCT-CNPq-FNDCT-CAPES) and the Millennium Initiative Program (CNPq) to D.S.S. and L.A.B. D.S.S. (CNPq, 304051/1975-06), L.A.B. (CNPq, 520182/99-5), and M.S.P. (CNPq, 500079/90-0) are Research Career Awardees of the National Research Council of Brazil (CNPq). A.B. is recipient of a Ph.D. student scholarship awarded by BNDES. L.A.R. and D.C.R. are recipients of M.Sc. student scholarships awarded by, respectively, CAPES and CNPq.

* Corresponding authors at: Centro de Pesquisas em Biologia Molecular e Funcional (CPBMF), Instituto Nacional de Ciência e Tecnologia em Tuberculose (INCT-TB), Pontifícia Universidade Católica do Rio Grande do Sul (PUCRS), Av. Ipiranga 6681 – Tecnopuc – Prédio 92-A, Porto Alegre 90619-900, RS, Brazil. Fax: +55 51 33203629.

E-mail addresses: luiz.basso@pucrs.br (L.A. Basso), diogenes@pucrs.br (D.S. Santos).

[1] *Abbreviations used:* ADP, adenosine 5′-diphosphate; ATP, adenosine 5′-triphosphate; CMP, cytosine 5′-monophosphate; CTP, cytosine 5′-triphosphate; dCMP, deoxycytosine 5′-monophosphate; DMSO, dimethyl sulfoxide; DNA, deoxyribonucleic acid; dTMP, deoxythymidine 5′-monophosphate; ESI-MS, electrospray ionization mass spectrometry; FDA, Food and Drug Administration; GTP, guanosine 5′-triphosphate; Hepes, *N*-2-hydroxyethylpiperazyne-*N*′-2-ethanesulfonic acid; HIV, human immunodeficiency virus; IPTG, isopropyl-β-D-thiogalactopyranoside; ITC, isothermal titration calorimetry; LB, Luria–Bertani; MDR, multidrug-resistant; *Mt*UMPK, uridine 5′-monophosphate kinase from *Mycobacterium tuberculosis*; NADH, nicotinamide adenine dinucleotide; NDP, nucleoside diphosphate; NMP, nucleoside monophosphate; NTP, nucleoside triphosphate; PCR, polymerase chain reaction; PDB, Protein Data Bank; RNA, ribonucleic acid; SDS–PAGE, sodium dodecyl sulfate–polyacrylamide gel electrophoresis; TB, Terrific Broth; TB, tuberculosis; Tris, tris(hydroxymethyl)aminomethane; UDP, uridine 5′-diphosphate; UMP, uridine 5′-monophosphate; UMPK, uridine 5′-monophosphate kinase; UTP, uridine 5′-triphosphate; XDR, extensively drug-resistant.

0003-9861/$ - see front matter © 2010 Elsevier Inc. All rights reserved.
doi:10.1016/j.abb.2010.10.019

the role played by proteins of essential and, preferentially, exclusive biochemical pathways for mycobacterial growth [5].

Rational inhibitor design relies on mechanistic and structural information on the target enzyme. Enzyme inhibitors make up roughly 25% of the drugs marketed in United States [6]. Enzymes offer unique opportunities for drug design that are not available to cell surface receptors, nuclear hormone receptors, ion channel, transporters, and DNA [6]. It has been pointed out that one of the lessons to be learned from marketed enzyme inhibitors is that the most potent and effective inhibitors take advantage of enzyme chemistry to achieve inhibition [7]. Moreover, the recognition of the limitations of high-throughput screening approaches in the discovery of candidate drugs has rekindled interest in rational design methods [8]. Accordingly, mechanistic analysis should always be a top priority for enzyme-targeted drug programs aiming at the rational design of potent enzyme inhibitors.

Nucleotides are important molecules present in all living organisms as they constitute the building blocks for nucleic acids and also serve as energy sources for many biochemical reactions [9]. Pyrimidine nucleotides can be synthesized by *de novo* and salvage pathways resulting in a common product, the nucleotide uridine 5′-monophosphate (UMP) [10]. Subsequent phosphorylation of UMP yields UDP that leads to the synthesis of all other pyrimidine nucleotides [11]. Nucleoside monophosphate (NMP) kinases play an important role in the biosynthesis of nucleotides and represent a homogeneous family of catalysts related to adenylate kinase (EC 2.7.4.3). They catalyze the synthesis of nucleoside diphosphates (NDPs), which will be converted to nucleoside triphosphates (NTPs) by a non-specific nucleoside diphosphate kinase [12]. UMP kinases (UMPKs) catalyze the reversible transfer of the γ-phosphoryl group from ATP to UMP in the presence of a divalent cation, usually Mg^{2+} (Fig. 1) [13]. In general, eukaryotic UMP/CMP kinases (EC 2.7.4.14) are monomers, phosphorylate with comparable efficiency both UMP and CMP, and are structurally similar to other NMP kinases (such as adenylate kinase) [12,14–16]. In contrast, bacterial UMPKs (EC 2.7.4.22) are specific for UMP, exist in solution as stable homohexamers, and do not resemble either UMP/CMP kinases or NMP kinases from other organisms based on sequence comparisons [17,18]. Kinetic studies have shown that bacterial UMPKs can be activated by GTP and/or be subject to feedback inhibition by UTP, the major product of the reaction they catalyze [17–21], regulating the balance of purine versus pyrimidine nucleoside triphosphates synthesis [13].

As pyrimidine biosynthesis is an essential step in the progression of TB, enzymes of this pathway are attractive antitubercular drug targets [22]. Homologs to enzymes in the pyrimidine pathway have been identified in the genome sequence of *M. tuberculosis* [23]. A rapid recombination method for screening and confirmation of gene essentiality has recently been proposed to allow identification of which of the approximately 4000 genes of *M. tuberculosis* are worthy of further study as drug targets [24]. The product of *pyrH* (Rv2883) gene has been shown to be essential for *M. tuberculosis* growth by the rapid screening method [24].

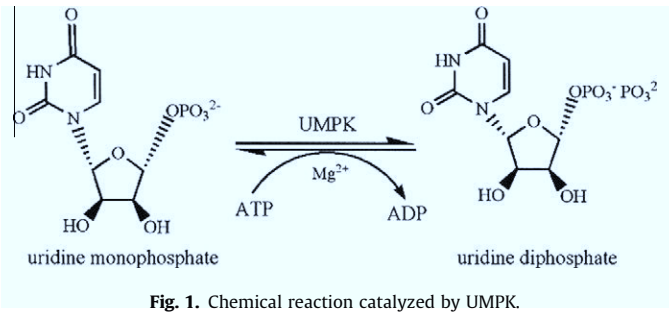

Fig. 1. Chemical reaction catalyzed by UMPK.

Genetic studies have provided evidence that UMPK is essential for growth in both Gram-negative (*Escherichia coli*) [25,26] and Gram-positive bacteria (*Streptococcus pneumoniae*) [19]. Although the *pyrH* gene has been proposed by sequence homology to encode a UMPK protein [23], there has been no formal biochemical proof as to ascertain the correct assignment to the open reading frame of *pyrH* gene in *M. tuberculosis*.

In the present work, the *pyrH* gene from *M. tuberculosis* strain H37Rv was PCR amplified, cloned, and recombinant UMPK (*Mt*UMPK) was purified to homogeneity. N-terminal amino acid sequencing and electrospray ionization mass spectrometry (ESI-MS) analyses were carried out to confirm the identity of the recombinant *Mt*UMPK protein. Initial velocity studies were performed to evaluate the kinetic parameters of the recombinant *Mt*UMPK. In addition, isothermal titration calorimetry study of substrates binding was carried out to demonstrate the order of substrate addition in the kinetic mechanism of *Mt*UMPK. Protein allosteric regulation by ATP, GTP, and UTP have also been demonstrated. These results represent an important step for the rational design of *Mt*UMPK inhibitors that can further be tested as anti-TB drugs.

Materials and methods

Amplification, cloning and DNA sequencing of the pyrH gene

The full-length *pyrH* (Rv2883c) coding region [23] was PCR amplified using the genomic DNA from *M. tuberculosis* H37Rv as template and a high fidelity proof-reading thermostable DNA polymerase (*Pfu*® DNA polymerase, Stratagene). The synthetic oligonucleotides used (forward primer, 5′-GTC ATA TGA CAG AGC CCG ATG TCG CCG GC-3′; and reverse primer, 5′-TAA AGC TTT CAG GTG GTG ACC AGC GTT CCG A-3′) were designed to contain, respectively, NdeI and HindIII (New England Biolabs) restriction sites (underlined). Dimethyl sulfoxide (DMSO) was added to a final concentration of 10%. The 786-bp amplicon was detected on 1% agarose gel and purified utilizing the Quick Gel Extraction kit (Invitrogen). The PCR fragment was cloned into pCR-Blunt® vector (Invitrogen) and, following transformation of *E. coli* strain DH10B (Novagen), the resulting plasmid was isolated utilizing the Qiaprep Spin Miniprep kit (Qiagen). Subsequently, the fragment was cleaved with NdeI and HindIII endonucleases and inserted into the pET-23a(+) expression vector (Novagen), previously digested with the same restriction enzymes. The complete *pyrH* nucleotide sequence was determined by automated DNA sequencing to corroborate sequence identity, integrity and to check the absence of mutations in the cloned fragment.

Expression and purification of recombinant MtUMPK

The recombinant plasmid pET-23a(+)::*pyrH* was transformed into BL21(DE3) *E. coli* electrocompetent cells (Novagen), and cells carrying the recombinant vector were selected on Luria–Bertani (LB) agar plates containing 50 μg mL^{-1} ampicillin [27]. A single colony was used to inoculate 50 mL of Terrific Broth (TB) medium containing the same antibiotic and grown overnight at 37 °C. Aliquots of this culture (2.5 mL) were used to inoculate 250 mL of TB medium in 5 × 1 L flasks supplemented with ampicillin (50 μg mL^{-1}) and grown at 37 °C and 180 rpm to an optical density (OD_{600nm}) of 0.4–0.6. When this OD_{600} value was reached, the temperature was lowered to 30 °C and protein expression was carried out without isopropyl-β-D-thiogalactopyranoside (IPTG) induction. After 24 h, the cells (12 g) were collected by centrifugation at 11,800*g* for 30 min at 4 °C and stored at −20 °C. The same protocol was employed for BL21 (DE3) *E. coli* cell transformed with pET-23a(+) as control. The expression of the recombinant protein was confirmed by 12% sodium

dodecyl sulfate–polyacrylamide gel electrophoresis (SDS–PAGE) stained with Coomassie Brilliant Blue [28].

Escherichia coli (2 g) cells overproducing the *Mt*UMPK were resuspended in 20 mL of 50 mM Tris–HCl, pH 7.5 (buffer A), stirred for 30 min at 4 °C in the presence of lysozyme (0.2 mg mL^{-1}, Sigma–Aldrich), and disrupted by sonication (eight pulses of 10 s, at an amplitude value of 60%). The lysate was centrifuged at 38,900*g* for 30 min to remove cell debris and the supernatant was treated with 1% (wt/vol) streptomycin sulfate (Sigma–Aldrich), stirred for 30 min, and the mixture was centrifuged at 38,900*g* for 30 min. The supernatant containing soluble *Mt*UMPK was dialyzed against 2 L of buffer A for 3 h.

All purification steps were carried out on an ÄKTA system (GE Healthcare) at 4 °C with UV detection at 215, 254, and 280 nm, and fractions were analyzed by SDS–PAGE. The crude extract was loaded on a HiPrep 16/10 Q XL (GE Healthcare) anion-exchange column pre-equilibrated with buffer A. Proteins were eluted using a 0–300 mM NaCl linear gradient at a flow rate of 1 mL min^{-1}. Fractions containing *Mt*UMPK in NaCl (ca. 280 mM) were pooled and $(NH_4)_2SO_4$ was added to a final concentration of 1 M, stirred for 30 min, and clarified by centrifugation at 38,900*g* for 30 min. The supernatant was loaded on a Butyl Sepharose High Performance (GE Healthcare) hydrophobic interaction column pre-equilibrated with 50 mM Tris–HCl, pH 7.5, containing 1 M $(NH_4)_2SO_4$. Proteins were eluted using a 0–100% linear gradient of buffer A at a flow rate of 1 mL min^{-1}. Pooled fractions containing *Mt*UMPK was dialyzed against buffer A to remove salt and loaded on a Mono Q 16/10 (GE Healthcare) anion-exchange column. *Mt*UMPK was eluted in a salt gradient (0–240 mM NaCl) at a flow rate of 1 mL min^{-1}. The pooled sample was dialyzed against 50 mM Tris–HCl, pH 7.5, containing 200 mM NaCl, concentrated using an AMICON (Millipore Corporation, Bedford, MA) ultra filtration membrane (MWCO = 10 kDa), and stored at −80 °C. Total protein concentration was determined by the method of Bradford [29], using the Bio-Rad protein assay kit (Bio-Rad Laboratories) and bovine serum albumin as standard.

Amino acid sequence and mass spectrometry analysis

The N-terminal amino acid residues of homogenous recombinant *Mt*UMPK were determined by automated Edman degradation sequencing using a PPSQ-21A gas-phase sequencer (Shimadzu) [30]. Recombinant *Mt*UMPK was analyzed by electrospray ionization mass spectrometry (ESI-MS) employing some adaptations made to the system described by Chassaigne and Lobinski [31]. Samples were analyzed on a Quattro-II triple-quadrupole mass spectrometer (Micromass; Altrincham, UK), using MassLynx and Transform softwares for data acquisition and spectrum handling.

Determination of MtUMPK molecular mass

Gel-filtration chromatography was performed on a Superdex 200 (HR 10/30) column (GE Healthcare) pre-equilibrated with 50 mM Tris HCl pH 7.5 containing 200 mM NaCl at a flow rate of 0.4 mL min^{-1}, with UV detection at 215, 254 and 280 nm. The LMW and HMW Gel Filtration Calibration Kits (GE Healthcare) were used to prepare a calibration curve. The elution volumes (V_e) of standard proteins (ferritin, catalase, aldolase, coalbumin, ovalbumin, ribonuclease A) were used to calculate their corresponding partition coefficient (K_{av}, Eq. (1)). Blue dextran 2000 (GE Healthcare) was used to determine the void volume (V_o). V_t is the total bead volume of the column. The K_{av} value for each protein was plotted against their corresponding molecular mass.

$$K_{av} = \frac{V_e - V_o}{V_t - V_o} \quad (1)$$

Multiple sequence alignment

The amino acid sequences of the following UMPK proteins, whose three-dimensional structures were solved, were included in the alignment: *E. coli* (NP_414713.1), *Ureaplasma parvum* (YP_001752598.1), *Pyrococcus furiosus* (NP_579136.1), *Sulfolobus solfataricus* (NP_342460.1), and *Bacillus anthracis* (NC_012659.1). The UMPK amino acid sequences of *S. pneumoniae* (YP_816317.1) and *B. subtilis* (NP_389533.2) [32] were also included in the alignment and compared with *M. tuberculosis* UMPK (NP_217399.1). Multiple amino acid sequence alignment was performed by ClustalW [33], using the Gonnet matrix for amino acids substitutions and considering gap penalties, to identify essential residues for nucleotide substrate(s) binding, as well as to infer possible similarities in their mechanism of catalysis. For alignment improvement, 8, 23, 11, 5, 5, and 29 amino acids residues were removed from the *E. coli*, *U. parvum*, *B. anthracis*, *S. pneumoniae*, *B. subtilis*, and *M. tuberculosis*, respectively.

Functional characterization of MtUMPK

*Mt*UMPK catalytic activity was measured for all purification steps in the forward direction at 25 °C, using a coupled spectrophotometric assay (0.5 mL final volume) as described elsewhere [34], on an UV-2550 UV/vis spectrophotometer (Shimadzu). In short, the reaction mixture contained 50 mM Tris–HCl, pH 7.5, 50 mM KCl, 5 mM $MgCl_2$ buffer; 1 mM phosphoenolpyruvate, 0.2 mM β-NADH, fixed concentrations of both ATP (3000 μM) and UMP (600 μM) substrates, 3 U of pyruvate kinase (EC 2.7.1.40) and 2.5 U of L-lactate dehydrogenase (EC 1.1.1.27). The reaction was started by the addition of *Mt*UMPK. The decrease in absorbance at 340 nm ($\varepsilon_{\beta\text{-NADH}} = 6.22 \times 10^{+3}\ M^{-1}\ cm^{-1}$) was continuously monitored and corrected for non-catalyzed chemical reactions in the absence of UMP. One unit of *Mt*UMPK is defined as the amount of enzyme necessary to convert 1 μmol of UMP in UDP per min in an optical path of 1 cm.

Steady-state kinetics

Determination of the apparent steady-state kinetic parameters were evaluated at varying concentrations of UMP (0–150 μM) and a fixed-saturating concentration of ATP (3000 μM), and at varying concentrations of ATP (0–3000 μM) and a fixed-saturating level of UMP (600 μM). Initial velocity data were analyzed by SigmaPlot (Systat Software, Inc.).

In order to evaluate the specificity for phosphate acceptor, UMP was replaced with other nucleoside monophosphates (CMP, dCMP or dTMP) at different concentrations. The specificity of the enzyme as regards the phosphoryl donors was tested by replacing ATP with 3 mM GTP, CTP, and UTP in the standard assay.

Inhibition studies were carried out in the presence of fixed non-saturating levels of ATP (1300 μM) and fixed-varied UTP concentration (0, 30, 50, and 70 μM) when UMP was the variable substrate. Inhibition studies were also carried out in the presence of fixed non-saturating concentration of UMP (40 μM) and fixed-varied UTP concentration (0, 20, 50, and 100 μM) when ATP was the variable substrate. In addition, saturation curves for UTP (0–400 μM) were carried out at three different sets of experiments: fixed-non-saturating ATP concentration (1300 μM) corresponding to its $K_{0.5}$, and saturating UMP concentration (600 μM = 19 × K_m); fixed-non-saturating ATP concentration (1300 μM) corresponding to its $K_{0.5}$, and non-saturating UMP concentration (30 μM ≅ K_m); and fixed-saturating ATP concentration (3000 μM = 2.3 × $K_{0.5}$) and non-saturating UMP concentration (30 μM ≅ K_m). The maximal rate for each reaction condition was determined in the absence of inhibitor. Initial velocity parameters were also analyzed as a

function of ATP concentrations at fixed-saturating UMP concentration (600 μM) either in the absence or presence of a fixed concentration of GTP (500 μM) to verify whether this substrate has any effect on the kinetic properties of *Mt*UMPK (70 nM). Initial velocity measurements were also carried out as a function of UMP concentration at fixed-saturating ATP concentration (3000 μM) in either absence or presence of GTP (500 μM).

Hyperbolic saturation curves were fitted by non-linear regression analysis to the Michaelis–Menten equation (Eq. (2)), in which v is the steady-state velocity, V_{max} is the maximal rate, [S] is the substrate concentration, and K_m is the Michaelis–Menten constant [35,36]. Sigmoidal curves were fitted to the Hill equation (Eq. (3)), where $K_{0.5}$ is the value of the substrate concentration where $v = 0.5\ V_{max}$, and n is the Hill coefficient (indicating the cooperative index) [35,36].

$$v = \frac{V_{max}[S]}{K_m + [S]} \tag{2}$$

$$v = \frac{V_{max}[S]^n}{K_{0.5}^n + [S]^n} \tag{3}$$

The K_i value for UTP towards UMP was calculated using the uncompetitive equation (Eq. (4)), in which [I] is the inhibitor concentration and K_i is the inhibition constant [35,36].

$$v = \frac{V_{max}[S]}{[S]\left(1 + \frac{[I]}{K_i}\right) + K_m} \tag{4}$$

The IC_{50} value, which defines the concentration of inhibitor required to half-saturate the enzyme population, was determined by fitting the data to Eq. (5), in which v_i and v_o are, respectively, the reaction velocity in the presence and in the absence of inhibitor, v_i/v_o represents the fractional activity remaining at a given inhibitor concentration (fraction of free enzyme), and n is the Hill coefficient [36].

$$\frac{v_i}{v_o} = \frac{1}{1 + \left(\frac{[I]}{IC_{50}}\right)^n} \tag{5}$$

Isothermal titration calorimetry (ITC)

ITC experiments were carried out using an iTC_{200} Microcalorimeter (MicroCal, Inc., Northampton, MA). The reference cell (200 μL) was loaded with Milli Q water during all experiments and the sample cell (200 μL) was filled with *Mt*UMPK at a concentration of 100 μM. The injection syringe (39.7 μL) contained substrates or effectors at different concentrations: ATP, ADP, GTP, and UTP at 1.5 mM, UMP at 3 mM, and UDP at 1.8 mM. In addition, titration was performed with the non-hydrolyzable ATP analog, adenosine 5′-(β,γ-imido)triphosphate tetralithium salt hydrate (AMP-PNP) at 1.2 mM to determine the ligand concentration necessary to saturate the enzyme active sites. Subsequently, UMP at 800 μM was titrated into the sample cell containing *Mt*UMPK (100 μM) and AMP-PNP at saturating concentration (250 μM). The latter permits evaluation of any effect that this ATP analog may have on UMP binding to *Mt*UMPK:AMP-PNP binary complex. The ligand binding isotherms were measured by direct titration (ligand into macromolecule). The enzyme was prepared for ITC analysis by dialysis against 50 mM Hepes at pH 7.5 containing 50 mM KCl, 5 mM $MgCl_2$, 200 mM NaCl. The same buffer was used to prepare all ligand solutions and Tris, used at the kinetic assays, was replaced with Hepes due to the high enthalpy of ionization of Tris [37,38]. The stirring speed was 500 rpm at a temperature of 25 °C for all ITC experiments. The first titration injection (0.5 μL), which was discarded in the data analysis, was followed by 17 injections of 2.2 μL each at 180 s intervals. Control titrations (ligand into buffer) were performed to subtract the heats of dilution and mixing for each experiment prior to data analysis. The data after peak integration of the isotherm generated by ITC, subtraction of control titration data and concentration normalization (heat normalized to the molar ratio), were analyzed by Origin 7 SR4 software (Microcal, Inc.).

The ΔG (Gibbs free energy) of binding was calculated using the relationship described in Eq. (6), in which R is the gas constant (8.314 J K^{-1} mol^{-1}), T is the temperature in K (T = °C + 273.15), and K_a is the association constant at equilibrium. The entropy of binding (ΔS) can also be determined by this mathematical formula. The initial estimates for n, K_a, and ΔH parameters were refined by standard Marquardt non-linear regression method provided in the Origin 7 SR4 software.

$$\Delta G^o = -RT \ln K_a = \Delta H^o - T\Delta S^o \tag{6}$$

Results and discussion

Amplification, cloning and sequencing of the pyrH gene

The 786-bp PCR amplicon was consistent with the *M. tuberculosis* H37Rv *pyrH* coding region (data not shown). The product was purified and ligated into pET-23a(+) expression vector as described in Section 'Amplification, cloning and DNA sequencing of the pyrH gene'. Automated DNA sequencing confirmed the identity and the absence of mutations in the cloned fragment.

Expression and purification of the recombinant MtUMPK

The resulting pET-23a(+)::*pyrH* recombinant plasmid was electroporated into BL21(DE3) *E. coli* cells and cultures were grown in TB medium for 24 h. Analysis by SDS–PAGE indicated that the supernatant of cell extract (Fig. 2A, lane 3), which was sonicated and centrifuged, contained a significant amount of protein with subunit molecular mass (ca. 27 kDa) in agreement with the predicted MW for *Mt*UMPK (27.4 kDa).

The overexpressed protein was purified by a three-step protocol consisting of an anion-exchange column (HiPrep Q XL), a hydrophobic interaction column (Butyl Sepharose HP) and a strong anion-exchange column (Mono Q). The target protein eluted at approximately 180 mM of NaCl from the Mono Q column, and

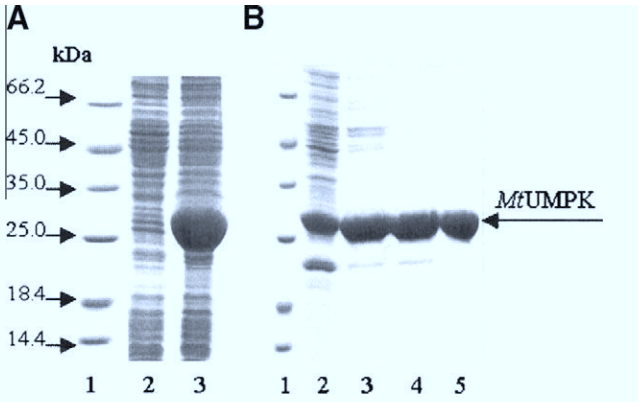

Fig. 2. (A) Twelve percent SDS–PAGE analysis of total soluble proteins. Expression of *Mt*UMPK of 24-h cell growth after reaching an $OD_{600\ nm}$ of 0.4–0.6 in TB medium without addition of IPTG. Lane 1, Protein Molecular Weight Marker (Fermentas); lane 2, soluble *E. coli* BL21 (DE3) [pET-23a(+) (control)] extract; lane 3, soluble *E. coli* BL21 (DE3) [pET-23a(+)::*pyrH*] extract. (B) Twelve percent SDS–PAGE analysis of pooled fractions from *Mt*UMPK purification steps. Lane 1, Protein Molecular Weight Marker (Fermentas); lane 2, crude extract; lane 3, HiPrep Q XL 16/10 elution; lane 4, Butyl Sepharose HP elution and Mono Q 16/10 elution.

Table 1
Purification of *Mt*UMPK from *E. coli* BL21 (DE3). Typical purification protocol from 2 g wet cell paste.

Purification step	Total protein (mg)	Total enzyme activity (U)	Specific activity (U mg^{-1})	Purification fold	Yield (%)
Crude extract	158	722	4.6	1.0	100
HiPrep Q XL	55	977	17.8	3.9	135
Butyl Sepharose	27	863	32	6.9	120
Mono Q	20	154	7.7	1.7	21

SDS–PAGE analysis showed that recombinant *Mt*UMPK was homogenous (Fig. 2B, lane 5). This 1.7-fold purification protocol yielded 20 mg of recombinant protein from 2 g of cells, indicating a 21% protein yield (Table 1). Enzyme kinetic measurements by NADH-coupled spectrophotometric assay showed that recombinant *Mt*UMPK indeed catalyzes the phosphorylation of UMP. Nevertheless, increase in the specific activity could be observed in the presence of high salt concentrations and a pronounced decrease after salt removal. This difference in activity may be attributed to ionic strength which, such as pH variations, is recognized to affect enzyme conformation, stability and activity [39,40]. Gagyi et al. [18] have also reported the addition of 100 mM NaCl as an approach to keep the *B. subtilis* UMPK stability. Accordingly, the homogenous protein was stored at −80 °C 50 mM Tris–HCl, pH 7.5, buffer containing 200 mM NaCl, which resulted in an apparent maximum velocity of 7.7 U mg^{-1} and allowed the kinetic assays to be carried out without affecting the coupled enzymes.

Mass spectrometry and N-terminal amino acid sequencing

The subunit molecular mass value was determined to be 27264.08 ± 13 Da by ESI-MS, which is lower than expected from the predicted amino acid sequence (27395.00 Da), indicating that the N-terminal methionine (130.92 Da) was removed.

The first 22 N-terminal amino acid residues identified by the Edman degradation method correspond to those predicted for the *pyrH* gene protein product and corroborate the N-terminal methionine removal. These results unambiguously identify the homogenous recombinant protein as the putative *Mt*UMPK.

MtUMPK molecular mass determination

The molecular mass of the native enzyme was determined by gel-filtration chromatography and yielded a single peak with elution volume corresponding to approximately 106 kDa, suggesting that *Mt*UMPK is a tetramer in solution (106,000 Da/27264.08 Da ≅ 3.9), differing from other bacterial homohexameric UMPKs [17–19].

Multiple sequence alignment

The currently available three-dimensional structures of UMPKs from several prokaryotic organisms deposited in the Protein Data Bank, such as *E. coli* (PDB code: 2BNE, 2BND, 2BNF, and 2V4Y) [13,41], *U. parvum* (PDB code: 2VA1) [21], *P. furiosus* (PDB code: 2BRI and 2BMU) [11], *S. solfataricus* (PDB code: 2J4J, 2J4K and 2J4L) [20] and *B. anthracis* (PDB code: 2JJX) [9], allow drug design based on a detailed model of the target binding site. The experimentally solved structures of *E. coli* UMPK [13,41] in complex with its substrates and the allosteric effector permit to propose the amino acid side chains in *M. tuberculosis* that are involved in ATP, UMP, and UDP binding as well as residues that participate in GTP-binding. To this end, multiple sequence alignment was carried out and

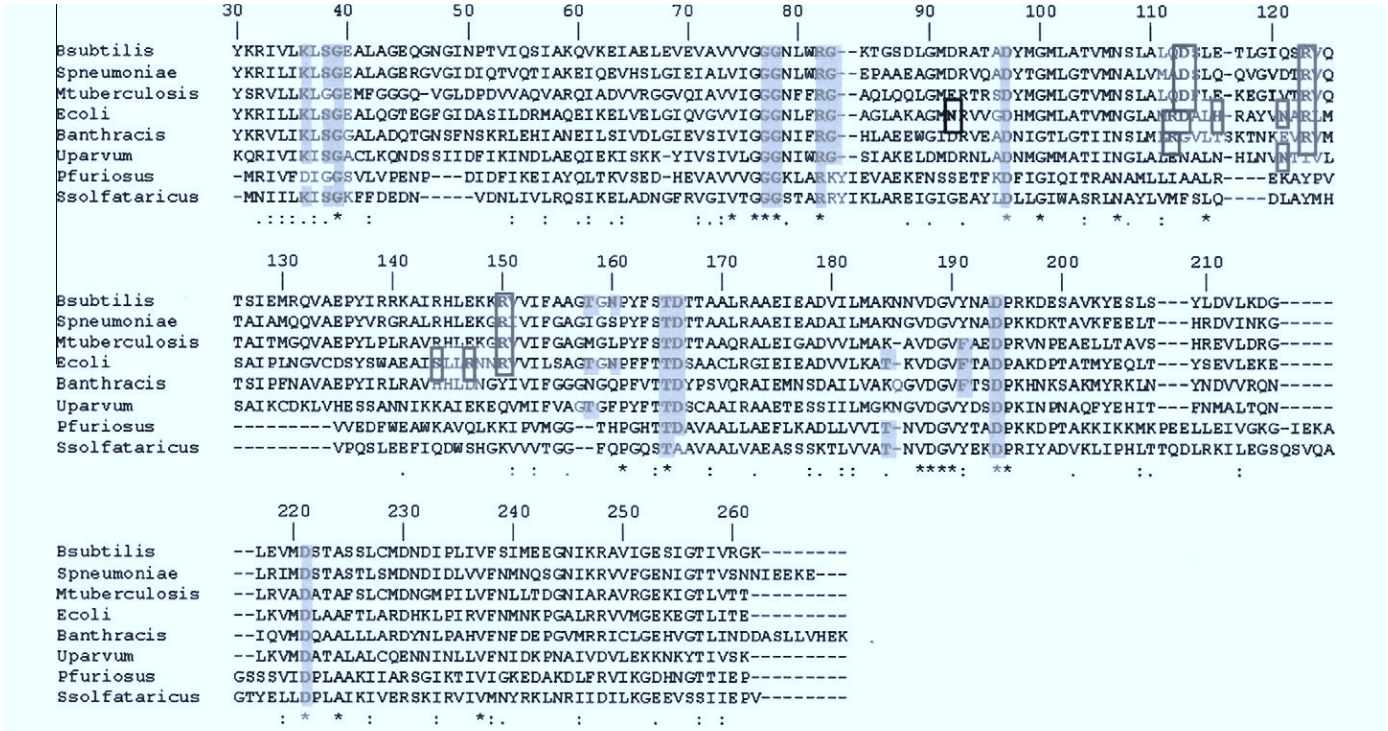

Fig. 3. Amino acids sequence alignment of UMPKs from eight prokaryotes. The residues inferred in *E. coli* as interacting with ATP, UMP or UDP are shaded in gray and the residues involved in GTP-binding are boxed [13,41]. (∗), (:), (.) and (–) indicate identity, strong similarity, weak similarity and gat inclusion among the residues, respectively. Amino acid residues were numbered after removing 29 N-terminal amino acids from the polypeptide sequence of *Mt*UMPK.

the results suggest that the conserved *Mt*UMPK Gly83 and Asp97 (*M. tuberculosis* numbering) amino acid residues are equivalent to residues in *E. coli* UMPK [13] that interact with the 2′-OH ribose ring of UMP (Fig. 3). The amino acids Gly77, Gly78, Arg82, and Thr165, which are involved in UMP α-phosphate interactions, are conserved among all sequences aligned. The main differences among UMP binding residues are those associated with uracil binding. The interactions between *E. coli* UMPK and the uracil moiety of UMP are between the hydrophilic Thr138 and Asn140 amino acids, whereas in *Mt*UMPK these interactions are made by the hydrophobic Met158 and Leu160 residues. As no structural data for *Mt*UMPK have been available to date, it is tempting to suggest that these differences may be related to the distinct quaternary structures of *Mt*UMPK (tetramer) and *E. coli* UMPK (hexamer), since site-directed mutagenesis of Thr138 and Asn140 residues suggested their involvement in subunit contacts in the quaternary structure of the latter [13]. The interactions between the enzyme and uracil, ribose, or the UDP α-phosphate moiety are very similar to those with UMP, although UDP binding involves three additional amino acid residues [13]. The Lys36 and Gly39 residues (*M. tuberculosis* numbering) are conserved, whereas Gly39 in *Mt*UMPK sequence replaces a serine residue present in *E. coli* UMPK.

The amino acids Lys36, Asp166, Phe191, Asp194, and Asp221 in *Mt*UMPK are likely involved in ATP interaction since they are conserved in the *E. coli* UMPK and *Mt*UMPK polypeptide sequences. On the other hand, Lys185 in *Mt*UMPK replaces a threonine residue present in ATP binding site of *E. coli* UMPK. It is interesting to note that the Lys residue involved in ATP binding replaces Thr in five UMPK sequences [43] as in *Mt*UMPK. In *E. coli* UMPK, the GTP-binding site is between two dimers of the hexamer and GTP promotes a rearrangement of its quaternary structure, resulting in a tighter dimer–dimer interaction [41]. Asp113, which interacts with the GTP purine moiety, Arg123 and Arg150, both interacting with the phosphate group, are the most conserved amino acid residues (Fig. 3). These residues are absent in *U. parvum* and *S. solfataricus* UMPKs and may explain the lack of GTP stimulation of these enzymes [20,21].

MtUMPK kinetic parameters

The dependence of velocity with UMP as variable substrate at fixed-saturating ATP concentration (3000 μM) followed hyperbolic Michaelis–Menten kinetics (Fig. 4A), and the apparent constant values were thus calculated fitting the data to Eq. (2), yielding the following values: $V_{max} = 7.5$ (±0.3) U mg^{-1} and $K_m = 31$ (±3) μM. These results permit estimate a value of 3.4 (±0.1) s^{-1} for the UMP catalytic constant (k_{cat}) and of 11 (±1) × 10^4 M^{-1}s^{-1} for the UMP specificity constant (k_{cat}/K_m). The Michaelis–Menten constant values are similar to those reported for *B. subtilis* ($K_m^{UMP} = 30$ μM) and *E. coli* ($K_m^{UMP} = 43$ μM at pH 7.4) UMPKs [18,41].

The saturation curve for ATP at fixed-saturating UMP concentration (600 μM) was sigmoidal (Fig. 4B), suggesting cooperative kinetics. Accordingly, the data were fitted to the Hill equation (Eq. (3)), yielding the following values: $V_{max} = 8.8$ (±0.2) U mg^{-1}, $K_{0.5} = 1299$ (±32) μM and $n = 3.9$ (±0.3). The k_{cat} for ATP is 4.0 (±0.1) s^{-1}. The limiting value for the Hill coefficient (n) is four since we showed that *Mt*UMPK is a homotetramer in solution. The n value of 3.9 thus indicates strong positive cooperativity for ATP.

As demonstrated for others UMPKs [17,20,21], *Mt*UMPK was specific for UMP as the phosphoryl group acceptor as no enzyme activity was detected with CMP, dCMP or dTMP. The specificity for the phosphoryl group donor was tested with GTP, CTP and UTP, and UMP as the acceptor substrate. No activity was detected with GTP and CTP. UTP acted as phosphoryl donor at a velocity value of 0.5 U mg^{-1}. This value is 18-fold lower than for ATP (8.8 U mg^{-1}), suggesting that ATP is the more likely physiological phosphate donor for *Mt*UMPK.

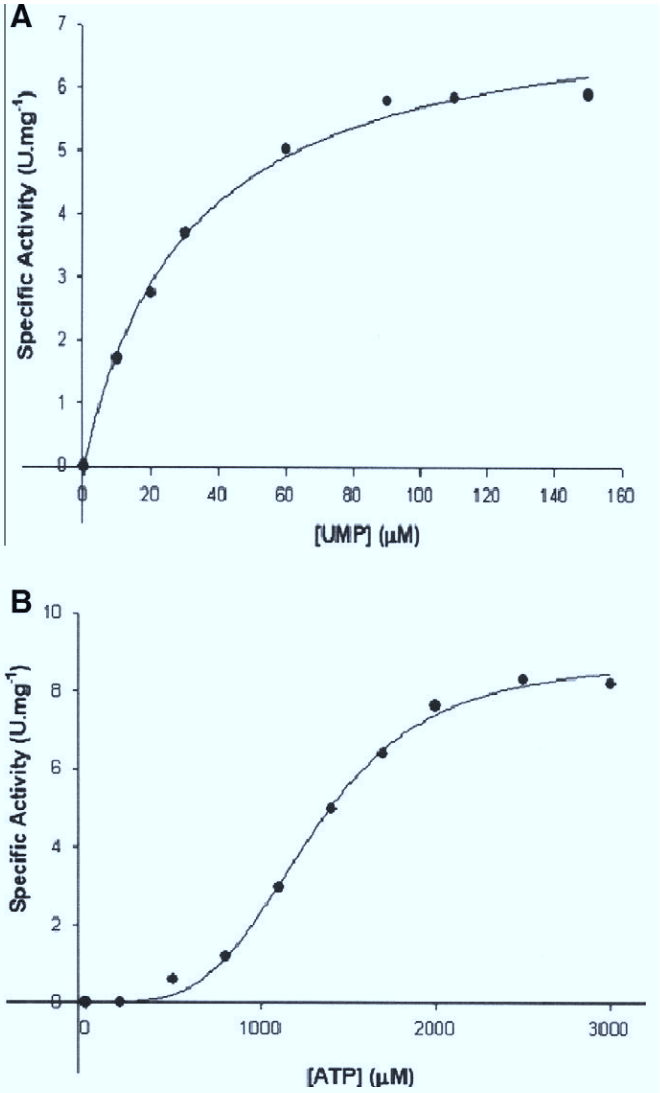

Fig. 4. Apparent steady-state kinetic parameters. (A) Specific activity (U mg^{-1}) versus [UMP] (μM) at fixed concentration of ATP (3000 μM). (B) Specific activity (U mg^{-1}) versus [ATP] (μM) at fixed concentration of UMP (600 μM). The *Mt*UMPK concentration was 70 nM on both assays.

UTP has been reported as a common negative regulator of UMPKs from Gram-negative bacteria, Gram-positive bacteria and archae [20,42,43]. To evaluate the inhibitory effect of UTP on *Mt*UMPK enzyme velocity, measurements of steady-state rates were carried out as described in Section 'Materials and methods'. Double-reciprocal plots at different UTP concentrations displayed a pattern of parallel lines, suggesting that UTP acts as an uncompetitive inhibitor towards UMP in which V_{max} and K_m values were simultaneously reduced (Fig. 5) at fixed non-saturating ATP concentration (1300 μM) and varying UMP concentration. Data fitting to Eq. (4) for uncompetitive inhibition yielded a K_i value of 87 (±5) μM for UTP. On the other hand, the plots of *Mt*UMPK activity versus ATP concentration in the presence of both non-saturating UMP (40 μM) and fixed-varied UTP concentrations (0, 30, 50, and 70 μM) were all sigmoidal. Although inhibition by UTP did not modify the sigmoidal shape of the curve, data fitting to Eq. (3) yielded increasing, though modest, values for apparent $K_{0.5}$, whereas V_{max} and the Hill coefficient values remained approximately constant (Table 2). These features appear to be a common

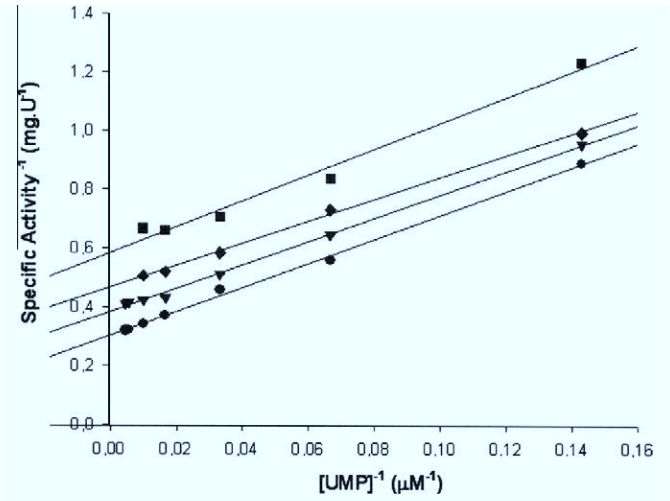

Fig. 5. Double-reciprocal plot of specific activity^{-1} (mg U^{-1}) versus [UMP]$^{-1}$ (μM^{-1}) at 0, 30, 50 and 70 μM UTP. The *Mt*UMPK concentration was 80 nM.

theme for UMPKs from Gram-positive and archae microorganisms [19,20,43].

The saturation curves for UTP inhibition in the presence of fixed-non-saturating ATP concentration and saturating UMP concentration, fixed-non-saturating ATP concentration and non-saturating UMP concentration, and fixed-saturating ATP concentration and non-saturating UMP concentration were all sigmoidal (data not shown). These data were thus fitted to Eq. (5), yielding estimates for IC_{50} values and the Hill coefficient (Table 3). The rates decreased with increasing UTP concentration, reaching a plateau of low enzyme activity (below 0.5 U mg^{-1}) at high UTP concentrations. The IC_{50} values of 80 μM (saturating UMP concentration) and 97 μM (non-saturating UMP concentration) were within experimental error. These results are in agreement with UTP acting as an uncompetitive inhibitor towards UMP (Fig. 5), thereby suggesting that UTP preferentially binds to a complex formed between *Mt*UMPK and UMP (it would have to be a ternary complex because we showed that ATP binding is followed by UMP binding). Stated otherwise, as the *Mt*UMPK enzyme mechanism is ordered (ATP binds first), the concentration of *Mt*UMPK:ATP binary complex, to which UMP binds, is unchanged as ATP concentration in both experiments were the same (1300 μM). It could be argued that increasing UMP fixed concentration (from 30 to 600 μM) would result in increasing concentration of *Mt*UMPK:ATP:UMP ternary complex, to which UTP binds, resulting in lower IC_{50} values for larger UMP concentrations. However, it should be kept in mind that the enzyme activity measurements here presented provide a value for the apparent K_m value of UMP and that this value represents an apparent dissociation constant that may be treated as the overall dissociation constant of all enzyme-bound species. In short, the true equilibrium dissociation constant of UMP from *Mt*UMPK:ATP:UMP ternary complex is not known, thereby precluding a proposal that increasing UMP concentration would result in increasing ternary complex concentration because the true dissociation constant value for UMP may be considerably larger than the concentrations employed here. In any case, the uncompetitive inhibition cannot be overcome by high UMP substrate concentrations, suggesting that UTP binds to an allosteric (regulatory) site. In addition, there was a decrease in the Hill coefficient (n) from 2.8 at non-saturating UMP concentration to 1.5 at saturating UMP concentration (Table 3). It thus appears that increasing UMP concentration results in decreasing degree of cooperativity. In the presence of saturating ATP concentration (3000 μM), there was a 2-fold increase in IC_{50} value for UTP, suggesting that UTP acts as a competitive inhibitor towards ATP. These data are consistent with ATP kinetics in which increasing fixed-varied concentrations of UTP in the presence of fixed-non-saturating UMP concentration yielded increasing values for apparent $K_{0.5}$ (Table 2). Moreover, since we have shown that UTP can act as a poor phosphoryl donor, it is thus likely that UTP can also bind to ATP binding site of *Mt*UMPK. These data suggest that UTP either binds to the ATP binding site with low affinity or to an allosteric site that results in uncompetitive inhibition towards UMP. Incidentally, it has been proposed that each subunit of bacterial UMPKs has three distinct nucleotide-binding sites [43].

Table 2
ATP kinetic parameters in the presence of fixed concentrations of UTP.

UTP concentration (μM)	V_{max}[a]	n[b]	$K_{0.5}$[c] (μM)
0	3.8 ± 0.3	2.4 ± 0.4	1.2 (±0.1) × 10^3
20	3.5 ± 0.3	2.1 ± 0.3	1.3 (±0.2) × 10^3
50	3.9 ± 0.4	2.5 ± 0.5	1.4 (±0.2) × 10^3
100	4 ± 1	2.3 ± 0.9	1.7 (±0.5) × 10^3

[a] V_{max} = maximal rate.
[b] n = the Hill coefficient.
[c] $K_{0.5}$ = value of the substrate concentration in which $v = 0.5\ V_{max}$.

Table 3
IC_{50} and n values for UTP in the presence of different fixed substrate concentrations.

Substrate concentrations	IC_{50}[a] (μM)	n[b]
ATP 1300 μM + UMP 600 μM	80 ± 4	1.5 ± 0.1
ATP 1300 μM + UMP 30 μM	97 ± 7	2.8 ± 0.4
ATP 3000 μM + UMP 30 μM	210 ± 6	3.6 ± 0.3

[a] IC_{50} = concentration of inhibitor required to half-saturate the enzyme population.
[b] n = the Hill coefficient.

GTP has been shown to be a positive effector for bacterial UMPKs [41,43]. The crystal structure of *E. coli* UMPK bound to GTP has recently been solved at 2.3 Å [41]. The presence of GTP (500 μM) resulted in both increased V_{max} values (from 2 to 3.2 U mg^{-1}) and affinity ($K_{0.5}$) of ATP for *Mt*UMPK (from 1335 to 545 μM) (Fig. 6). In addition, the Hill coefficient value of 4.4 in the absence of GTP decreased to 1.6 in the presence of GTP (500 μM), suggesting that this nucleotide decreased the degree of cooperativity of ATP upon *Mt*UMPK enzyme activity (Fig. 6). These results are in agreement with previously published results on UMPKs from Gram-positive bacteria [19,43]. On the other hand, the effect of GTP on UMP kinetics displayed a slight increase in the V_{max} values (from 1.63 ± 0.03 U mg^{-1} in the absence to 2.07 ± 0.05 U mg^{-1} in the presence of GTP), and no change of K_m values for UMP (data not shown).

Equilibrium binding of ligands assessed by ITC

To further elucidate the *Mt*UMPK kinetic mechanism, titration microcalorimetry of ligand binding to the recombinant enzyme was carried out. Equilibrium binding values of ligands were measured directly by ITC, determining the heat generated or consumed upon ligand–macromolecule binary complex formation at constant temperature and pressure. The measured of the heat released upon binding of the ligands allowed us to derive the binding enthalpy (ΔH) of the process, to estimate the stoichiometry of the interaction (n) and the association constant at equilibrium (K_a). The dissociation constant at equilibrium (K_d) could be calculated as the inverse of K_a ($K_d = 1/K_a$). Moreover, the Gibbs free energy (ΔG) and entropy (ΔS) of binding were determined from the association constant values at equilibrium as described in Eq. (6). The ITC data for binding of ligands to *Mt*UMPK (Fig. 7) are summarized in Table 4. The overall binding isotherms for ATP, ADP, UDP or

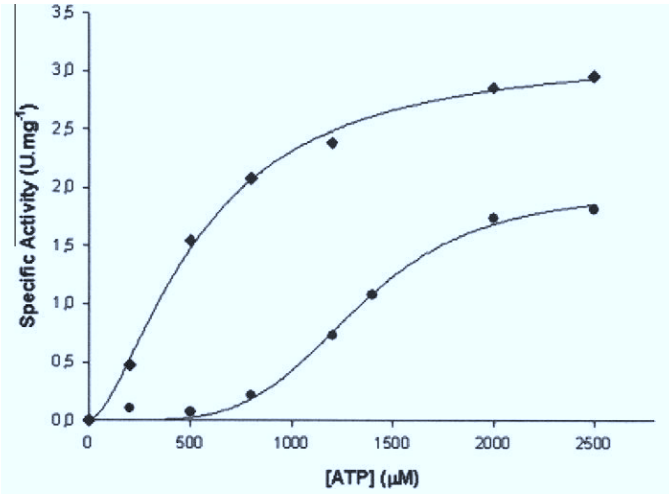

Fig. 6. Effect of GTP (500 μM) on ATP saturation curves. In the absence of effector (•), the curve is sigmoidal. In the presence of effector (♦), the sigmoidicity is reduced though still present. The *Mt*UMPK concentration was 70 nM.

GTP-binding to *Mt*UMPK were best fitted to a model of one set of sites (Table 4). The UTP binding isotherm was not well defined to obtain an adequate fit of the data to any model, probable because this substrate may exert different and simultaneous effects on *Mt*UMPK.

The mechanism of phosphoryl transfer of NMP kinases has been reported to follow a sequential random bi bi kinetic mechanism [12]. The *Mt*UMPK appears to deviate from this type of mechanism, since no significant heat changes were obtained for UMP binding, suggesting that it cannot bind to free enzyme. In contrast, all other ligands tested do bind to the free enzyme and exhibit exothermic reactions, as seen by negative changes in the binding enthalpy (Fig. 7). Interestingly, the binding isotherm of an ATP molecule does not appear to influence the affinity for the subsequent one, as the thermodynamic parameters for ATP binding provide single ΔH and K_a values. How can one reconcile these data with positive cooperativity displayed by the saturation curve (Fig. 4B) of steady-state kinetics for ATP in the presence of UMP? These data suggest that ATP binding has a positive heterotropic effect upon UMP binding to *Mt*UMPK:ATP binary complex, since UMP does not bind to the free enzyme. The *n* value of 0.57 sites for the ATP binding refers to the event of two subunits of *Mt*UMPK in the cell associating with each ATP molecule injected. In summary, we propose that ATP binding triggers a conformational change of *Mt*UMPK that results in increased affinity for UMP. To provide further experimental evidence for the proposed positive heterotropic effect of ATP, titration of UMP into a solution containing *Mt*UMPK:AMP-PNP binary complex (a non-hydrolyzable ATP analog) was carried out. The ligand binding isotherms showed no ITC signal upon UMP binding to free *Mt*UMPK enzyme (Fig. 7, panel E). On the other hand, the ITC signal for titration of *Mt*UMPK:AMP-PNP with UMP showed changes in the degree of heat response upon *Mt*UMPK:AMP-PNP:UMP ternary complex formation, displaying exothermic and endothermic responses (Fig. 7, panel F). The ITC data were analyzed with a model assuming a cooperative ligand binding interaction for a tetrameric protein. The UMP binding exhibited biphasic behavior (Fig. 7, panel F), which could be assessed by the endothermic and exothermic profile of the heat response. The ITC data showed a cooperative pattern and demonstrated that UMP binds to *Mt*UMPK:AMP-PNP binary complex (Table 4), even though it could not be demonstrated an obvious positive cooperative effect with increasing affinity for UMP as the binding sites are sequentially occupied. However, positive cooperativity is generally more difficult to distinguish from ITC studies alone, since the tendency is for the binding sites on any single molecule to saturate together unless the difference in affinity values between the sites were large. Notwithstanding, the ITC data are in agreement with the steady-state kinetics results showing that UMP binds to *Mt*UMPK:ATP binary complex and that ATP has a cooperative effect on tetrameric *Mt*UMPK enzyme.

The UDP product binds to free *Mt*UMPK enzyme with higher affinity than ADP product (Table 4), and both ligands displayed a stoichiometry of one ligand binding to each monomer of the tetrameric enzyme. The larger association constant of UDP as compared to ADP appears to be enthalpy driven (Table 4). These ITC results suggest that product release is random. The GTP-binding affinity is in the same range of UDP (Table 4). These ITC results demonstrate that GTP is capable of binding to free *Mt*UMPK enzyme with a stoichiometry close to unity. It is interesting to note that ATP (substrate) as compared to ADP (product) binding display approximately the same association constant at equilibrium (or Gibbs free energy), which is a result of the ubiquitous phenomenon of enthalpy–entropy compensation meaning that entropy losses often negate enthalpy gains [8]. In short, ITC and steady-state kinetic results provide evidence *Mt*UMPK follows an sequential ordered mechanism, in which ATP binds first to free enzyme followed by UMP binding to the *Mt*UMPK:ATP binary complex (Fig. 8). Release of products is, however, random. The mechanism for *S. solfataricus* UMPK has been shown to be random order for either addition of substrates or release of products [20].

Summary

Bacterial UMPKs have been proposed to be attractive drug targets because their primary amino acid sequence and three-dimensional structures are divergent from their eukaryotic counterparts. They are unique members of the NMP kinases family of enzymes and several research groups have demonstrate its essentiality for different organisms [17,19,25,26,44], and to *M. tuberculosis* in particular [24]. Moreover, they are oligomers with an exclusive and complex control of activity by GTP and UTP, representing an interesting model of allosteric regulation [43]. The elucidation of the mode of action of *Mt*UMPK is thus warranted. Although the *pyrH* gene has been proposed by *in silico* analysis to encode a UMPK enzyme [23], formal biochemical proof was still lacking as regards the correct assignment to its open reading frame in *M. tuberculosis*. Accordingly, here we describe PCR amplification of the *pyrH* coding region, cloning, heterologous expression, and purification of recombinant protein to homogeneity. N-terminal amino acid sequence and ESI-MS confirmed the identity of the homogeneous recombinant protein. Steady-state kinetic measurements confirmed that the *pyrH* gene encodes a UMPK enzyme in *M. tuberculosis*. Size exclusion chromatography showed that *Mt*UMPK is a tetramer in solution. Multiple sequence alignment analysis allowed identification of residues involved in substrate binding and/or catalysis.

Steady-state kinetic measurements showed that *Mt*UMPK is specific for both ATP and UMP substrates. This specificity for UMP is not surprising since it has been shown that the Rv1712 locus in *M. tuberculosis* codes for a functional cytosine monophosphate kinase that preferentially phosphorylates CMP and dCMP, and that UMP is a poor substrate [45]. In agreement with these results, *E. coli* has two distinct enzymes that display substrate specificity for UMP (UMPK) or CMP (CMP kinase) [46]. Steady-state kinetics and ITC data suggest a sequential ordered mechanism for substrate addition to *Mt*UMPK, in which ATP binds first to free enzyme followed by UMP binding; and a random order for release of products.

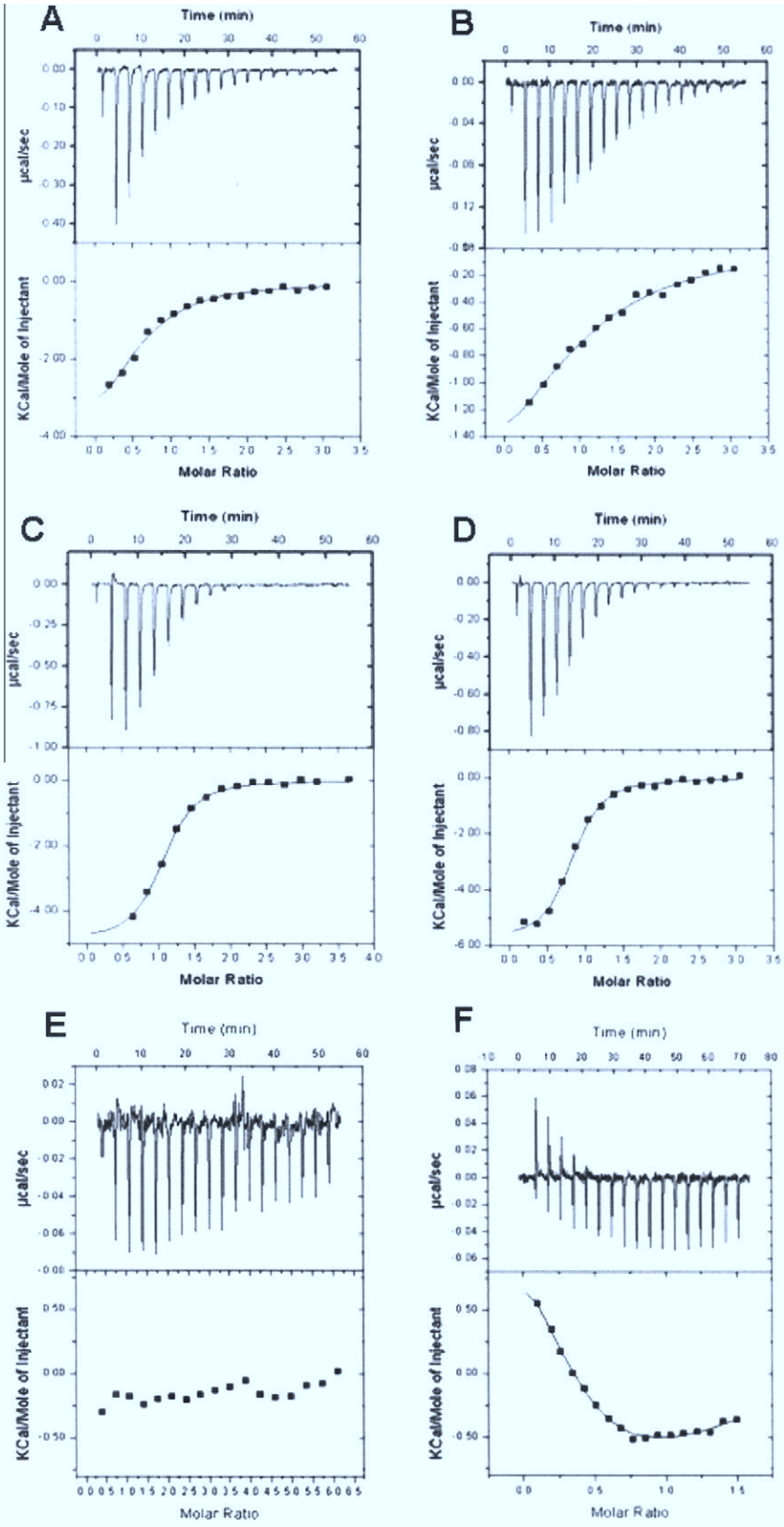

Fig. 7. Isothermal titration calorimetric curves of binding of ligands to *Mt*UMPK (100 µM). (A) Titration of the ATP substrate at a final concentration of 248 µM. (B) Titration of the ADP product at a final concentration of 248 µM. (C) Titration of the UDP product at a final concentration of 398 µM. (D) Titration of the allosteric effector GTP at a final concentration of 248 µM. (E) Titration of the UMP substrate at a final concentration of 497 µM. (F) Titration of the UMP substrate at a final concentration of 132 µM in the presence of the non-hydrolyzable ATP analog (AMP-PNP). The experiments were carried out at constant temperature and pressure.

Table 4
Association constants and thermodynamic parameters of different ligands binding to *Mt*UMPK.

Ligands	n[a]	K_a[b] (M^{-1})	ΔH°[c] (kcal mol^{-1})	ΔG°[d] (kcal mol^{-1})	ΔS°[e] (cal mol^{-1} K^{-1})	K_d[f] (μM)
ATP	0.57 ± 0.06	$3.0e^4 \pm 5.7e^3$	−4.8 ± 0.6	−6.1 ± 1.2	4.3 ± 0.8	33.3 ± 6.3
ADP	1.0 ± 0.1	$1.5e^4 \pm 3.5e^3$	−2.1 ± 0.4	−5.7 ± 1.3	12.1 ± 2.8	66 ± 15
UDP	1.01 ± 0.01	$2.1e^5 \pm 2.4e^4$	−4.9 ± 0.1	−7.3 ± 0.8	7.9 ± 0.9	4.8 ± 0.5
GTP	0.80 ± 0.01	$2.0e^5 \pm 2.6e^4$	−5.8 ± 0.1	−7.2 ± 0.9	4.6 ± 0.6	5.0 ± 0.6
UMP		$2.4e^5 \pm 1.5e^5$	0.68	−7.34	26.9	4.2 ± 2.6
		$7.5e^4 \pm 3.8e^4$	−2.3	−6.63	14.6	13.3 ± 6.8
		$1.5e^5 \pm 9.3e^4$	−3.0	−7.03	13.4	6.7 ± 4.2
		$1.0e^5 \pm 5.3e^4$	7.9	−6.84	49.5	10 ± 5.3

[a] n = number of sites.
[b] K_a = association constant.
[c] ΔH° = binding enthalpy.
[d] ΔG° = Gibbs free energy.
[e] ΔS° = binding entropy.
[f] K_d = dissociation constant.

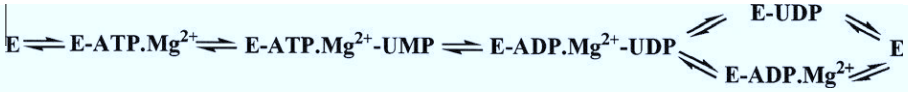

Fig. 8. Proposed kinetic mechanism for *Mt*UMPK.

The cooperative kinetics with respect to ATP, activation by GTP, and inhibition by UTP, showed that *Mt*UMPK is an allosteric enzyme that is subject to a complex control by these metabolites. The results here described also show that *Mt*UMPK belongs to the *K* system. This term was originally proposed by Monod et al. [47], in which the enzyme exists at equilibrium between two states with the same catalytic activities, but different substrate affinities (T of low affinity, and R of high affinity). In the absence of effectors, ATP has a positive heterotropic effect on UMP binding to *Mt*UMPK to form the catalytically competent ternary complex. This degree of cooperativity is decreased in the presence of GTP as there is a lowering of the Hill coefficient value, and a decrease in $K_{0.5}$ value for ATP, thereby suggesting increased ATP affinity for *Mt*UMPK. This model may also be applicable to UTP inhibition, in which binding of UTP displaces the equilibrium for the state with lower affinity for ATP with no effect on the Hill coefficient and maximum velocity. Moreover, as UTP is an uncompetitive inhibitor towards UMP, it appears that UTP can have a dual inhibitory effect on *Mt*UMPK enzyme activity depending on which substrate is varied. The results on *Mt*UMPK mode of action show that its cooperativity is more pronounced than that observed for other UMPKs (n values of 1.28–2.5) [19,21,43]. In general, the Hill coefficient does not represent the actual number of sites, unless the cooperativity is high [35]. Our findings show that the n value of ATP (3.9) for tetrameric *Mt*UMPK indicates strong positive cooperativity and it may correspond to the actual number of protomers. Activation of *Mt*UMPK by GTP and feedback inhibition by UTP imply a role for this enzyme in coordinating the synthesis of purine versus pyrimidine nucleoside triphosphates, and highlights the likely relevance of UMPK in the metabolism of *M. tuberculosis*.

The currently available repertoire of antimycobacterial agents reveals only a handful of comprehensively validated targets, namely RNA polymerase, DNA gyrase, NADH-dependent enoyl-ACP reductase, and ATP synthase [48]. The complete genome sequencing of *M. tuberculosis* H37Rv strain has accelerated the study and validation of molecular targets aiming at the rational design of anti-TB drugs [23]. The target-based rational design of new agents with anti-TB activity includes functional and structural efforts. However, the first step to enzyme target validation must include experimental data demonstrating that a gene predicted by *in silico* analysis to encode a particular protein catalyzes the proposed chemical reaction. Moreover, it has recently been pointed out that recognition of the limitations of high-throughput screening approaches in the discovery of candidate drugs has rekindled interest in rational design methods [8]. Understanding the mode of action of *Mt*UMPK will inform us on how to better design inhibitors targeting this enzyme with potential therapeutic application in TB chemotherapy. Accordingly, it is hoped that the results here described may be useful to the rational design of anti-TB agents and that they may contribute to our understanding of the biology of *M. tuberculosis*.

References

[1] C. Dye, S. Scheele, P. Dolin, V. Pathania, M.C. Raviglione, J. Am. Med. Assoc. 282 (1999) 677–686.
[2] World Health Organization, Global Tuberculosis Control: A Short Update to the 2009 Report, 2010.
[3] W.W. Yew, C.C. Leung, Respirology 13 (2008) 21–46.
[4] A.A. Velayati, P. Farnia, M.R. Masjedi, T.A. Ibrahim, P. Tabarsi, R.Z. Haroun, H.O. Kuan, J. Ghanavi, P. Farnia, M. Varahram, Eur. Respir. J. 34 (2009) 1202–1203.
[5] R.G. Ducati, L.A. Basso, D.S. Santos, Curr. Drug Targets 8 (2007) 423–435.
[6] J.G. Robertson, Biochemistry 44 (2005) 5561–5571.
[7] J.G. Robertson, Curr. Opin. Struct. Biol. 17 (2007) 674–679.
[8] J.E. Ladbury, G.K. Klebe, E. Freire, Nat. Rev. Drug Discov. 9 (2010) 23–27.
[9] C. Meier, L.G. Carter, S. Sainsbury, E.J. Mancini, R.J. Owens, D.I. Stuart, R.M. Esnouf, J. Mol. Biol. 381 (2008) 1098–1105.
[10] G.E. Shambaugh, Am. J. Clin. Nutr. 32 (1979) 1290–1297.
[11] C. Marco-Marín, F. Gil-Ortiz, V. Rubio, J. Mol. Biol. 352 (2005) 438–454.
[12] H. Yan, M.D. Tsai, Adv. Enzymol. Relat. Areas Mol. Biol. 73 (1999) 103–134.
[13] P. Briozzo, C. Evrin, P. Meyer, L. Assairi, N. Joly, O. Barzu, A. Gilles, J. Biol. Chem. 280 (2005) 25533–25540.
[14] H.J. Müller-Dieckmann, G.E. Schulz, J. Mol. Biol. 236 (1994) 361–367.
[15] J. Liou, G.E. Dutschman, W. Lam, Z. Jiang, Y. Cheng, Cancer Res. 62 (2002) 1624–1631.
[16] K. Scheffzek, W. Kliche, L. Wiesmüller, J. Reinstein, Biochemistry 35 (1996) 9716–9727.
[17] L. Serina, C. Blondin, E. Krin, O. Sismeiro, A. Danchin, H. Sakamoto, A.M. Gilles, O. Bârzu, Biochemistry 34 (1995) 5066–5074.
[18] C. Gagyi, N. Bucurenci, O. Sîrbu, G. Labesse, M. Ionescu, A. Ofiteru, L. Assairi, S. Landais, A. Danchin, O. Bârzu, A. Gilles, Eur. J. Biochem. 270 (2003) 3196–3204.
[19] F. Fassy, O. Krebs, M. Lowinski, P. Ferrari, J. Winter, V. Collard-Dutilleul, Biochem. J. 384 (2004) 619–627.
[20] K.S. Jensen, E. Johansson, K.F. Jensen, Biochemistry 46 (2007) 2745–2757.
[21] L. Egeblad-Welin, M. Welin, L. Wang, S. Eriksson, FEBS J. 274 (2007) 6403–6414.
[22] K.A. Kantardjieff, C. Vasquez, P. Castro, N.M. Warfel, B.S. Rho, T. Lekin, C.Y. Kim, B.W. Segelke, T.C. Terwilliger, B. Rupp, Acta Crystallogr. D: Biol. Crystallogr. 61 (2005) 355–364.
[23] S.T. Cole, R. Brosch, J. Parkhill, T. Garnier, C. Churcher, D. Harris, S.V. Gordon, K. Eiglmeier, S. Gas, C.E. Barry, F. Tekaia, K. Badcock, D. Basham, D. Brown, T. Chillingworth, R. Connor, R. Davies, K. Devlin, T. Feltwell, S. Gentles, N. Hamlin, S. Holroyd, T. Hornsby, K. Jagels, A. Krogh, J. McLean, S. Moule, L. Murphy, K.

Oliver, J. Osborne, M.A. Quail, M.A. Rajandream, J. Rogers, S. Rutter, K. Seeger, J. Skelton, R. Squares, S. Squares, J.E. Sulston, K. Taylor, S. Whitehead, B.G. Barrell, Nature 393 (1998) 537–544.
[24] D. Robertson, P. Carroll, T. Parish, Tuberculosis 87 (2007) 450–458.
[25] K. Yamanaka, T. Ogura, H. Niki, S. Hiraga, J. Bacteriol. 174 (1992) 7517–7526.
[26] J.C. Smallshaw, R.A. Kelln, Genetics (Life Sci. Adv.) 11 (1992) 59–65.
[27] J. Sambrook, D.W. Russel, Molecular Cloning: A Laboratory Manual, Spring Harbor Laboratory Press, New York, 2001.
[28] U.K. Laemmli, Nature 227 (1970) 680–685.
[29] M.M. Bradford, Anal. Biochem. 72 (1976) 248–254.
[30] B. Monson de Souza, M.S. Palma, Biochim. Biophys. Acta 1778 (2008) 2797–2805.
[31] H. Chassaigne, R. Lobinski, Analyst 123 (1998) 2125–2130.
[32] D.A. Benson, I. Karsch-Mizrachi, D.J. Lipman, J. Ostell, E.W. Sayers, Nucleic Acids Res. 37 (2009) D26–D31.
[33] J.D. Thompson, D.G. Higgins, T.J. Gibson, Nucleic Acids Res. 22 (1994) 4673–4680.
[34] J.S. Oliveira, C.A. Pinto, L.A. Basso, D.S. Santos, Protein Expr. Purif. 22 (2001) 430–435.
[35] I. Segel, Enzyme Kinetics, Behavior and Analysis of Rapid Equilibrium and Steady-State Enzyme Systems, John Wiley and Sons, New York, 1975.
[36] R.A. Copeland, Evaluation of Enzyme Inhibitors in Drug Discovery, John Wiley and Sons, Inc., New Jersey, 2005.
[37] R.G. Bates, H.B. Hetzer, J. Phys. Chem. 65 (1961) 667–671.
[38] H. Fukada, K. Takahashi, Proteins 33 (1998) 159–166.
[39] M.C. Pinna, A. Salis, M. Monduzzi, B.W. Ninham, J. Phys. Chem. B 109 (2005) 5406–5408.
[40] Y. Zhang, P.S. Cremer, Curr. Opin. Chem. Biol. 10 (2006) 658–663.
[41] P. Meyer, C. Evrin, P. Briozzo, N. Joly, O. Bârzu, A. Gilles, J. Biol. Chem. 283 (2008) 36011–36018.
[42] L. Serina, N. Bucurenci, A.M. Gilles, W.K. Surewicz, H. Fabian, H.H. Mantsch, M. Takahashi, I. Petrescu, G. Batelier, O. Bârzu, Biochemistry 35 (1996) 7003–7011.
[43] C. Evrin, M. Straut, N. Slavova-Azmanova, N. Bucurenci, A. Onu, L. Assairi, M. Ionescu, N. Palibroda, O. Bârzu, A. Gilles, J. Biol. Chem. 282 (2007) 7242–7253.
[44] S.E. Lee, S.Y. Kim, C.M. Kim, M. Kim, Y.R. Kim, K. Jeong, H. Ryu, Y.S. Lee, S.S. Chung, H.E. Choy, J.H. Rhee, Infect. Immun. 75 (2007) 2795–2801.
[45] C. Thum, C.Z. Schneider, M.S. Palma, D.S. Santos, L.A. Basso, J. Bacteriol. 191 (2009) 2884–2887.
[46] N. Bucurenci, H. Sakamoto, P. Briozzo, N. Palibroda, L. Serina, R.S. Sarfati, G. Labesse, G. Briand, A. Danchin, O. Bărzu, A.M. Gilles, J. Biol. Chem. 271 (1996) 2856–2862.
[47] J. Monod, J. Wyman, J.P. Changeux, J. Mol. Biol. 12 (1965) 88–118.
[48] T.S. Balganesh, P.M. Alzari, S.T. Cole, Trends Pharmacol. Sci. 29 (2008) 576–581.

Anexo E

RECOMBINANT *Escherichia coli* GMP REDUCTASE: KINETIC, CATALYTIC AND CHEMICAL MECHANISMS, AND THERMODYNAMICS OF ENZYME-LIGAND BINARY COMPLEX FORMATION.

Leonardo Krás Borges Martinelli, Rodrigo Gay Ducati, Leonardo Astolfi Rosado, Ardala Breda, Bruna Pelegrim Selbach, Diógenes Santiago Santos, Luiz Augusto Basso

Artigo publicado (Epub)
Molecular Biosystems, 2011, Fev 07.
DOI: 10.1039/c0mb00245c

Molecular BioSystems

Cite this: DOI: 10.1039/c0mb00245c

www.rsc.org/molecularbiosystems

PAPER

Recombinant *Escherichia coli* GMP reductase: kinetic, catalytic and chemical mechanisms, and thermodynamics of enzyme–ligand binary complex formation

Leonardo Krás Borges Martinelli,[ab] Rodrigo Gay Ducati,[a] Leonardo Astolfi Rosado,[ac] Ardala Breda,[ab] Bruna Pelegrim Selbach,[ab] Diógenes Santiago Santos*[ab] and Luiz Augusto Basso*[ab]

Received 22nd October 2010, Accepted 18th January 2011
DOI: 10.1039/c0mb00245c

Guanosine monophosphate (GMP) reductase catalyzes the reductive deamination of GMP to inosine monophosphate (IMP). GMP reductase plays an important role in the conversion of nucleoside and nucleotide derivatives of guanine to adenine nucleotides. In addition, as a member of the purine salvage pathway, it also participates in the reutilization of free intracellular bases. Here we present cloning, expression and purification of *Escherichia coli guaC*-encoded GMP reductase to determine its kinetic mechanism, as well as chemical and thermodynamic features of this reaction. Initial velocity studies and isothermal titration calorimetry demonstrated that GMP reductase follows an ordered bi–bi kinetic mechanism, in which GMP binds first to the enzyme followed by NADPH binding, and $NADP^+$ dissociates first followed by IMP release. The isothermal titration calorimetry also showed that GMP and IMP binding are thermodynamically favorable processes. The pH-rate profiles showed groups with apparent p*K* values of 6.6 and 9.6 involved in catalysis, and p*K* values of 7.1 and 8.6 important to GMP binding, and a p*K* value of 6.2 important for NADPH binding. Primary deuterium kinetic isotope effects demonstrated that hydride transfer contributes to the rate-limiting step, whereas solvent kinetic isotope effects arise from a single protonic site that plays a modest role in catalysis. Multiple isotope effects suggest that protonation and hydride transfer steps take place in the same transition state, lending support to a concerted mechanism. Pre-steady-state kinetic data suggest that product release does not contribute to the rate-limiting step of the reaction catalyzed by *E. coli* GMP reductase.

Introduction

Purine nucleoside and nucleotide biosynthesis is a fundamental and well-established pathway in the metabolism of avian, mammalian and microbial cells.[1] Guanosine monophosphate (GMP) reductase (NADPH:GMP oxidoreductase; EC 1.6.6.8) catalyzes the reductive deamination of GMP to inosine monophosphate (IMP)[2] (Fig. 1). GMP reductase plays an important role in the conversion of nucleoside and nucleotide derivatives of guanine (Gua) to adenine (Ade) nucleotides, and in the maintenance of the intracellular balance between Gua and Ade nucleotides.[3] As part of the purine salvage pathway, it also participates in the reutilization of free intracellular bases.[2] In *Escherichia coli*, the *guaC*-encoded GMP reductase is induced by GMP,[4] and is also regulated by cyclic adenosine monophosphate (cAMP),[5] by the intracellular ratio of purine nucleotides, and by glutamine and its analogs.[6] In addition to its role as an enzyme for the interconversion of purine nucleotides, GMP reductase provides a nitrogen source *via* its deamination activity.[6] In addition, it is inhibited by adenosine triphosphate (ATP) and is reactivated by the presence of guanosine triphosphate (GTP).[3] GMP reductase is not normally necessary for efficient bacterial growth, since the lack of its activity leaves the *de novo* synthesis of purine nucleotides *via* IMP intact.[4] However, when the route of IMP is blocked, GMP reductase activity becomes necessary to provide AMP when Gua and its derivatives are the purine sources.[7] In purine auxotroph mutants that are blocked prior to the formation of IMP, *guaC* mutations prevent the use of Gua or xanthine derivatives as sources of purine.[3]

[a] *Centro de Pesquisas em Biologia Molecular e Funcional (CPBMF), Instituto Nacional de Ciência e Tecnologia em Tuberculose (INCT-TB), Pontifícia Universidade Católica do Rio Grande do Sul (PUCRS), 6681/92-A Av. Ipiranga, 90619-900, Porto Alegre, RS, Brazil. E-mail: luiz.basso@pucrs.br, diogenes@pucrs.br; Fax: +55 51-33203629; Tel: +55 51-33203629*
[b] *Programa de Pós-Graduação em Biologia Celular e Molecular, Pontifícia Universidade Católica do Rio Grande do Sul (PUCRS), Porto Alegre, RS, Brazil*
[c] *Programa de Pós-Graduação em Medicina e Ciências da Saúde, Pontifícia Universidade Católica do Rio Grande do Sul (PUCRS), Porto Alegre, RS, Brazil*

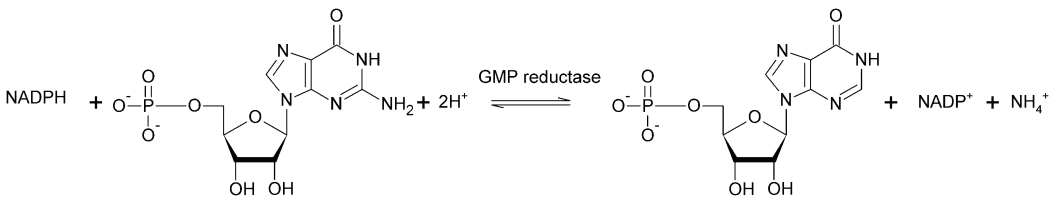

Fig. 1 Chemical reaction catalyzed by GMP reductase.

GMP reductases have been found and characterized in a number of organisms, including *E. coli*,[3] *Salmonella typhimurium*,[6] *Artemia salina*,[8] *Leishmania donovani*,[9] and *Homo sapiens*.[10] The human homologue is responsible for the only known metabolic step by which Gua nucleotides can be converted to the pivotal precursor of both Ade and Gua nucleotides.[11] Human deficiency of this enzyme has not been related to any known disease, which can be explained by several possibilities, the main one being that the lack of this enzyme is invariably lethal.[12] Human GMP reductase has been identified as two isoenzymes, hGMPR1[11] and hGMPR2[2] (the second being shown to promote monocytic differentiation of HL-60 leukemia cells).[13] Salvatore and co-workers[14] studied the role of GMP reductase in non-shivering thermogenesis, a process required for the survival of rodents during cold stress, and determined that the enzyme plays a critical role in this process, evidenced by significant increases in its expression during cold exposure. GMP reductases have been shown to be involved in various biological functions, including maintenance of the balance of purine nucleotides,[3] as a possible target for antileishmanial[9] and anticancer drugs,[15] and involvement in human cell differentiation.[13] Moreover, GMP reductases are similar across the species at the amino acid level.[16] Accordingly, the need to further investigate *E. coli* GMP reductase to elucidate the kinetic, catalytic and chemical mechanisms to provide a basis on which to design species-specific inhibitors is warranted. Understanding the mode of action of *E. coli* GMP reductase may also be useful to chemical biologists interested in designing function-based chemical compounds to elucidate the biological role of this enzyme in the context of whole *E. coli* cells. In addition, availability of recombinant *E. coli* GMP reductase may provide a tool for determination of substrate specificity of cyclic nucleotide phosphodiesterases (PDEs).

Results

Amplification and cloning of the *E. coli guaC* gene

A PCR amplification product consistent with the expected size for the *E. coli guaC* (1038 bp) coding sequence was detected by agarose gel electrophoresis (data not shown), purified, and cloned into the pCR-Blunt vector. The cloned sequence was extracted from the cloning vector, purified and subcloned into the pET-23a(+) expression vector. DNA sequence identity of the fragment cloned in the expression vector was confirmed by enzyme restriction analysis and automated DNA sequencing.

Expression and purification of recombinant GMP reductase

The recombinant pET-23a(+)::*guaC* plasmid was transformed into *E. coli* BL21(DE3) host cells by electroporation.

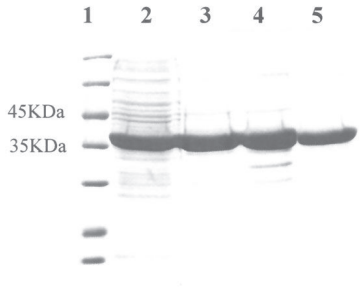

Fig. 2 SDS-PAGE (12%) analysis for the three chromatographic steps of purification of recombinant *E. coli* GMP reductase that yielded homogeneous protein. Lane 1, Molecular Weight Protein Marker (Fermentas); lane 2, crude extract; lane 3, Q-Sepharose anion exchange column; lane 4, Sephacryl S-200 size exclusion; lane 5 MonoQ High Resolution anion exchange column.

Sodium dodecyl sulfate–polyacrylamide gel electrophoresis (SDS-PAGE) analysis revealed expression of a protein in the soluble fraction with an apparent subunit molecular mass of ~38 kDa, consistent with *E. coli* GMP reductase (37 383.6 Da). The expression of the recombinant protein was monitored at different periods of cell growth after an OD_{600nm} value of approximately 0.4–0.6 was reached. The best result was achieved at 24 h of cell growth at 37 °C in LB medium without isopropyl-β-D-thio-galactopyranoside (IPTG) induction (data not shown). Recombinant GMP reductase was efficiently purified to homogeneity (Fig. 2) by a three-step purification protocol yielding 45 mg of homogeneous recombinant GMP reductase from 2.8 g of cells (Table 1). Homogeneous enzyme was stored at −80 °C with no loss of activity.

Quaternary structure analysis of *E. coli* GMP reductase

The subunit molecular mass of *E. coli* GMP reductase was determined as 37 382 Da by electrospray ionization mass spectrometry (ESI-MS) and suggests that there was no removal of the N-terminal methionine residue (theoretical molecular mass of 37 383.6 Da). Amino acid sequencing of *E. coli* GMP reductase confirmed approximately 85% of the sequence.

The protein native molecular mass was determined by gel filtration chromatography and revealed a single peak with elution volume consistent with a molecular mass of 155.98 kDa (data not shown), indicating that *E. coli* GMP reductase is a tetramer in solution.

Determination of apparent steady-state kinetic constants and initial velocity pattern

The determination of the apparent steady-state kinetic constants was performed using either GMP or NADPH as

Table 1 Purification protocol of recombinant *E. coli* GMP reductase (2.8 g wet cell paste)

Purification step	Total protein (mg)	Total enzyme activity (U)	Specific activity (U mg^{-1})	Purification fold	Yield (%)
Crude extract	210	89	0.47	1.0	100
Q-Sepharose FF	81	68	0.84	2	76
Sephacryl S-200	47	20	0.44	1.1	23
Mono-Q	45	30	0.66	1.6	34

the variable substrate, and the data were fitted to eqn (1) (hyperbolic equation), which indicates that the GMP reductase catalyzed reaction follows Michaelis–Menten kinetics.[17] The apparent K_M and V_{max} values for GMP (at 100 μM NADPH fixed concentration) were, respectively, 6.9 (±0.3) μM and 0.065 (±0.001) U mg^{-1}; and the apparent K_M and V_{max} values for NADPH (at 100 μM GMP fixed concentration) were, respectively, 11.1 (±1.2) μM and 0.40 (±0.01) U mg^{-1}. No *E. coli* GMP reductase activity could be detected for varying NADH concentrations (up to 200 μM) in the presence of saturating concentration of GMP. In addition, no enzymatic activity could be detected when, in the presence of saturating levels of NADPH, varying AMP concentrations (up to 1000 μM) were substituted for GMP.

To both determine the true steady-state kinetic parameters and GMP reductase enzyme mechanism, initial velocity as a function of substrate concentration (either GMP or NADPH) was plotted as a linear function of reciprocal of initial velocity against the reciprocal of substrate concentration (double-reciprocal or Lineweaver–Burk plot). The double-reciprocal plots showed a family of lines intersecting to the left of the *y*-axis (Fig. 3), which is consistent with ternary complex formation and a sequential mechanism. Data were plotted in reciprocal form and fitted to the equation for a sequential initial velocity pattern (eqn (2)), yielding the following values for the true steady-state kinetic parameters: k_{cat} = 0.28 (±0.02) s^{-1}, K_{GMP} = 5.5 (±1.0) μM, K_{NADPH} = 14.7 (±2.5) μM, k_{cat}/K_{GMP} = 5.1 (±0.9) × 10^4 M^{-1} s^{-1}, and k_{cat}/K_{NADPH} = 1.9 (±0.3) × 10^4 M^{-1} s^{-1}.

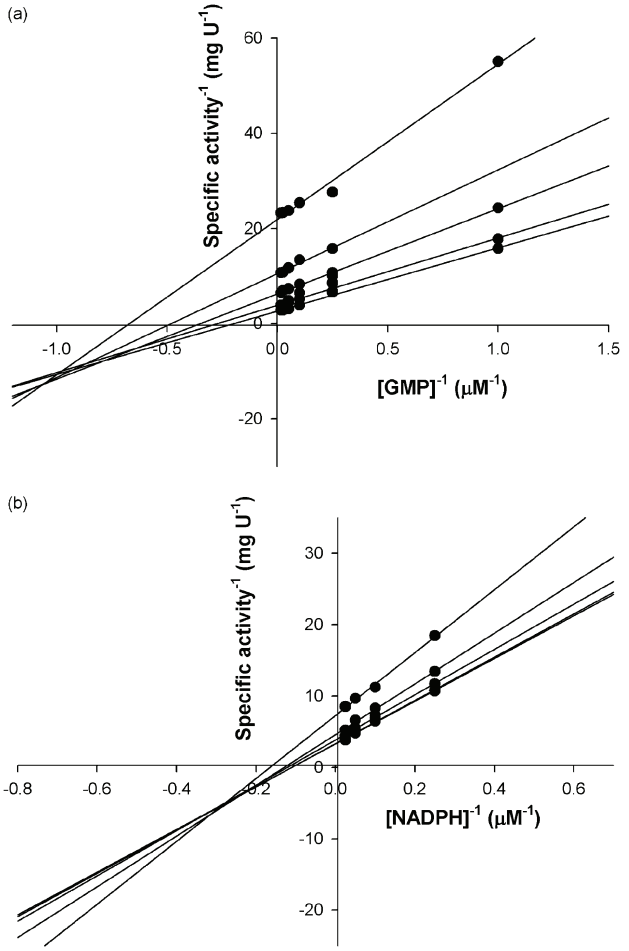

Fig. 3 Intersecting initial velocity patterns for GMP reductase using either GMP (a) or NADPH (b) as the variable substrate. Each curve represents varied-fixed levels of the cosubstrate.

Isothermal titration calorimetry (ITC)

Isothermal titration calorimetry (ITC) experiments were carried out to both determine the relative affinities of substrate(s)/product(s) binding to *E. coli* GMP reductase and provide support for the proposed enzyme mechanism. ITC measurements of ligand equilibrium binding to the enzyme followed the amount of heat generated or consumed upon formation of the binary complex, at constant temperature and pressure. The measure of heat released (exothermic process) upon binding of a ligand provides the binding enthalpy (ΔH)

Table 2 ITC measurements of either GMP or IMP binding to *E. coli* GMP reductase. ΔG = Gibbs free energy changes; ΔS = entropy changes; ΔH = enthalpy changes; K_d = dissociation constants

	Subunit 1	Subunit 2	Subunit 3	Subunit 4
	GMP			
ΔG (kcal mol^{-1})	−5.5 (±8.6)	−6.6 (±5.2)	−6.2 (±9.1)	−5.1 (±6.1)
ΔS (cal mol^{-1} deg^{-1})	−35.1 (±55.4)	133 (±105)	−53 (±78.4)	−4.1 (±4.8)
ΔH (cal mol^{-1})	−16 (±9) × 10^3	3.3 (±3.2) × 10^4	−2.2 (±7.2) × 10^4	−6.3 (±1.1) × 10^3
K_d (μM)	87 (±130)	50 (±39)	15 (±22)	160 (±198)
	IMP			
ΔG (kcal mol^{-1})	−5.6 (±8.5)	−5.3 (±6.6)	−6.9 (±7.5)	−6.2 (±9.0)
ΔS (cal mol^{-1} deg^{-1})	−23 (±34)	100 (±125)	−115 (±125)	−5.4 (±7.8)
ΔH (cal mol^{-1})	−12 (±3) × 10^3	2.4 (±1.9) × 10^4	−1.0 (±2.7) × 10^4	−7.8 (±9.0) × 10^3
K_d (μM)	61 (±92)	142 (±177)	7.8 (±8.5)	26 (±37)

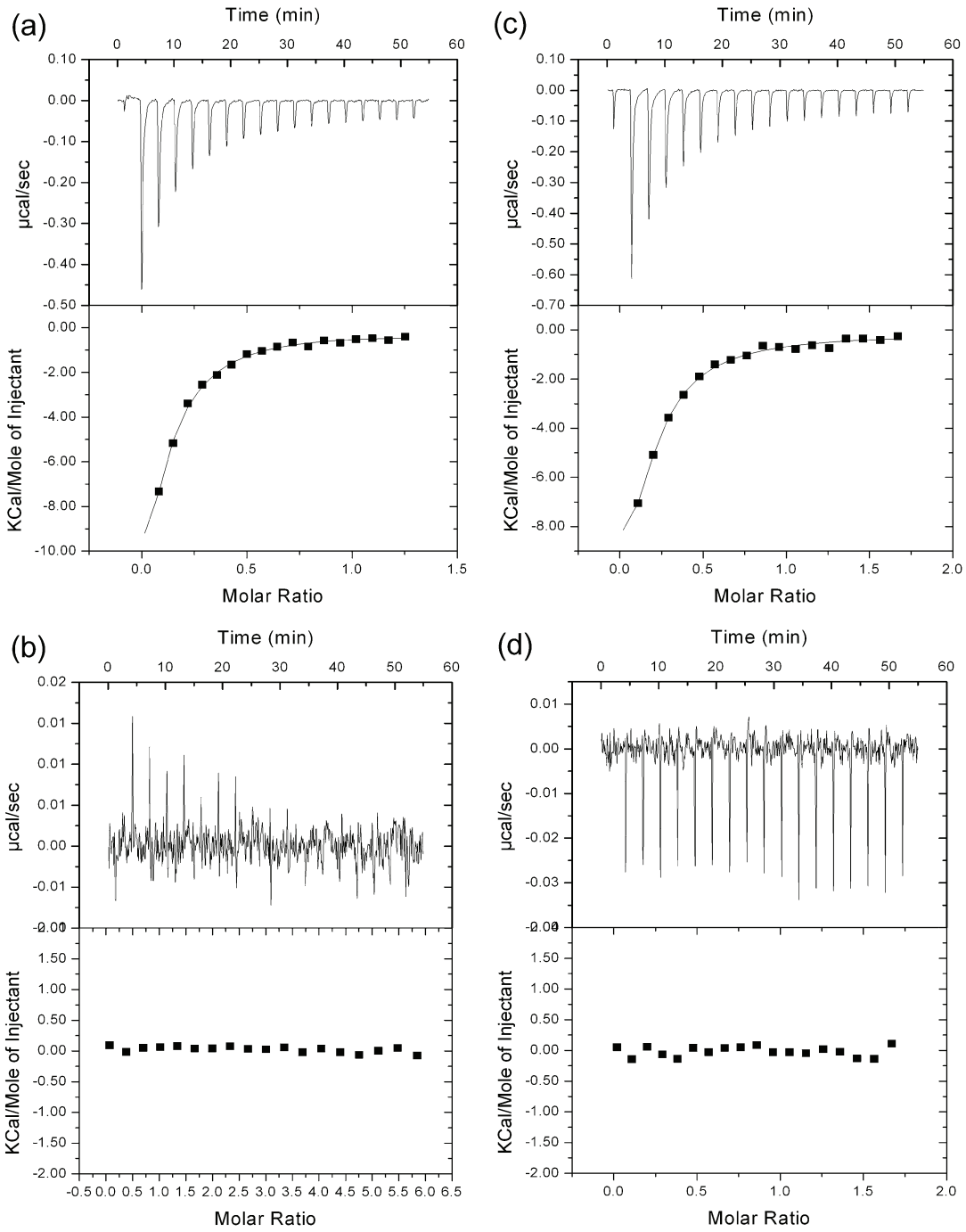

Fig. 4 Isothermal titration calorimetry (ITC) analysis of *E. coli* GMP reductase titration with GMP (a), NADPH (b), IMP (c), and $NADP^+$ (d). The top panels show raw data of the heat pulses resulting from titration of *E. coli* GMP reductase. The bottom panels show the integrated heat pulses, normalized per mole of injectant as a function of the molar ratio (ligand concentration/*E. coli* GMP reductase concentration). These binding curves were best fitted to a sequential binding sites model equation.

of the process, an estimate for the stoichiometry of the interaction (n) and the equilibrium binding constant (K_{eq}). These values allow the Gibbs free energy (ΔG) and the entropy (ΔS) of the process to be calculated.

The ITC data for binding of ligands to *E. coli* GMP reductase are summarized in Table 2. The ITC results showed significant heat changes upon binding of GMP to free *E. coli* GMP reductase enzyme (Fig. 4a), and data fitting to the sequential binding sites model yielded a value of 4 for n, consistent with the quaternary structure determined by gel filtration. This model provides values of ΔH, ΔS, K_{eq} for the binding sites of each subunit. The binding of IMP to the free enzyme also showed significant heat changes (Fig. 4c), and the best fit was also to the sequential binding sites model yielding an n value of 4. No heat change upon the addition of either NADPH or $NADP^+$ to *E. coli* GMP reductase could be detected, suggesting that neither ligand can bind to free enzyme (Fig. 4b and d).

Multiple sequence alignment and *E. coli* GMPR structural analysis

Sequence alignment of GMP reductases from *E. coli* strain K12 (GMPR NC_010473.1) and both human isoforms (hGMPR1 NP_006868.3 and hGMPR2 NP_001002000.1) was performed using the CLUSTALW program.[18] The sequence alignment reveals that the homologues present high similarity (Fig. 5). At the amino acid level, *E. coli* GMP reductase is 65% identical with hGMPR1 and 68% identical with hGMPR2. The proposed catalytic site loop that acts as a lid that closes upon GMP binding is comprised of the conserved residues 179–187[16] (Fig. 5). Based on structural comparison and model building for hGMPR2, it has been suggested that the amino acid residues 129–133 are involved in NADPH binding.[16] These residues are all conserved in *E. coli* GMP reductase (Fig. 5). In addition, the residues involved in GMP binding, which are located in a flexible binding region of hGMPRs,[16] are all conserved in *E. coli* GMP reductase (residues 268–290). Moreover, the N7 of the guanine moiety of GMP makes hydrogen bonds with Met269 and the O6 atom with Ser270 and Gly290, which are all conserved (Fig. 5). It has been shown for hGMPR1 that Ser288 makes hydrogen bonds with N1 and N2 atoms of guanine base.[16] However, this residue is not conserved in *E. coli* GMP reductase, being replaced by Ala288 (Fig. 5). Amino acid residues involved in interactions with the ribose (Asp219 and Arg286) and phosphate (Ser184, Gly221, Gly242, and Gly243) moieties of GMP are all conserved. A disulfide bond between Cys68 and Cys95 side chains has been observed in the crystal structure of hGMPR2, and it has been proposed that it may play a role in stabilization of the tetramer. Interestingly, there are no corresponding residues in *E. coli* GMP reductase indicating that such a disulfide bridge plays no part in stabilization of the tetramer.

The three-dimensional model of *E. coli* GMP reductase was built by restrained-based homology modeling implemented in MODELLER9v1 using the human type 2 GMP reductase structure as a template, as described in more detail in the Experimental procedures section. The three-dimensional model of *E. coli* GMPR indicates high conservation of its tertiary structure as compared to the hGMPR2 structural template, with a RMSD value of 0.61 Å, which is in agreement with the 68% identity at the amino acid level. The model presented no stereochemical parameters violation, as evaluated by PROCHECK package (data not shown), in which 99.2% of *E. coli* GMP reductase amino acids are within allowed regions of the Ramachandran plot. Amino acids involved in GMP binding are almost all conserved in the bacterial homologue (Fig. 5). In addition, there are minor conformational deviations even for the conserved amino acid residues (Fig. 6). The H-bond network of side chains and main chains of these amino acid residues to bound GMP is maintained in both human and *E. coli* GMP reductases. A

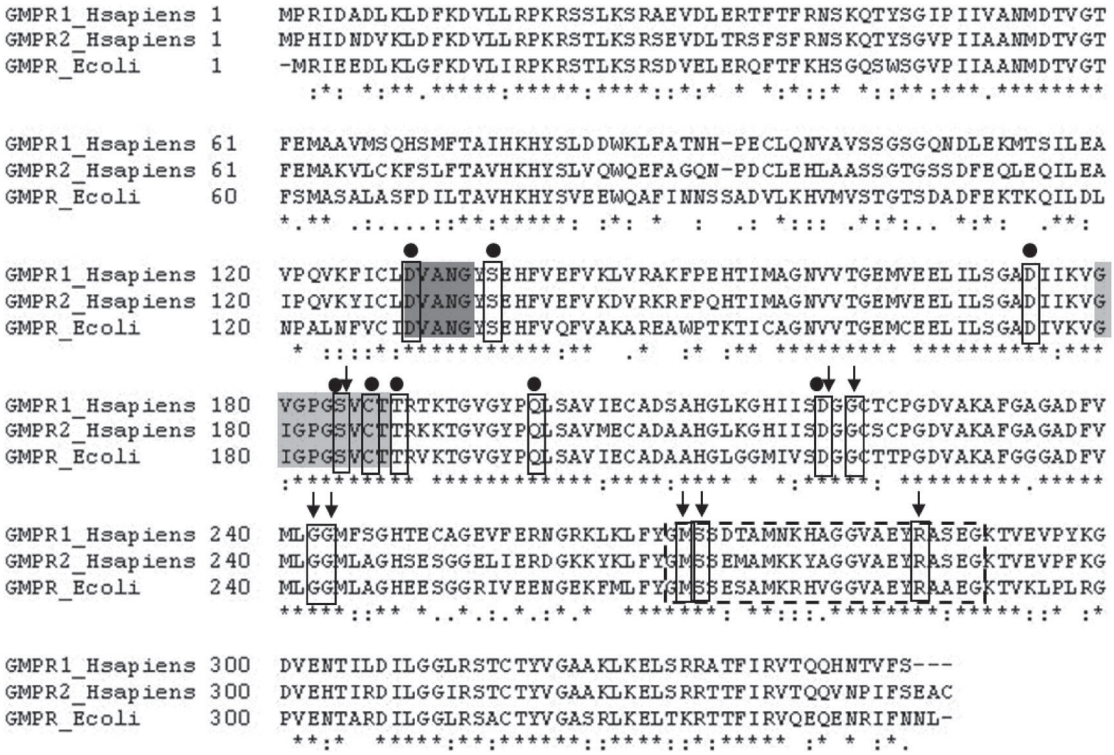

Fig. 5 Multiple sequence alignment of *E. coli* GMP reductase with both human enzymes (GMPR1_Hsapiens and GMPR2_Hsapiens) using the program CLUSTAL W. (*), (:), (.) and (–) indicate, respectively, identity, strong similarity and weak similarity among the residues. The residues in the proposed catalytic site (active site loop that acts as a lid that closes upon GMP binding) were shaded in light gray, the amino acid residues in the proposed NADPH binding site were shaded in dark gray, and amino acid residues in the GMP binding site were boxed by a dashed line. Conserved amino acid residues that are important for catalysis or binding were boxed by a solid line. Black dots above the conserved residue indicate residues involved in catalysis, and black arrows indicate residues involved in substrate binding.

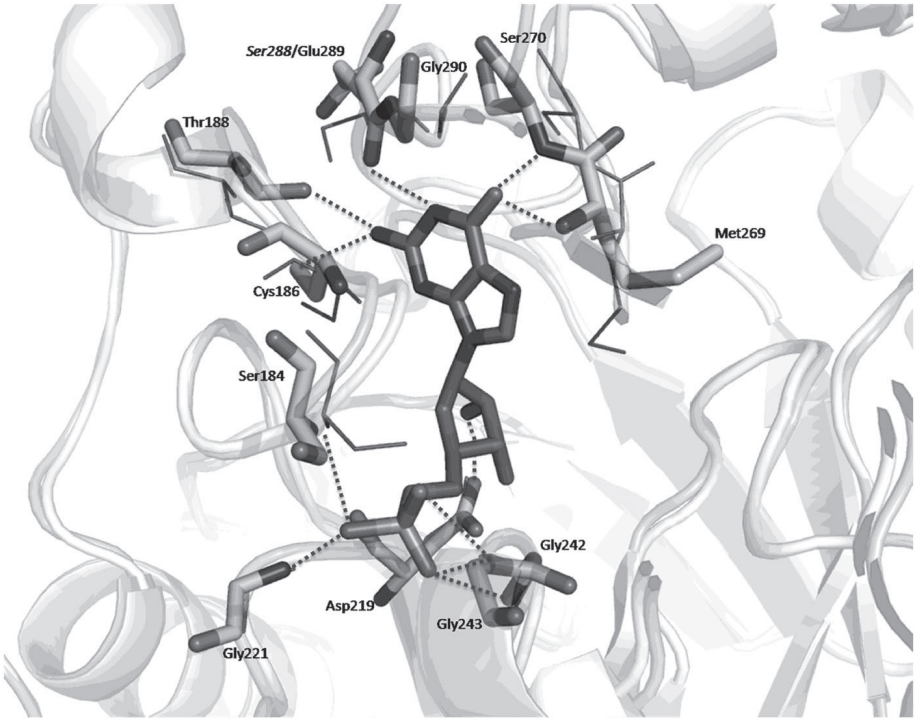

Fig. 6 *E. coli* GMP reductase model superimposed on experimentally solved the human type 2 GMP reductase (hGMPR2) structure. Amino acid residues of *E. coli* GMP reductase involved in GMP binding (light gray) and the GMP molecule (dark gray) are shown as sticks. The corresponding amino acids of the hGMPR2 template are depicted as thin gray sticks. It is noteworthy that Glu289 *E. coli* GMP reductase substitutes for Ser288 in hGMPR2 (italics). H-bonds between amino acid residues of *E. coli* GMP reductase and GMP are shown as dotted lines.

noticeable exception is the Gly290 amino acid residue that is displaced by 1.3 Å away from the substrate binding site in *E. coli* GMP reductase (Fig. 6). Therefore, there is no H-bond between Gly290 and GMP O6 atom since its distance raised from 3.12 Å in the template to 4.4 Å in *E. coli* GMP reductase. The hGMPR2 template structure indicates that the conserved Asp219 residue makes two H-bonds between its carboxyl oxygen atoms and O2′ and O3′ atoms of the GMP ribose moiety. However, our proposed model showed just one H-bond to the O2′ atom of GMP. Although Glu289 *E. coli* GMP reductase substitutes for Ser288 in hGMPR2, there is either no gain or loss of H-bonds between the amino acid side chain at this position and GMP. The H-bond between N1 of the guanine moiety of GMP and the main chain oxygen atom of Glu289 in *E. coli* GMP reductase replaces the same interaction made between the main chain oxygen atom of Ser288 in hGMPR2. The catalytic Cys186 residue that likely plays a critical role in *E. coli* GMP reductase catalysis makes an H-bond to the C2 exocyclic amino group of the guanine moiety of GMP (Fig. 6). Another H-bond is made between Thr188 side chain and the C2 exocyclic amino group of GMP (Fig. 6). Interestingly, according to the PDB coordinates of hGMPR2, there is only one H-bond that is made between Thr188 side chain and the C2 exocyclic amino group of GMP, and Cys186 side chain is H-bonded to Thr188.

pH-rate profiles

To probe for acid–base catalysis, pH dependence studies of k_{cat}, and k_{cat}/K_M for GMP and NADPH were performed. The pH-rate profiles are shown in Fig. 7. The bell-shaped pH-rate data for k_{cat} were fitted to eqn (3), yielding apparent pK values of 6.6 (±0.6) and 9.6 (±1.2) (Fig. 7a), with slopes of +1 for the acidic limb and −1 for the basic limb. These results indicate participation of a single ionizable group in each limb, in which protonation of a group with an apparent pK value of 6.6 and deprotonation of another group with a pK value of 9.6 play critical roles in *E. coli* GMP reductase enzyme catalysis. The pH-rate data for of k_{cat}/K_{GMP} were fitted to eqn (4) and indicate that both protonation of two groups with apparent pK values of 7.1 (±0.8) and deprotonation of two groups with apparent pK values of 8.6 (±1.1) (Fig. 7b) are required for binding of GMP. The data of the pH-rate profile for k_{cat}/K_{NADPH} were fitted to eqn (5), which suggests that protonation of two groups with apparent pK values of 6.2 (±1.0) abolish NADPH binding to *E. coli* GMP reductase (Fig. 7c).

Energy of activation

The energy of activation for the enzyme-catalyzed chemical reaction was assessed by measuring the dependence of k_{cat} on temperature (Fig. 8). These data were fitted to eqn (6), yielding a value of 4.4 kcal mol^{-1}, which represents the minimal amount of energy necessary to initiate the chemical reaction catalyzed by *E. coli* GMP reductase. The linearity of the Arrhenius plot (Fig. 8) also suggests that there is no change in the rate-limiting step over the temperature range utilized in the assay.

Deuterium kinetic isotope effects and proton inventory

To probe for rate-limiting steps and determine the stereospecificity of hydride transfer, measurements of primary

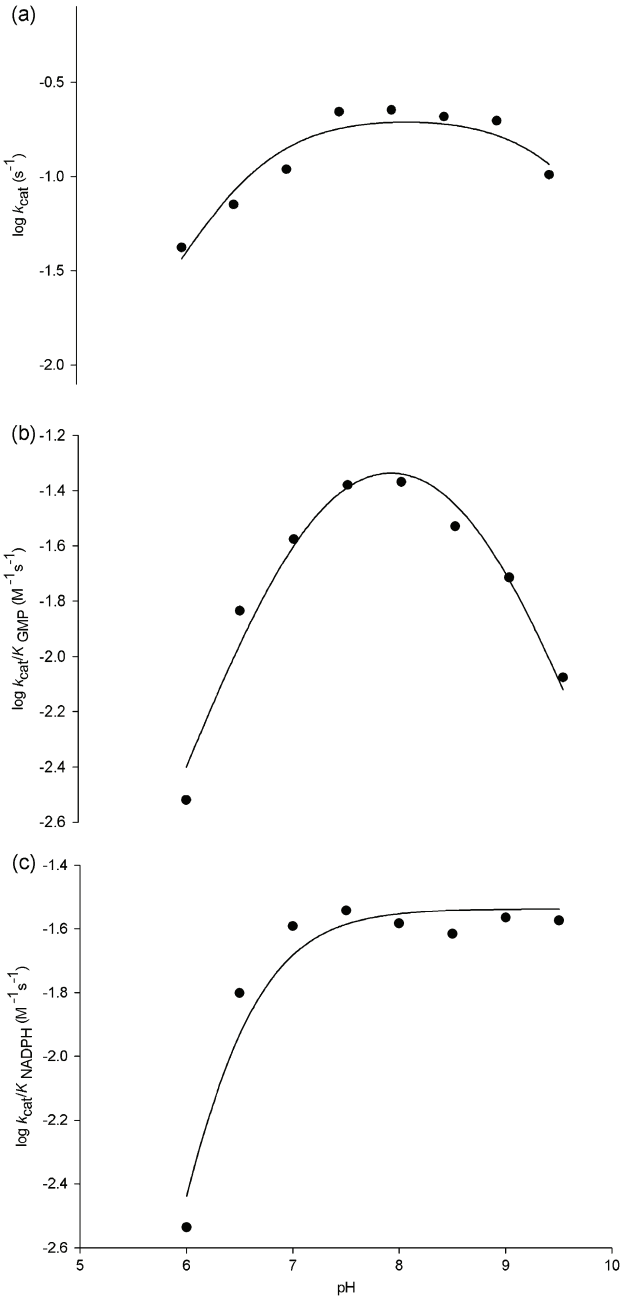

Fig. 7 Dependence of kinetic parameters on pH. (a) pH dependence of log k_{cat} data were fitted to eqn (3); (b) log k_{cat}/K_{GMP} data were fitted to eqn (4); (c) pH dependence of log k_{cat}/K_{NADPH} data were fitted to eqn (5).

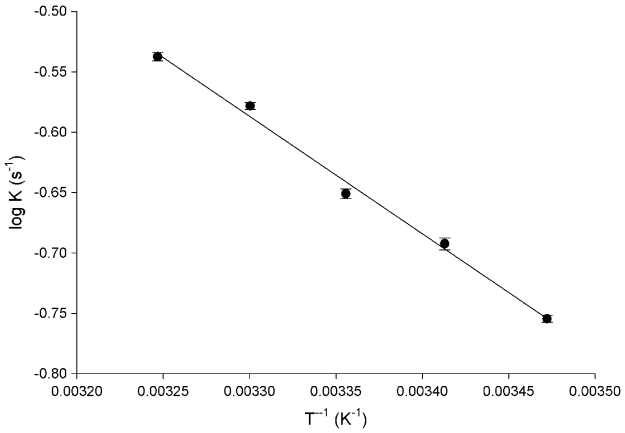

Fig. 8 Temperature dependence of log k_{cat}. Saturating concentrations of NADPH and GMP substrates were employed to measure the maximum velocity as a function of temperature ranging from 15 to 35 °C. The data were fitted to eqn (6). The linearity of the Arrhenius plot suggests that there is no change in the rate-limiting step over the temperature range utilized in the assay.

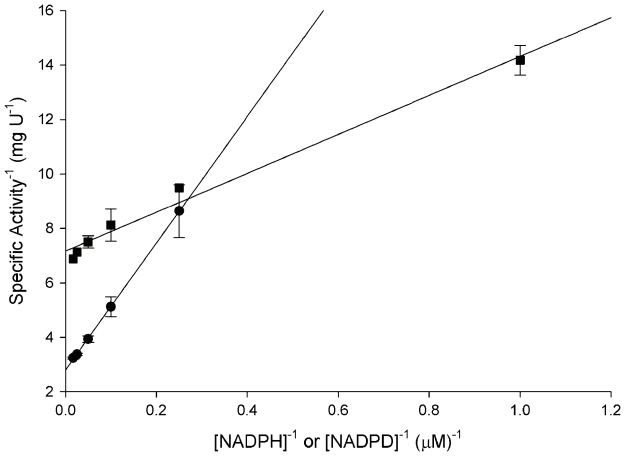

Fig. 9 Primary deuterium kinetic isotope effects using either NADPH (●) or NADPD (■) as the variable substrate in the presence of saturating concentration of GMP (100 μM). The data were fitted to eqn (7).

deuterium kinetic isotope effects were carried out (Fig. 9). The data were fitted to eqn (7) for kinetic isotope effects on both V and V/K, yielding values of 2.50 (±0.04) for $^{D}V_{NADPH}$ and 0.40 (±0.04) for $^{D}V/K_{NADPH}$ (Table 3). The corresponding values for GMP were 1.05 (± 0.06) for $^{D}V_{GMP}$ and 1.03 (± 0.07) for $^{D}V/K_{GMP}$ (Table 3).

To evaluate the contribution of proton-transfer from the solvent to the GMP reductase catalyzed reaction, solvent kinetic isotope effects were determined and the data fitted to eqn (7). The following values were found for the solvent kinetic isotope effects (Table 3): $^{D_2O}V_{NADPH}$ = 0.99 (±0.03)

Table 3 Kinetic isotope effects for *E. coli* GMP reductase[a]

Parameter	Isotope effect
$^{D}V/K_{NADPH}$	0.40 ± 0.04
$^{D}V_{NADPH}$	2.50 ± 0.04
$^{D}V/K_{GMP}$	1.03 ± 0.07
$^{D}V_{GMP}$	1.05 ± 0.06
$^{D_2O}V/K_{NADPH}$	0.67 ± 0.09
$^{D_2O}V_{NADPH}$	0.99 ± 0.03
$^{D_2O}V/K_{GMP}$	0.82 ± 0.03
$^{D_2O}V_{GMP}$	1.30 ± 0.01
$^{D_2O}V/K_{NADPD}$	1.50 ± 0.17
$^{D_2O}V_{NADPD}$	1.00 ± 0.02
$^{D}K_{eq}$	0.82

[a] Value ± standard error obtained upon data fitting to the appropriate equations.

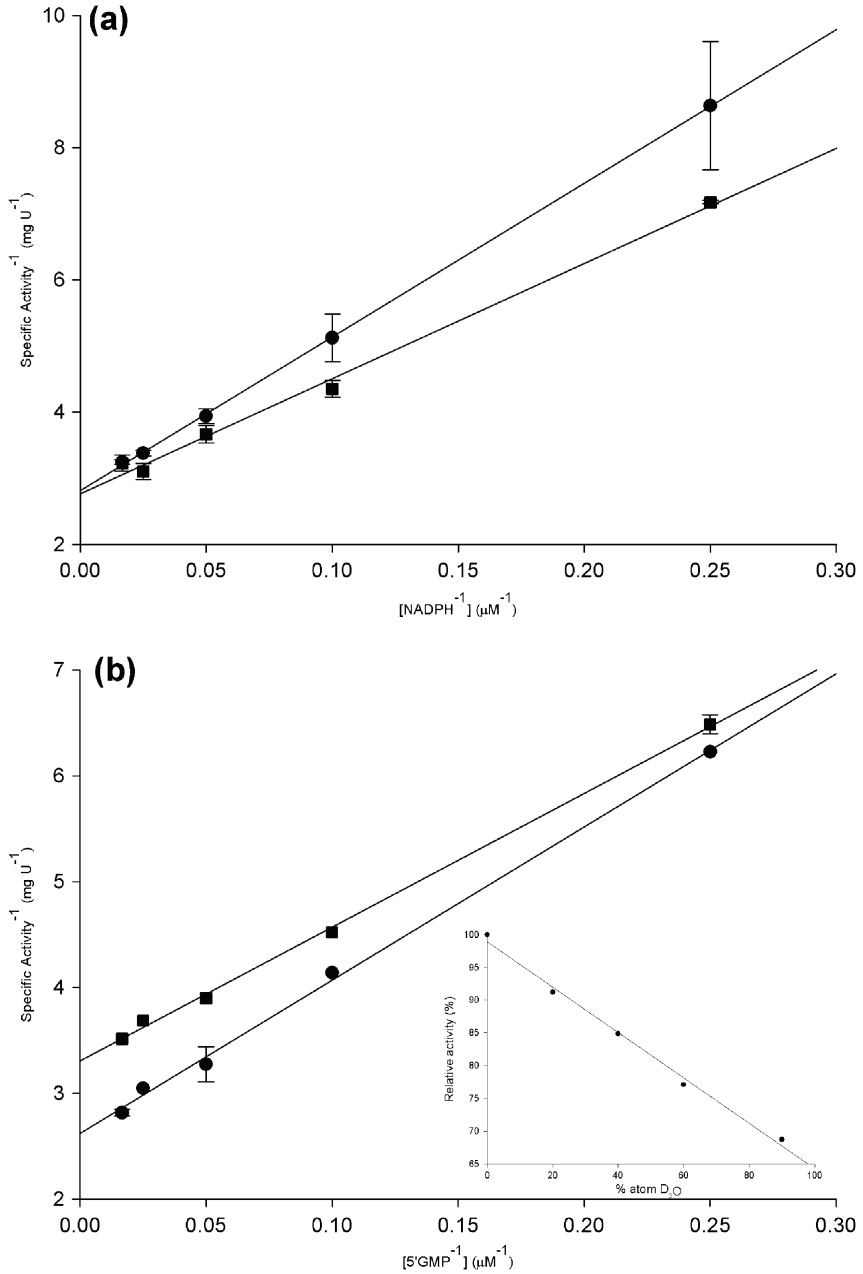

Fig. 10 Solvent isotope effects for GMP reductase. (a) NADPH was used as the variable substrate (4–60 μM), with a saturating concentration of GMP (100 μM). (b) GMP was used as the variable substrate (4–60 μM), with a saturating concentration of NADPH (100 μM). Both reactions mix contained either 0 (●) or 90 (■) atom% D_2O. The inset of (b) represents the proton inventory (0, 20, 40, 60, and 90 atom% D_2O) measuring GMP reductase enzyme activity with both substrates at saturating concentrations (100 μM).

and $^{D_2O}V/K_{NADPH}$ = 0.67 (±0.09) (Fig. 10a), and $^{D_2O}V_{GMP}$ = 1.30 (±0.01) and $^{D_2O}V/K_{GMP}$ = 0.82 (±0.03) (Fig. 10b). In an attempt to determine the number of protons transferred during the solvent isotope-sensitive step, a proton inventory experiment was conducted. A linear relationship between V and the mole fraction of D_2O for GMP reductase (Fig. 10b—inset) was found, suggesting that a single proton is transferred during this step.

Multiple isotope effects are capable of discriminating if two different isotopic substitutions affect the same or distinct chemical steps. Accordingly, solvent kinetic isotope effects were measured using NADPD as the varied substrate. Isotope effect values on $^{D_2O}V_{NADPD}$ and $^{D_2O}V/K_{NADPD}$ were, respectively, 1.00 (±0.02) and 1.50 (±0.17) (Fig. 11; Table 3). The isotope effect on the equilibrium constant, $^{D}K_{eq}$, was determined in order to assess whether the deuterium substitution could affect the internal equilibrium of the reaction. A value of 0.82 was determined for the equilibrium isotope effect ($^{D}K_{eq}$; Table 3).

Pre-steady-state kinetics

In an attempt to determine whether product release contributes to some extent to the rate limiting step, pre-steady-state

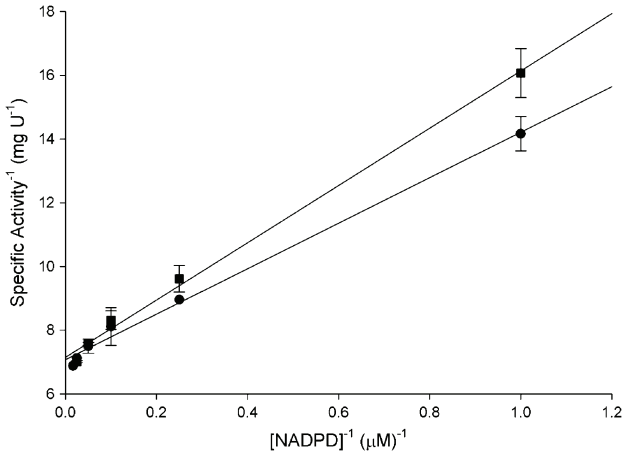

Fig. 11 Multiple kinetic isotope effects using NADPD as the variable substrate in the presence of saturating concentration of GMP (100 μM) and either 0 (●) or 80 (■) atom% D_2O. The data were fitted to eqn (7).

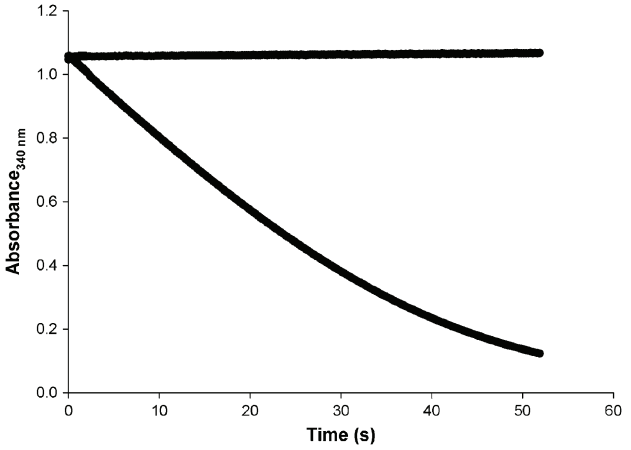

Fig. 12 Representative stopped-flow trace for product formation, measuring the decrease in absorbance at 340 nm upon conversion of NADPH to $NADP^+$ catalyzed by 10 μM of recombinant *E. coli* GMP reductase (mixing chamber concentration) in the presence of GMP. The data were fitted to eqn (10) for a single exponential decay, yielding a value of 0.204 s^{-1} for the apparent first-order constant of product formation. The top stopped-flow trace represents the control experiment in the absence of the GMP substrate.

analysis of the reaction catalyzed was performed. Fitting the pre-steady-state data to eqn (10), which describes a single exponential decay, yielded a value of 0.204 (±0.002) s^{-1} for the apparent first-order rate constant (Fig. 12). This result is in agreement with the value of 0.28 (±0.02) s^{-1} for the catalytic rate constant (k_{cat}) determined by initial velocity study measurements.

Discussion

Amplification, cloning, expression and purification of recombinant *E. coli* GMP reductase

The *guaC* gene was successfully amplified from the *E. coli* genome, cloned into the pCR-Blunt vector, and subcloned into the pET-23a(+) expression vector. The automatic DNA sequencing confirmed the integrity of the gene and the absence of mutations. *E. coli* GMP reductase was expressed after 24 h of cell growth in the absence of IPTG induction. The pET expression system makes use of a powerful T7 polymerase, under control of the IPTG-inducible *lacUV5* promoter to transcribe genes of interest, which are positioned downstream of the bacteriophage T7 late promoter.[19] Expression of recombinant GMP reductase showed that even in the absence of the inducer, high levels of protein production could be obtained in the stationary phase, as has been previously reported for other enzymes.[20–22] It has been proposed that uninduced expression of *lac*-controlled genes occurs when cells approach the stationary phase in complex medium and that cAMP, acetate and low pH are required to produce high level expression in the absence of IPTG induction, which perhaps is part of a general response to carbon-limiting conditions.[23] Nevertheless, more recently, it has been shown that unintended induction in the pET system is due to the presence of as little as 0.0001% of lactose in the medium.[24] The recombinant *E. coli* GMP reductase was purified to homogeneity by a three-step purification protocol using standard anionic exchange and size exclusion columns with 33% of protein yield.

Quaternary structure analysis of *E. coli* GMP reductase

The results of mass spectrometry analysis combined with the amino acid sequencing demonstrated, unequivocally, that the homogeneous protein is, indeed, recombinant *E. coli* GMP reductase. The gel filtration chromatography showed that the enzyme from *E. coli* has the same tetrameric quaternary structure of hGMPR2, demonstrated by X-ray diffraction.[16]

Determination of apparent steady-state kinetic constants and initial velocity pattern

The results of the apparent steady-state kinetic data for *E. coli* GMP reductase indicate a K_M value for GMP of 6.9 μM, which is 2.5-fold lower than that for hGMPR2 (17.4 μM),[2] and 3-fold lower than the enzyme from *L. donovani* (21.2 μM).[9] The same pattern occurs for NADPH, with a K_M value of 11.1 μM, which is 2.3-fold lower than that for hGMPR2 (26.6 μM).[2] As for its human counterparts, *E. coli* GMP reductase cannot catalyze conversion of GMP to IMP using NADH as the hydride donor up to 200 μM concentration (data not shown).

Lineweaver–Burk analysis (Fig. 3) suggests that ping-pong and rapid equilibrium ordered mechanisms can be ruled out for *E. coli* GMP reductase. The former mechanism gives double reciprocal plots displaying parallel lines and the latter a family of lines intersecting on the *y*-axis. These data are consistent with ternary complex formation and a sequential mechanism. A sequential mechanism was also reported for hGMPR1[11] and hGMPR2.[2]

It has been shown that the true K_M values for erythrocyte hGMPR1 are 2.6 μM for GMP and 16.9 μM for NADPH,[11] which are in the same concentration range as *E. coli* GMP reductase true steady-state kinetic parameters. These results suggest that *E. coli* GMP reductase possesses a similar overall

dissociation constant for both substrates when compared to hGMPR1. However, the erythrocyte human enzyme presents a bimodal GMP substrate saturation curve,[11] which is usually attributed to the existence of independent isoenzymes with different kinetic constants or to a single multisubunit enzyme with multiple sites that can interact in a negatively cooperative manner.[25] Deng and co-workers[2] identified the hGMPR2 isoenzyme, making the bimodal substrate-saturation kinetic found in hGMPR likely to be a result of a mixture of both isoenzymes. At any rate, a sequential addition of substrates to form a ternary complex has also been proposed for hGMPR2 enzyme.[2]

Isothermal titration calorimetry

ITC is an important and well-established technique for the study of thermodynamics of macromolecular interactions, and is unique in that it is capable of measuring simultaneously the association and thermodynamic constants of binding.[26] Binding experiments using ITC combined with the initial velocity study demonstrated that the reaction catalyzed by *E. coli* GMP reductase follows an ordered bi–bi kinetic mechanism, in which GMP is the first substrate to bind to free enzyme, followed by the binding of NADPH to form the ternary complex capable of undergoing catalysis; and $NADP^+$ is the first product to dissociate from the enzyme, followed by the dissociation of IMP (Fig. 13). This mechanism is in agreement with both human GMP reductases, for which a sequential kinetic mechanism has been reported.[2,11] Notwithstanding, the results reported here provide, to the best of our knowledge, the first experimental evidence for both order of addition of substrate and release of products.

The ITC measurements of GMP binding provided dissociation constant values (K_d), one for each subunit, where $K_{d1} > K_{d2} > K_{d3}$, suggesting a positive homotropic cooperativity, since the binding of one molecule of GMP increases the affinity for the next molecule which will bind to the next subunit. The K_{d4} value is higher than the others, indicating a lower affinity for the last subunit to bind GMP. Interestingly, this finding is consistent with the crystal structure of hGMPR2, as no GMP binding could be observed for one of the subunits of this enzyme.[16] However, the large errors do not warrant to ascertain whether or not there is cooperativity on GMP binding to *E. coli* GMP reductase. The ΔG values for all four subunits are negative, which demonstrate that GMP binding to *E. coli* GMP reductase is a thermodynamically favorable process. The thermodynamic analysis revealed different types of interactions between the ligand and the enzyme subunits, ranging from favorable hydrogen bonds and/or van der Waals interactions (negative ΔH), release of "bound" water molecules to the bulk solvent (positive ΔS) to conformational changes in either or both of the molecules (negative ΔS).[27] As can be seen in Table 2, with the exception of subunit 2, the analyses of ΔH and ΔS reveal that the binding of GMP is coupled with favorable hydrogen bonds (negative ΔH) and conformational changes (negative ΔS).[28] This finding appears to be consistent with the hGMPR2 structure,[16] in which GMP was located on the top of the α/β barrel surrounded by a hydrophilic surface formed by the active site loop and the flexible binding loop that would close upon GMP binding to the enzyme.

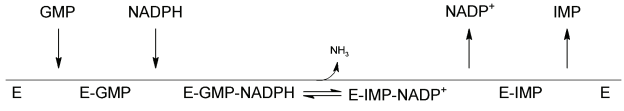

Fig. 13 Proposed enzyme mechanism for *E. coli* GMP reductase.

The IMP binding to *E. coli* GMP reductase yielded four different K_d values (Table 2). However, the large errors do not allow us to propose that there is either positive or negative cooperativity among the subunits upon IMP binding. The analysis of the Gibbs free energy revealed that the binding of IMP is thermodynamically favorable for all subunits of *E. coli* GMP reductase (negative ΔG), and the analysis of ΔH and ΔS for IMP follows a similar pattern as observed for GMP. The determination of the crystal structure of *E. coli* GMP reductase in complex with IMP may shed light on these thermodynamic features.

The rather large standard errors (Table 2) are a direct consequence of the shape of the binding isotherm (*C* value), which will dictate how accurately the thermodynamics parameters can be determined.[27] The shape of the binding is dependent on K_d and the concentration of the macromolecule. The latter is limited by the need to obtain large quantities and/or solubility. Another consideration is that for the experimental set-up it is important to obtain an isotherm that provides maximum data points for the fitting process,[27] and the loss of the plateau in the beginning of the titration curve might have contributed to the large standard errors. We were unable to determine the initial points due to rather small ΔH values. At any rate, the ITC data provided clear-cut experimental evidence of GMP and IMP binding to free *E. coli* GMP reductase enzyme (Fig. 4a and c) that allowed the proposal of an ordered bi–bi kinetic mechanism with GMP binding first (Fig. 13). In addition, the ITC data provided thermodynamic signatures of non-covalent interactions between *E. coli* GMP reductase and either GMP or IMP.

pH-rate profiles

The Cys186 amino acid side chain has been shown to play a key role in catalysis for hGMPR2 since the Cys186Ala mutant displayed less than 5% activity as compared to wild-type enzyme.[16] The pH dependence of k_{cat} and sequence alignment analyses suggest that the conserved Cys186 is likely the residue with an apparent p*K* value of 9.6 that plays a critical role in *E. coli* GMP reductase catalysis. The cysteine thiol group usually ionizes at slightly alkaline pH values, and the resulting thiolate anion is the reactive species that acts as a nucleophile, which is one of the most reactive functional groups found in proteins.[29] It is possible that the Cys186 side chain, which has been shown to interact with GMP in the crystal structure of hGMPR2,[16] interacts with the exocyclic amino group bound to C2 of the guanine moiety of GMP thereby facilitating both hydride transfer to C2 and the amino leaving group. In addition, the proposed model of *E. coli* GMP reductase indicates that this residue makes an H-bond to the C2 exocyclic amino group of the guanine moiety of GMP (Fig. 6). Notwithstanding, site-directed mutagenesis studies

are in progress to confirm the role of Cys186, if any, in *E. coli* GMP reductase enzyme catalysis. The bell-shaped pH profile for k_{cat} (Fig. 7a) also showed participation of a single ionizable group with an apparent pK value of 6.6 that has to be deprotonated for catalysis. Sequence alignment showed conservation of Asp129 in *E. coli* GMP reductase (Fig. 7) that has been shown to be located in the active site loop in hGMPR2.[16] Although the pK value of the β-carboxyl group of Aspartate residues are usually in the 3.9–4.0 range, it is not unlikely that this pK value may be displaced by a neighbouring chemical group. However, assigning a definite catalytic role to Asp129 in *E. coli* GMP reductase is not warranted and site-directed mutagenesis studies should be carried out. Although the apparent pK value of 6.6 that plays a role in catalysis could tentatively be ascribed to the imidazole side chain of a Histidine residue (pK usually in the 6.0–7.0 range), His278 is located in the GMP binding site of *E. coli* GMP reductase whereas it is not present in hGMPR2 (Fig. 7).

The pH-rate data for of k_{cat}/K_{GMP} indicate that both protonation of two groups with apparent pK values of 7.1 and deprotonation of two groups with apparent pK values of 8.6 (Fig. 7b) are required for GMP binding. These dissociation constants can be in the ligand and the other in the enzyme, or both can be in one or the other. The crystal structure of hGMPR2 in complex with GMP demonstrated that this substrate is surrounded by a hydrophilic surface formed by the active site loop (residues 179–187 in hGMPR2) and the flexible GMP binding region (residues 268–290 in hGMPR2).[16] Sequence alignment of GMP reductases (Fig. 5) shows a relatively good conservation of these two regions in *E. coli* GMP reductase (active site loop: residues 179–187; GMP binding region: 268–290). The pK value for the N7 atom of the guanine moiety of GMP is 3.6, and the ribose 2′,3′-diol only loses a proton above pH 12. The guanine base becomes protonated on one of the ring nitrogens rather than on the exocyclic amino group since this does not interfere with delocalization of the NH_2 electron lone pair into the aromatic system. In the case of monoesters, the phosphate group of GMP loses one proton at pH 1 and a second proton at pH 7. The proximity of negative charge on the phosphate residues has a secondary effect, making the ring nitrogens more basic ($\Delta pK \approx +0.4$) and the amine protons less acidic ($\Delta pK \approx +0.6$). It is thus likely that the pH-rate profile does not reflect any ionization of the guanine moiety of GMP. On the other hand, it is possible that the apparent pK values reflect change in ionization of His278 in the GMP binding site, and change in ionization of the phosphate group of GMP and, for instance, Asp219 that makes H-bonds with the ribose hydroxyl groups of the pentose.

The pH-rate profile for k_{cat}/K_{NADPH} indicated that protonation of two groups with apparent pK values of 6.2 abolish NADPH binding to *E. coli* GMP reductase (Fig. 7c). Although there was no diffraction pattern to allow identification of the NADPH binding site in hGMPR2, structural comparison and model building has been employed to suggest that the amino acid residues 129–133 are involved in NADPH binding.[16] These residues are conserved in *E. coli* GMP reductase (Fig. 5). The adenine-C2′-ribose phosphate group has a pK value of 6.1. It is thus tempting to suggest that protonation of NADPH phosphate and the putative Asp129 residue located in the NADPH binding site can account for the k_{cat}/K_{NADPH} pH-rate profile.

Deuterium kinetic isotope effects and proton inventory

Measurements of kinetic isotope effects in enzyme catalyzed reactions aim at examining the contribution of proton transfer(s) to rate-limiting step(s). However, the maximal velocity may be dependent on several rate-contributing or partially rate-limiting steps instead of one rate-determining step.[30]

Isotope effects on V report on events following the ternary complex formation capable of undergoing catalysis (fully loaded enzyme), which include the chemical steps, possible enzyme conformational changes, and product release (leading to regeneration of free enzyme). Isotope effects on V/K report on steps in the reaction mechanism from binding of the isotopically labeled substrate to the first irreversible step, usually considered to be the release of the first product (that is, all rate constants from reactant binding until the first irreversible step).[30] Any substrate can be varied; it does not need to be the labeled one, but one obtains $^{D}V/K$ effect for the varied substrate rather than for the labeled one. Although the apparent classical limit for primary deuterium kinetic isotope effects on V is approximately 8, values as low as 2 have sometimes been accepted as evidence of a rate-determining step.[30,31] For reactions involving NAD(P)H oxidation, primary deuterium isotope effects ranging from 1 to 3 have been found.[32] The magnitude of primary deuterium isotope effect depends on the chemical nature of the transition state.[33] This isotope effect reaches a maximum value when the hydrogen is symmetrically placed between the donor atom from which cleavage occurs and the acceptor atom to which a new bond is formed, and decreases for reactant- or product-like transition states. The value of 2.5 for the observed primary deuterium kinetic isotope effect on V for *E. coli* GMP reductase using either NADPH or [4*S*-^{2}H]-NADPH ($^{D}V_{NADPH}$) as a variable substrate indicates that hydride transfer is involved in a rate-limiting step and that the transition state may be either substrate- (early) or product-like (late). However, the symmetry of the transition state can only be inferred from the magnitude of a deuterium kinetic isotope effect if it is for the specific step in an enzymatically catalyzed reaction at which the isotopically substituted bond is broken by passing through a single transition state (that is, the intrinsic kinetic isotope effect). Enzyme-catalyzed chemical reactions proceed through many steps and the rate constants for several steps are usually consequential to the composite rate constant for the overall reaction, consequently the observed deuterium kinetic isotope effect is less than or equal to the intrinsic deuterium isotope effect for the step in which the hydrogen is transferred. In any case, the observed primary deuterium kinetic isotope effect on V for *E. coli* GMP reductase indicates that hydride transfer is from C4-*proS* hydrogen of NADPH and that it is partially rate-limiting. On the other hand, the inverse primary deuterium kinetic effect on V/K for NADPH ($^{D}V/K_{NADPH} = 0.4$) is somewhat puzzling. Incidentally, there have been numerous reports of inverse isotope effects on V/K of unknown origin.[34,35]

The expression of deuterium kinetic isotope effect on V/K includes the intrinsic isotope effect, commitment factors (forward and reverse) and equilibrium isotope effect.[33] An equilibrium isotope effect may be invoked to account for the inverse effect on V/K, providing that the reverse commitment factor is large and the forward commitment factor is small. The inverse deuterium isotope effect on the equilibrium constant ($^{D}K_{eq}$ = 0.82) suggests that the deuterated product is more stiffly bonded than the deuterated substrate[36] and the internal equilibrium might dominate the observed kinetic isotope effect. The inverse isotope effect indicates that once the hydride is transferred it becomes more tightly bonded to the corresponding product (IMP) when compared to the substrate. The magnitude of this isotope effect is a direct consequence of the difference in the bonds of the substrate and product, with deuterium becoming enriched in the stiffest bond and the hydrogen in the looser one (deuterium accumulates where binding is tighter).[37] In addition, isotope effects on V/K are a combination of binding and catalytic events. Binding isotope effects can contribute in the opposite direction of kinetic isotope effects that arise from transition state chemistry. An inverse binding isotope effect may arise when binding of the molecule containing the heavier isotope atom (NADPD) is increased as bonds to the isotopic label are tighter in the bound complex. Although it is conceivable that the inverse $^{D}V/K_{NADPH}$ value reflects an inverse binding isotope effect, it cannot be experimentally assessed as NADPH (enzyme mechanism proposed here) binds to the *E. coli* GMP reductase:GMP binary complex to form the catalytic competent ternary complex. Accordingly, the inverse $^{D}V/K_{NADPH}$ value is likely due to the inverse deuterium isotope effect on the equilibrium constant. Isotope effects can provide further experimental evidence for a specific enzyme mechanism. In the case of an ordered mechanism, the V/K for the first substrate (GMP) to bind (at saturating concentrations of the second substrate: NADPH) is the on-rate for the reactant binding to enzyme, a non-isotope sensitive step.[33] The value of 1.03 ($\pm$ 0.07) for $^{D}V/K_{GMP}$ (Table 3) provides further support for an ordered enzyme mechanism as suggested by the initial velocity pattern and ITC data.

To evaluate the contribution of proton transfer from solvent to a rate-limiting step, measurements of solvent isotope effects on V and V/K were carried out. As rule of thumb, deuterium accumulates where binding is tighter (that is, fractionation factor is larger than one). Transition state proton contributes the reciprocal of its respective fractionation factor to the solvent isotope effect, whereas the contribution of a reactant state proton to the solvent isotope effect is equal to its fractionation factor.[32] Reactant state fractionation by enzyme cysteine thiol groups (S–H group of cysteine) can make large inverse contributions to solvent isotope effects.[32,33] It is thus conceivable that the value of 0.82 for $^{D_2O}V/K_{GMP}$ reflects participation of Cys186 of free enzyme, which has been shown to interact with GMP in the hGMPR2 crystal structure,[16] and the value of 0.67 for $^{D_2O}V/K_{NADPH}$ reflects an inverse contribution of conserved Cys127 of free enzyme, located near the NADPH binding site of *E. coli* GMP reductase (Fig. 5). The value of 0.99 for $^{D_2O}V_{NADPH}$ suggests no participation of the proton solvent in catalysis. On the other hand, solvent proton transfer appears to play a modest role in catalysis since a value of 1.30 was found for $^{D_2O}V_{GMP}$. In addition, proton inventory data (Fig. 10b—inset) suggest that this modest solvent kinetic isotope effect arises from a single protonic site. The difference found between the primary deuterium and solvent kinetic isotope effects suggests that the hydride and proton transfer may occur in distinct reaction steps, as found in other NADPH-dependent reductive reactions.[34] Nevertheless, it is not possible to ascertain whether or not hydride transfer and protonation steps occur in a single transition state (concerted mechanism) or in distinct transition states (stepwise mechanism) based solely on primary and solvent isotope effects.

Multiple isotope effects (double isotope effects) allow us to determine whether two different isotopic substitutions affect the same (concerted) or different (stepwise) chemical steps.[38] This method uses the normal effect of deuterium to slow down one step of a reaction mechanism while observing changes in the expression of another isotope effect,[38] the effects in question being the protonation and the hydride transfer. If the protonation and hydride transfer occur in the same transition state, the solvent isotope effect will be larger or unchanged with the deuterium substitution (NADPD) when compared with NADPH. However, if the effects take place in different steps, the solvent isotope effect will decrease with NADPD, once the hydride transfer will become more rate-limiting.[34,35,38] As can be seen in Table 3, the results of the multiple isotope effects showed similar values for $^{D_2O}V_{NADPD}$ (1.00) and $^{D_2O}V_{NADPH}$ (0.99), suggesting that hydride transfer and solvent proton transfer steps take place in the same transition state (concerted mechanism). In addition, the value for the solvent isotope effect on V/K with NADPD (1.50) is larger than with NADPH (0.67), thereby lending support to a concerted mechanism.

Pre-steady-state kinetics

In the study of the transient phase of enzyme reactions, the data obtained are generally expressed by a single exponential curve for the first order reaction.[39] The analysis of the data allows us to determine the apparent first order rate constant, which was in the same range as the first order in the steady-state kinetics. The observation of burst during a time course in the transient phase is evidence of a significant build-up of product formation along the reaction pathway.[39] If a burst is observed during the transient phase, and the concentration of $NADP^+$ produced is approximately equal to the initial *E. coli* GMP reductase subunit concentration, it would indicate that the chemical step of the reaction is much faster than the release of the first product ($NADP^+$). As there is no burst of $NADP^+$ formation (Fig. 12), the stopped-flow result demonstrates that product release does not contribute to the rate-limiting step of the chemical reaction catalyzed by *E. coli* GMP reductase.

Conclusion

A rational inhibitor design relies on mechanistic and structural information on the target enzyme. Enzyme inhibitors make up roughly 25% of the drugs marketed in United States.[40] Enzymes catalyze multistep chemical reactions to achieve rate

accelerations by stabilization of transition state structure(s).[40] Accordingly, mechanistic analysis should always be a top priority for enzyme-targeted drug programs aiming at the rational design of potent enzyme inhibitors. Moreover, ITC has been used as an important technique for the direct determination of thermodynamic and kinetic parameters of enzymatic reactions.[41] The recognition of the limitations of high-throughput screening approaches in the discovery of candidate drugs has rekindled interest in rational design methods.[42] Understanding the mode of action of *E. coli* GMP reductase will inform us on how to better design inhibitors targeting this enzyme. In addition, understanding the mode of action of an enzyme can be used to inform functional annotation of newly determined sequences and structures, to select appropriate enzyme scaffolds for engineering new functions, and to refine definitions in the current EC classifications.[43] The elucidation of the mode of action of *E. coli* GMP reductase and its availability in recombinant form may also provide a tool for determination of substrate specificity of cyclic nucleotide phosphodiesterases (PDEs). PDEs belong to a superfamily of proteins with medical relevance that play a major role in cell signaling by catalyzing the hydrolysis of cyclic AMP (cAMP) and cyclic GMP (cGMP).[44] PDE enzymes are distinguished by their substrate specificity. The PDE activity cannot be directly assayed, being necessary to couple an accessory enzyme. As recombinant *E. coli* GMP reductase is specific for GMP, it may be employed to determine the substrate specificity of PDE enzymes. Among the 11 families of PDEs, only PDE 5, PDE 6 and PDE 9 are specific for cGMP, which are targets for, respectively, treatment of erectile dysfunction (sildenafil), visual alterations, and behavioral state regulations and learning.[45] The results here presented may also help chemical biologists to design function-based chemical compounds to carry out either loss-of-function (inhibitors) or gain-of-function (activators) experiments to reveal the biological role of GMP reductase in the context of whole *E. coli* cells.[46] It is also hoped that the results presented here may be useful to understand the role that GMP reductase plays in the *E. coli* salvage pathway.

Experimental procedures

Materials

All chemicals were of analytical or reagent grade and were used without further purification, unless stated otherwise. 5′GMP, NADPH, IMP, and $NADP^+$ along with lysozyme and streptomycin sulfate were purchased from Sigma-Aldrich. Deuterium oxide (99.9 atom% D_2O) was from Cambridge Isotope Laboratories. Fast performance liquid chromatography (FPLC) protein purification (4 °C) was carried out using an Äkta Purifier from GE Healthcare; all chromatographic columns and the LMW and HMW Gel Filtration Calibration Kit were also from GE Healthcare. Bovine serum albumin and Bradford reagent were from Bio-Rad Laboratories. All steady-state activity assays were performed in an UV-2550 UV/Visible spectrophotometer (Shimadzu). Dithiothreitol (DTT) was from Acros Organics. *Pfu* DNA polymerase was from Stratagene. Restriction enzymes and T4 DNA ligase and pCR-Blunt cloning vector were from Invitrogen and pET-23a(+) expression vector and *E. coli* BL21(DE3) were from Novagen. The mass spectrometer LTQ-XL and LTQ Orbitrap Discovery were from Thermo and the nanoLC Ultra 1D plus was from Eksigent. An iTC_{200} Microcalorimeter was from MicroCal Inc (Northampton, MA). Pre-steady-state measurements were carried out using an Applied Photophysics SX.18MV-R stopped-flow spectrofluorimeter on absorbance mode.

E. coli GMP reductase comparative homology modeling

A *E. coli* three-dimensional model was built by comparative homology modeling using the human type 2 GMP reductase structure as template (PDB ID: 2A7R; hGMPR2),[16] solved by X-ray crystallography at 3.0 Å in complex with GMP. The template structure was used for *E. coli* GMP reductase modeling, as well as to evaluate GMP binding mode to the bacterial enzyme active site. Template selection was based on high primary sequence conservation (68.5% identity and 16.47% strong similarity), and the presence of enzyme substrate bound to its active site. Target and template pair-wise sequence alignment required a single gap inclusion in human GMP reductase primary sequences. The *E. coli* GMP reductase model was built by restrained-based homology modeling implemented in MODELLER9v1,[47] with the standard protocol of the comparative protein structure modeling methodology, by satisfaction of spatial restrains.[48,49] Atomic coordinates of GMP heteroatoms were copied from the template structure into the *E. coli* GMP reductase model. The best model was selected according to MODELLER objective function[50] and subjected to energy minimization for amino acid side chain and main chain rearrangements with the GROMACS package[51] using the 43a1 force-field. The system was submitted to an initial steepest descent energy minimization in vacuum with a maximum number of 400 minimization steps, followed by a maximum of 3000 steps of conjugate gradient energy minimization. The program PROCHECK[52] was employed to analyze the stereochemical quality of the model, as previously described.[53] Structural correspondence between the *E. coli* model and human GMP reductase template was evaluated by their root-mean square deviation (RMSD). H-bond interactions were evaluated with LIGPLOT v4.4.2,[54] considering an atomic distance cut off of 3.9 Å (program default values). Images were generated with PyMOL Molecular Graphic System V1.3 (Schrödinger, LLC).

Amplification and cloning of the *E. coli guaC* gene

The oligonucleotide primer sequences of the *E. coli guaC* structural gene were 5′-AA*CATATG*CGTATTGAAGAA-GATCTGAAGTTAGGTTTTAAAGACG-3′ (forward) and 3′-AA*GGATCC*TCATTACAGGTTGTTGAAGATGCGG TTTTCTTGTTCC-5′ (reverse). The primers were designed to contain, respectively, *Nde*I and *Bam*HI restriction sites (in italics). The DNA fragment (1038 bp) was amplified using *Pfu* DNA polymerase, ligated into the pCR-Blunt cloning vector, and transformed into *E. coli* DH10B cells. Plasmid DNA recovered from these cells was digested with the

restriction enzymes *Nde*I and *Bam*HI, and the isolated insert was ligated into the pET-23a(+) expression vector, previously treated with the same restriction enzymes. The sequence of the *E. coli guaC* gene was determined by automated DNA sequencing to confirm the identity, integrity, and absence of PCR-introduced mutations in the cloned fragment.

Expression of recombinant GMP reductase

The recombinant plasmid pET-23a(+)::*guaC* was transformed into *E. coli* BL21(DE3) cells, and these were selected on Luria-Bertani (LB) agar plates containing 50 μg mL^{-1} ampicillin. LB medium (60 mL) containing 50 μg mL^{-1} ampicillin was inoculated with a single colony and cells were grown overnight. The culture (10 mL) was inoculated in LB medium (500 mL) with the same antibiotic concentration, and, as soon as $OD_{600\ nm}$ reached a value of 0.6, culture was grown for additional 24 h at 180 rpm and 37 °C without IPTG induction. Cells (15 g) were harvested by centrifugation at 7690*g* for 30 min at 4 °C and were stored at –20 °C. Soluble and insoluble fractions were analyzed by 12% SDS-PAGE and Coomassie staining.

Purification of recombinant GMP reductase

Approximately 2.8 g of frozen cells were resuspended in 14 mL of 100 mM tris(hydroxymethyl)aminomethane (Tris; buffer A), pH 7.8, and incubated with lysozyme (0.2 mg mL^{-1}) for 30 min with stirring. Cells were disrupted by sonication, and centrifuged at 38 900*g* for 30 min to remove cells debris. Streptomycin sulfate was added to the supernatant up to 1% (wt/vol), stirred for 30 min to precipitate nucleic acids, and centrifuged at 38 900*g* for 30 min. The resulting supernatant was dialyzed against buffer A (2 × 2 L; 2 h each) using a dialysis tubing with a molecular weight exclusion limit of 12–14 kDa. The sample was clarified by centrifugation at 38 900*g* for 30 min and loaded on a FPLC 2.6 cm × 8.2 cm Q-Sepharose Fast Flow anion exchange column, pre-equilibrated with buffer A, washed with 5 column volumes of buffer A, and the adsorbed material was eluted with a linear gradient (0-40%) of 20 column volumes of 100 mM Tris pH 7.8 containing 500 mM NaCl (buffer B) at 1 mL min^{-1}. The adsorbed recombinant GMP reductase was eluted at approximately 145 mM NaCl concentration, with substantial removal of contaminants. All fractions were analyzed by SDS-PAGE electrophoresis, and the ones containing the target protein were pooled and concentrated to 8.5 mL using an Amicon ultrafiltration cell (molecular weight cutoff 30 kDa). The soluble sample was loaded on a 2.6 cm × 60 cm HiPrep Sephacryl S-200 High Resolution size exclusion column, which was previously equilibrated with buffer A, and isocratically eluted with buffer A at a flow rate of 0.25 mL min^{-1}. This step was employed to further purify the recombinant protein and to remove salt from the sample, thereby allowing protein preparation for the next chromatographic step. Fractions containing the target protein were pooled and the soluble sample was loaded on a 1.6 cm × 10 cm Mono Q High Resolution anion exchange column, pre-equilibrated with buffer A. The column was washed with 5 column volumes, and the adsorbed proteins were eluted with a linear gradient (0–40%) of 20 column volumes of buffer B, and the target protein eluted at approximately 155 mM NaCl concentration. The active fractions containing the target protein were pooled and dialyzed against buffer A (2 × 2 L; 2 h each) in order to remove the remaining salt. Protein concentration was determined by Bradford's method using bovine serum albumin as standard.[55]

Quaternary structure analysis of *E. coli* GMP reductase

The homogeneous sample was submitted to ESI-MS in order to confirm the identity of *E. coli* GMP reductase. The protein was also digested with trypsin and the resulting peptides were separated and analyzed by liquid chromatography associated with mass spectrometry with fragmentation collision induced, and the results were used to identify the amino acid sequence through a search software (Protein Discoverer, Thermo).

The molecular mass of recombinant GMP reductase was determined by gel filtration chromatography using a 1.0 cm × 30 cm High Resolution Superdex 200 column pre-equilibrated with 50 mM Tris, pH 7.5, containing 200 mM NaCl at a flow rate of 0.4 mL min^{-1}. The LMW and HMW Gel Filtration Calibration Kit were used as the protein molecular mass standards in the calibration curve, measuring the elution volumes of several standards (ferritin, catalase, aldolase, ovalbumin, coalbumin, ribonuclease A, and blue dextran 2000), calculating their partition coefficients (K_{av}), and plotting these values against the logarithm of their molecular mass. The K_{av} values were determined as $K_{av} = (V_e - V_o)/(V_t - V_o)$, where V_e is the sample elution volume, V_t is the total bed volume of the column, and V_o is the column void volume, which had been determined by loading blue dextran 2000 into the column. Protein elution was monitored at 215, 254, and 280 nm.

Synthesis of [4*S*-^{2}H]-NADPH

[4*S*-^{2}H]-NADPH was synthesized according to the method of Ottolina and co-workers[56] and purified on a 1.0 cm × 10 cm Mono Q High Resolution anion exchange column. The column was washed with 1 column volume of 100 mM *N*-2-hydroxyethylpiperazine-*N*′-2-ethanesulfonic acid (Hepes), pH 7.0, and the material was eluted with a linear gradient (0–100%) of 5 column volumes of 100 mM Hepes containing 1.0 M NaCl, pH 7.0, at a flow rate of 0.5 mL min^{-1}. The fractions with $A_{260\ nm}/A_{340\ nm} \leq 2.3$ were pooled.

Enzyme activity assay of *E. coli* GMP reductase

The recombinant GMP reductase activity was determined by a continuous spectrophotometric assay monitoring the conversion of NADPH to $NADP^+$ at 340 nm. The standard assay was performed at 25 °C in 100 mM Tris, pH 7.8, with 10 mM DTT, unless stated otherwise.

Determination of apparent steady-state kinetic constants and initial velocity pattern

In order to determine the apparent steady-state kinetic constants, GMP reductase activity was measured (in duplicates) in the presence of varying concentrations of GMP (5–80 μM) and fixed NADPH concentration (100 μM), and varying concentrations of NADPH (5–120 μM) and fixed GMP concentration (100 μM), in 100 mM Tris, pH 7.8, buffer

containing 10 mM DTT in a total volume of 500 μL. The enzyme specificity for NADPH was evaluated measuring the enzymatic activity in the presence of varying concentrations of NADH (20–200 μM) at a fixed-saturating concentration of GMP (100 μM). To determine the true steady-state kinetic parameters and initial velocity patterns, enzymatic activity was measured in the presence of varying concentrations of GMP (1–60 μM) and several fixed-varied NADPH concentrations (1–60 μM). Enzyme activity was determined in an UV-2550 UV/Visible spectrophotometer (Shimadzu) by monitoring the decrease in absorbance at 340 nm (ε_{340nm} = 6220 M^{-1} cm^{-1}) upon GMP reductase-catalyzed conversion of NADPH to $NADP^+$. One unit of enzyme activity was defined as the amount of protein that catalyzes the consumption of 1 μmol of NADPH per minute at 25 °C.

Isothermal titration calorimetry

ITC experiments were carried out using the iTC_{200} Microcalorimeter. The reference cell (200 μL) was loaded with water during all experiments and the sample cell (200 μL) was filled with *E. coli* GMP reductase at a concentration of 122 μM in buffer A. The injection syringe (39.7 μL) was filled with substrates or products at different concentrations, GMP at 0.75 mM, NADPH at 3.5 mM, $NADP^+$ at 1.0 mM, and IMP at 1.0 mM, and the ligand binding isotherms were measured by direct titration (ligand into macromolecule). The same buffer was used to prepare all ligand solutions. The stirring speed was 500 rpm at 25 °C with constant pressure for all ITC experiments. Titration first injection (0.5 μL) was not used in data analysis and was followed by 17 injections of 2.2 μL each at 180 s intervals. Control titrations (ligand into buffer) were performed in order to subtract the heats of dilution and mixing for each experiment prior to data analysis. All data were evaluated utilizing the Origin 7 SR4 software (Microcal, Inc.).

pH-rate profiles

The dependence of kinetic parameters on pH was determined by measuring initial velocities in the presence of varying concentrations of one substrate and saturating levels of the other, in a buffer mixture of 500 mM 2-(*N*-morpholino)-ethanesulfonic acid (MES)/Hepes/2-(*N*-cyclohexylamino)-ethanesulfonic acid (CHES) over the following pH values: 6.0 (10–160 μM varying GMP concentration and fixed concentration of NADPH at 240 μM, and 10–160 μM varying NADPH concentration and fixed concentration of GMP at 240 μM), 6.5 (2–60 μM varying GMP concentration and fixed concentration of NADPH at 100 μM, and 2–60 μM varying NADPH concentration and fixed concentration of GMP at 100 μM), 7.0 (2–60 μM varying GMP concentration and fixed concentration of NADPH at 100 μM, and 2–60 μM varying NADPH concentration and fixed concentration of GMP at 100 μM), 7.5 (5–80 μM varying GMP concentration and fixed concentration of NADPH at 100 μM, and 5–80 μM varying NADPH concentration and fixed concentration of GMP at 100 μM), 8.0 (5–80 μM varying GMP concentration and fixed NADPH concentration at 100 μM, and 5–80 μM varying NADPH concentration and fixed concentration of GMP at 100 μM), 8.5 (5–60 μM varying GMP concentration and fixed concentration of NADPH at 100 μM, and 5–60 μM varying NADPH concentration and fixed concentration of GMP at 100 μM), 9.0 (5–60 μM varying GMP concentration and fixed concentration of NADPH at 100 μM, and 5–60 μM varying NADPH concentration and fixed concentration of GMP at 100 μM), and 9.5 (2–60 μM varying GMP concentration and fixed concentration of NADPH at 100 μM, and 2–60 μM varying NADPH concentration and fixed concentration of GMP at 100 μM). Prior to performing the pH-rate profiles, the recombinant enzyme was incubated over a broader pH range and assayed under standard conditions to identify denaturing pH values and to ensure enzyme stability at the tested pH range.

Energy of activation

In order to determine the energy of activation of the GMP reductase-catalyzed reaction, initial velocities were measured in the presence of varying concentrations of one (GMP 1–60 μM) (NADPH 1–80 μM) substrate and saturating levels of the other (100 μM), at temperatures ranging from 15 to 35 °C. GMP reductase was incubated for several minutes in all temperatures tested and assayed under standard conditions to ensure enzyme stability under all temperatures.

Deuterium kinetic isotope effects and proton inventory

Primary deuterium kinetic isotope effects were determined by measuring initial rates using a saturating level of GMP (100 μM) and varying concentrations of either NADPH (4–60 μM) or [4*S*-^{2}H]-NADPH (1–60 μM).

Solvent kinetic isotope effects were determined by measuring initial velocities using a saturating level of one substrate (100 μM) and varying concentrations of the other (GMP: 4–60 μM; NADPH: 4–60 μM) in either H_2O or 90 atom% D_2O. The proton inventory was determined using saturating concentrations of both substrates (100 μM) at various mole fractions of D_2O.

Multiple kinetic isotope effects were measured by determining the solvent isotope effects using [4*S*-^{2}H]-NADPH (NADPD) as the varied substrate.

An equilibrium isotope effect ($^DK_{eq}$) was determined by measuring the equilibrium constant in the presence of either NADPH or [4*S*-^{2}H]-NADPH. These equilibrium constants were measured as described by Leu and Cook.[57] In short, the ratio of [NADPH]/[$NADP^+$] was fixed at 1 and the ratio of [IMP]/[GMP] were varied from 0.1 to 30 at fixed concentration of NH_4Cl. A plot of the change in NADPH concentration *versus* [IMP]/[GMP] ratio crosses the abscissa at a value equal to K_{eq}.[57]

The notation utilized to express isotope effects is that of Northrop[30] as extended by Cook and Cleland.[58]

Pre-steady-state kinetics

Pre-steady-state kinetic measurements of the reaction catalyzed by *E. coli* GMP reductase were performed to determine whether product release is part of the rate-limiting step. The decrease in absorbance was monitored at 340 nm (1 mm split width = 4.65 nm spectral band), at 25 °C, using a split time base (2–50 s; 400 data points for each time base). The experimental conditions were 10 μM *E. coli* GMP reductase,

10 mM DTT, 250 μM GMP and 250 μM NADPH in 100 mM Tris-HCl, pH 7.8 (mixing chamber concentrations). The experimental conditions for the control experiment were 10 μM *E. coli* GMP reductase, 10 mM DTT, and 250 μM NADPH in 100 mM Tris-HCl, pH 7.8 (mixing chamber concentrations). The dead time of the stopped-flow equipment is 1.37 ms.

Data analysis

Values of the kinetic parameters and their respective errors were obtained by fitting the data to the appropriate equations by using the nonlinear regression function of SigmaPlot 9.0 (SPSS, Inc.). Initial rate data at single concentration of the fixed substrate and varying concentrations of the other were fitted to eqn (1).[17]

$$v = \frac{VA}{K + A} \tag{1}$$

The family of lines intersecting to the left of the *y*-axis in double-reciprocal plots was fitted to eqn (2), which describes a mechanism involving ternary complex formation and a sequential substrate binding.[59]

$$v = \frac{VAB}{K_{ia}K_b + K_aB + K_bA + AB} \tag{2}$$

For eqn (1) and (2), v is the initial velocity, V is the maximal initial velocity, A and B are the concentrations of the substrates (GMP and NADPH), K_a and K_b are their respective Michaelis constants, and K_{ia} is the dissociation constant for enzyme–substrate A binary complex formation.

pH-rate profiles data were fitted to eqn (3), (4) or (5), where y is the kinetic parameter, C is the pH-independent value of y, H is the proton concentration, and K_a and K_b are, respectively, the apparent acid and base dissociation constants for ionizing groups, and K_0 is the product of two apparent dissociation constants.[60]

$$\log y = \log\left(\frac{C}{1 + \frac{H}{K_a} + \frac{K_b}{H}}\right) \tag{3}$$

$$\log y = \log\left(\frac{C}{1 + \frac{H}{K_a} + \frac{H^2}{K_0} + \frac{K_b}{H} + \frac{K_0}{H^2}}\right) \tag{4}$$

$$\log y = \log\left(\frac{C}{1 + \left(\frac{H}{K_{a1}}\right)\left(1 + \frac{H}{K_{a2}}\right)}\right) \tag{5}$$

Eqn (3) describes a bell-shaped pH profile for a group that must be protonated for binding/catalysis and another group that must be unprotonated for binding/catalysis, and participation of a single ionizing group for the acidic limb (slope value of +1) and participation of a single ionizing group for the basic limb (slope value of −1). Eqn (4) describes a bell-shaped pH-rate profile that starts with a slope of +2 in the acidic limb and goes to an eventual slope of −2 in the basic limb, suggesting participation of two ionizing groups in each limb. Eqn (5) describes a pH-rate profile for two groups that need to be unprotonated for binding (slope of +2 for the acidic limb). Unless the p*K*s of the groups are at least 3 pH units apart, there will not be a linear region with a slope of +1.

The data for temperature effects were fitted to eqn (6), where k is the maximal reaction rate, E_a is the energy of activation, T is the temperature in Kelvin, R is the gas constant (1.987 cal K^{-1} mol^{-1}), and A is a pre-exponential factor that correlates collision frequency and the probability of the reaction occurring when reactant molecules collide.

$$\log k = -\left(\frac{E_a}{2.3R}\right)\left(\frac{1}{T}\right) + \log A \tag{6}$$

Kinetic isotope effects data were fitted to eqn (7), which assumes isotope effects on both V/K and V. In this equation, $E_{V/K}$ and E_V are the isotope effects minus 1 on V/K and V, respectively, and F_i is the fraction of isotopic label in substrate A.[36]

$$v = \frac{VA}{K(1 + F_iE_{V/K}) + A(1 + F_iE_V)} \tag{7}$$

ITC data were fitted to eqn (8), where ΔH is the enthalpy of process given by the ITC experiment, ΔG is the Gibbs free energy changes, ΔS is the entropy changes, T is the temperature of the experiment in Kelvin, R is the gas constant (1.987 cal K^{-1} mol^{-1}), and K_{eq} is the equilibrium binding constant. The dissociation constant, K_d, is the inverse of the equilibrium binding constant, K_{eq}, described in eqn (9).

$$\Delta G = \Delta H - T\Delta S = -RT\ln K_{eq} \tag{8}$$

$$K_d = \frac{1}{K_{eq}} \tag{9}$$

The pre-steady-state time course of the reaction was fitted to eqn (10) for a single exponential decay, in which A is the absorbance at time t, A_0 is the absorbance at time zero, and k is the apparent first-order rate constant for product formation.[39]

$$A = A_0e^{-kt} \tag{10}$$

Acknowledgements

This work was supported by funds of Millennium Initiative Program (CNPq) and National Institute of Science and Technology on Tuberculosis (INCT-TB), MCT-CNPq, Ministry of Health—Department of Science and Technology (DECIT)—Secretary of Health Policy (Brazil) to D.S.S. and L.A.B. D.S.S. (CNPq, 304051/1975-06) and L.A.B. (CNPq, 520182/99-5) are Research Career Awardees of the National Research Council of Brazil (CNPq). R.G.D. is a postdoctoral fellow of CNPq. L.A.R. acknowledges an MSc scholarship awarded by CAPES, A.B. acknowledges her PhD scholarship awarded by BNDES, and L.K.B.M. a PhD scholarship awarded by CNPq.

References

1 H. J. J. Nijkamp and P. G. DeHaan, *Biochim. Biophys. Acta*, 1967, **147**, 31–40.
2 Y. Deng, Z. Wang, K. Ying, S. Gu, C. Ji, Y. Huang, X. Gu, Y. Wang, Y. Xu, Y. Li, Y. Xie and Y. Mao, *Int. J. Biochem. Cell Biol.*, 2002, **34**, 1035–1050.
3 S. C. Andrews and J. R. Guest, *Biochem. J.*, 1988, **255**, 35–43.
4 R. E. Roberts, C. I. Lienhard, C. G. Gaines, J. M. Smith and J. R. Guest, *J. Bacteriol.*, 1988, **170**, 463–467.
5 C. E. Benson, B. A. Brehmeyer and J. S. Gots, *Biochem. Biophys. Res. Commun.*, 1971, **403**, 1089–1094.
6 B. B. Garber, B. U. Jochimsen and J. S. Gots, *J. Bacteriol.*, 1980, **143**, 105–111.
7 A. I. Kessler and J. S. Gots, *J. Bacteriol.*, 1985, **164**, 1288–1293.
8 M. F. Renart and A. Silero, *Biochim. Biophys. Acta*, 1976, **341**, 178–186.
9 T. Spector and T. E. Jones, *Biochem. Pharmacol.*, 1982, **31**, 3891–3897.
10 J. J. Mackenzie and L. B. Sorensen, *Biochim. Biophys. Acta*, 1973, **327**, 282–294.
11 T. Spector, T. E. Jones and R. L. Miller, *J. Biol. Chem.*, 1979, **254**, 2308–2315.
12 S. Henikoff and J. M. Smith, *Cell (Cambridge, Mass.)*, 1989, **58**, 1021–1022.
13 J. Zhang, W. Zhang, D. Zou, G. Chen, T. Wan, M. Zhang and X. Cao, *J. Cancer Res. Clin. Oncol.*, 2003, **129**, 76–83.
14 D. Salvatore, T. Bartha and P. R. Larsen, *J. Biol. Chem.*, 1998, **273**, 31092–31096.
15 T. Page, S. J. Jacobsen, R. M. Smejkal, J. Scheele, W. L. Nyhan, J. H. Magnun and R. K. Robbins, *Cancer Chemother. Pharmacol.*, 1985, **15**, 59–62.
16 J. Li, Z. Wei, M. Zheng, X. Gu, Y. Deng, R. Qiu, F. Chen, C. Ji, W. Gong, Y. Xie and Y. Mao, *J. Mol. Biol.*, 2006, **355**, 980–988.
17 V. Henri, L. Michaelis and M. L. Menten, *Biochem. Z.*, 1913, **49**, 333–369.
18 J. D. Thompson, D. G. Higgins and T. J. Gibson, *Nucleic Acids Res.*, 1994, **22**, 4673–4680.
19 K. C. Kelley, K. J. Huestis, D. A. Austen, C. T. Sanderson, M. A. Donohue, S. K. Stickel, E. S. Kawasaki and M. S. Osburne, *Gene*, 1995, **156**, 33–36.
20 C. Rizzi, J. Frazzon, F. Ely, P. G. Weber, I. O. Fonseca, M. Gallas, J. S. Oliveira, M. A. Mendes, B. M. Souza, M. S. Palma, D. S. Santos and L. A. Basso, *Protein Expression Purif.*, 2005, **40**, 23–30.
21 G. Biazus, C. Z. Schneider, M. S. Palma, L. A. Basso and D. S. Santos, *Protein Expression Purif.*, 2009, **66**, 185–190.
22 Z. A. Sanchez-Quitian, C. Z. Schneider, R. G. Ducati, W. F. de Azevedo, Jr., C. Bloch, Jr., L. A. Basso and D. S. Santos, *J. Struct. Biol.*, 2010, **169**, 413–423.
23 T. H. Grossman, E. S. Kawasaki, S. R. Punreddy and M. S. Osburne, *Gene*, 1998, **209**, 95–103.
24 F. W. Studier, *Protein Expression Purif.*, 2005, **41**, 207–234.
25 A. Levitzki and D. E. Koshland, Jr, *Proc. Natl. Acad. Sci. U. S. A.*, 1969, **62**, 1121–1128.
26 A. Velazquez-Campoy and E. Freire, *Biophys. Chem.*, 2005, **115**, 115–124.
27 J. E. Ladbury and M. L. Doyle, *Biocalorimetry II*, Wiley, London, 2004, 1st edn, p. 259.
28 P. Kwong, M. L. Doyle, D. J. Casper, C. Cicala, S. A. Leavitt, S. Majeed, T. D. Steenbeke, M. Venturi, I. Chaiken, M. Fung, H. Katinger, P. W. Parren, J. Robinson, D. Van Ryk, L. Wang, D. R. Burton, E. Freire, R. Wyatt, J. Sodroski, W. A. Hendrickson and J. Arthos, *Nature*, 2002, **420**, 678–682.
29 G. Bulaj, T. Kortemme and D. P. Goldenberg, *Biochemistry*, 1998, **37**, 8965–8972.
30 D. B. Northrop, *Biochemistry*, 1975, **14**, 2644–2651.
31 J. H. Richards, *Enzymes*, Academic Press, New York, 1970, 2nd edn, p. 321.
32 P. F. Cook, *Enzyme Mechanism from Isotope Effects*, CRC Press, Boca Raton, 1991, pp. 203–228.
33 P. F. Cook, *Isot. Environ. Health Stud.*, 1998, **34**, 3–17.
34 M. P. Patel, W. Liu, J. West, D. Tew, T. D. Meek and S. H. Thrall, *Biochemistry*, 2005, **44**, 16753–16765; R. G. Silva, L. P. S. de Carvalho, J. S. Blanchard, D. S. Santos and L. A. Basso, *Biochemistry*, 2006, **45**, 13064–13073.
35 D. B. Northrop, *Methods*, 2001, **24**, 117–124.
36 P. F. Cook and W. W. Cleland, *Enzyme Kinetics and Mechanism*, Garland Science Publishing, New York, 2007, ch. 9, pp. 253–323.
37 P. F. Cook, J. S. Blanchard and W. W. Cleland, *Biochemistry*, 1980, **19**, 4853–4858.
38 J. G. Belasco, W. J. Albery and J. R. Knowles, *J. Am. Chem. Soc.*, 1983, **105**, 2475–2477.
39 K. Hiromi, *Kinetics of Fast Enzyme Reactions: Theory and Practice*, Kodansha Ltd., Tokyo, 1979, ch. 4, pp. 188–253.
40 J. G. Robertson, *Biochemistry*, 2005, **44**, 5561–5571; J. G. Robertson, *Curr. Opin. Struct. Biol.*, 2007, **17**, 674–679.
41 M. L. Bianconi, *Biophys. Chem.*, 2007, **126**, 59–64.
42 J. E. Ladbury, G. K. Klebe and E. Freire, *Nat. Rev. Drug Discovery*, 2010, **9**, 23–27.
43 D. E. Almonacid, E. R. Yera, J. B. O. Mitchell and P. C. Babbitt, *PLoS Comput. Biol.*, 2010, **6**(3), e1000700.
44 C. Lugnier, *Pharmacol. Ther.*, 2006, **109**, 366–398.
45 H. T. Zhang, *Curr. Pharm. Des.*, 2009, **15**, 1688–1698.
46 A. C. Bishop and V. L. Chen, *J. Chem. Biol.*, 2010, **2**, 1–9.
47 A. Sali and T. L. Blundell, *J. Mol. Biol.*, 1993, **234**, 779–815.
48 M. A. Martí-Renom, A. C. Stuart, A. Fiser, R. Sánchez, F. Melo and A. Sali, *Annu. Rev. Biophys. Biomol. Struct.*, 2000, **29**, 291–325.
49 A. Sali and J. P. Overington, *Protein Sci.*, 1994, **3**, 1582–1596.
50 M. Y. Shen and A. Sali, *Protein Sci.*, 2006, **15**, 2507–2524.
51 D. van der Spoel, E. Lindahl, B. Hess, G. Groenhof, A. E. Mark and H. J. C. Berendsen, *J. Comput. Chem.*, 2005, **26**, 1701–1718.
52 R. A. Laskowski, M. W. MacArthur, D. S. Moss and J. M. Thornton, *J. Appl. Crystallogr.*, 1993, **26**, 283–291.
53 I. O. Fonseca, R. G. Silva, C. L. Fernandes, O. N. de Souza, L. A. Basso and D. S. Santos, *Arch. Biochem. Biophys.*, 2007, **457**, 123–133.
54 A. C. Wallace, R. A. Laskowski and J. M. Thornton, *Protein Eng., Des. Sel.*, 1995, **8**, 127–134.
55 M. M. Bradford, R. A. Mcroire and W. L. Williams, *Anal. Biochem.*, 1976, **72**, 248–254.
56 G. Ottolina, S. Riva, G. Carrea, B. Danieli and A. F. Buckman, *Biochim. Biophys. Acta*, 1989, **998**, 173–178.
57 L. S. Leu and P. F. Cook, *Biochemistry*, 1994, **33**, 2667–2671.
58 P. F. Cook and W. W. Cleland, *Biochemistry*, 1981, **20**, 1790–1796.
59 I. H. Segel, *Enzyme kinetics, behavior and analysis of rapid equilibrium and steady-state enzyme systems*, John Wiley & Sons, Inc., New York, 1975, p. 957.
60 P. F. Cook and W. W. Cleland, *Enzyme Kinetics and Mechanism*, Garland Science Publishing, New York, 2007, ch. 10, pp. 325–366.